# Single molecule electronics

Shaikh, Ahson Jabbar

# Single Molecule Electronics

A Systematic Approach to Study the Properties of

Single Porphyrin Molecules

Ahson Jabbar Shaikh

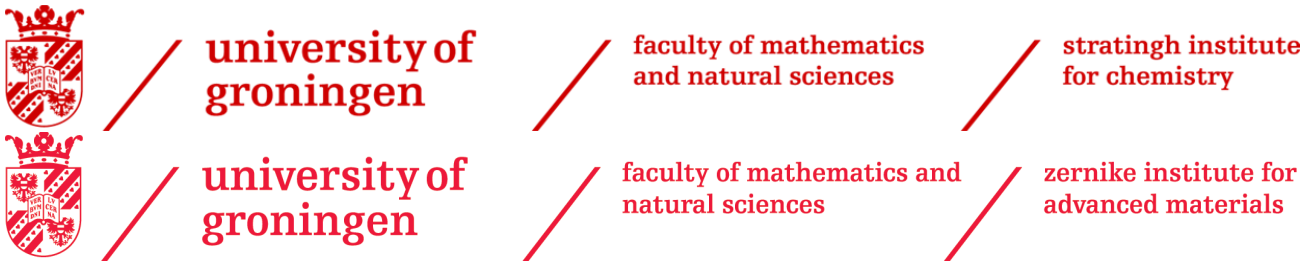


The work described in this thesis was performed in the research group Self-Assembling Systems (now Advanced Soft Matter) at the Department of Chemical Engineering, Delft University of Technology, The Netherlands. The work described in Chapter 6 of this thesis was performed in the research group Molecular Electronics and Devices, Department of Quantum Nanoscience, The Kavli Institute of Nanoscience Delft, Delft University of Technology, The Netherlands by our collaborators. This research work was partly financially supported by the Stratingh Institute for Chemistry and the Zernike Institute for Advanced Materials, University of Groningen, The Netherlands.

Cover design: Ahson Jabbar Shaikh

Stratingh Institute for Chemistry
Zernike Institute PhD thesis series 2013-16
ISSN: 1570-1530
ISBN: 978-90-367-6326-4 (printed version)
ISBN: 978-90-367-6327-1 (electronic version)

**RIJKSUNIVERSITEIT GRONINGEN**

# Single Molecule Electronics

## A systematic approach to study the properties of single porphyrin molecules

**Proefschrift**

ter verkrijging van het doctoraat in de
Wiskunde en Natuurwetenschappen
aan de Rijksuniversiteit Groningen
op gezag van de
Rector Magnificus, dr. E. Sterken,
in het openbaar te verdedigen op
vrijdag 27 september 2013
om 16.15 uur

door

**Ahson Jabbar Shaikh**

geboren op 17 januari 1979
te Karachi, Pakistan

| | |
|---|---|
| Promotores: | Prof. dr. J.C. Hummelen<br>Prof. dr. J.H. van Esch |
| Beoordelingscommissie: | Prof. dr. S.J. Picken<br>Prof. dr. J.G. Roelfes<br>Prof. dr. A.E. Rowan |

# TABLE OF CONTENTS

# CHAPTER 1

# About this Thesis

## 1.1 Single molecule electronics: a systematic approach to study the properties of single porphyrin molecules

The work described in this thesis is concerned with molecular electronics, which sometimes is also referred to as moletronics.[1] It is an interdisciplinary subject matter in nanotechnology, which extends over chemistry, physics, materials science and sometimes to biosciences.[2, 3] There is a wide variety of molecular building blocks, which have been used or are being used for the fabrication of electronic components.[4-8] The main theme in molecular electronics lies around the concept of size reduction offered by molecular-level control of properties by the use of small ensembles or even individual molecules as functional building blocks in electronic circuitry. In the chase for smaller, faster and smarter computer chips, scientists focus on miniaturization, that a molecular electronic device can potentially be as small as a single molecule. Our focus is on single-molecule applications.[9-12]

The miniaturization for integrating billions of silicon-based building blocks in a millimeter-scale chip of electronic devices has been progressed rapidly due to the advanced silicon technology.[13] However, it is becoming increasingly difficult to make these small features using top-down, mostly lithographic, approaches. Single-molecule devices appear to be ideal candidates for future nano-electronics, as they possess the potential for creating high-density devices with low power consumption in combination with high speed. The molecules which are typically utilized for the purpose of single molecule electronics are designed in such a way that they have properties which resemble traditional electronic components such as the wire, the transistor, the rectifier, the switch, memory elements and logic gates etc.[14]

Technological advancement has now enabled us to fabricate single-molecule junctions, which led to significant progress for understanding electron transport in molecular systems at the

single-molecule level. However, a long-standing desire of scientists for various potential device applications is the ability to completely understand, control, and exploit charge transport at the level of single molecule.[15]

The manufacturing of ICs with single-molecule building blocks is the main goal of molecular electronics. It can be achieved by assembly of a large numbers of nanoscale objects i.e. molecules, nanoparticles, nanotubes and nanowires to form new devices and circuit architectures.[16] The concept of making a functional device based on the properties inherent in a single molecule offers, in principle, unlimited possibilities for technological development because the potentially diverse electronic functions of the component molecules can be tailored by chemical design and synthesis. The great diversity of molecular structures with their associated energy levels may permit tuning electronic properties and modification of energy gaps over a wide range, and incorporation of sensors into microelectronic circuits. This approach will significantly reduce the fabrication costs, compared to usual semiconductor technologies. If molecular devices can take advantage of self-assembly processes, manufacturing costs can be further lowered by achieving high device yields.[13]

Numerous strategies have been reported to date for the fabrication, design, and characterization of molecular electronic devices, but a broadly accepted example showing relationship between molecular structure and current–voltage characteristics has not yet emerged. Also to create accessible, easily transportable, standard molecule-based device with reproducibility has proven difficult to find in molecular electronics due to instability. Low yield reproducibility, consistency across several laboratories and experimental prototypes, rational design, manufacturability, thermal stability and integration with commercial materials and structures, like hybrid devices with conventional semiconductor structures are issues, still to be resolved. A robust molecular junction with reproducible electronic behavior and , exploitation of new functions enabled by molecular components are also needed.[17] Some measurements on single molecules are carried out in cryogenic temperatures (close to absolute zero) which is very energy consuming. Therefore it is essential to examine the device performance and durability of single-molecule junctions in a practical environment.

There is still a long way to go before single-molecule electronic devices can be used in practical applications as entire electronic circuits exclusively made of molecules. The current focus is on finding interesting molecules with required properties and finding ways to obtain

reliable and reproducible contacts by major improvements in device fabrication methods. Nevertheless, the field is progressing rapidly from both scientific and technological viewpoints encouraging further advances in single-molecule electronics.

## 1.2 Porphyrins in single molecule electronics

We chose to study porphyrins (figure 1) in single molecule devices as they are complex, highly conjugated aromatic molecules with interesting optical properties, great architectural flexibility, chemically stable structures, and the ability to self-assemble on surfaces as well as in solution. [18-21] Porphyrins are interesting molecules for scientist to study for their conductivity properties, e.g., a single porphyrin molecule conductance was measured, which was held between a STM tip and a gold substrate. Conductance in two states was observed and was attributed to conformational changes in the molecule.[22] Similar studies were performed with porphyrin wires of various sizes.[21] Additionally, the conductivity of molecules using the Scanning Tunneling Microscope break-junction (STM-BJ) method was measured, where the length dependence of charge transport of porphyrin wires (oligomers) was evaluated in planar edge-fused tapes, alkyne-linked oligomers and twisted singly linked chains.[23] Some studies have also been conducted on planarly absorbed porphyrin molecules on metal interface, which is however less interesting for our studies.[24, 25]

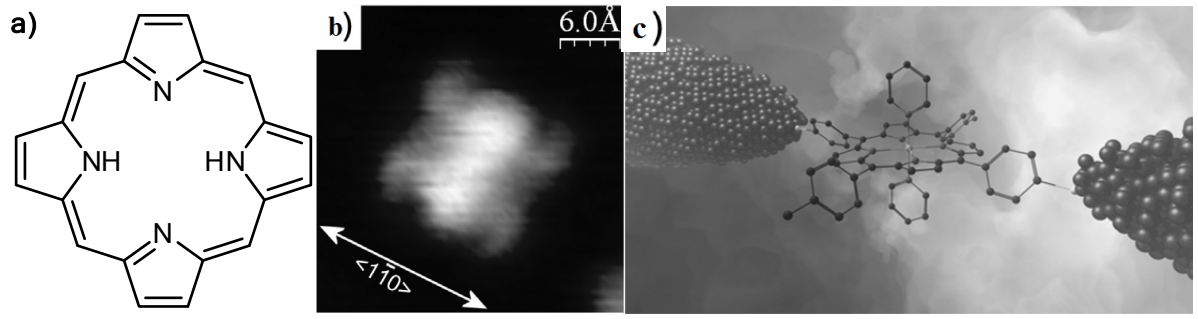


Fig. 1: (a) Basic porphyrin molecular structure, which has alternate double bonds in a fully conjugated manner, (b) conduction through porphyrins as studied by STM on planarly adsorbed porphyrins on metal surfaces, adopted from reference [24], and (c) porphyrins between nanoelectrodes, forcing charge transport parallel to plane.

## 1.3 Thesis outline

In chapter 2 of this thesis, we show the application of molecules either as bulk or as single molecule in the construction of electronic devices. For this purpose, we designed and successfully synthesized amino and thiol-functionalized porphyrin molecules (chapter 3), which have the required conjugated structure and linkers at proper positions to incorporate them in single molecule devices.[26-28]

With the ultimate aim of studying these molecules in gold or platinum nanojunctions, in chapter 4 we investigated binding interaction of synthesized porphyrin molecules with gold nanoparticles and gold nanorods to act as model systems for the nanoelectrodes in single molecule devices.[27, 29, 30] The results of these studies show that binding is static on fluorescence time scales, and is dependent on the number of linker moieties present on the porphyrin molecules, while the diamino porphyrins and dithiol porphyrins show similar binding constants. Interestingly, the trans-dithiol porphyrins show specific binding interaction of nanoparticles in selective combination of solvents by formation of dimers or trimers of nanoparticles, without making cluster formation, as observed by SEM pictures.

Once the binding of thiol and amine porphyrins to gold nanoparticles was established, we also investigated binding interaction of porphyrins with PbSe quantum dots (chapter 5) in order to study charge and energy transfer properties.[31-35] While the amine- and thiol porphyrins functionalized porphyrins did not interact with the PbSe quantum dots, it was found that carboxylate-functionalized porphyrins and PbSe quantum dots have a strong interaction, though dynamic on fluorescence time scale. These studies indicated that indeed photo-induced charge transfer from the porphyrins to quantum dots occurs, but photo-induced charge transfer from quantum dots to porphyrins did not take place. Therefore these molecules can further be used for charge transfer through nanoelectrodes.

The final part of this thesis was focused on single molecule electronic behavior of porphyrins, which have significant potential for both bulk and single molecule electronics. In the last chapter (chapter 6), porphyrins were studied as single molecules using three terminal devices prepared through a platinum electromigration technique, and a mechanical control break junction.[19-21] Current-voltage characteristics of porphyrins were studied at room and near absolute zero temperatures. Overall, single molecule electrical measurements on

functionalized porphyrins in nanoscale electronic devices show that it is possible to use this type of molecules for the formation of stable single molecule junctions. Detailed analysis of such measurements reveals that the porphyrins can exist in several differently conducting configurations in these nanogaps, depending both on the device and on the molecular structure of the porphyrin. Moreover, the configuration can change rapidly and repeatedly over time. It is not unlikely that this behavior is not limited to porphyrins, and future design of single molecule electronic junctions should take this behavior into account.

As a result, these studies increase our understanding on the influence of metal – molecule interactions and electron transport in a single molecule, which is crucial for further development in nanoscale electronics.

## 1.4 References


1. Lent, C.S., *Molecular electronics - Bypassing the transistor paradigm.* Science, 2000. **288**(5471): p. 1597-+.
2. Tour, J.M., *Molecular Electronics. Synthesis and Testing of Components.* Accounts of Chemical Research, 2000. **33**(11): p. 791-804.
3. Mallajosyula, S.S. and S.K. Pati, *Effect of Protonation on the Electronic Properties of DNA Base Pairs: Applications for Molecular Electronics.* The Journal of Physical Chemistry B, 2007. **111**(40): p. 11614-11618.
4. Baer, R. and D. Neuhauser, *Phase Coherent Electronics: A Molecular Switch Based on Quantum Interference.* Journal of the American Chemical Society, 2002. **124**(16): p. 4200-4201.
5. Klare, J.E., et al., *Cruciform π-Systems for Molecular Electronics Applications.* Journal of the American Chemical Society, 2003. **125**(20): p. 6030-6031.
6. Martin, C.A., et al., *Fullerene-based anchoring groups for molecular electronics.* Journal of the American Chemical Society, 2008. **130**(40): p. 13198-13199.
7. Vondrak, T., et al., *Interfacial Electronic Structure in Thiolate Self-Assembled Monolayers: Implication for Molecular Electronics.* Journal of the American Chemical Society, 2000. **122**(19): p. 4700-4707.
8. Watson, M.D., et al., *A Hexa-peri-hexabenzocoronene Cyclophane: An Addition to the Toolbox for Molecular Electronics.* Journal of the American Chemical Society, 2004. **126**(5): p. 1402-1407.
9. Andrews, D.Q., et al., *Single Molecule Electronics: Increasing Dynamic Range and Switching Speed Using Cross-Conjugated Species.* Journal of the American Chemical Society, 2008. **130**(51): p. 17309-17319.
10. Erin, V.I., E.-K. Mahnaz, and E.C.H. Sykes, *Scanning Tunneling Microscopy and Single Molecule Conductance*, in *Nanotechnology in Undergraduate Education*. 2009, American Chemical Society. p. 123-133.
11. Müllen, K. and J.P. Rabe, *Nanographenes as Active Components of Single-Molecule Electronics and How a Scanning Tunneling Microscope Puts Them To Work.* Accounts of Chemical Research, 2008. **41**(4): p. 511-520.
12. Venkataraman, L., et al., *Electronics and Chemistry: Varying Single-Molecule Junction Conductance Using Chemical Substituents.* Nano Letters, 2007. **7**(2): p. 502-506.
13. Tsutsui, M. and M. Taniguchi, *Single Molecule Electronics and Devices.* Sensors, 2012. **12**(6): p. 7259-7298.
14. Okawa, Y., et al., *Chemical Wiring and Soldering toward All-Molecule Electronic Circuitry.* Journal of the American Chemical Society, 2011. **133**(21): p. 8227-8233.
15. Song, H., M.A. Reed, and T. Lee, *Single Molecule Electronic Devices.* Advanced Materials, 2011. **23**(14): p. 1583-1608.
16. Vuillaume, D., *Molecular Nanoelectronics.* Proceedings of the Ieee, 2010. **98**(12): p. 2111-2123.
17. McCreery, R.L. and A.J. Bergren, *Progress with Molecular Electronic Junctions: Meeting Experimental Challenges in Design and Fabrication.* Advanced Materials, 2009. **21**(43): p. 4303-4322.
18. Anderson, H.L., *Building molecular wires from the colours of life: conjugated porphyrin oligomers.* Chemical Communications, 1999(23): p. 2323-2330.

19. Noguchi, Y., et al., *Fowler-Nordheim tunneling in electromigrated break junctions with porphyrin molecules.* Japanese Journal of Applied Physics Part 1-Regular Papers Brief Communications & Review Papers, 2007. **46**(4B): p. 2683-2686.
20. Kang, B.K., et al., *Length and temperature dependence of electrical conduction through dithiolated porphyrin arrays.* Chemical Physics Letters, 2005. **412**(4-6): p. 303-306.
21. Sedghi, G., et al., *Single molecule conductance of porphyrin wires with ultralow attenuation.* Journal of the American Chemical Society, 2008. **130**(27): p. 8582-+.
22. Qian, G., S. Saha, and K.M. Lewis, *Two-state conductance in single Zn porphyrin molecular junctions.* Applied Physics Letters, 2010. **96**(24): p. 243107-3.
23. Sedghi, G., et al., *Comparison of the Conductance of Three Types of Porphyrin-Based Molecular Wires: β,meso,β-Fused Tapes, meso-Butadiyne-Linked and Twisted meso-meso Linked Oligomers.* Advanced Materials, 2012. **24**(5): p. 653-657.
24. Brede, J. and et al., *Dynamics of molecular self-ordering in tetraphenyl porphyrin monolayers on metallic substrates.* Nanotechnology, 2009. **20**(27): p. 275602.
25. Beggan, J.P., et al., *Control of the axial coordination of a surface-confined manganese(III) porphyrin complex.* Nanotechnology, 2012. **23**(23): p. 235606.
26. Pollard, M.M. and J.C. Vederas, *A convenient preparation of thioether functionalized porphyrins.* Tetrahedron, 2006. **62**(51): p. 11908-11915.
27. Gryko, D.T., C. Clausen, and J.S. Lindsey, *Thiol-derivatized porphyrins for attachment to electroactive surfaces.* Journal of Organic Chemistry, 1999. **64**(23): p. 8635-8647.
28. Abdelrazzaq, F.B., R.C. Kwong, and M.E. Thompson, *Photocurrent generation in multilayer organic-inorganic thin films with cascade energy architectures.* Journal of the American Chemical Society, 2002. **124**(17): p. 4796-4803.
29. Cormode, D.P., J.J. Davis, and P.D. Beer, *Anion sensing porphyrin functionalized nanoparticles.* Journal of Inorganic and Organometallic Polymers and Materials, 2008. **18**(1): p. 32-40.
30. Kanehara, M., H. Takahashi, and T. Teranishi, *Gold(0) porphyrins on gold nanoparticles.* Angewandte Chemie-International Edition, 2008. **47**(2): p. 307-310.
31. Frasco, M.F., V. Vamvakaki, and N. Chaniotakis, *Porphyrin decorated CdSe quantum dots for direct fluorescent sensing of metal ions.* Journal of Nanoparticle Research, 2010. **12**(4): p. 1449-1458.
32. Hashimoto, T., et al., *Theoretical study of the Q and B bands of free-base, magnesium, and zinc porphyrins, and their derivatives.* Journal of Physical Chemistry A, 1999. **103**(12): p. 1894-1904.
33. Wen, Y.N., et al., *Activation of porphyrin photosensitizers by semiconductor quantum dots via two-photon excitation.* Applied Physics Letters, 2009. **95**(14).
34. Zenkevich, E., et al., *Nanoassemblies designed from semiconductor quantum dots and molecular arrays.* Journal of Physical Chemistry B, 2005. **109**(18): p. 8679-8692.
35. Zenkevich, E.I., et al., *Identification and assignment of porphyrin-CdSe hetero-nanoassemblies.* Journal of Luminescence, 2007. **122**: p. 784-788.

# CHAPTER 2

# Single Molecule Electronics

## 2.1 Molecular electronics

Molecular electronics, also sometimes referred to as *moletronics*, is an interdisciplinary subject matter in nanotechnology, which extends over chemistry, physics, biology and materials science. Molecular building blocks are used for the fabrication of electronic components, e.g. resistive wires and transistors. The concept of molecular-scale electronics has considerable appeal from the viewpoint of size reduction and the chase for smaller, faster and smarter computer chips down to the molecular scale by molecular-level control of properties. Molecular electronics also provides means for scientists to focus and broaden Moore's Law beyond the foreseen limits of small-scale standard silicon integrated circuits.[1]

Organic semiconductors, when compared to traditional inorganic materials such as silicon, have unique properties and advantages, e.g. low-temperature processing on flexible substrates, their low cost, high-speed fabrication and tunable electronic properties. These materials are based on π-conjugated organic molecules and polymers. Within the organic semiconductors, most of the materials are *p*-channel (hole-transporting), whereas *n*-channel (electron-transporting) materials are relatively rare.[2, 3]

The fabrication of molecular electronic devices can be achieved by using supramolecular chemistry techniques and self-assembly of organic molecules, carbon nanotubes, DNA and proteins and others. In molecular electronics experiments, electrically active molecules can drastically change their behavior depending on whether they are surrounded by electrodes or by other materials, an effect that is currently receiving increasing attention.[4-6].

Molecular electronics can be divided into two sub-disciplines. *Molecular materials for electronics*, which utilizes the properties of the molecules to affect the bulk properties of a material,[7, 8] while *molecular scale electronics* focuses on single-molecule applications.[9]

### 2.1.1 Applications of thin film molecular electronics

Organic electronics can play an important role in the development of flexible thin-film device technologies.[10] Photovoltaic solar cells, organic light emitting diodes (OLEDs), and plastic electronics are some of the applications of thin film molecular electronics. The next generation of electronic products includes flexible displays, low cost radio frequency identification tags and printable sensors.[2] Development of new photoresist materials and photolithography can be applied to fabricate complex organic electronic and hybrid organic/inorganic circuitry and full-color organic displays.[11]

#### 2.1.1.1 Photovoltaic solar cells

Photovoltaic solar cells are one of the most important current fields of focus for application of thin film molecular electronics. π-conjugated polymeric semiconductor materials are utilized as light absorbing and charge carrier transporting materials in these devices.[12, 13] The molecular design and the supramolecular ordering of these materials are of particular importance for the efficiency of such devices.[14]

#### 2.1.1.2 Organic light emitting diodes

Organic light emitting diodes (OLEDs) are another important application of thin film molecular electronics. During the past two decades the development of OLEDs has been the focus of an intensive multidisciplinary research effort. In recent years, beside the development of a new generation of display devices, lighting applications such as light-emitting field-effect transistors or organic lasers are attracting substantial interest. OLEDs have various functions and are used as a backlight unit in full-color single-panel LCD microdisplay systems.[15] Most of the screens in handheld electronic devices nowadays are based on OLEDs and even OLED-based televisions up to 55 inch of diagonal screen have been introduced to the market.

Porphyrins, a class of π-conjugated organic molecules, which are also the molecules of interest in this thesis, have been used for OLEDs, where linear and cyclic porphyrin hexamers were used as near-infrared emitters.[16]. Devices based on luminophores possessing hole transporting units have been successfully developed by taking advantage of the intrinsic charge-transport properties of some π-conjugated systems or by introduction of hole-

transporting blocks in the structure. Some of the bipolar blue, green and red molecular emitters, showing both electron and hole injection and transport, have shown promising device efficiencies.[17] High photoluminescence efficiency, synthetic accessibility and process ability can be combined by design with additional functions such as hole and/or electron injection and transport. Molecular design can be applied to generate the required colored fluorescent materials for use in OLED displays, where there is relationship between the molecular structure and the electronic properties of the molecular emitters. [17, 18] Recent advancements in this field show evenly separated red, green and blue OLED colors, which can bring OLEDs into the next generation of full-color displays and the solid-state lighting market. [19]

#### 2.1.1.3 Plastic electronics

Plastic electronics is a branch of electronics, which deals with electricity conducting polymers, and is an alternative to silicon technology. Plastic electronics are low-cost, large-scale, transparent and flexible electronics, and are one of the most highlighted applications of organic electronics. In plastic electronics, the active organic based materials are deposited as printable inks onto polymer-based substrates using various printing technologies, rather than relying on conventional, rigid and brittle silicon chips to process information. Plastic electronic circuits have the potential to be printed in a small laboratory containing one or two printing tools, whereas state-of-the-art microchip factories are about the size of three football fields and require purpose-built facilities. Polyacetylene, polypyrrole, and polyaniline or their mixed polymers are examples of generally used organic materials which are conducting and used in plastic electronics.

Molecular orientation effects of organic thin films strongly affects the performance of organic electronic devices, such as the light absorption, charge transport, interfacial charge transfer, ionization potential and energy level alignment.[20] Organic and polymer layer based molecular memories, which have either capacitive or resistive based electrical storage behavior, show the potential of organic electronics in general and plastic electronics specifically.[21] Plastic electronic devices containing electrophysiological, temperature, and strain sensors, transistors, light-emitting diodes, photodetectors, radio frequency inductors, capacitors, oscillators, and rectifying diodes, solar cells and wireless coils, as high-performance electronic functionality have been described. These devices are laminated tightly

and reliably onto the skin which has thickness, effective elastic moduli, bending stiffnesses, and areal mass densities matched to the epidermis. Electrical activity produced by the heart, brain, and skeletal muscles can be measured by such devices.[22]

## 2.2 Single Molecule Electronics

### 2.2.1 Concept

Single molecule electronics is defined as a branch of molecular electronics that uses single molecules as electronic components. Moore's law describes a trend, where the number of transistors, which can be placed inexpensively on an integrated circuit of constant area size, will be approximately doubled every two years. This law has basically been used in the semiconductor industry to guide long-term planning and to set targets for research and development. The current size of functional elements on electronic chips is 22 nm, and Intel and Samsung have announced 14 nm and 10 nm chips for future releases. However, it becomes increasingly difficult to make these small features using top-down, mostly lithographic, approaches. In that respect, single molecules are the smallest stable structures imaginable as electrical circuits, and could as such be applied to further down-scale future electronic devices.

The molecules which are typically utilized for the purpose of single molecule electronics are designed in such a way that they have properties which resemble traditional electronic components such as the wire, the transistor, the rectifier and the switch. In 1988 Aviram and coworkers[23] provided evidence of switching and rectification by a single molecule, effected with scanning tunneling microscope (STM) tip. Joachim and coworkers reported the first study of electrical contact with an individual molecule ($C_{60}$) and measurement of the conductance of a single molecule using an STM tip in 1995.[24, 25]

In 1996[26], Tour *et al* presented evidence of conducting molecular wires, by use of STM (figure 1). The molecular wire candidate was ethyl-substituted 4,4'-di(phenylene-ethynylene)-benzothioacetate, which was already shown to self-assemble on gold.[27] Molecular wires were inserted into nonconducting n-dodecanethiol self-assembled monolayers on Au{111}and were probed by STM to assess their electrical properties. The inserted conjugated molecules

formed single molecule wires that showed very high conductivity as compared the surrounding alkanethiolates.

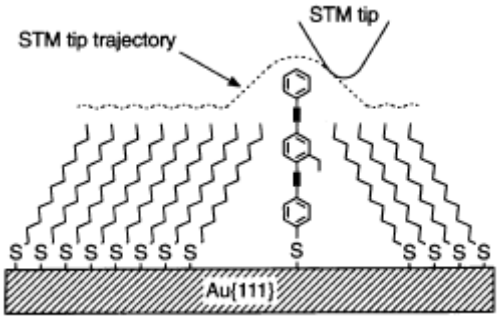


Fig. 1: Adapted from Ref.[26]; Conducting wire shows very high conductivity as compared to dodecane thiolate.

The first evidence of conductance of a molecular junction was reported in 1997 by Mark Reed and co-workers.[28] They used benzene-1,4-dithiol, self-assembled onto the two facing gold electrodes of a mechanically controllable break junction. They observed charge transport through the molecules and a conductance-voltage curve showing two steps in both bias directions. That study provided a quantitative measure of the conductance of a junction containing a single molecule, which was a fundamental step towards the development of molecular-scale electronics.

The field of single molecule electronics progressed rapidly after the first examples of conductive single molecules. Advances in the preparation of nano-electrodes made it possible to measure conduction properties of simple organic molecules directly. Early theoretical predictions have been confirmed to a significant extent, and technological progress in nanoscience has improved both the experimental and theoretical study of (single) molecule electronics. Especially, development of the scanning tunneling microscope (STM) and the atomic force microscope (AFM) have facilitated manipulation of single molecules and their use in single-molecule electronics.[29, 30]

Rotaxanes and catenanes can also be applied as molecular components in molecular electronic devices such as low bit-density memory circuits and ultra-high density memory circuits, where the electrochemical switching characteristics of these molecules are used together with novel patterning methods.[31-33] The semiconductor industry is also involved in exploring carbon nanotubes, graphene layers and nanoribbons as carbon-based electronics. Additionally,

field-effect transistors based on semiconductor nanotubes and graphene nanoribbons have been demonstrated.[34]

#### 2.2.1.1 Conduction of electrons through single molecules

At the single molecule level, the terms “conductance” and “conductivity” are used synonymously,[35, 36] however the term conductance is prevalent. Different classes of molecules will have different conductivities, for instance conjugated structures will in general be more conductive than simple alkanes. An overview of the difference in conductance between different classes of molecules is described by Martin *et al*.[37] Some studies have been performed in order to study the effect of conductance as a function of molecular length.[36, 38, 39] Mostly, simple molecules have been studied in detail, e.g. substituted benzenes, alkanes and alkenes with different linker groups.

The basic idea of molecular electronics or single molecule electronics is to conduct charge carriers through molecular wires, transistors or rectifiers.[40, 41] The linkers between the molecules and the electrodes must be able to connect with nano-electrodes, typically made of gold, platinum or other metals. The electrical contacts must be reproducible and reliable, showing strong binding e.g. thiols with gold electrodes, amines with platinum electrodes.[36, 42, 43]

The conductance G ($G = I / V$) of a single molecule [44] is dependent on various conditions of the surroundings, e.g. pH, temperature, pressure as well as the properties of measuring device, e.g. the surface morphology of the electrode and the atomic-scale molecule-electrode contact geometry. Experimentalists and theorists still face many challenges in single molecule electronics, although many experimental techniques have been developed so far to measure conductivity (figure 2).[45, 46]

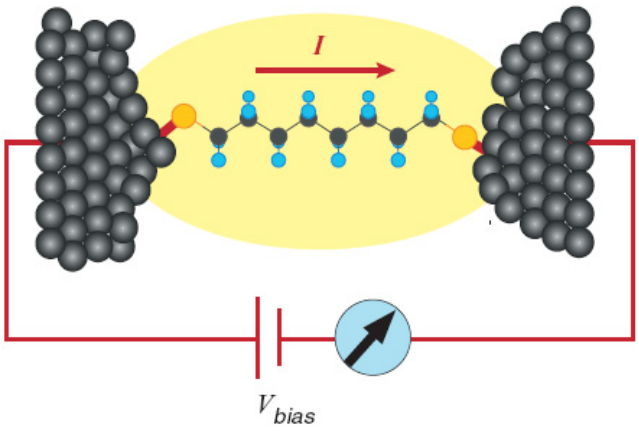


Fig. 2: Representation of a single molecule interaction; adapted from [45]

An important prerequisite to determine the conductance of a single molecule is to establish that the measured conductance results from only a single molecule and not several molecules, and therefore the molecule has to be properly attached to the two probing electrodes.[47]

In 2001, Cui *et al.* were able to measure the resistance of a single octanedithiol molecule. Non-bonded contacts to octanethiol monolayers were at least four orders of magnitude more resistive, demonstrating that the measurement of basic molecular properties requires chemically bonded contacts.[48] The delocalization of molecular electronic orbitals and their connection to the metallic contacts is responsible for the electrical conduction through conjugated molecules. However, for non-conjugated molecules such as octanethiol, conduction is attributed to the large band gap of molecules with the highest occupied molecular orbital (HOMO) being close to the Fermi level. For a positive substrate Pt/Ge(001) bias, the electrons tunnel from the STM tip through the molecule to the surface, giving rise to higher current compared to a negatively biased Pt/Ge(001) substrate.[49] Dadosh *et al.* studied the effect of conjugation-breaking groups within a conjugated molecule on the electrical conduction. They found that the presence of oxygen or methylene groups between conjugated structures suppresses the electrical conduction. [38].

#### 2.2.1.2 Coulomb blockade

An important aspect of miniaturization down to the single molecule level is that at these length scales quantum effects start to play a role.[50] In the case of conventional electronic components, electrons added or removed from for instance a wire are more or less like a continuous flow of charge, whereas in the case of single molecules, the transfer of a single

electron changes the system significantly. Essentially, when an electron is transferred from the source electrode to the molecule, the molecule gets charged and repels any other incoming electron. This mechanism is known as Coulomb blockade (CB).[51] At low bias voltages, the resistance of the device increases to infinity and for zero bias no current flows because of the CB. Quantum mechanics put severe restraints on the orbitals (or energy levels) for the number of electrons in a single molecule. These states basically determine the energy and spatial distribution of an electron and hence the electronic properties of the complete single molecule setup. Although the molecules seem small and simple when drawn schematically, the possible electronic states can only be deduced approximately, which limits the predictability of the molecular electronic properties.

#### 2.2.1.3 Fermi levels of electrodes and frontier molecular orbitals

In metals, the Fermi Level is defined as the highest occupied molecular orbital in the valence band at 0 K, so that there are many states available to accept electrons. When a bias voltage is applied, the Fermi energy levels of the electrodes are changed, and electron tunneling from one electrode to the other is driven by this potential difference (figure 3).

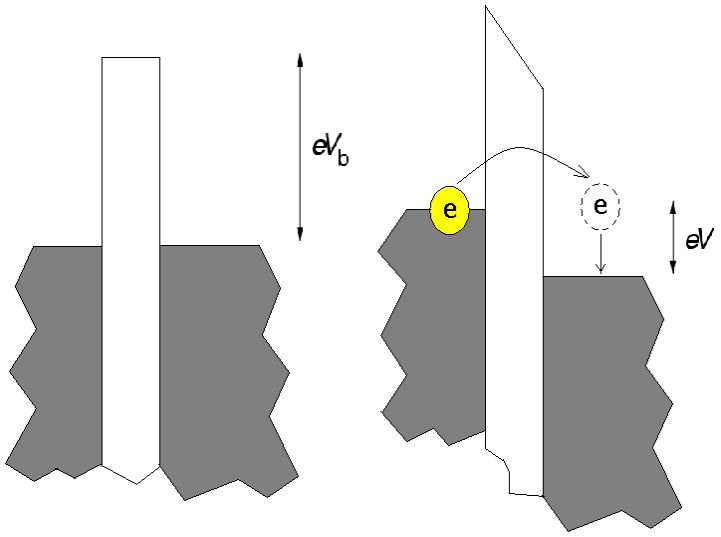


Fig. 3: Cartoon diagram showing tunneling of electrons from one electrode to the other, where "*e*" represents an electron, which tunnels through a barrier of height $eV_b$ (vertical dimension is energy), V is the bias voltage leading to a current flowing between the right and the left "electrode" (side of the barrier).

Now, if a molecule is placed between the two electrodes, then the HOMO-LUMO energy levels of the molecule play an important role in the electron conductance between the

electrodes. In the following diagram (figure 4), it can be seen that a certain energy level of the molecule should be in line with the Fermi level in order to transfer the electron most efficiently through the molecule and if the Fermi level is not aligned with one of the frontier orbitals, charge transfer is not efficient. Additionally the Fermi level of the electrode on the other side should be at a lower level, so that the electron can be transferred from the molecule to the electrode, allowing the process to continue. At any certain moment, there can only be one electron passing through the molecule. In order for an electron to tunnel through a molecule, a third electrode (gate) can also be introduced to change the energy levels of the single molecule.

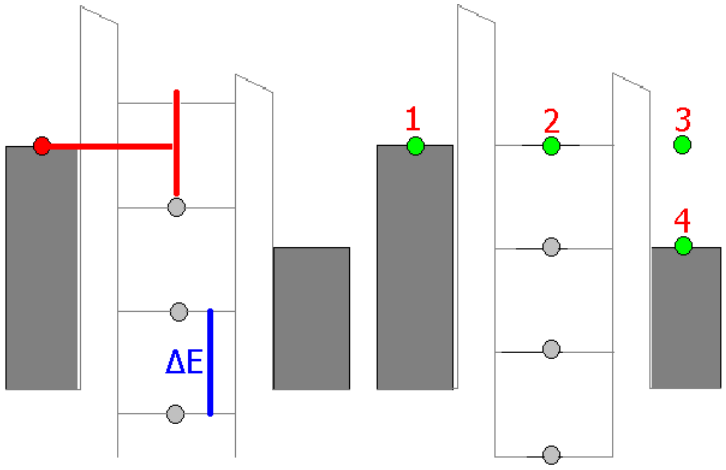


Fig. 4: Possibility of electron transfer through the molecule with the specified energy levels of the molecule (additional details below)

In figure 4 above, the blocking state (left part) and the transmitting state (right part) are represented, where energy levels of source, island and drain (from left to right in each part) in a single electron transistor are shown. In the blocking state, no accessible energy levels are within tunneling range of the electron (red) on the source contact. All energy levels on the island electrode with lower energies are occupied. When a positive voltage is applied to the gate electrode the energy levels of the island electrode are lowered. The electron (green **1**) can tunnel onto the island (**2**), occupying a previously vacant energy level. From there it can tunnel onto the drain electrode (**3**) where it in-elastically scatters and reaches the drain electrode Fermi level (**4**). The energy levels of the island electrode are evenly spaced with a separation of ΔE.

### 2.2.2 Techniques to measure conductance of single molecule

A major problem when measuring single molecules is to establish reproducible electrical contacts to only one molecule.[52] Conceptually, a simple method to measure single-molecule conductance is to fabricate two facing electrodes on a solid substrate and place a molecule with proper anchoring groups bridging the two electrodes.[53] As the size of the molecule is small as compared to the electrodes, care has to be taken that shortcut of the electrodes does not occur. This requires a method to fabricate electrodes with a molecular scale gap, which proves to be a difficult task. The current conventional micro- and nanofabrication photolithographic techniques are unable to produce electrode gaps that are small enough; therefore alternative strategies are considered and used nowadays for measuring the electronic properties of single molecules (see below). Furthermore, connecting single molecules reliably to a larger scale circuit has proven to be a great challenge and constitute a significant hindrance to application of such devices up till now.

#### 2.2.2.1 Scanning probe techniques

STM and AFM have played a unique role in measuring conductance of single molecules. STM is able to image individual molecules absorbed on a conductive substrate with sub-molecular resolution. Electrical measurements were performed to identify simultaneously the number and type of organic molecules within metal–molecule–metal junctions by combining analyses of single-molecule conductance and inelastic electron tunneling spectra using a nanofabricated mechanically controllable break junction.[54] The tip can also be used to manipulate atoms and molecules on surfaces. Although AFM generally has lower resolution than STM, it can measure both mechanical and electrical properties of single molecules.[26, 30, 48, 50, 55-59].

#### 2.2.2.2 Mechanically controllable break junction

When an electrical junction is formed by pulling a wire apart in such a manner that it produces two electrodes, separated by only a few atomic distances, it is called a break junction. A piezoelectric crystal (actuator) is often used to apply the necessary force to pull a metal wire apart to the sides in this technique. Piezoelectric materials can be elongated and controlled to atomic scale precision, when voltage is applied to it, which is proportional to the

resulting mechanical movement. This movement acts as a vertical push rod, which bends the horizontal flexible substrate, resulting in atomic sized gaps by breaking the metallic wire on top of the substrate in a controlled manner. As the wire breaks, the separation between the electrodes can be controlled by relaxing the force on the substrate, while continuously monitoring the electrical current through the junction (figure 5).

A single molecule in an MCBJ is deposited by coating an unbroken electrode with a single layer of molecules, after which the wire is broken and the electrodes are pulled away from each other. The molecules which are bonded between these two electrodes start to detach one by one, until only single molecule is connected. The atomic-level geometry of the tip-electrode contact has an effect on the molecular conductance and varies from one experiment to the other experiment, so generally many measurements are taken. A junction formation with precise contact geometry is one of the main issues with this approach. This effect is described in detail in the next section.

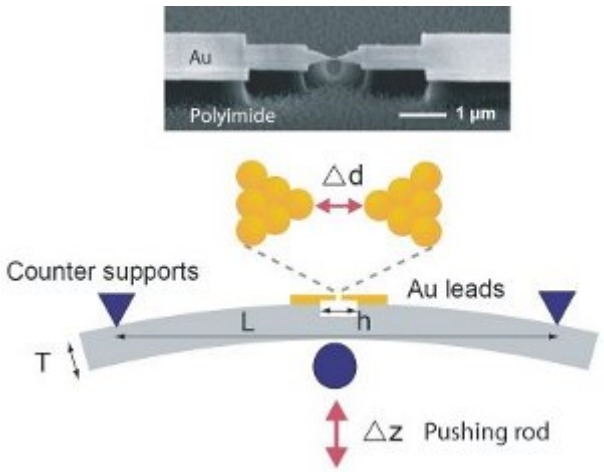


Fig. 5: (Top) a SEM picture shows a free-standing Au wire on top of a polyimide-coated stainless steel substrate. Adapted from http://www.nanoelectronics.ch/research/molecular.php. (Bottom) diagram depicting the principle of the MCBJ.

### 2.2.2.3 Other single molecule junctions

Certain unconventional techniques are used to fabricate electrodes with a molecular scale gap e.g. electromigration,[60, 61] electrochemical etching or deposition[62-65] and other novel methods[66-70]

There are a few methods to prepare nanogaps using electrochemical methods. Templates can be used for the synthesis of nanowires. A simple automated method to fabricate nanowires supported on a solid substrate with electrochemical etching and deposition is described.[63, 64] Fabrication techniques on insulating substrates using combination of lithographic and electrochemical methods, to reach separations on 1 nm scale were achieved.[65] An etching method to reproducibly make gaps with distance control on the single-atom level is also described.[62, 71] Tornow *et al* fabricated nanometer spaced metal electrodes with precisely predetermined spacing using etching methods to get monolayer precision.[69] Kubatkin *et al*.[67] described another multistep method to prepare nano sized gaps between two electrodes by using a shadow mask to deposit the gold lead electrodes. Further Zhitnev and Bao from the Bell laboratories [70] fabricated metal single electron transistors (SETs) on scanning tips by exploiting the smallness of the tip geometry with shadow angle evaporation. A paper published in 2005 [66] reported another method by the combination of lithography techniques and electromigration methods.

In summary, there is a range of special methods that are used to create nanoscale gaps electrodes.[72] Many techniques exist, each with their own advantages and shortcomings. For each type of measurement the most appropriate technique has to be selected.

### 2.2.3 Single molecules

The limitations of the present day lithographic methods and continuous demand for more computing power in smaller sized circuits will possibly bring one day molecular electronics in everyday use.[73, 74] One of the common features for the structure of organic molecules to be utilized in molecular electronics is that they contain alternating single and multiple (double or triple) bonds (figure 6), generally classified as a conjugated system.[75-77] The delocalization of molecular orbitals makes it possible for electrons to move freely over the conjugated area. There are various kinds of functions of molecules in single molecule devices, such as wires, transistors, rectifiers, logic gates and switches etc.[78]

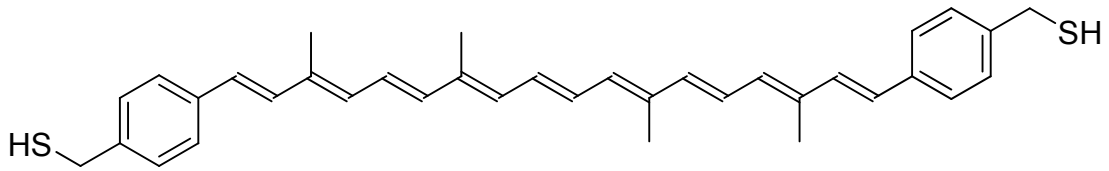


Fig. 6: A carotene molecule with alternating double bonds, synthesized to study electron transport properties through single molecules.[30]

Considerable progress has been made for the advancement of molecular electronics in recent years. Molecules with robust electronic functionalities, such as switches, diodes, and memory elements, showing consistent electrical properties across various experimental circumstances are still needed. The diversity of molecular structures containing functional molecular components e.g. transistors, rectifiers, switches and logic gates etc. require self-assembly on electrode surfaces, thermally stable contacts, and functional electronic coupling with electrodes. There are various factors that affect the behavior of molecules and their electronic function, such as the structure of molecule, type of device, device fabrication method, the molecule-device-interface, and the type of surface.[79]

The resistance of the junctions in molecular electronics is strongly affected by both the structure and size of the molecule, and the way the molecule is attached to the surface. [80, 81] Molecular junction design and development improves device yield and reproducibility, as well as reducing deviations in intrinsic electrical characteristics.

The torsion angle φ between two phenyl rings in biphenyl-dithiol derivatives also affects the conductivity of the molecules.[82-84]. The conductance of the molecular junctions is roughly proportional to the square of the cosine of the torsion angle between the two benzene rings of the biphenyl core.[85, 86] The role of sulfur-gold couplings and molecular conformation, such as gauche defects in the alkyl chains and the torsion angle between two phenyl rings has been demonstrated with detailed molecular-level understanding of the electronic structure and transport characteristics. Redox-active molecules such as thiol-terminated derivatives of viologens show transistor- or diode-like behavior.[87]

#### 2.2.3.1 Molecular wires

Molecular wires are molecules that conduct electrical current. They are one of the fundamental building blocks for molecular electronic devices. As a rule of thumb, higher

conductivities originate from highly conjugated systems. The sole purpose of molecular wires is to electrically connect different parts of a molecular electrical circuit. They consist of a molecular unit connected to two continuum reservoirs of electrons, which are usually metallic electrodes.[88] In molecular conductance junctions, the connection between the molecule and the electrodes greatly affects the current-voltage characteristics.[89] A main problem with molecular wires is to obtain good electrical contact with the electrodes so that the electrons can move freely in and out of the wire. The connectors (linkers) should have covalent bonding to ensure reproducible transport and contact properties. The focus of current research in single molecule electronics is mainly concerned with thiol or amine functionalized molecules, which can be connected to gold or platinum nanoelectrodes. Recently, electrical properties of oligoenes as molecular wires have been measured by using a scanning tunneling microscope-based break-junction technique. The electrical conductance can be specified through the molecule by modulating to which particular site on the oligoene chain the electrode binds. The result is a device that functions as a potentiometer at the single molecule level.[90] Conjugated porphyrin oligomers constitute another example of molecular wires, which have extraordinary electro-optical and non-linear optical properties.[91] Conjugated oligophenylenetriazole wires were also synthesized and electrically characterized with varied chain lengths.[92] The influence of molecular length, temperature, and applied voltage on the transport properties of such wires is of particular importance.[93] The most promising families of molecular wires are conjugated hydrocarbons, carbon nanotubes, porphyrin oligomers and DNA.[94]

#### 2.2.3.2 Transistors

A transistor is a semiconductor device, which is used to amplify and switch electronic signals and power. Single molecule transistors differ from the ones known from bulk electronics. The gate electrode in a conventional transistor determines the conductance between the source and drain electrode by controlling the density of charge carriers between them, or in other words, a voltage on the insulated gate electrode can induce a conducting current between the source and drain electrodes. The gate electrode in a single molecule transistor controls the probability of a single electron to jump in and out of the molecule by modifying the energy of HOMO and LUMO orbitals of the molecule. As a result, a single molecule transistor has a binary character, i.e. it is either on or off,[95] which is different to the bulk counterparts, which have

quadratic response to gate voltage. When compared to molecular wires, the electronic levels of the transistor molecule must not be well integrated with the Fermi-levels of the electrodes. If the molecular energy levels and the Fermi-level of the electrodes are at the same level, then the electron cannot be located on the molecule or the electrodes and the molecule will function as a wire.

Molecular orbital gating by a single molecule transistor was recently observed. The transistor, which has a 1,4-benzenedithiol molecule attached to gold contacts, could behave just like a silicon transistor. The molecule's different energy states can be manipulated by varying the voltage applied to it through the source and drain electrodes, and by manipulating the energy states by a gate electrode, the current passing through the molecule can be controlled.[96]

#### 2.2.3.3 Rectifiers

An electrical device that converts alternating current (AC) to direct current (DC) is called as rectifier and this process is known as rectification. Rectifiers are generally made of solid state diodes, vacuum tube diodes, mercury arc valves, and other components. Almost all rectifiers are comprised of a number of diodes in a specific arrangement for efficiently converting AC to DC, which is not possible with only one diode.

When molecules are synthesized in such a way that they can accept electrons from one end and not the other, then these type of molecules are called molecular rectifiers. These molecular rectifiers are mimics of their bulk counterparts. These molecules must constitute an electron acceptor on one end and an electron donor on the other end. The electron current would be expected to pass only from the acceptor part of the molecule towards the donor part of the molecule.

The electron acceptor (electron-poor) subunit of the molecule is electron withdrawing. On the other side, the electron donor (electron-rich) subunit of the molecule has increased π-electron density and this subunit lowers the ionization potential. The result is that an electric current can be drawn through the molecule if the electrons are added via the cathode to the acceptor end of the molecule, but if the electrons are added through the donor end of the molecule, the electric current cannot be passed through the molecule. One classical example of a theoretical molecular rectifier contains tetracyanoquinodimethane (TCNQ) as an acceptor and

tetrathiofulvalene (TTF) as a donor part of the molecule.[97] Another example of diode molecule is 'dipyrimidinyl diphenyl', which behaves as a molecular rectifier at room temperature. The dipyrimidinyl block is electron-deficient, and the diphenyl group is electron rich, resulting in an energy diagram reminiscent of a classic pn junction.[98]

#### 2.2.3.4 Molecular switches

A molecular switch is a molecule that can be reversibly shifted between two or more stable states. Synthetic molecular switches are of interest in the field of nanotechnology for application in molecular computers. Photochromic molecular switches are able to switch between electronic configurations when irradiated by light of a specific wavelength.[99-101] Each state has a specific absorption maximum which can then be read out by UV-VIS spectroscopy. Members of this class include azobenzenes, diarylethenes, dithienylethenes, fulgides, stilbenes, spiropyrans and phenoxynaphthacene quinones. Single dithienylcyclopentene molecule which is also a photochromic molecular switch has been studied using mechanically controlled break junction technique to measure electronic transport. These molecules consist of conjugated units, connected by a switching element. By exposing the molecule to light of specific frequencies, the covalent bonds in the switching element rearrange, and the conjugation throughout the molecule can be turned on and off.[102] The donor/acceptor substituents in molecular switches also play an important role in the electronic transport of molecular devices.[103] Single porphyrin molecule, i.e. free base 'tetraphenyl-porphyrin', anchored to a silver surface has also shown to function as a molecular conductance switch.[104]

#### 2.2.3.5 Molecular logic gates

A molecular logic gate is a molecule that performs a logical operation on one or more logic inputs and produces a single logic output. These molecular machines are also called moleculators, because of their potential utility in simple arithmetic calculations. Molecular logic gates work with input signals based on chemical processes and with output signals based on spectroscopy.[105-108]

In a recent example, trinaphthylene molecule is shown to have logic gate functionality, which was characterized by scanning tunneling spectroscopy.[109]

### 2.2.3.6 Porphyrins in single molecule devices

The work described in this thesis is based on the electronic conductance measurements of porphyrins, therefore some discussion on use of porphyrins for single molecule electronics is described below.

In biology, porphyrins and metalloporphyrins act as catalysts, small molecule transporters, electrical conduits, and energy transducers in photosynthesis, which make porphyrins an obvious class of molecules to investigate for molecular electronic functions.[110] Porphyrins (figure 7) have a highly conjugated aromatic heterocyclic nature.[91, 111, 112] Ligands can be attached to the sides of a porphyrin by coordination to a range of different cations in the internal ring, and both cation incorporation and ligand coordination generally result in changes in electronic properties. Porphyrins are architecturally flexible so that they can be synthesized with various functional groups, including a range of groups that can act as molecular clips to attach with metal electrodes. They are stable at high temperatures, and have already been studied extensively in solution with very interesting physical and optoelectronic properties. Theoretical studies on conductance of porphyrin molecules have been studied as well. [113]

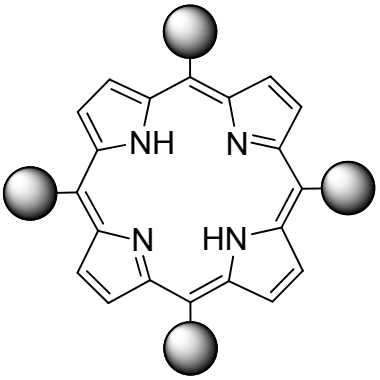


Fig. 7: A porphyrin molecule with linker groups at meso-carbons, represented as black dots.

Porphyrin-based short chain molecular wires as single molecules could be useful in nanoelectronic devices as electrical measurements of single-molecule junctions show that the conductance of the oligo-porphyrin wires show a very low attenuation factor, which is considerably lower than generally observed for π-conjugated organic bridges. These wires have a strong dependence on temperature, and a weak dependence on the length of the

wire.[111, 112] Chapter 3 is dedicated to discussions about the design and synthetic strategies of porphyrin molecules for molecular electronics, issues related to synthesis and finally characterization of synthesized porphyrin molecules.

### 2.2.4 Anchoring of molecules to inorganic surfaces

In general, the most commonly used method to connect molecules to electrodes is to make use of sulphur (e.g. the thiol functional group), which has a high affinity for gold surfaces.[114] Molecules are designed and synthesized in a way that sulfur atoms are strategically placed to function as anchors, connecting the molecules to the gold electrodes. Although this method is useful, anchoring is non-specific and connects the molecules randomly to any part of the gold surface. Contact resistance is highly dependent on the precise atomic geometry around the site of anchoring, resulting in issues of reproducibility of the thiol-Au connection. The conductive properties of the molecule are also dependent on the Au-S bond in Au-S-molecule-S-Au system, where thiol is the linker moiety, because Au-surface geometry can be different e.g. gold (100), (110) or (111).[115-119]

In order to obtain better reproducibility in conductivity measurements, experiments reveal that fullerenes (figure 8) could be potential candidates for use as an alternative to sulfur. The large conjugated π-system[120] can electrically contact many more atoms at once when attached to a gold surface as compared to a single atom of sulfur.[121, 122] Amines have also shown interaction with gold surfaces, but to a weaker extent, when compared with the thiol-gold bond.[39, 122-125] Other functional groups of interests are carboxylic acid functional groups[126], diphenylphosphine[127], carbodithiolate[128], isothiocyanate[129], dimethylphosphine,[130] pyridine,[131] methyl sulphides,[132] isocyanide[133] and isonitrile functional groups,[134, 135]

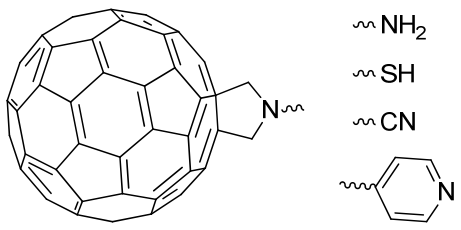


Fig. 8: A few examples of molecular linkers.

Side groups effects on the electronic transport in molecular devices have also been studied theoretically.[136]

Single molecule electronics is an emerging field, but entire electronic circuits exclusively made of molecules are still very far from being realized. At this moment, the focus is on finding interesting molecules with required properties and finding ways to obtain reliable and reproducible contacts between the molecular components and nanoscale electrodes.

## 2.3 Nanoparticles in Molecular Electronics

### 2.3.1 Introduction

The bottom-up approach in the field of molecular electronics also requires inorganic metallic interfaces, and the nanoscopic arrangement of nanoparticles and their charge transport properties could be of significant importance. Metallic and semiconductor nanoparticles reveal quantized optical and electronic properties that can be used in the design of nanoelectronic devices. Exploring the potential of nanoparticles in the field of nano- and molecular electronics has been of great interest in recent years. In certain cases, it requires careful and precise organization of nanoparticles into specifically designed structural arrangements.[137]

### 2.3.2 Metallic nanoparticles

Gold nanoparticles (Au-NPs) are used in combination with organic molecules, polymers[138, 139] and biological molecules[140] for various functionalities,[141] where such molecules act as ligands or stabilizing agents for nanoparticles. Au-NPs can act as model gold surfaces in solution for molecules, which are supposed to be used for molecular electronic studies. Using the conductive properties of gold nanoparticles and specifically designed organic molecules, conjugates with new functionalities and properties could be obtained.

Gold nanoparticles have been used in combination with various classes of molecules for molecular electronic studies, e.g. single dithiolated molecules, [142] functionalized reduced graphene oxide for nonvolatile memory devices,[143] and photoconductance properties e.g. oligo(phenylene vinylene) molecules.[144] Growth of functional molecular wires using

mercaptoaniline on gold nanoparticles,[145] and use of single nanoparticle as a bridge for molecular electronic studies [146] are another applications of gold nanoparticles for molecular electronics.

Networks of gold nanoparticles (Au-NPs) linked by organic molecules have attracted considerable interest because of their potential applications in nanoscale molecular electronics. Two-dimensional nanoparticle arrays also represent a suitable platform to build a large number of molecular junctions for molecular electronics, as they are stable at room temperature in air, enabling the formation of robust molecular junctions, and can resist common organic solvents.[147] Due to the inherently small size of nanoparticles, ultra dense logic and memory, nano- and molecular devices could be realized. Assembly of molecules or NPs in pre-patterned electrodes can provide electronic transport information in the electrode gap.[148] The charge transport properties of such gold nanoparticle networks linked by organic molecules could possibly be used in nano-scale electronics, where millions of Au-NPs contribute to the transport. The important parameters to describe the charge transport behaviors of bulk networks are the charging energy of the Au-NP and the tunneling resistance of the linker molecule.[149]

#### 2.3.2.1 Metal nanorods as nanoelectrodes

Gold nanorods can be possibly used in molecular electronic studies as nanoelectrodes. There are various methods in the literature to prepare gold nanorods of various sizes and aspect ratios. [150-157]

Au nanorods have been known to align and make end-to-end contact with each other. e.g. dimers of Au-NRs were formed via aromatic and aliphatic dithiols[158, 159] and long chains of aligned gold nanorods were formed using lysine and aspartic acid [160], cysteine and 3-mercaptopropionic acid[161, 162], biotin-streptavidin[163-165], and alanine, valine, and glycine ligands [162]. Additional methods to align gold nanorods include use of antibodies using biomolecular recognition system[166], oligonucleotide hybridization[167] and growth of nanoparticles to nanorods aligned via dithiol-functionalized polyethylene glycol[168], citrate anions[169], amphiphilic triblock copolymers [170], and cysteine and glutathione[171].

The idea that aligned gold nanorods with molecular spacing between them can act as two well defined electrodes was a concept generated in our group in collaboration with the molecular electronics group in Delft (figure 9). However, while work was in progress, a similar concept was published elsewhere.[168, 172, 173].

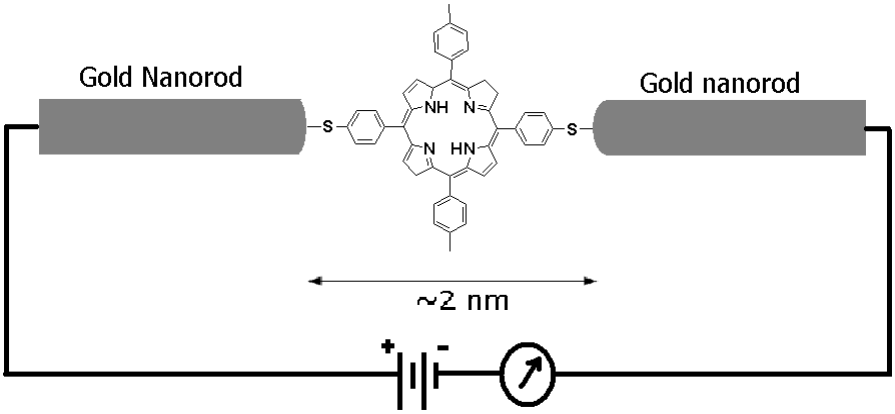


Fig. 9: Cartoon diagram of a single porphyrin molecule placed in between two gold nanorods. The relative size of molecule and rods is not according to scale.

In the diagram above, a single porphyrin molecule is placed between two nanorods with spacing of ~2 nm, which is roughly the size of one porphyrin molecule. The rods could be connected to micro electrodes.

### 2.3.3 Semiconductor Nanoparticles (Quantum dots)

In the field of molecular electronics, it is important to know the energy and charge transfer characteristics of molecules, in order to better understand their behavior in real molecular electronic devices. Although metallic nanoparticles have been used for charge or energy transfer studies,[174] semiconductor nanoparticles or quantum dots are generally used for such studies, because of their high photostability and size-tunable optical properties. Quantum dots are also interesting because in some cases multi-exciton generation is reported, which could have profound implications for the construction of efficient solar cells.[175-179] Energy transfer of quantum dots can be used for the detection of organic molecules, [180] whereas charge transfer between molecules and quantum dots have been exploited in solar cells and light emitting diodes.[181].

#### 2.3.3.1 Charge / Energy transfer studies between molecules and QDs

Charge or energy transfer studies between molecules and quantum dots as donor and acceptor are interesting model systems which provide insight details at a molecular level, which is important for molecular electronics. Charge and energy transfer are of central importance to the design of organic-inorganic blend photovoltaic devices and LEDs. Various studies have been performed in order to understand electron and/or energy transfer processes via different mechanisms in quantum dots.[176, 182] Different charge transfer mechanisms occur due to interfacial chemistry effects, changes in surface ligands of quantum dots, chemical changes on the quantum dot surface or polymer and quantum dot interactions.[183]

## 2.4 Conclusions

In this chapter we have shown how molecules are applied in the construction of electronic devices. In these devices, molecules can be applied in bulk or as single molecules. Single molecule electronic devices are among the smallest theoretically possible electronic structural elements and might as such be applied in future computers, in line with the continuing demand for smaller and denser integrated circuits. The electronic behavior of single molecule devices can be hugely different from those constructed using bulk material. In single molecule devices, quantum effects have to be taken into account, and the molecular configuration and attachment to the inorganic electrodes can have a large impact on for instance the conductance through a single molecule.

Since, we are interested to study porphyrins as single molecule, therefore initial part of this thesis will be devoted to porphyrin synthesis, and to study their attachment to inorganic nanoparticles, to act as model systems for the nanoelectrodes in single molecule devices. Final part of this thesis will be focused towards single molecule electronic behavior of porphyrins, which are a widely applied class of aromatic molecules with significant potential for both bulk and single molecule electronics.

## 2.5 References


1. Blum, A.S., et al., *Molecular electronics based nanosensors on a viral scaffold.* Biosensors and Bioelectronics, 2011. **26**(6): p. 2852-2857.
2. Usta, H., A. Facchetti, and T.J. Marks, *n-Channel Semiconductor Materials Design for Organic Complementary Circuits.* Accounts of Chemical Research, 2011. **44**(7): p. 501-510.
3. Wu, Q., et al., *Dicyanomethylene-Substituted Fused Tetrathienoquinoid for High-Performance, Ambient-Stable, Solution-Processable n-Channel Organic Thin-Film Transistors.* Chemistry of Materials, 2011. **23**(13): p. 3138-3140.
4. Service, R.F., *Can chemists assemble a future for molecular electronics?* Science, 2002. **295**(5564): p. 2398-2399.
5. Service, R.F., *Molecular electronics - Nanodevices make fresh strides toward reality.* Science, 2003. **302**(5649): p. 1310-1310.
6. Service, R.F., *Molecular electronics - Next-generation technology hits an early midlife crisis.* Science, 2003. **302**(5645): p. 556-+.
7. Akkerman, H.B., et al., *Electron tunneling through alkanedithiol self-assembled monolayers in large-area molecular junctions.* Proceedings of the National Academy of Sciences, 2007. **104**(27): p. 11161-11166.
8. Gergel-Hackett, N., *Vapor phase deposition of oligo(phenylene ethynylene) molecules for use in molecular electronic devices.* J. Vac. Sci. Technol. B, 2007. **25**(1): p. 252.
9. Kamenetska, M., et al., *Conductance and Geometry of Pyridine-Linked Single-Molecule Junctions.* Journal of the American Chemical Society. **132**(19): p. 6817-6821.
10. Beaujuge, P.M. and J.M.J. Fréchet, *Molecular Design and Ordering Effects in π-Functional Materials for Transistor and Solar Cell Applications.* Journal of the American Chemical Society, 2011. **133**(50): p. 20009-20029.
11. Zakhidov, A.A., et al., *Orthogonal processing: A new strategy for organic electronics.* Chemical Science, 2011. **2**(6): p. 1178-1182.
12. Facchetti, A., *π-Conjugated Polymers for Organic Electronics and Photovoltaic Cell Applications†.* Chemistry of Materials, 2010. **23**(3): p. 733-758.
13. Sonar, P., et al., *High mobility organic thin film transistor and efficient photovoltaic devices using versatile donor-acceptor polymer semiconductor by molecular design.* Energy & Environmental Science, 2011. **4**(6): p. 2288-2296.
14. Beaujuge, P.M. and J.M.J. Frechet, *Molecular Design and Ordering Effects in pi-Functional Materials for Transistor and Solar Cell Applications.* Journal of the American Chemical Society, 2011.
15. Woo, S., et al., *Full-Color LCD Microdisplay System Based on OLED Backlight Unit and Field-Sequential Color Driving Method.* International Journal of Photoenergy, 2011. **2011**.
16. Fenwick, O., et al., *Linear and Cyclic Porphyrin Hexamers as Near-Infrared Emitters in Organic Light-Emitting Diodes.* Nano Letters, 2011. **11**(6): p. 2451-2456.
17. Zhu, X.-H., et al., *Solution-processable single-material molecular emitters for organic light-emitting devices.* Chemical Society Reviews, 2011. **40**(7): p. 3509-3524.
18. Zhu, M., et al., *Efficient Solution-Processed Nondoped Deep-Blue Organic Light-Emitting Diodes Based on Fluorene-Bridged Anthracene Derivatives Appended with Charge Transport Moieties.* The Journal of Physical Chemistry C, 2011. **115**(36): p. 17965-17972.
19. Chen, S., et al., *White Organic Light-Emitting Diodes with Evenly Separated Red, Green, and Blue Colors for Efficiency/Color-Rendition Trade-Off Optimization.* Advanced Functional Materials, 2011. **21**(19): p. 3785-3793.

20. Chen, W., et al., *Organic–Organic Heterojunction Interfaces: Effect of Molecular Orientation.* Advanced Functional Materials, 2011. **21**(3): p. 410-424.
21. De Salvo, B., J. Buckley, and D. Vuillaume, *Recent results on organic-based molecular memories.* Current Applied Physics, 2011. **11**(2, Supplement): p. e49-e57.
22. Kim, D.-H., et al., *Epidermal Electronics.* Science, 2011. **333**(6044): p. 838-843.
23. Aviram, A., C. Joachim, and M. Pomerantz, *Evidence of Switching and Rectification by a Single Molecule Effected with a Scanning Tunneling Microscope.* Chemical Physics Letters, 1988. **146**(6): p. 490-495.
24. Joachim, C., et al., *Electronic Transparency of a Single C-60 Molecule.* Physical Review Letters, 1995. **74**(11): p. 2102-2105.
25. Joachim, C. and J.K. Gimzewski, *Analysis of Low-Voltage I(V) Characteristics of a Single C(60) Molecule.* Europhysics Letters, 1995. **30**(7): p. 409-414.
26. Bumm, L.A., et al., *Are single molecular wires conducting?* Science, 1996. **271**(5256): p. 1705-1707.
27. Tour, J.M., et al., *Self-Assembled Monolayers and Multilayers of Conjugated Thiols, Alpha,Omega-Dithiols, and Thioacetyl-Containing Adsorbates - Understanding Attachments between Potential Molecular Wires and Gold Surfaces.* Journal of the American Chemical Society, 1995. **117**(37): p. 9529-9534.
28. Reed, M.A., et al., *Conductance of a molecular junction.* Science, 1997. **278**(5336): p. 252-254.
29. Grill, L., et al., *Nano-architectures by covalent assembly of molecular building blocks.* Nat Nano, 2007. **2**(11): p. 687-691.
30. Ramachandran, G.K., et al., *Electron transport properties of a carotene molecule in a metal-(single molecule)-metal junction.* Journal of Physical Chemistry B, 2003. **107**: p. 6162-6169.
31. Beckman, R., et al., *Spiers Memorial Lecture - Molecular mechanics and molecular electronics.* Faraday Discussions, 2006. **131**: p. 9-22.
32. Miljanic, O.S., et al., *Structural and co-conformational effects of alkyne-derived subunits in charged donor-acceptor [2]catenanes.* Journal of the American Chemical Society, 2007. **129**(26): p. 8236-8246.
33. Kim, H., et al., *Free Energy Barrier for Molecular Motions in Bistable [2]Rotaxane Molecular Electronic Devices.* Journal of Physical Chemistry A, 2009. **113**(10): p. 2136-2143.
34. Avouris, P., Z.H. Chen, and V. Perebeinos, *Carbon-based electronics.* Nature Nanotechnology, 2007. **2**(10): p. 605-615.
35. Xiao, Xu, and N.J. Tao, *Measurement of Single Molecule Conductance: Benzenedithiol and Benzenedimethanethiol.* Nano Letters, 2004. **4**(2): p. 267-271.
36. Xing, Y., et al., *Optimizing Single-Molecule Conductivity of Conjugated Organic Oligomers with Carbodithioate Linkers.* Journal of the American Chemical Society, 2010. **132**(23): p. 7946-7956.
37. Martin, C.A., et al., *Lithographic mechanical break junctions for single-molecule measurements in vacuum: possibilities and limitations.* New Journal of Physics, 2008. **10**.
38. Dadosh, T., et al., *Measurement of the conductance of single conjugated molecules.* Nature, 2005. **436**(7051): p. 677-680.
39. Hybertsen, M.S. and et al., *Amine-linked single-molecule circuits: systematic trends across molecular families.* Journal of Physics: Condensed Matter, 2008. **20**(37): p. 374115.
40. Diez-Perez, I., et al., *Controlling single-molecule conductance through lateral coupling of [pi] orbitals.* Nat Nano, 2011. **6**(4): p. 226-231.

41. Tao, N.J., *Electron transport in molecular junctions.* Nat Nano, 2006. **1**(3): p. 173-181.
42. Dell'Angela, M., et al., *Relating Energy Level Alignment and Amine-Linked Single Molecule Junction Conductance.* Nano Letters, 2010. **10**(7): p. 2470-2474.
43. Venkataraman, L., et al., *Electronics and Chemistry: Varying Single-Molecule Junction Conductance Using Chemical Substituents.* Nano Letters, 2007. **7**(2): p. 502-506.
44. Moth-Poulsen, K. and T. Bjørnholm, *Molecular electronics with single molecules in solid-state devices.* Nature Nanotechnology, 2009. **4**: p. 551-556.
45. Chen, F., et al., *Measurement of single-molecule conductance.* Annual Review of Physical Chemistry, 2007. **58**: p. 535-564.
46. Pontes, R.B., et al., *Adsorption of Benzene-1,4-dithiol on the Au(111) Surface and Its Possible Role in Molecular Conductance.* Journal of the American Chemical Society, 2006. **128**(28): p. 8996-8997.
47. Chen, F., et al., *Measurement of Single-Molecule Conductance.* Annual Review of Physical Chemistry, 2007. **58**(1): p. 535-564.
48. Cui, X.D., et al., *Reproducible measurement of single-molecule conductivity.* Science, 2001. **294**(5542): p. 571-574.
49. Kumar, A., et al., *Controlled transport through a single molecule.* Journal of Physics: Condensed Matter, 2012. **24**(8): p. 082201.
50. Andres, R.P., et al., *"Coulomb staircase" at room temperature in a self-assembled molecular nanostructure.* Science, 1996. **272**(5266): p. 1323-1325.
51. Tilke, A.T., et al., *Coulomb blockade in silicon nanostructures.* Progress in Quantum Electronics, 2001. **25**(3): p. 97-138.
52. Song, H., M.A. Reed, and T. Lee, *Single Molecule Electronic Devices.* Advanced Materials, 2011. **23**(14): p. 1583-1608.
53. Zalinge, H.v., et al., *Nanoscale electrode gaps to study single molecule conduction.* Microelectron. Eng., 2011. **88**(8): p. 2707-2709.
54. Taniguchi, M. and et al., *Inelastic electron tunneling spectroscopy of single-molecule junctions using a mechanically controllable break junction.* Nanotechnology, 2009. **20**(43): p. 434008.
55. Langlais, V.J., et al., *Spatially resolved tunneling along a molecular wire.* Physical Review Letters, 1999. **83**(14): p. 2809-2812.
56. Samanta, M.P., et al., *Electronic conduction through organic molecules.* Physical Review B, 1996. **53**(12): p. R7626-R7629.
57. Tao, N.J., *Probing potential-tuned resonant tunneling through redox molecules with scanning tunneling microscopy.* Physical Review Letters, 1996. **76**(21): p. 4066-4069.
58. Nazin, G.V., X.H. Qiu, and W. Ho, *Visualization and spectroscopy of a metal-molecule-metal bridge.* Science, 2003. **302**(5642): p. 77-81.
59. Repp, J., et al., *Imaging bond formation between a gold atom and pentacene on an insulating surface.* Science, 2006. **312**(5777): p. 1196-1199.
60. Liang, W.J., et al., *Kondo resonance in a single-molecule transistor.* Nature, 2002. **417**(6890): p. 725-729.
61. Park, J., et al., *Coulomb blockade and the Kondo effect in single-atom transistors.* Nature, 2002. **417**(6890): p. 722-725.
62. Kervennic, Y.V., et al., *Charge transport in three-terminal molecular junctions incorporating sulfur-end-functionalized tercyclohexylidene spacers.* Angewandte Chemie-International Edition, 2006. **45**(16): p. 2540-2542.
63. Li, C.Z., et al., *Fabrication of stable metallic nanowires with quantized conductance.* Nanotechnology, 1999. **10**(2): p. 221-223.

64. Li, X.L., et al., *Measurement of electron transport properties of molecular junctions fabricated by electrochemical and mechanical methods.* Surface Science, 2004. **573**(1): p. 1-10.
65. Morpurgo, A.F., C.M. Marcus, and D.B. Robinson, *Controlled fabrication of metallic electrodes with atomic separation.* Applied Physics Letters, 1999. **74**(14): p. 2084-2086.
66. Ghosh, S., et al., *Device structure for electronic transport through individual molecules using nanoelectrodes.* Applied Physics Letters, 2005. **87**(23).
67. Kubatkin, S., et al., *Single-electron transistor of a single organic molecule with access to several redox states.* Nature, 2003. **425**(6959): p. 698-701.
68. Lee, J.O., et al., *Absence of strong gate effects in electrical measurements on phenylene-based conjugated molecules.* Nano Letters, 2003. **3**(2): p. 113-117.
69. Luber, S.M., et al., *Nanometre spaced electrodes on a cleaved AlGaAs surface.* Nanotechnology, 2005. **16**(8): p. 1182-1185.
70. Zhitenev, N.B., H. Meng, and Z. Bao, *Conductance of small molecular junctions.* Physical Review Letters, 2002. **88**(22).
71. Kervennic, Y.V., et al., *Planar nanocontacts with atomically controlled separation.* Applied Physics Letters, 2003. **83**(18): p. 3782-3784.
72. Zhou, J., F. Chen, and B. Xu, *Fabrication and Electronic Characterization of Single Molecular Junction Devices: A Comprehensive Approach.* Journal of the American Chemical Society, 2009. **131**(30): p. 10439-10446.
73. Choi, H. and C.C.M. Mody, *The Long History of Molecular Electronics: Microelectronics Origins of Nanotechnology.* Social Studies of Science, 2009. **39**(1): p. 11-50.
74. Weiss, E.A., et al., *The study of charge transport through organic thin films: mechanism, tools and applications.* Philosophical Transactions of the Royal Society a-Mathematical Physical and Engineering Sciences, 2007. **365**(1855): p. 1509-1537.
75. Moth-Poulsen, K., Bj, and T. rnholm, *From Nanofabrication to Self-fabrication Tailored Chemistry for Control of Single Molecule Electronic Devices.* CHIMIA International Journal for Chemistry, 2010. **64**(6): p. 404-408.
76. Park, Y.S., et al., *Frustrated Rotations in Single-Molecule Junctions.* Journal of the American Chemical Society, 2009. **131**(31): p. 10820-10821.
77. Wu, S., et al., *Molecular junctions based on aromatic coupling.* Nat Nano, 2008. **3**(9): p. 569-574.
78. Browne, W.R. and B.L. Feringa, *Light and Redox Switchable Molecular Components for Molecular Electronics.* CHIMIA International Journal for Chemistry, 2010. **64**(6): p. 398-403.
79. Bergren, A.J. and R.L. McCreery, *Analytical Chemistry in Molecular Electronics.* Annual Review of Analytical Chemistry, 2011. **4**(1): p. 173-195.
80. Kim, B., et al., *Molecular Tunnel Junctions Based on π-Conjugated Oligoacene Thiols and Dithiols between Ag, Au, and Pt Contacts: Effect of Surface Linking Group and Metal Work Function.* Journal of the American Chemical Society, 2011.
81. Tan, A., et al., *Effect of Length and Contact Chemistry on the Electronic Structure and Thermoelectric Properties of Molecular Junctions.* Journal of the American Chemical Society, 2011. **133**(23): p. 8838-8841.
82. Mishchenko, A., et al., *Influence of Conformation on Conductance of Biphenyl-Dithiol Single-Molecule Contacts.* Nano Letters, 2009. **10**(1): p. 156-163.
83. Bürkle, M., et al., *Conduction mechanisms in biphenyl dithiol single-molecule junctions.* Physical Review B, 2012. **85**(7): p. 075417.

84. Vonlanthen, D., et al., *Synthesis of Rotationally Restricted and Modular Biphenyl Building Blocks.* European Journal of Organic Chemistry, 2010. **2010**(1): p. 120-133.
85. Mishchenko, A., et al., *Single-Molecule Junctions Based on Nitrile-Terminated Biphenyls: A Promising New Anchoring Group.* Journal of the American Chemical Society, 2010. **133**(2): p. 184-187.
86. Vonlanthen, D., et al., *Chemically Controlled Conductivity: Torsion-Angle Dependence in a Single-Molecule Biphenyldithiol Junction.* Angewandte Chemie International Edition, 2009. **48**(47): p. 8886-8890.
87. Li, C., et al., *Charge Transport with Single Molecules An Electrochemical Approach.* CHIMIA International Journal for Chemistry, 2010. **64**(6): p. 383-390.
88. Emberly, E. and G. Kirczenow, *Electrical conductance of molecular wires.* Nanotechnology, 1999. **10**(3): p. 285-289.
89. Nitzan, A. and M.A. Ratner, *Electron transport in molecular wire junctions.* Science, 2003. **300**(5624): p. 1384-1389.
90. Meisner, J.S., et al., *A Single-Molecule Potentiometer.* Nano Letters, 2011. **11**(4): p. 1575-1579.
91. Anderson, H.L., *Building molecular wires from the colours of life: conjugated porphyrin oligomers.* Chemical Communications, 1999(23): p. 2323-2330.
92. Luo, L. and C.D. Frisbie, *Length-Dependent Conductance of Conjugated Molecular Wires Synthesized by Stepwise "Click" Chemistry.* Journal of the American Chemical Society, 2010. **132**(26): p. 8854-8855.
93. Luo, L., S.H. Choi, and C.D. Frisbie, *Probing Hopping Conduction in Conjugated Molecular Wires Connected to Metal Electrodes†.* Chemistry of Materials, 2010. **23**(3): p. 631-645.
94. Robertson, N. and C.A. McGowan, *A comparison of potential molecular wires as components for molecular electronics.* Chemical Society Reviews, 2003. **32**(2): p. 96-103.
95. Andréasson, J., et al., *All-Photonic Multifunctional Molecular Logic Device.* Journal of the American Chemical Society, 2011. **133**(30): p. 11641-11648.
96. Song, H., et al., *Observation of molecular orbital gating.* Nature, 2009. **462**(7276): p. 1039-1043.
97. Aviram, A. and M.A. Ratner, *Molecular rectifiers.* Chemical Physics Letters, 1974. **29**(2): p. 277-283.
98. Hihath, J., et al., *Inelastic Transport and Low-Bias Rectification in a Single-Molecule Diode.* Acs Nano, 2011. **5**(10): p. 8331-8339.
99. Koumura, N., et al., *Light-driven monodirectional molecular rotor.* Nature, 1999. **401**(6749): p. 152-155.
100. Browne, W.R. and B.L. Feringa, *Making molecular machines work.* Nat Nano, 2006. **1**(1): p. 25-35.
101. Staykov, A., et al., *Electrochemical and Photochemical Cyclization and Cycloreversion of Diarylethenes and Diarylethene-Capped Sexithiophene Wires.* Acs Nano, 2011. **5**(2): p. 1165-1178.
102. Dulić, D., et al., *One-Way Optoelectronic Switching of Photochromic Molecules on Gold.* Physical Review Letters, 2003. **91**(20): p. 207402.
103. Xia, C.J.L., Han Chen; Wang, Jing, *Electronic Transport Properties of the Azobenzene-Based Optical Molecular Switch with Different Substituents.* Advanced Materials Research, 2011. **284-286**: p. 816-819.
104. Auwarter, W., et al., *A surface-anchored molecular four-level conductance switch based on single proton transfer.* Nat Nano, 2012. **7**(1): p. 41-46.

105. Kompa, K.L. and R.D. Levine, *A molecular logic gate.* Proceedings of the National Academy of Sciences, 2001. **98**(2): p. 410-414.
106. Maeda, K., et al., *Logic Operations of Chemically Assembled Single-Electron Transistor.* Acs Nano, 2012. **6**(3): p. 2798-2803.
107. Joachim, C., N. Renaud, and M. Hliwa, *The Different Designs of Molecule Logic Gates.* Advanced Materials, 2012. **24**(2): p. 312-317.
108. Prauzner-Bechcicki, J.S., S. Godlewski, and M. Szymonski, *Atomic- and molecular-scale devices and systems for single-molecule electronics.* physica status solidi (a), 2012. **209**(4): p. 603-613.
109. Soe, W.-H., et al., *Manipulating Molecular Quantum States with Classical Metal Atom Inputs: Demonstration of a Single Molecule NOR Logic Gate.* Acs Nano, 2011. **5**(2): p. 1436-1440.
110. Jurow, M., et al., *Porphyrins as molecular electronic components of functional devices.* Coordination Chemistry Reviews, 2010. **254**(19-20): p. 2297-2310.
111. Sedghi, G., et al., *Single molecule conductance of porphyrin wires with ultralow attenuation.* Journal of the American Chemical Society, 2008. **130**(27): p. 8582-+.
112. Sedghi, G., et al., *Long-range electron tunnelling in oligo-porphyrin molecular wires.* Nat Nano, 2011. **6**(8): p. 517-523.
113. Welack, S., et al., *Single-Electron Counting Spectroscopy: Simulation Study of Porphyrin in a Molecular Junction.* Nano Letters, 2008. **8**(4): p. 1137-1141.
114. Lu, J.-Q., et al., *Electronic transport mechanism of a molecular electronic device: structural effects and terminal atoms.* Physics Letters A, 2004. **323**(1-2): p. 154-158.
115. Guan, L., et al., *Relaxation and electronic states of Au(100), (110) and (111) surfaces.* Solid State Communications, 2009. **149**(37-38): p. 1561-1564.
116. Bilic, A., J.R. Reimers, and N.S. Hush, *Adsorption of pyridine on the gold(111) surface: Implications for "alligator clips" for molecular wires.* Journal of Physical Chemistry B, 2002. **106**(26): p. 6740-6747.
117. Carbó-Argibay, E., et al., *The Crystalline Structure of Gold Nanorods Revisited: Evidence for Higher-Index Lateral Facets.* Angewandte Chemie International Edition, 2010. **49**(49): p. 9397-9400.
118. Carbo-Argibay, E., et al., *Growth of pentatwinned gold nanorods into truncated decahedra.* Nanoscale, 2010. **2**(11): p. 2377-2383.
119. Tran, E., et al., *Experimental Approaches for Controlling Current Flowing through Metal–Molecule–Metal Junctions.* Advanced Materials, 2006. **18**(10): p. 1323-1328.
120. Quek, S.Y., et al., *Length Dependence of Conductance in Aromatic Single-Molecule Junctions.* Nano Letters, 2009. **9**(11): p. 3949-3953.
121. Cuniberti, G., et al., *Fullerene based devices for molecular electronics.* Physica E-Low-Dimensional Systems & Nanostructures, 2002. **12**(1-4): p. 749-752.
122. Martin, C.A., et al., *Fullerene-based anchoring groups for molecular electronics.* Journal of the American Chemical Society, 2008. **130**(40): p. 13198-13199.
123. Venkataraman, L., et al., *Single-molecule circuits with well-defined molecular conductance.* Nano Letters, 2006. **6**(3): p. 458-462.
124. Miller, D.J., et al., *Static SIMS studies of fatty alcohols, amines and esters on gold and aluminium–magnesium alloy surfaces.* Surface and Interface Analysis, 2005. **37**(5): p. 499-508.
125. Quek, S.Y., et al., *Amine-gold linked single-molecule circuits: Experiment and theory.* Nano Letters, 2007. **7**(11): p. 3477-3482.
126. Miller, D.J., et al., *Static SIMS studies of carboxylic acids on gold and aluminium-magnesium alloy surfaces.* Surface and Interface Analysis, 2003. **35**(5): p. 463-476.

127. Parameswaran, R., et al., *Reliable Formation of Single Molecule Junctions with Air-Stable Diphenylphosphine Linkers.* Journal of Physical Chemistry Letters, 2010. **1**(14): p. 2114-2119.
128. Xing, Y.J., et al., *Optimizing Single-Molecule Conductivity of Conjugated Organic Oligomers with Carbodithioate Linkers.* Journal of the American Chemical Society, 2010. **132**(23): p. 7946-7956.
129. Ko, C.-H., et al., *Superior Contact for Single-Molecule Conductance: Electronic Coupling of Thiolate and Isothiocyanate on Pt, Pd, and Au.* Journal of the American Chemical Society, 2009. **132**(2): p. 756-764.
130. Kamenetska, M., et al., *Formation and Evolution of Single-Molecule Junctions.* Physical Review Letters, 2009. **102**(12): p. 126803.
131. Quek, S.Y., et al., *Mechanically controlled binary conductance switching of a single-molecule junction.* Nat Nano, 2009. **4**(4): p. 230-234.
132. Park, Y.S., et al., *Contact Chemistry and Single-Molecule Conductance: A Comparison of Phosphines, Methyl Sulfides, and Amines.* Journal of the American Chemical Society, 2007. **129**(51): p. 15768-15769.
133. Angelici, R.J. and M. Lazar, *Isocyanide Ligands Adsorbed on Metal Surfaces: Applications in Catalysis, Nanochemistry, and Molecular Electronics†.* Inorganic Chemistry, 2008. **47**(20): p. 9155-9165.
134. Kanters, R.P.F., et al., *Isonitrile-Containing Platinum-Gold Phosphine Clusters.* Journal of Organometallic Chemistry, 1990. **388**(1-2): p. 233-242.
135. Hipps, K.W., *Molecular electronics - It's all about contacts.* Science, 2001. **294**(5542): p. 536-537.
136. Fan, Z.-Q. and K.-Q. Chen, *First-principles study of side groups effects on the electronic transport in conjugated molecular device.* Physica E: Low-dimensional Systems and Nanostructures, 2010. **42**(5): p. 1492-1496.
137. Zheng, J., et al., *Two-Dimensional Nanoparticle Arrays Show the Organizational Power of Robust DNA Motifs.* Nano Letters, 2006. **6**(7): p. 1502-1504.
138. Baker, C.O., et al., *Size Control of Gold Nanoparticles Grown on Polyaniline Nanofibers for Bistable Memory Devices.* Acs Nano, 2011. **5**(5): p. 3469-3474.
139. Tang, J., et al., *PHEMA functionalization of gold nanoparticles for vapor sensing: Chemi-resistance, chemi-capacitance and chemi-impedance.* Sensors and Actuators B: Chemical, 2011(0).
140. Huschka, R., et al., *Light-Induced Release of DNA from Gold Nanoparticles: Nanoshells and Nanorods.* Journal of the American Chemical Society, 2011. **133**(31): p. 12247-12255.
141. Pissuwan, D., T. Niidome, and M.B. Cortie, *The forthcoming applications of gold nanoparticles in drug and gene delivery systems.* Journal of Controlled Release, 2011. **149**(1): p. 65-71.
142. Morita, T. and S. Lindsay, *Determination of Single Molecule Conductances of Alkanedithiols by Conducting-Atomic Force Microscopy with Large Gold Nanoparticles.* Journal of the American Chemical Society, 2007. **129**(23): p. 7262-7263.
143. Cui, P., et al., *Nonvolatile Memory Device Using Gold Nanoparticles Covalently Bound to Reduced Graphene Oxide.* Acs Nano, 2011. **5**(9): p. 6826-6833.
144. Mangold, M.A., et al., *Resonant Photoconductance of Molecular Junctions Formed in Gold Nanoparticle Arrays.* Journal of the American Chemical Society, 2011. **133**(31): p. 12185-12191.

145. Ashwell, G.J., B. Urasinska-Wojcik, and L.J. Phillips, *In Situ Stepwise Synthesis of Functional Multijunction Molecular Wires on Gold Electrodes and Gold Nanoparticles.* Angewandte Chemie International Edition, 2010. **49**(20): p. 3508-3512.
146. Jafri, S.H.M., et al., *Assessment of a nanoparticle bridge platform for molecular electronics measurements.* Nanotechnology, 2010. **21**(43): p. 435204.
147. Jianhui, L., et al., *Interlinking Au nanoparticles in 2D arrays via conjugated dithiolated molecules.* New Journal of Physics, 2008. **10**(6): p. 065019.
148. Cheon, D., S. Kumar, and G.-H. Kim, *Assembly of gold nanoparticles of different diameters between nanogap electrodes.* Applied Physics Letters, 2010. **96**(1): p. 013101-3.
149. Noguchi, Y., et al., *Charge transport in various dimensions of small networks composed of gold nanoparticles and terthiophene wire-molecules.* Applied Physics Letters, 2011. **98**(26): p. 263114-3.
150. Park, W.M., Y.S. Huh, and W.H. Hong, *Aspect-ratio-controlled synthesis of high-aspect-ratio gold nanorods in high-yield.* Current Applied Physics, 2009. **9**(2): p. E140-E143.
151. Wu, H.Y., W.L. Huang, and M.H. Huang, *Direct high-yield synthesis of high aspect ratio gold nanorods.* Crystal Growth & Design, 2007. **7**(4): p. 831-835.
152. Nikoobakht, B. and M.A. El-Sayed, *Preparation and growth mechanism of gold nanorods (NRs) using seed-mediated growth method.* Chemistry of Materials, 2003. **15**(10): p. 1957-1962.
153. Gole, A. and C.J. Murphy, *Seed-mediated synthesis of gold nanorods: Role of the size and nature of the seed.* Chemistry of Materials, 2004. **16**(19): p. 3633-3640.
154. Wu, H.Y., et al., *Seed-mediated synthesis of high aspect ratio gold nanorods with nitric acid.* Chemistry of Materials, 2005. **17**(25): p. 6447-6451.
155. Busbee, B.D., S.O. Obare, and C.J. Murphy, *An Improved Synthesis of High-Aspect-Ratio Gold Nanorods.* Advanced Materials, 2003. **15**(5): p. 414-416.
156. Perez-Juste, J., et al., *Gold nanorods: Synthesis, characterization and applications.* Coordination Chemistry Reviews, 2005. **249**(17-18): p. 1870-1901.
157. Guo, H., et al., *Correlating the Shape, Surface Plasmon Resonance, and Surface-Enhanced Raman Scattering of Gold Nanorods.* The Journal of Physical Chemistry C, 2009. **113**(24): p. 10459-10464.
158. Pramod, P. and K.G. Thomas, *Plasmon Coupling in Dimers of Au Nanorods.* Advanced Materials, 2008. **20**(22): p. 4300-4305.
159. Joseph, S.T.S., et al., *Gold nanorods to nanochains: Mechanistic investigations on their longitudinal assembly using alpha,omega-alkanedithiols and interplasmon coupling.* Journal of Physical Chemistry B, 2006. **110**(1): p. 150-157.
160. Joshi, H., et al., *Isothermal titration calorimetry studies on the binding of amino acids to gold nanoparticles.* Journal of Physical Chemistry B, 2004. **108**(31): p. 11535-11540.
161. Varghese, N., et al., *A calorimetric investigation of the assembly of gold nanorods to form necklaces.* Chemical Physics Letters, 2008. **450**(4-6): p. 340-344.
162. Hu, X.G., et al., *Well-ordered end-to-end linkage of gold nanorods.* Nanotechnology, 2005. **16**(10): p. 2164-2169.
163. Gole, A. and C.J. Murphy, *Biotin-streptavidin-induced aggregation of gold nanorods: Tuning rod-rod orientation.* Langmuir, 2005. **21**(23): p. 10756-10762.
164. Caswell, K.K., et al., *Preferential end-to-end assembly of gold nanorods by biotin-streptavidin connectors.* Journal of the American Chemical Society, 2003. **125**(46): p. 13914-13915.
165. Zareie, M.H., X.D. Xu, and M.B. Cortie, *In situ organization of gold nanorods on mixed self-assembled-monolayer substrates.* Small, 2007. **3**(1): p. 139-145.

166. Chang, J.Y., et al., *Oriented assembly of Au nanorods using biorecognition system.* Chemical Communications, 2005(8): p. 1092-1094.
167. Pan, B.F., et al., *End-to-end self-assembly and colorimetric characterization of gold nanorods and nanospheres via oligonucleotide hybridization.* Nanotechnology, 2005. **16**(9): p. 1776-1780.
168. Jain, T., et al., *Self-Assembled Nanogaps via Seed-Mediated Growth of End-to-End Linked Gold Nanorods.* Acs Nano, 2009. **3**(4): p. 828-834.
169. Kawamura, G., Y. Yang, and M. Nogami, *End-to-end assembly of CTAB-stabilized gold nanorods by citrate anions.* Journal of Physical Chemistry C, 2008. **112**(29): p. 10632-10636.
170. Nie, Z.H., et al., *Self-assembly of metal-polymer analogues of amphiphilic triblock copolymers.* Nature Materials, 2007. **6**: p. 609-614.
171. Sudeep, P.K., S.T.S. Joseph, and K.G. Thomas, *Selective detection of cysteine and glutathione using gold nanorods.* Journal of the American Chemical Society, 2005. **127**(18): p. 6516-6517.
172. Ni, W., et al., *Evidence for Hydrogen-Bonding-Directed Assembly of Gold Nanorods in Aqueous Solution.* The Journal of Physical Chemistry Letters, 2010. **1**(8): p. 1181-1185.
173. Tang, Q., et al., *Self-assembled nanogaps for molecular electronics.* Nanotechnology, 2009. **20**(24): p. 245205.
174. Kissling, G.P., D.O. Miles, and D.J. Fermin, *Electrochemical charge transfer mediated by metal nanoparticles and quantum dots.* Physical Chemistry Chemical Physics, 2011.
175. Matylitsky, V.V., et al., *Ultrafast Charge Separation in Multiexcited CdSe Quantum Dots Mediated by Adsorbed Electron Acceptors.* Journal of the American Chemical Society, 2009. **131**(7): p. 2424-2425.
176. Boulesbaa, A., et al., *Competition between Energy and Electron Transfer from CdSe QDs to Adsorbed Rhodamine B.* The Journal of Physical Chemistry C, 2009. **114**(2): p. 962-969.
177. Huang, J., et al., *Multiple Exciton Dissociation in CdSe Quantum Dots by Ultrafast Electron Transfer to Adsorbed Methylene Blue.* Journal of the American Chemical Society, 2010. **132**(13): p. 4858-4864.
178. Beard, M.C., *Multiple Exciton Generation in Semiconductor Quantum Dots.* The Journal of Physical Chemistry Letters, 2011. **2**(11): p. 1282-1288.
179. Trinh, M.T., et al., *In Spite of Recent Doubts Carrier Multiplication Does Occur in PbSe Nanocrystals.* Nano Letters, 2008. **8**(6): p. 1713-1718.
180. Liu, X., et al., *Anodic Electrochemiluminescence of CdTe Quantum Dots and Its Energy Transfer for Detection of Catechol Derivatives.* Analytical Chemistry, 2007. **79**(21): p. 8055-8060.
181. Huang, J., et al., *Photoinduced Ultrafast Electron Transfer from CdSe Quantum Dots to Re-bipyridyl Complexes.* Journal of the American Chemical Society, 2008. **130**(17): p. 5632-5633.
182. Lutich, A.A., et al., *Energy Transfer versus Charge Separation in Type-II Hybrid Organic−Inorganic Nanocomposites.* Nano Letters, 2009. **9**(7): p. 2636-2640.
183. Noone, K.M., et al., *Absence of Photoinduced Charge Transfer in Blends of PbSe Quantum Dots and Conjugated Polymers.* Acs Nano, 2009. **3**(6): p. 1345-1352.

# CHAPTER 3

## Synthesis of *trans*-functionalized porphyrins for single molecule electronic studies

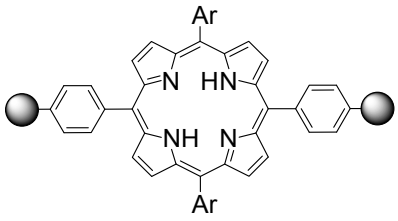


= Linker moieties = -$NH_2$, -SH

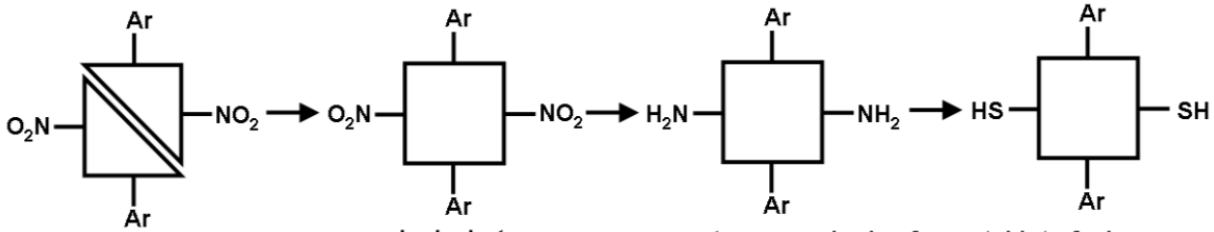


With the ultimate goal to study porphyrins as single molecules, we devised a quick and easy synthetic route to obtain amine and thiol functionalized pure *trans*-porphyrins in high yields, avoiding isomerization and scrambling of the functionalities. We used the mono-carbinol strategy by monoacylation of dipyrromethane and further reduction to mono-carbinol with subsequent cyclisation to synthesize *trans*-nitro porphyrin, which was converted by reduction to the *trans*-amino porphyrin, which is a highly versatile intermediate for the synthesis of a wide variety of other functionalized porphyrins, making use of common amine converting strategies. The *trans*-amino functionalized porphyrin was converted to bis-thiol-porphyrin by Leuckart thiophenol synthesis. These amino and thiol-functionalized porphyrin molecules have the required conjugated structure and linkers at proper positions to study their single molecule properties.

## 3.1 Introduction

Porphyrin molecules are highly conjugated[1] heterocyclic aromatic macrocyles with 26 π electrons in the core ring structure. They are commonly present in nature, forming the reactive sites of haemoglobin, myoglobin and cytochrome enzymes. The macrocyclic structure and chemical reactivity of porphyrins offers architectural flexibility and facilitates the tailoring of chemical[2], physical[3] and optoelectronic properties.[4] Different metal ions can be incorporated in the internal ring of the porphyrin molecule, which alter the optical and electronic properties of these highly conjugated systems. Combined with outstanding chemical and thermal stabilities, porphyrins find widespread application in molecular electronic devices.[5]

Hans Fisher thought up the first system of nomenclature for porphyrins, which was straight forward for naming porphyrins, but with increasing complexity of porphyrin molecules, with different substitutents on the β- (1-8 carbon atoms in Fisher numbering system shown in figure 1) and *meso*-positions (α, β, γ, δ carbon atoms in Fisher numbering system shown in figure 1), the system becomes unwieldy and even contradictory. Since the nomenclature systems have to be self-consistent, a new and more systematic IUPAC nomenclature was introduced, which numbered all the atoms including nitrogen atoms, in the macrocycle as shown in figure 1.

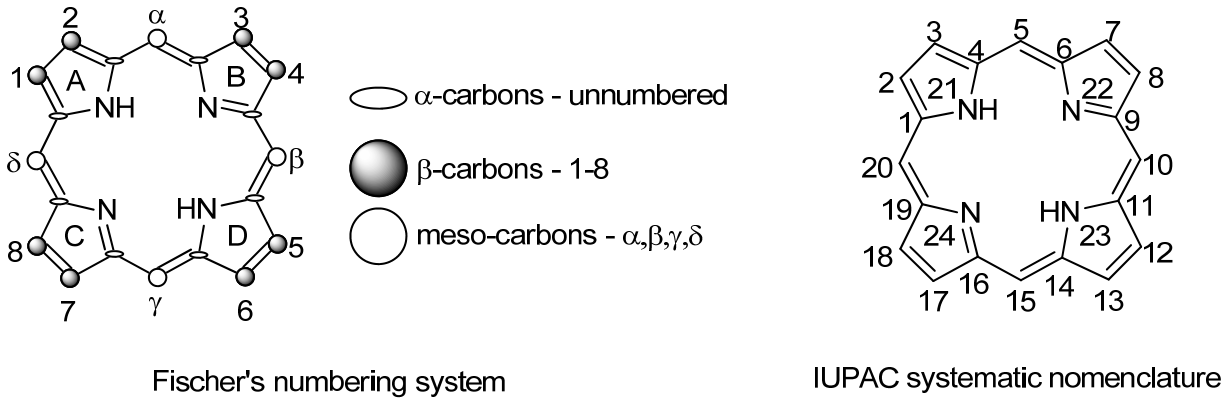


Fig. 1: Nomenclature of porphyrins used in Fischer's numbering system and IUPAC system.

We are interested in studying the interaction of porphyrin molecules with gold and platinum surfaces and particles.[6, 7] These studies require the synthesis of various porphyrin molecules with amine and thiol functional groups to link them with these metal interfaces,[3, 8-10] as thiols are known to have high affinity for gold surfaces and amines have more interaction with platinum surfaces. Variations at the *meso* positions rather than the *β*-positions (of the pyrrole rings) was chosen because of symmetry considerations required for applications in molecular electronic devices. Likewise, these applications require the porphyrins to exist as purely *trans* isomers as shown in figure 2.

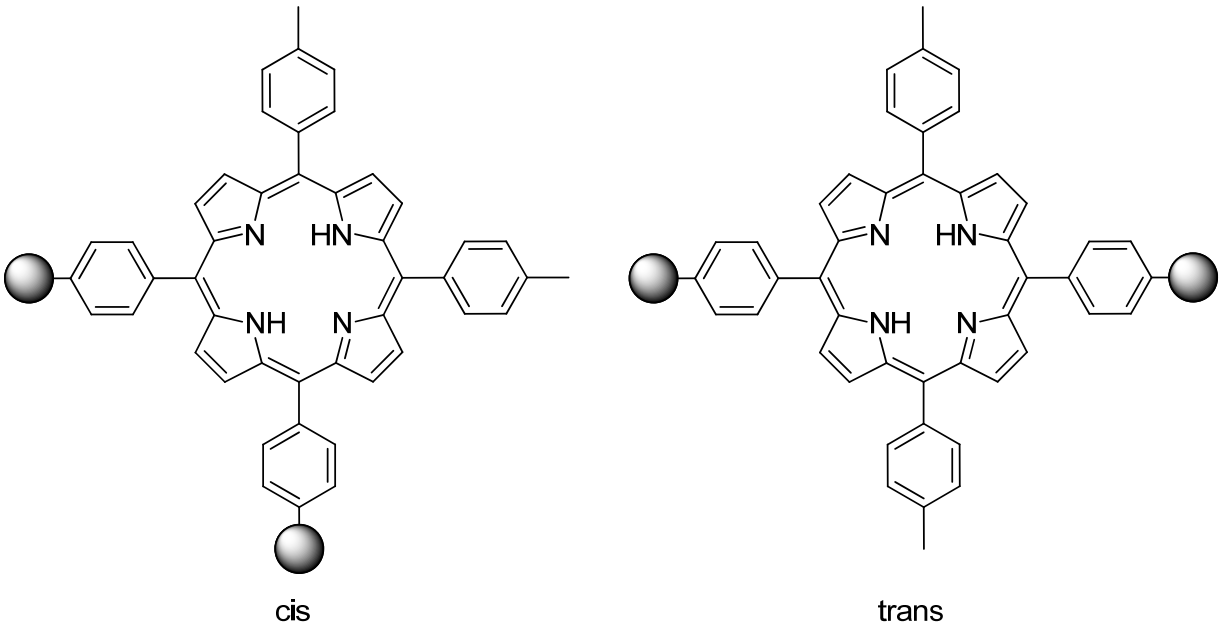


Fig. 2: *Cis* and *trans* functional groups at meso positions of porphyrin molecules. *Trans* functionalized porphyrin molecules with amine (-$NH_2$) or thiol (-SH) functional groups as linkers are required for molecular devices.

However, most strategies to obtain pure *trans*-porphyrin isomers rely on the statistical formation of six different isomers (figure 3b), followed by tedious chromatographic procedures to separate them. As such, the classical porphyrin synthesis under Adler conditions[11] (figure 3a) using a mixture of aldehydes results in very low yield of the desired porphyrin. In addition to that, in certain cases it is impossible to separate the *cis* and *trans* isomers.[12]

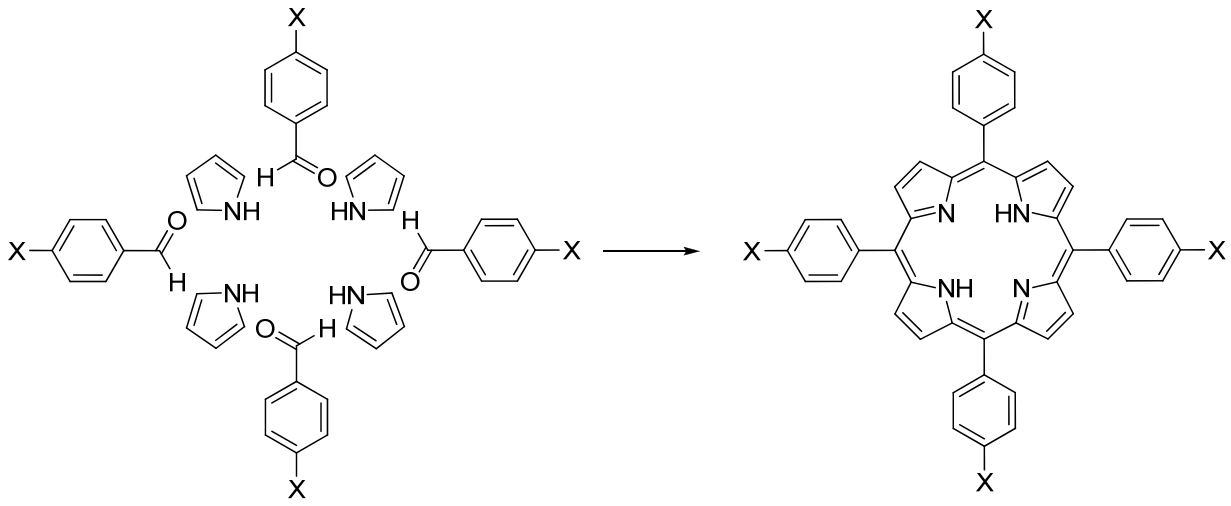

Fig. 3(a): Porphyrin synthesis with four symmetrical groups using one aldehyde only. X represents any functional group. Four aldehyde and four pyrrole molecules combined to make a single porphyrin molecule.

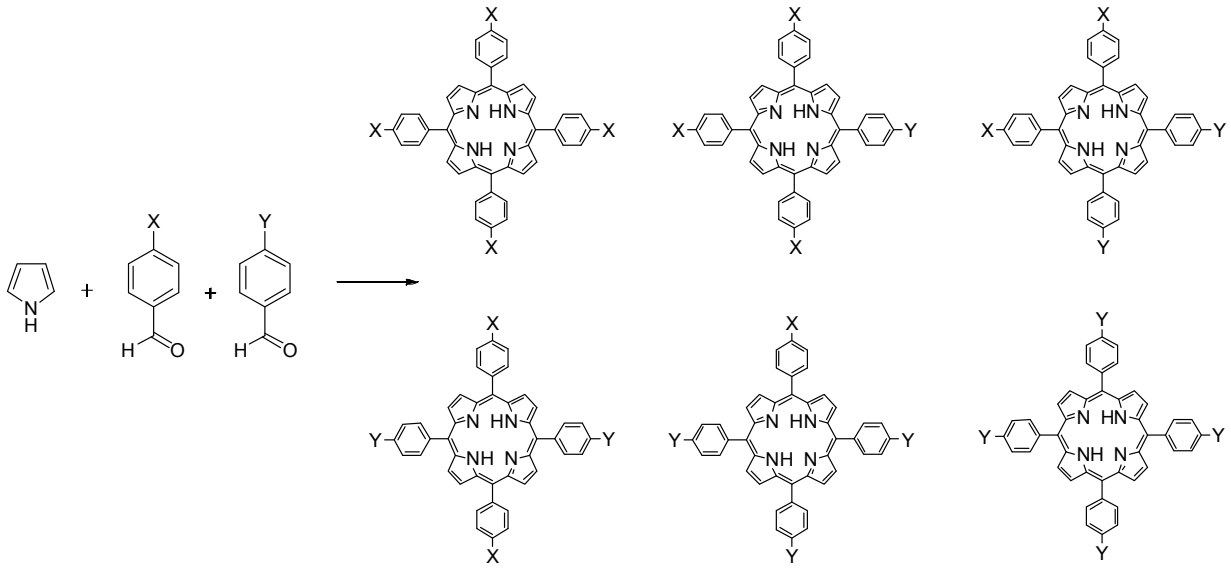

Fig. 3(b): Six different isomers as obtained from mixed aldehyde condensation method. X and Y represents different functional groups.

The widely applied dipyrromethane route[13] (figure 4) is also not practical because the required acidic conditions for the condensation reaction generally cause scrambling of the meso-aryl substituents.[14] However, dipyrromethane route is a very good synthetic approach for trans-

$A_2B_2$-porphyrins derived from dipyrromethanes containing ortho-disubstituted arylgroups. The reason is not completely understood, but possibly it is due to the kinetic hindrance in acidolysis of the dipyrromethane species. With less bulky groups scrambling can marginally be avoided by careful adjustment of reaction conditions, resulting in low yields of isolated trans-porphyrins.[14-16]

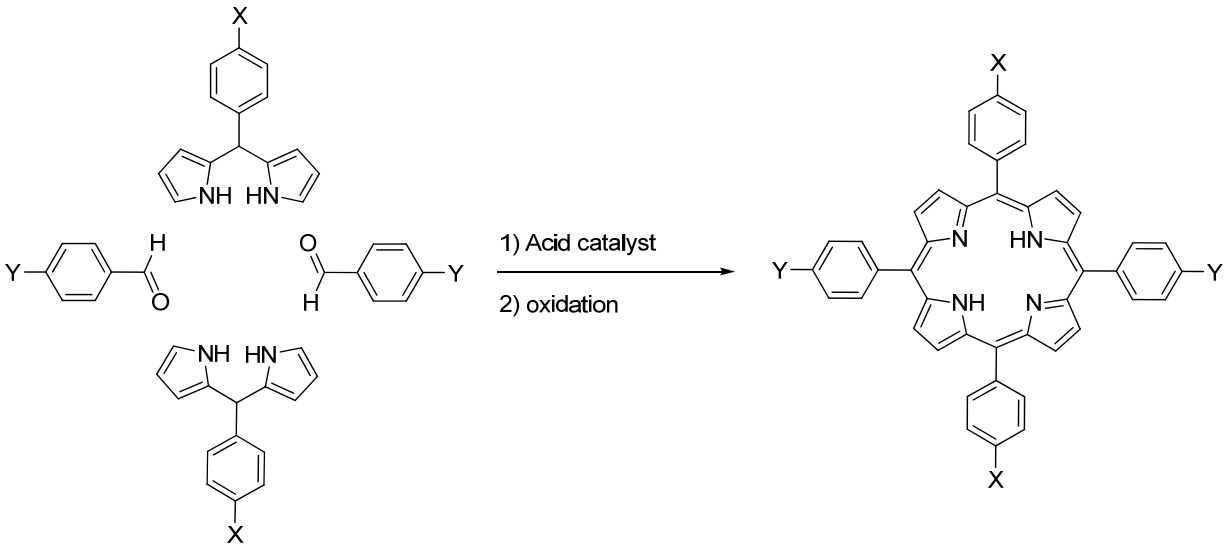


Fig. 4: Dipyrromethane route to obtain pure *trans*-porphyrins is also limited to very few sterically hindered groups

Another approach to functionalized porphyrins is via tetraphenylporphyrin, e.g nitration. In this case, apart from long reaction times, mixtures of mono, di, tri and tetra isomers are formed (figure 5), which again require tedious separation procedures.[17-20]

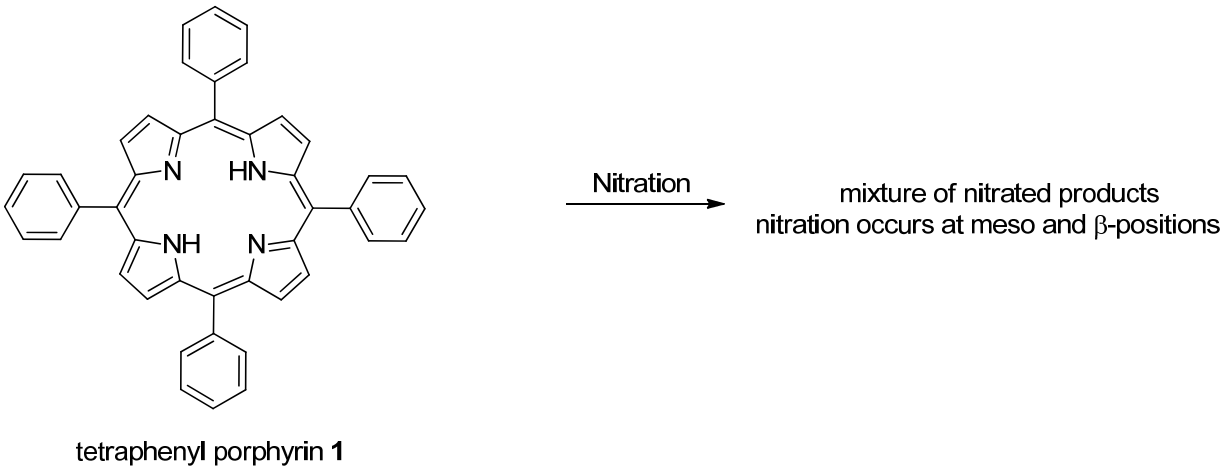


Fig. 5: Nitration of TPP results in various isomers e.g. nitration occurs at phenyl groups (meso positions) and at β-positions.

Only a few direct strategies are known for making solely *trans*-porphyrin isomers.[21-26] The most powerful approach till date consists of self-condensation of dipyrromethane-monocarbinols, pioneered by Lindsey and coworkers.[27, 28] A downside to the published procedures is that for every change in the substitution pattern, the procedure needs to be repeated for almost every step of the synthesis. There is still a lack of general methodology which provides us the immediate access to various porphyrins in a single step from an easily obtainable precursor.

Here we report a new method that allows easy access to a variety of pure *trans*-porphyrins, with *trans*-dinitroporphyrin as a key intermediate. First, *trans*-dinitro porphyrin is synthesized using the dipyrromethane-monocarbinol strategy.[27] Second, reduction of the nitro functionalities yields the *trans*-diamino porphyrin, a versatile substrate for a wide range of amine-converting synthetic procedures, including the Sandmeyer-type diazonium substitutions, transition metal catalyzed aminations, reductive amination and amide forming methodologies. In this way, the synthesis of large amounts of pure *trans*-diamino porphyrin allows a facile entry into many different pure *trans*-functionalized aryl porphyrins. For our particular purpose, the amine intermediate was subsequently converted to the *trans*-dithiol porphyrin using the Leuckart thiophenol reaction. In this reaction, a diazonium ion is formed as an intermediate. This is followed by nucleophilic attack of a xanthate ester and finally hydrolysis by potassium

hydroxide, yielding pure *trans*-dithiol porphyrin as the desired product. The facile synthesis of isomerically pure *trans* amine and thiol functionalized porphyrins facilitates application in molecular electronic devices.

## 3.2 Results and discussion

In our efforts to synthesize 5,15-di-(*p*-tolyl)-10,20-di-(*p*-thiolphenyl)porphyrin **4'**, for future applications in molecular devices, we were unable to successfully reproduce the only method present in the literature, a method for the synthesis and deprotection of 5,15-di-(*p*-tolyl)-10,20-di-(*p*-thiomethoxyphenyl)-porphyrin **4**.[29] Using the reported dipyrromethane strategy, in all cases we obtained a mixture of isomers, which was the result of acid-induced scrambling of the aryl substituents during the condensation.

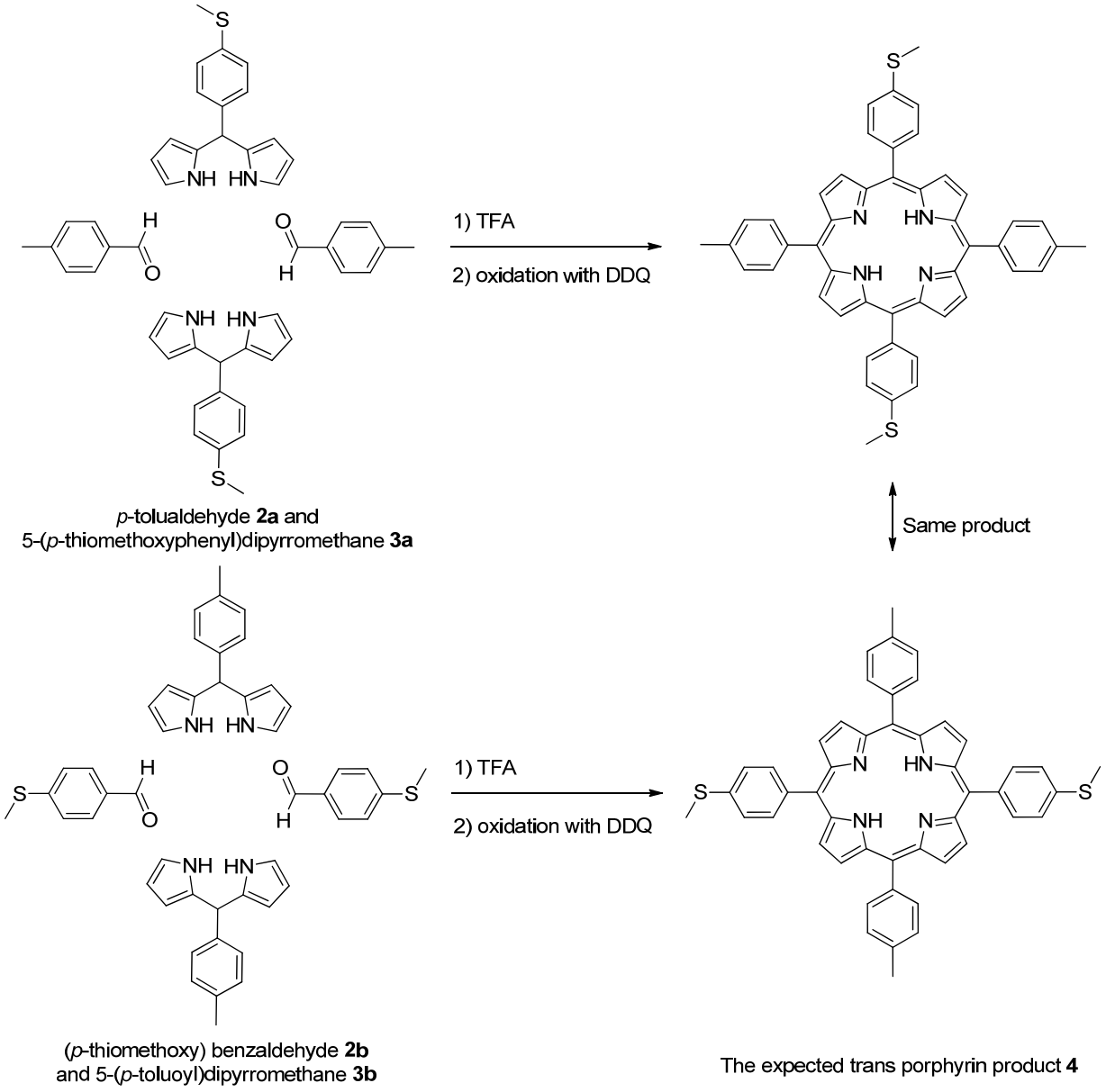


Fig. 6: Two different strategies to prepare same *trans* substituted porphyrin **4**. Scrambling occurs in both cases.

Apart from the reported trifluoroacetic acid, we attempted the use of other acid sources e.g. Amberlyst 15 (dry) ion exchange resin,[30] $BF_3{\cdot}O(Et)_2$,[13] and triethyl orthoacetate [30] but to no avail. Reaction in nitrogen atmosphere, under dark conditions, or changing the oxidant from DDQ to chloranil [30] also did not help. Chromatographic separation of the reaction mixture

afforded all isomers in pure form, except for the desired *cis* and *trans* isomers, which proved impossible to separate from each other (figure.7).

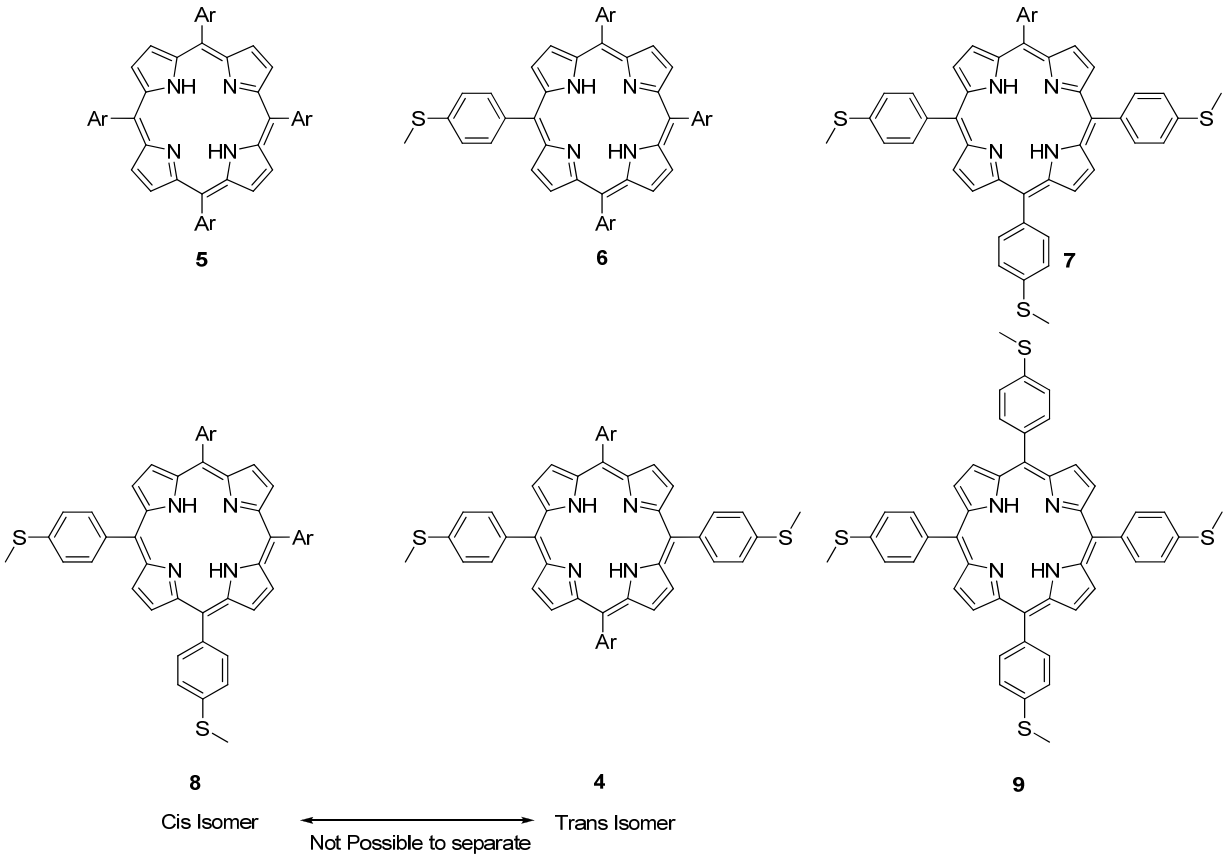


Fig. 7: Scrambling occurs, when the dipyrromethane route was applied. All six possible isomers were obtained as expected from the mixed aldehyde method.

Additionally, for the pyrollic protons (β-positions, figure 8) highlighted in small circles, $^{1}$H-NMR of the *cis*/*trans* mixture showed only a single absorption (figure 9) making it impossible to characterize *cis* and *trans* isomers of the porphyrin, even if they were pure.

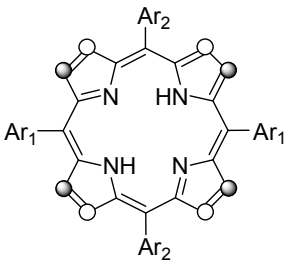


Fig. 8: Protons at β-positions are shown in circles. Black and white circles represent two chemically inequivalent sets of protons when $Ar^1 \neq Ar^2$.

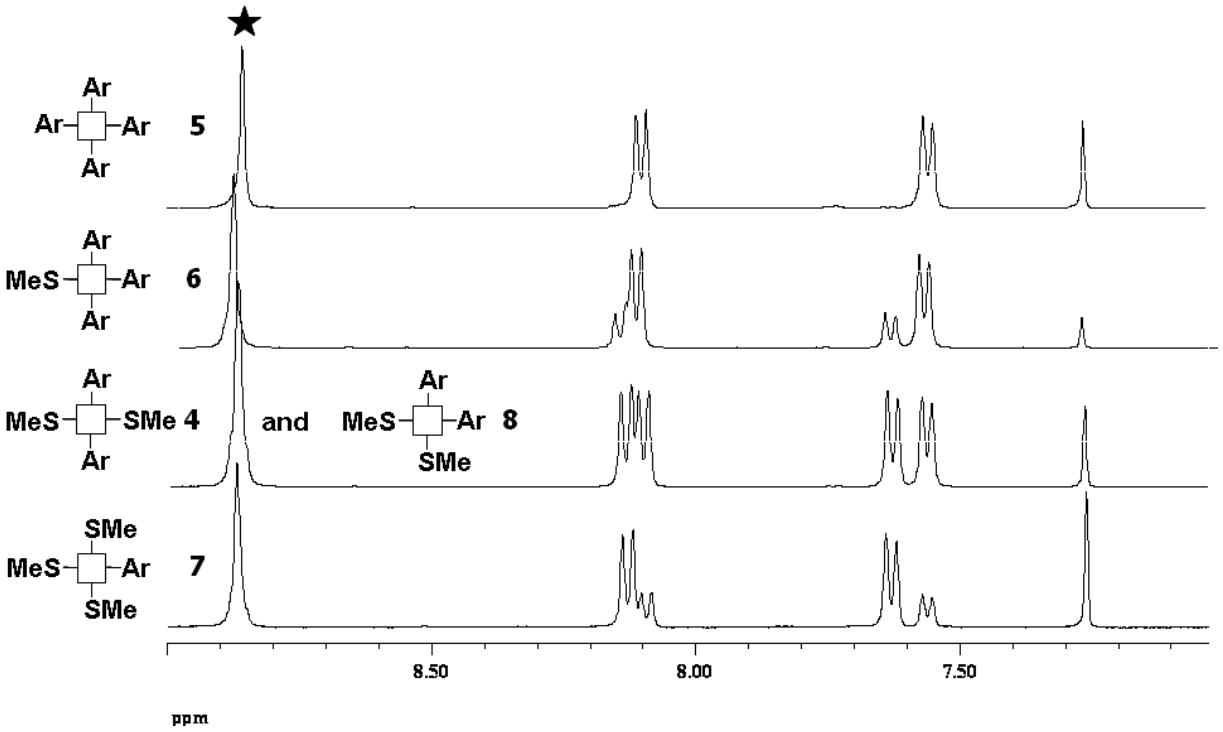


Fig. 9: NMR (400 MHz, $CDCl_3$) of thiomethoxy-substituted porphyrins. The pyrrolic protons (marked ★) show a single resonance, irrespective of the substitution pattern, making it impossible to distinguish between *trans* **4** and *cis* **8** isomers. Ar = p-tolyl; MeS = p-thiomethoxyphenyl.

Attempts to cleave off the thioether methyl groups of the mixture of *cis* and *trans* isomers to give a possibly separable mixture of free thiol porphyrins failed. The cleavage of thiomethoxy groups to provide free thiol groups was not successful. The starting material was either mono

thiomethoxy substituted porphyrin, dithiomethoxy substituted porphyrin or tri thiomethoxy substituted porphyrins.

Although, one of the next steps on the mixture of porphyrins was used to observe the metal insertion behaviour in the porphyrin core and it appears that metal insertion in free porphyrins was quick and quantitative reaction, when Zn was introduced as a metal atom.[31]

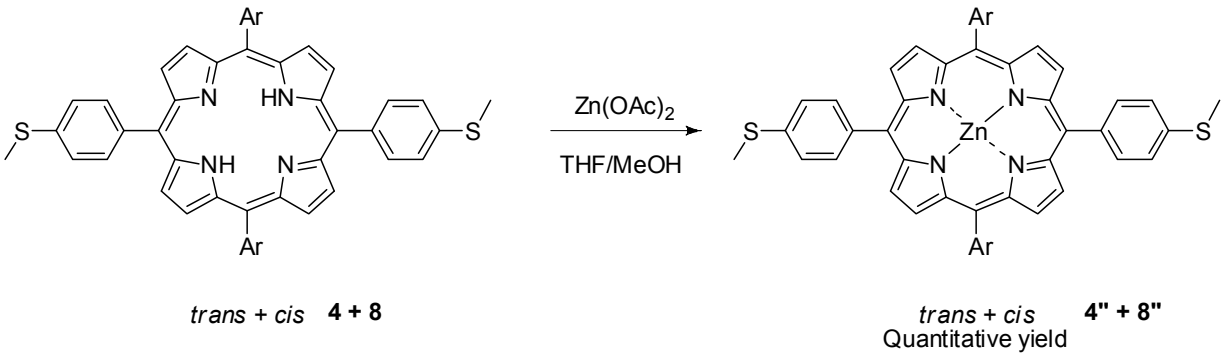


Fig. 10: Zn-metal insertion in porphyrin ring is a simple and easy reaction.

We then considered other strategies to obtain the desired trans-substituted porphyrins, such that it would include a possibility to analyze the isomeric constitution from the pyrrolic protons in $^{1}$H-NMR. We adapted a synthetic strategy developed by Lindsey and coworkers[27], which allowed us to obtain isomerically pure *trans* porphyrins from *trans*-nitro- and *trans*-aminoporphyrin intermediates (vide infra), structures that show distinctly split pyrrolic proton resonances (figure 12). It is important, because a distinct pyrrolic proton resonance gives us clear indication of pure *trans* isomer of porphyrin obtained.

Lindsey's approach can be easily understood in figure 11 below, where a retro synthetic analysis is shown. First, monoacylation of a dipyrromethane is performed. In the next step, the monoacylated product is reduced to carbinol which is expected to self-condense quickly to produce pure *trans*-porphyrin molecule. The dipyrromethane carbinol still has the possibility to scramble, but here the kinetics of the reaction are prevalent, as observed from the visual appearance of the reaction i.e. immediate change of colour to dark red in few seconds. As soon as

the porphyrinogen ring is formed, scrambling cannot occur. This porphyrinogen ring on oxidation, forms the porphyrin molecule.

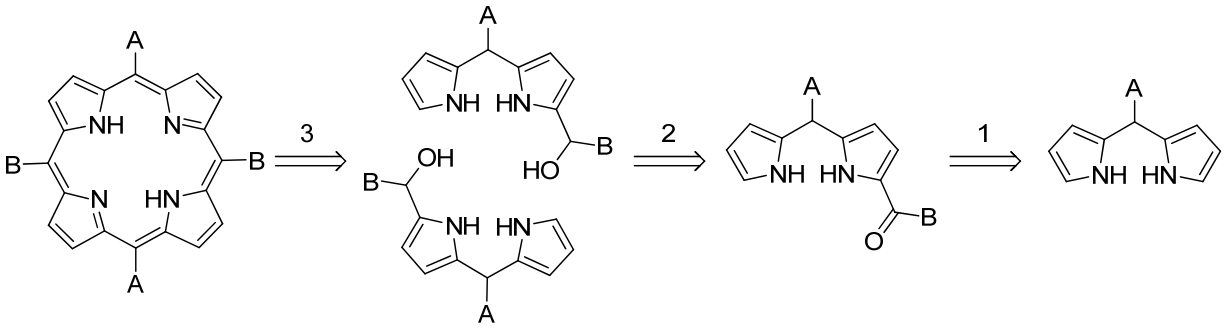


Fig. 11: Mechanism of Lindsey's approach. Step 1 shows the monoacylation of dipyrromethane, step 2 shows reduction of the carbonyl group and step 3 shows self-condensation of two monocarbinols to yield a pure porphyrin molecule.

The construction of the porphyrin scaffolds involved first synthesizing pyridyl thioesters **11a-e** using a slightly modified literature procedure,[27] as explained in the experimental section (scheme 1).

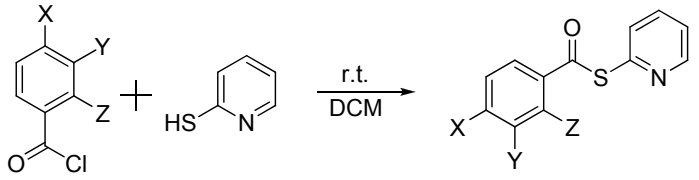


**9a**) X=$NO_2$, Y=H, Z=H
**9b**) X=H, Y=$NO_2$, Z=H
**9c**) X=Br, Y=H, Z=H
**9d**) X=SMe, Y=H, Z=H
**9e**) X=H, Y=H, Z=$CH_3$

**10**

**11a**) X=$NO_2$, Y=H, Z=H; 88%
**11b**) X=H, Y=$NO_2$, Z=H; 70%
**11c**) X=Br, Y=H, Z=H; 97%
**11d**) X=SMe, Y=H, Z=H; 70%
**11e**) X=H, Y=H, Z=$CH_3$; 50%

Scheme 1. Synthesis of various pyridyl thioesters 11a-e.

The dipyrromethanes **3** were prepared according to the literature procedure,[27, 28] with improved isolated yields as compared to reported values (scheme 2).

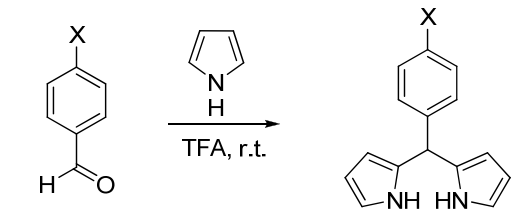


**2a**) X = $CH_3$
**2b**) X = SMe
**2c**) X = $NO_2$

**3a**) X = $CH_3$; 51%
**3b**) X = SMe; 55%
**3c**) X = $NO_2$; 65%

Scheme 2. Synthesis of tolyldipyrromethane.

Coupling of the pyridyl thioesters of **11a-e** to *para* substituted dipyrromethanes **3a-b** was achieved using 2.5 equivalents of Grignard reagent. Deprotonation occurs on one of the pyrrole rings, resulting in mono acylated dipyrromethanes **12a-c**, in good yields (scheme 3).

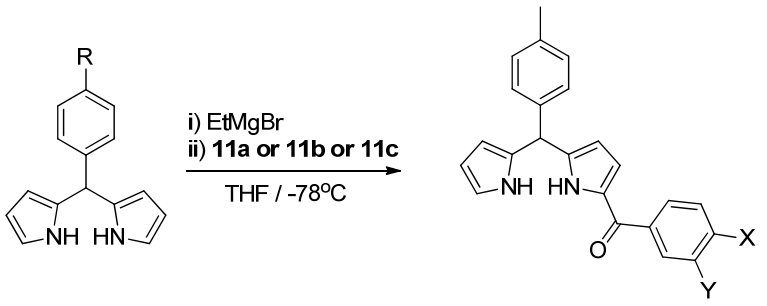


**3a** R=Me
**3b** R=SMe

**12a**) R=Me, X=$NO_2$, Y=H; 75%
**12b**) R=Me, X=H, Y=$NO_2$; 58%
**12c**) R=SMe, X=Br, Y=H; 89%

Scheme 3. Coupling of dipyrromethane and pyridyl thioesters to yield monoacylated dipyrromethanes.

The coupling of **3c** (5-(*p*-nitrobenzene)-dipyrromethane) and **11e** (S-2-pyridyl-2-methylbenzothioate) did not work, possibly due to electron withdrawing nature of nitro group attached. We did not further investigate on coupling of **3c**.

The monoacylated products **12a** and **12b** were reduced to monocarbinols **12a'** and **12b'** respectively with sodium borohydride. These monocarbinols were immediately self-condensed in presence of TFA yielding porphyrinogens, which were oxidized by DDQ to obtain the pure *trans* isomers of the desired meso substituted pure *trans* dinitrophenyl porphyrins **13a** and **13b** (scheme 4).

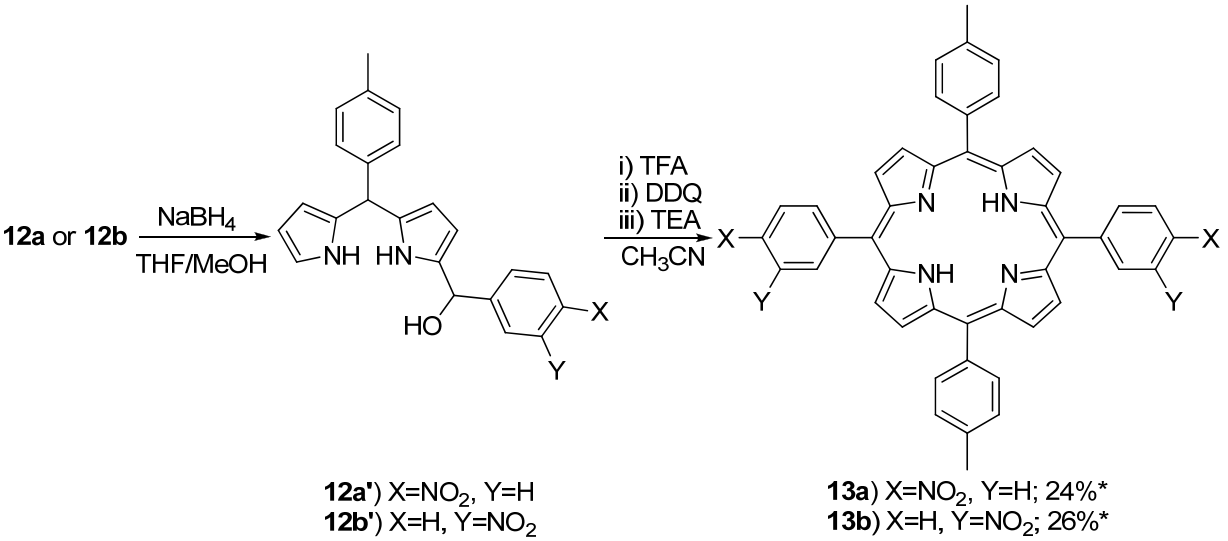


Scheme 4. Reduction of monoacylated dipyrromethanes and subsequent coupling to form pure *trans* nitroporphyrins. *Yield is calculated over two steps.

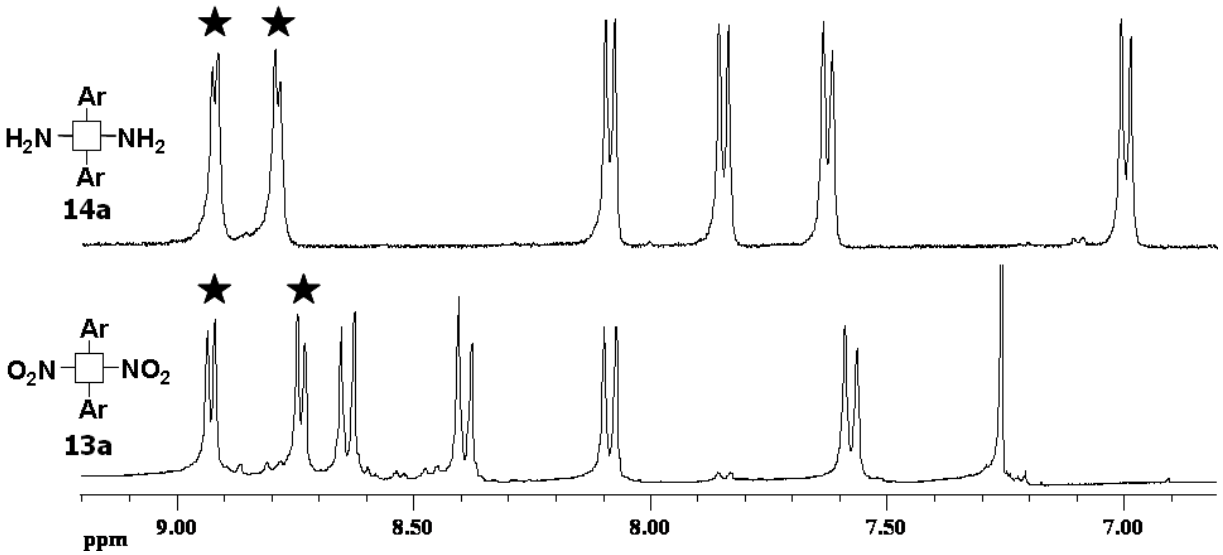


Fig. 12: NMR (400 MHz) of nitro- and amino-substituted trans-porphyrins (**13a**, $CDCl_3$; **14a**, DMSO-$d_6$). Both spectra show distinctly split patterns of the pyrrolic protons (marked ★), facilitating the characterization of the substitution patterns and purity based on the symmetry of the spectra. Minor secondary resonances can be observed in the baseline, resulting from porphyrin stacking in solution, as identified from their concentration dependence.

Subsequent reduction of *trans*-$A_2B_2$-Bis(4-nitrobenzene)porphyrins **13a** and **13b** was accomplished using excess tin(II) chloride in the presence of concentrated hydrochloric acid,[32] to obtain pure *trans*-bisamino porphyrins **14a** and **14b** quantitatively (scheme 5).

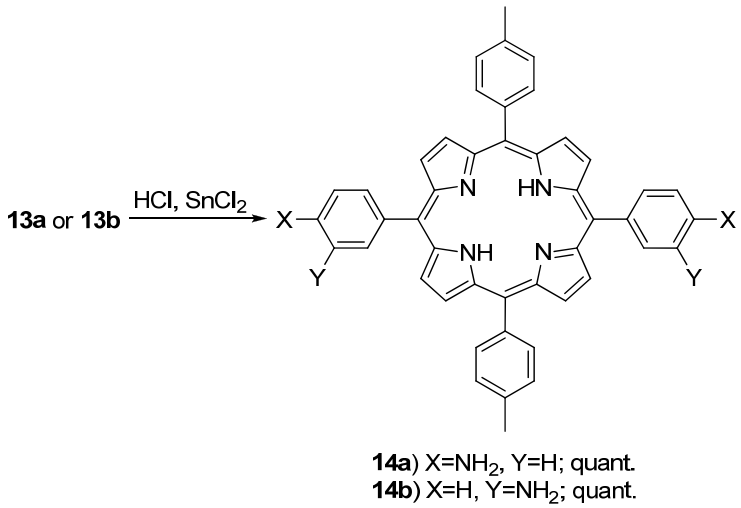


Scheme 5. Reduction of nitrogroups to form pure *trans* aminoporphyrins.

Aniline type of compounds such as **14a** and **14b** are versatile intermediates for further functionalisation. Since a lot of chemistry is known about the transformation of amine groups to wide variety of groups, from this product alone, we possibly can synthesize porphyrin molecules with any choice of functional group transformation which is possible with aniline type of compounds, e.g. amine group in aniline via diazotization can be transformed to hydroxyl, thiol, Ar-S-Ar sulphide, Ar-S-R, Ar-S-CN, Ar-S-Me, ArI, ArF, Azo compounds, ArMe, arylation. Some of the examples include azo coupling, reaction replacements by halogens, Sandmeyer reaction, Gomberg-Bachmann reaction, Schieman reaction, Craig method, Meerwein arylation, Bamberger triazine synthesis, Widman-Stoermer synthesis, hydrolysis yielding alcohols etc.[33]

As we were interested in thiol functionalized porphyrins, we decided to proceed with Leuckart thiophenol synthesis,[34] which was applied to make the di-xanthate ester derivative of porphyrin **14a**. This was achieved via diazotization and subsequent treatment of the diazonium ion with potassium ethyl xanthate. The intermediate product was finally converted to pure *trans*-bisthiol porphyrin **4'** by hydrolysis with potassium hydroxide, in an excellent overall yield (scheme 6).

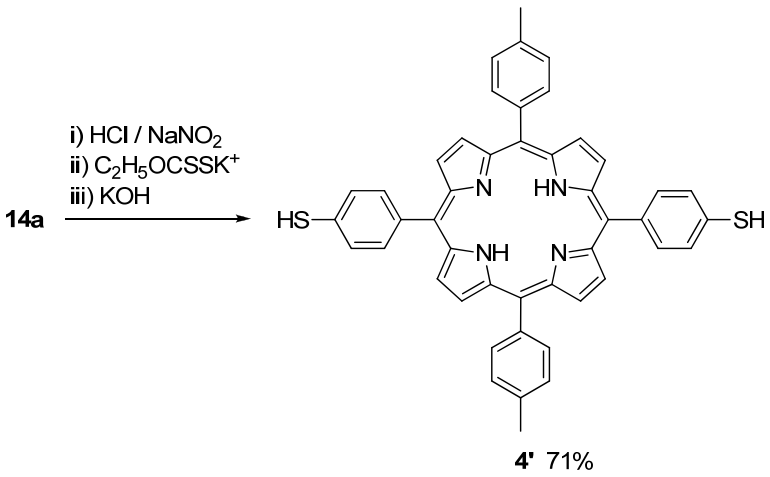


Scheme 6. Conversion of *trans* diamino porphyrins to *trans* dithiol porphyrins.

### 3.2.1 Synthesis of porphyrin molecules with four equal groups at meso positions

To understand I-V characteristics of various porphyrin molecules and to compare them with *trans* functionalized porphyrins in later studies (Chapter 4-6 of this thesis), we synthesized a variety of tetrasubstituted porphyrins using literature procedures.

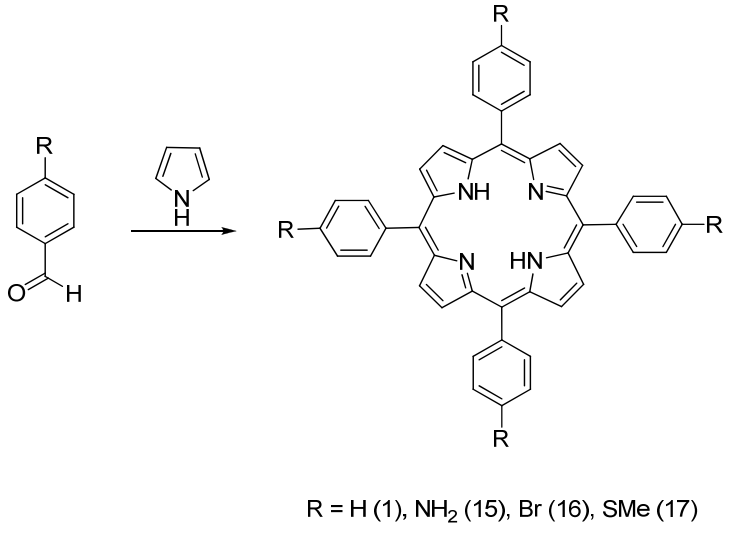


Fig. 13: Various tetrasubstituted porphyrins synthesized via Alder and Longo method.

Tetraphenylporphyrin (**1**), para-substituted tetrabromophenyl porphyrin **16** and tetra(thiomethoxy) porphyrin **17** were synthesized according to the classical Adler and Longo method [11, 35], whereas para-substituted tetraaminophenyl porphyrin (**15**) was synthesized by making tetranitrophenyl porphyrin as a modified method of Adler and subsequently reducing nitro groups with $SnCl_2$/HCl mixture. This method is also described in literature.[32]

### 3.2.2 Metal insertion in *trans*-bisthiol porphyrin 4', tetraaminophenyl porphyrin 15

Zinc metal insertion in **4'** and **15** was done according the method described in [31] and yielded the Zn-porphyrins **18** and **19** (figure 14) in a quantitative manner.

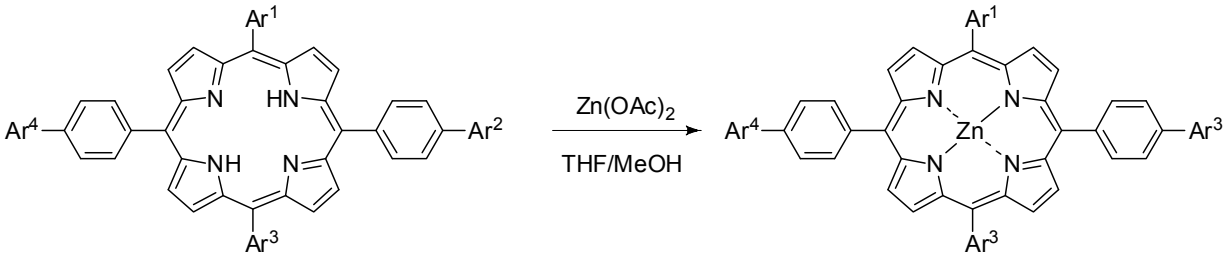


**4'** ) $Ar^1 = Ar^3$ = -PhMe; $Ar^2 = Ar^4$ = -PhSH
**15**) $Ar^1 = Ar^2 = Ar^3 = Ar^4$ = -$PhNH_2$

**18**) $Ar^1 = Ar^3$ = -PhMe; $Ar^2 = Ar^4$ = -PhSH
**19**) $Ar^1 = Ar^2 = Ar^3 = Ar^4$ = -$PhNH_2$

Quantitative yield

Fig. 14: Metal insertion in porphyrin ring.

### 3.2.3 Porphyrins with four different functional groups

After we were able to make the required pure *trans* porphyrins, an idea to prepare two different asymmetric monomers to yield four different functional groups on the *meso*-positions of the porphyrin molecules arose. Although, there are methods present in literature to prepare porphyrins with four different functional groups,[36] this was an interesting side project (figure 15)

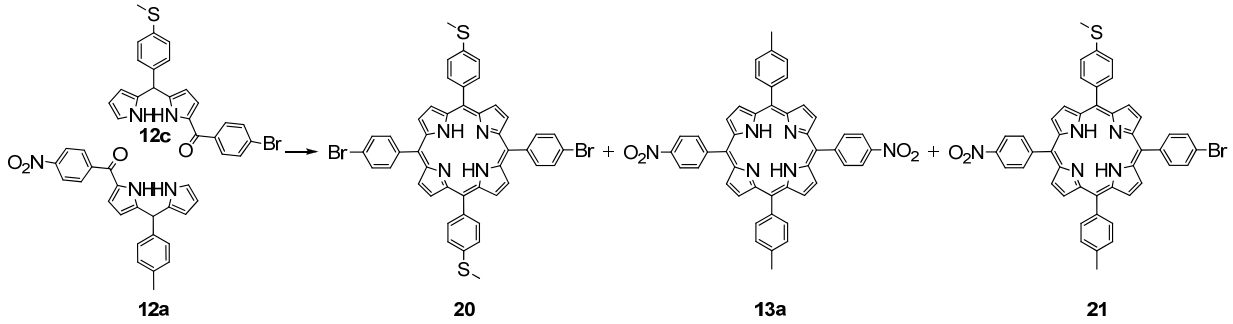


Fig. 15: Two different monomers **12a** and 1**2c**, each with two different functional groups result in three different porphyrins **20**, **13a** and **21**. One of the porphyrins (**21**) has four different substituents (functional groups).

Two different monoacylated dipyrromethanes (**12a** and **12c**) as monomers were prepared (scheme 3), were reduced together to monocarbinols (scheme 4) to yield a mixture of three porphyrins **13a**, **20**, and **21** only (figure 15), resulting in the possibility of getting any kind of functional groups of our choice at four different meso positions of the porphyrin molecule. The chosen functional groups were thiomethoxy, bromo, nitro and methyl substituents. The formation of these three porphyrins was confirmed by mass spectrometry. Separation seemed to be difficult as the overall polarity of these three products was similar as observed from TLC. Before we had the chance to come up with a selection of substituents that would allow a more facile separation, publication [24] similar to this project was published, which describes rational routes from 1-acyldipyrromethanes to obtain *meso*-substituted porphyrins. We did not continued further with this project.

## 3.3 Conclusions

In conclusion, we have devised an efficient route to synthesize exclusively *trans*-functionalized porphyrins. *Trans*-nitro porphyrin, obtained using the mono-carbinol strategy, is converted by reduction to the *trans*-amino porphyrin, which is a highly versatile intermediate for the synthesis of a wide variety of other functionalized porphyrins, making use of common amine converting strategies. This allows for the production of trans-functionalized porphyrins in high yields, and less purification steps, avoiding isomerization and scrambling, as we have shown for the synthesis of *trans*-thiol porphyrin. The amino and thiol-functionalized porphyrin molecules

synthesized will possibly broaden the applications of these molecules for attachment to inorganic surfaces and particles, in the field of molecular electronics, material sciences as well as in biological systems.

## 3.4 Experimental

### 3.4.1 General information

Starting materials were commercially available and were used without further purification. Silica gel grade 9385 (230-400 mesh) was used for column chromatography, in combination with the Teledyne Isco CombiFlash Companion with UV-detection. All solvents used for dry reactions were purified with the use of the MBRAUN solvent purification system MB SPS-800. $^{1}$H NMR spectra were recorded on a Bruker Avance 400 spectrometer (at 400 MHz) at 25ºC. The splitting patterns are noted as follows: s (singlet), d (doublet), dd (double doublet), t (triplet), q (quartet), m (multiplet) and bs (broad singlet). $^{13}$C NMR spectra were recorded on a Bruker Avance 400 spectrometer (at 100 MHz). Chemical shifts are given in δ (ppm) referenced to residual solvent peaks, $^{1}$H: DMSO δ = 2.50 and $CDCl_3$ δ = 7.26 or to TMS δ = 0; $^{13}$C: DMSO δ = 39.43 and $CDCl_3$ δ = 77.0. Coupling constants J are given in Hz. ESI-MS was performed on a SHIMADZU LCMS-2010, equipped with an LC-8A pump and a SPD-M20 diode array detector. Melting point measurements were performed on a Barnstead Electrothermal IA9300 Digital melting point apparatus. UV/Vis measurements were performed on an AnalytikJena Specord 250 spectrometer, using quartz cuvets with 1 cm path-lengths. FT-IR measurements were performed on a Perkin Elmer Spectrum One FT-IR spectrometer with a Universal ATR sampling accessory.

### 3.4.2 Reaction conditions used for cleavage of methyl groups 4+8, 6 & 7

The method specific to deprotect methyl from aryl-S-methyl group [37] is the use of *t*-BuSNa (2 equiv.) in dimethylformamide at 160$^{o}$C for four hours. First, we followed the method described in [29] to deprotect the methyl groups from thiomethoxy substituents using NaSMe in HMPA (hexamethylphosphoramide) under nitrogen atmosphere at 100 $^{o}$C. Upon repeated trials to cleave

of methyl groups from 4+8, 6 or 7 were unsuccessful. It has to be considered that HMPA is highly malodorous and carcinogenic compound.

We then tried DMF (dimethylformamide) as a solvent (standard condition). The temperature range was from 100-160 $^{o}$C. *t*-BuSNa (upto 10 equivalents per methylsulfide group) were used as cleaving agents. In all of the reactions with different conditions, TLC did not show any sign of product formation. Other issues involved were non-solubility of porphyrins in DMF. HMPA has a boiling point of 232 $^{o}$C, which was difficult to remove even after washing with brine and dilute HCl solution. The reaction times were upto 24 hours of stirring at high temperatures. Porphyrins were not soluble in diethyl ether so that they could be extracted, as HMPA remains in the aqueous phase. Porphyrins and HMPA were soluble in dichloromethane, so extraction did not work with dichloromethane. All reactions to cleave off the methyl groups were perfomed in dry conditions. Zn-porphyrin complexes also show the same behaviour.

One last attempt was to treat the thiomethoxy porphyrins with 47% HBr in water (method used to cleave arylmethylethers), but this also did not result in cleavage of the methyl groups from aryl-S-methyl porphyrins.

## 3.4.3 5,10,15,20-tetraphenyl porphyrin (1)

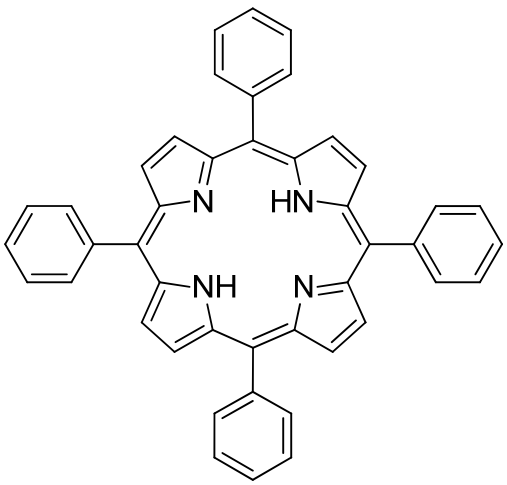


The classical Adler and Longo method [11] was used to synthesize 5,10,15,20-tetraphenyl porphyrin (TPP). Freshly distilled pyrrole (18.73 mL, 0.27 mole) and reagent grade benzaldehyde (27.51 mL, 0.27 mol) were added to 1L of refluxing reagent grade propionic acid. After 30 minutes, the solution was cooled down to room temperature and filtered. The filter cake was washed thoroughly with methanol and with hot water. The resulting purple crystals were dried in vacuum oven yielding **1** of tetraphenyl porphyrin (TPP) (8.06 g, 13.1 mmol, 20 %). $^{1}$H NMR was similar to the reported values.[38]: $^{1}$H NMR ($CDCl_3$): δ -2.77

(s, 2H, pyrrole NH), 7.73 – 7.79 (m, 12H, 5,10,15,20-Ar 3,4,5-H), 8.22 (d, J = 6.8 Hz, 8H, 5,10,15,20-Ar 2,6-H), 8.85 (s,8H, β-pyrrole); MS ($ESI^-$) m/z $\{M+H\}^+$ calcd for $C_{44}H_{31}N_4$ 615.2, obsd 615.2.

### 3.4.4 5-(4-Methylthiophenyl)dipyrromethane (3a)

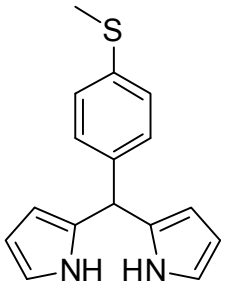


A general procedure for the preparation of 5-substituted dipyrromethanes (scheme 2) [39]was used. Pyrrole (50.0 mL, 720 mmol) and 4-(methylthio)benzaldehyde **2b** (3.83 mL, 28.8 mmol) were added to a 250 mL flask and degassed with stream of nitrogen. TFA (0.22 mL, ~2.9 mmol) was added, and the mixture was stirred under argon at room temperature for 5 minutes and then quenched with 0.1 M NaOH. Ethyl acetate was then added, and the organic phase was washed with water and dried ($Na_2SO_4$). Solvent was removed under vacuum to afford an orange oil. Bulb-to-bulb distillation (230-240 °C, 0.03 mbars) gave a yellow oil. The oil was dissolved in ethanol, and addition of a water resulted in white crystals of **3a** (4.21 g, 55 %); $^1$H NMR was similar to the reported values: $^1$H NMR ($CDCl_3$) δ 2.47 (s, 3H, S-$CH_3$), 5.44 (s, 1H, *meso* CH), 5.92 (s, 2H, pyrrole 3-H), 6.16 (d, J = 2.4 Hz, 2H, pyrrole 4-H), 6.70 (s, 2H, pyrrole 5-H), 7.14 (d, 2H, Ar-H), 7.21 (d, 2H, Ar-H), 7.91 (br s, 2H, pyrrole NH).

### 3.4.5 5-(4-Methylphenyl)dipyrromethane (3b)

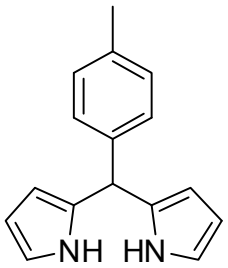


A general procedure for the preparation of 5-substituted dipyrromethanes[28] (scheme 2) was used. Pyrrole (50.0 mL, 720 mmol) and p-tolualdehyde **2a** (3.46 g, 28.8 mmol) were added together as described in the literature. The bulb-to-bulb distillation was carried out at 180 °C (0.02 mm Hg); the oil obtained was crystallized from ethyl acetate:hexanes and was recrystallized from ethanol:water 4:1) giving **3b** as colorless crystals. Yield: 3.47 g, 14.7 mmol, 51%; $^1$H NMR was similar to the reported values: $^1$H NMR ($CDCl_3$) δ 2.34 (s, 3H, Ar-$CH_3$), 5.45 (s, 1H, *meso* CH), 5.93 (s, 2H, pyrrole 3-H), 6.16 (q, J = 2.9 Hz, 2H, pyrrole 4-H), 6.69 (s, 2H, pyrrole 5-H), 7.10-7.15 (m, 4H, Ar-H), 7.91 (br s, 2H, pyrrole NH).

### 3.4.6 5-(4-Nitrophenyl)dipyrromethane (3c)

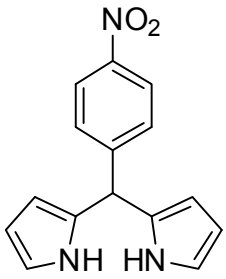


5-(4-Nitrophenyl)dipyrromethane (**3c**) was synthesized using a general literature procedure [28] (scheme 2). Pyrrole (50.0 mL, 720 mmol) and 4-nitrobenzaldehyde **2c** (4.35 g, 28.8 mmol) were added together as described in the literature. However, the crude product was not distilled but was crystallized from ethanol giving **3c** (5.00 g, 65%) as green crystals. $^{1}$H NMR was similar to the reported values: $^{1}$H NMR ($CDCl_3$) δ 5.59 (s, 1H, *meso* CH), 5.87 (s, 2H, pyrrole 3-H), 6.17 (d, J = 2.8 Hz, 2H, pyrrole 4-H), 6.75 (s, 2H, pyrrole 5-H), 7.37 (d, J = 8.8 Hz, 2H, Ar 3,5-H), 8.01 (br s, 2H, pyrrole NH), 8.17 (d, J = 8.8 Hz, 2H, Ar 1,3-H).

### 3.4.7 S-2-pyridyl 4-nitrobenzothioate (11a)

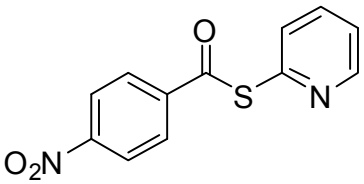


S-2-pyridyl 4-nitrobenzothioate (**11a**) was synthesized using a modified literature procedure[27] (scheme 1).

A solution of p-nitro benzoyl chloride **9a** (9.28 g, 50.0 mmol) in $CH_2Cl_2$ (100 mL) was added over 10 min to a stirred solution of 2-mercaptopyridine **10** (5.56 g, 50.0 mmol) in $CH_2Cl_2$ (250 mL) at room temperature. In 10-15 minutes, the precipitation of yellow solid was observed. Stirring was continued up to 45 minutes. Filtration of the reaction mixture gave 11.5 g of a pale yellow solid, which appeared to be the pure product as observed from $^{1}$H NMR. Yield: 11.5 g, 44.0 mmol, 88%; mp 135-137 °C; $^{1}$H NMR (DMSO-$d_6$) δ 7.28 (dd, J = 7.4 Hz, 5.0 Hz, 1H, pyridine 5-H), 7.62 (d, J = 8.0 Hz, 1H, pyridine 3-H), 7.81 (dt, J = 8.0 Hz, 1.6 Hz, 1H, pyridine 4-H), 8.11 (d, J = 8.8 Hz, 2H, Ar 3,5-H), 8.25 (d, J = 8.8 Hz, 2H, Ar 2,6-H), 8.47 (d, J = 4.8 Hz, 1H, pyridine 6-H); $^{13}$C NMR (DMSO) δ 120.2, 122.2, 123.8, 130.8, 136.5, 138.8, 149.3, 150.0, 157.0, 165.8; MS ($ESI^+$) m/z $\{M+H\}^+$ calcd for $C_{12}H_9N_2O_3S$ 261.0, obsd 261.0.

### 3.4.8 S-2-pyridyl 3-nitrobenzothioate (11b)

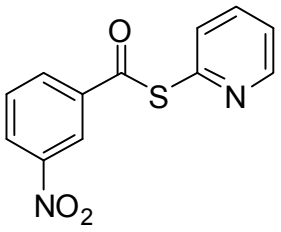


A solution of m-nitro benzoyl chloride **9b** (9.28 g, 50.0 mmol) in $CH_2Cl_2$ (100 mL) was added over 10 min to a stirred solution of 2-mercaptopyridine **10** (5.56 g, 50.0 mmol) in $CH_2Cl_2$ (250 mL) in presence of 50.0 mmol of triethylamine at room temperature (Scheme 1). The solution was stirred overnight and then 10 mL sat. $NaHCO_3$ (aq.) was added. The two layers were separated, the organic phase was washed with water (2 x 20 mL), dried with $Na_2SO_4$, filtered and the solvent removed to yield a yellow amorphous solid. Purification was done by recrystallisation with ethanol and water to yield pale yellow crystalline **11b**. Yield: 9.10 g, 35.0 mmol, 70%; mp 89-90 °C; $^1$H NMR ($CDCl_3$) δ 7.40 (dd, J = 7.4 Hz, 4.9 Hz, 1H, pyridine 5-H), 7.70-7.76 (m, 2H, pyridine 3-H, Ar 5-H), 7.84 (dt, J = 7.7 Hz, 1.7 Hz, 1H, pyridine 4-H), 8.33 (d, J = 8.0 Hz, 1H, Ar 6-H), 8.48 (d, J = 8.0 Hz, 1H, Ar 4-H), 8.71 (d, J = 4.8 Hz, 1H, pyridine 6-H), 8.86 (s, 1H, Ar 2-H); $^{13}$C NMR ($CDCl_3$) δ 122.4, 123.9, 124.4, 128.0, 130.1, 130.8, 132.9, 137.7, 148.3, 149.8, 150.5, 187.4; MS ($ESI^+$) m/z $\{M+H\}^+$ calcd for $C_{12}H_9N_2O_3S$ 261.0, obsd 261.0.

### 3.4.9 S-2-pyridyl 4-bromobenzothioate (11c)

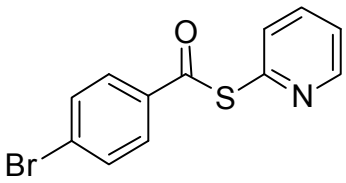


S-2-pyridyl 4-bromobenzothioate (**9c**) was synthesized using literature procedure[36, 40, 41] (scheme 1). A solution of 4-bromobenzoyl chloride **11c** (10.973 g, 50.0 mmol) in $CH_2Cl_2$ (100 mL) was added over 10 min to a stirred solution of 2-mercaptopyridine **10** (5.56 g, 50.0 mmol) in $CH_2Cl_2$ (250 mL) at room temperature. Stirring was continued up to 45 minutes. 1 N NaOH was added. The organic phase was isolated, washed with water, and dried with $Na_2SO_4$, and the solvent removed to afford offwhite solid. Recrystallization with Ethylacetate/hexanes afforded 14.3 g of white crystals, which appeared to be the pure product as observed from $^1$H NMR. Yield: 14.3 g, 48.6 mmol, 97%; $^1$H NMR ($CDCl_3$) δ 7.35 (ddd, J = 7.4 Hz, 4.9 Hz, 1.1 Hz, 1H, pyridine 5-H), 7.64 (d, J = 8.7 Hz, 2H, Ar 3,5-H), 7.66-7.72 (m, 1H, pyridine 3-H), 7.80 (dt, J = 7.8 Hz, 1.9 Hz, 1H, pyridine 4-H), 7.88 (d, J = 8.8 Hz, 2H, Ar 2,6-H), 8.68 (dd, J = 4.8 Hz, 0.9 Hz, 1H, pyridine 6-H).

### 3.4.10 S-2-pyridyl 4-(methylthio)benzothioate (11d)

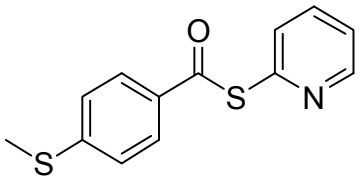

S-2-pyridyl 4-(methylthio)benzothioate (**11d**) was synthesized using literature procedure [27] (scheme 1). A solution of 4-(methylthio)benzoyl chloride **9d** (0.93 g, 5.0 mmol) in $CH_2Cl_2$ (15 mL) was added over 2 min to a stirred solution of 2-mercaptopyridine **10** (0.56 g, 5.0 mmol) in $CH_2Cl_2$ (25 mL) at room temperature. Stirring was continued up to 45 minutes. 1 N NaOH was added. The organic phase was isolated, washed with water, and dried with $Na_2SO_4$, and the solvent removed to afford white solid. Recrystallization with Ethylacetate/hexanes afforded 0.92 g of transparent crystals, which appeared to be pure product **11d** as observed from $^1$H NMR. Yield: 0.92 g, 3.5 mmol, 70%; mp 90-91 °C; $^1$H NMR ($CDCl_3$) δ 2.53 (s, 3H, S-$CH_3$) 7.29 (d, J = 8.8 Hz, 2H, Ar 3,5-H), 7.34 (ddd, J = 7.2 Hz, 4.9 Hz, 1.1 Hz, 1H, pyridine 5-H), 7.74 (d, J = 8.0 Hz, 1H, pyridine 3-H), 7.80 (dt, J = 7.8 Hz, 7.7 Hz, 1.9 Hz, 1H, pyridine 4-H), 7.93 (d, J = 8.8 Hz, 2H, Ar 2,6-H), 8.68 (d, J = 4.8 Hz, 1H, pyridine 6-H); MS ($ESI^+$) m/z $\{M+H\}^+$ calcd for $C_{13}H_{11}NOS_2$ 262.0, obsd 261.9.

### 3.4.11 S-2-pyridyl 2-methylbenzothioate (11e)

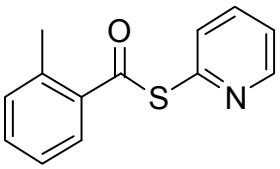

S-2-pyridyl 2-methylbenzothioate (**11e**) was synthesized using literature procedure [27] (scheme 1). A solution of *o*-toluoyl chloride **9e** (1.55 g, 1.30 mL, 10.0 mmol) in $CH_2Cl_2$ (20 mL) was added over 5 min to a stirred solution of 2-mercaptopyridine **10** (1.11 g, 10.0 mmol) in $CH_2Cl_2$ (50 mL) at room temperature. Stirring was continued up to 1 hour. The reaction mixture was neutralized with dilute NaOH. Organic phase was separated, washed twice with water and finally dried with $Na_2SO_4$. Removal of solvent provided brown oil, which was crystallized with Ethylacetate and hexane resulting in bright yellow crystals. Yield: 1.15 g, 5.0 mmol, 50%; mp 85-86 °C; $^1$H NMR ($CDCl_3$) δ 2.52 (s, 3H, Ar-$CH_3$), 7.29 (d, J = 7.6 Hz, 1H, Ar 3-H), 7.32 – 7.36 (m, 2H, Ar 5-H, pyridine 5-H), 7.45 (t, J = 7.6 Hz, 1H, Ar 4-H), 7.75 (d, J = 8.0 Hz, 1H, pyridine 3-H), 7.81 (dt, J = 7.6 Hz, 1.6 Hz, 1H, pyridine 4-H), 7.96 (d, J = 8.0 Hz, 1H, Ar 6-H), 8.71 (d, J = 4.0 Hz, 1H, pyridine 6-H); MS ($ESI^+$) m/z $\{M+MeOH\}^+$ calcd for $C_{13}H_{11}NOS$ 261.08, obsd 261.1.

### 3.4.12 1-(4-Nitrobenzoyl)-5-tolyldipyrromethane (12a)

Dipyrromethane monoacylation (scheme 3) was carried out by modification of a literature procedure[27]. A solution of EtMgBr (25.0 mL, 25.0 mmol, 1.0 M in THF) was carefully added via syringe to a stirred solution of 5-(4-methylphenyl)dipyrromethane **3a** (2.36 g, 10.0 mmol) in THF (10 mL) under Ar. The mixture was stirred at room temperature for 10 min and then cooled to -78 °C. Because of the insoluble nature of the compound, (p-nitrobenzoyl)pyridyl thioester **11a** (2.60 g, 10.0 mmol) was then added directly to the reaction mixture with a positive flow of nitrogen. Alternatively a suspension of **11a** in THF could also be used. The solution was maintained at -78 °C for 10 min, and then the cooling bath was removed. TLC (silica; $CH_2Cl_2$) showed complete conversion of the pyridyl thioester after 15 min, so the reaction was quenched with saturated aqueous $NH_4Cl$. The mixture was allowed to warm to room temperature, poured into $CH_2Cl_2$, washed with water, and then dried ($Na_2SO_4$) and the solvent removed to afford a dark foam. Purification by gradient flash column chromatography (silica; 80% $CH_2Cl_2$ in hexanes to 100% $CH_2Cl_2$ gradient) afforded a bright yellow amorphous solid **12a**. Yield: 2.89 g, 7.50 mmol, 75%; mp 82-83$^oC$; $^1H$ NMR ($CDCl_3$) δ 2.34 (s, 3H, Ar-$CH_3$), 5.53 (s, 1H, *meso* CH), 6.0 (s, 1H, pyrrole 3-H), 6.14 (t, J = 3.2 Hz, 1H, pyrrole(subst) 3-H), 6.17 (dd, J = 5.7 Hz, 2.8 Hz, 1H, pyrrole 4-H), 6.70 (d, J = 1.2 Hz, 1H, pyrrole 5-H), 6.77-6.78 (dd, 3.7 Hz, 2.5 Hz, 1H, pyrrole(subst) 4-H), 7.12 (app q, J = 8.0 Hz, 4H, $CH_3$-Ar 2,3,5,6-H), 7.93 (d, J = 8.8 Hz, 2H, $NO_2$-Ar 2,6-H), 8.06 (bs, 1H, pyrrole NH), 8.31 (d, J = 8.8 Hz, 2H, $NO_2$-Ar 3,5-H), 9.72 (bs, 1H, pyrrole(subst) NH); $^{13}C$ NMR ($CDCl_3$) δ 21.0, 43.8, 107.8, 108.7, 111.2, 117.8, 121.5, 123.5, 128.2, 129.6, 129.7, 129.9, 130.6, 137.2, 137.3, 143.3, 143.7, 149.5, 181.9; MS (ESI$^-$) m/z {M-H}$^-$ calcd for $C_{23}H_{18}N_3O_3$ 384.1, obsd 384.2.

### 3.4.13 1-(3-Nitrobenzoyl)-5-tolyldipyrromethane (12b)

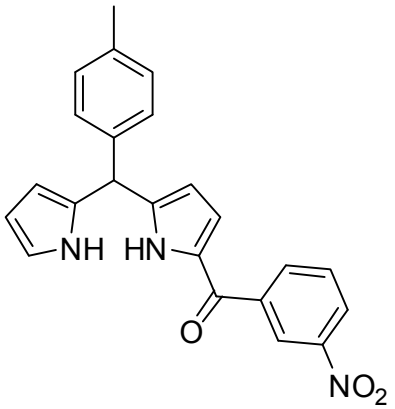


A solution of EtMgBr (12.5 mL, 12.5 mmol, 1.0 M in THF) was carefully added via syringe to a stirred solution of 5-(4-methylphenyl)dipyrromethane **3a** (1.18 g, 5.0 mmol) in THF (10 mL) under Ar. The mixture was stirred at room temperature for 10 min and then cooled to -78 °C, (m-nitrobenzoyl)pyridyl thioester **11b** (1.30 g, 5.0 mmol) in THF (10 mL) was then added into the reaction mixture over one minute. The solution was maintained at -78 °C for 10 min, and then the cooling bath was removed. TLC (silica; $CH_2Cl_2$) showed complete conversion of the pyridyl thioester after 15 min, so the reaction was quenched with saturated aqueous $NH_4Cl$. The mixture was allowed to warm to room temperature, poured into $CH_2Cl_2$, washed with water, and then dried ($Na_2SO_4$) and the solvent removed to afford a dark foam. Purification by gradient flash column chromatography (silica; 80% $CH_2Cl_2$ to pure $CH_2Cl_2$) afforded **12b** as a dark brown oil (1.12g, 58%, 2.91 mmol); $^1$H NMR ($CDCl_3$) δ 2.32 (s, 3H, Ar-$CH_3$), 5.55 (s, 1H, *meso* CH), 5.99 (s, 1H, pyrrole 3-H), 6.15-6.17 (m, 2H, pyrrole 4-H, pyrrole(subst) 3-H), 6.68 (s, 1H, pyrrole 5-H), 6.81-6.82 (m, 1H, pyrrole(subst) 4-H), 7.07-7.12 (m, 4H, $CH_3$-Ar 2,3,5,6-H), 7.65 (t, J = 8.0 Hz, 1H, $NO_2$-Ar 5-H), 8.10 (d, J = 8.0 Hz, 1H, $NO_2$-Ar 6-H), 8.19 (bs, 1H, pyrrole NH), 8.39 (d, J = 8.0 Hz, 1H, $NO_2$-Ar 4-H), 8.66 (s, 1H, $NO_2$-Ar 2-H), 10.05 (bs, 1H, pyrrole(subst) NH); $^{13}$C NMR ($CDCl_3$) δ 20.9, 43.6, 107.6, 108.3, 111.2, 117.7, 121.8, 123.7, 125.9, 127.6, 128.0, 128.4, 128.9, 129.3, 129.7, 130.8, 134.5, 136.8, 137.5, 139.6, 144.0, 147.8, 181.5; MS ($ESI^+$) m/z $\{M+H\}^+$ calcd for $C_{23}H_{20}N_3O_3$ 386.1, obsd 386.1.

### 3.4.14 1-(4-bromobenzoyl)-5-(4-(methylthio)phenyl)dipyrromethane (12c)

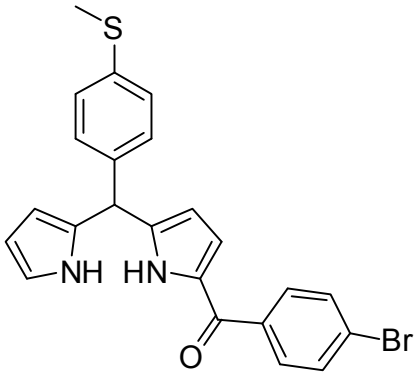


Dipyrromethane monoacylation (scheme 3) was carried out using a literature procedure[27]. A solution of EtMgBr (12.5 mL, 12.5 mmol, 1.0 M in THF) was carefully added via syringe to a stirred solution of 5-(4-Methylthiophenyl)dipyrromethane (**3b**) (2.68 g, 10.0 mmol) in THF (10 mL) under Ar. The mixture was stirred at room temperature for 10 min and then cooled to -78 °C. A solution of (*p*-bromobenzoyl) pyridyl thioester **11c** (2.94 g, 10.0 mmol) in THF (10 mL) was then added over 1 minute. The solution was maintained at -78 °C for 10 min, and then the cooling bath was removed. TLC (silica; Heptane / $CH_2Cl_2$) showed complete conversion of the pyridyl thioester after 15 min, so the reaction was quenched with saturated aqueous $NH_4Cl$. The mixture was allowed to warm to room temperature, poured into $CH_2Cl_2$, washed with water, and then dried ($Na_2SO_4$) and the solvent removed to afford a dark foam. Purification by gradient flash column chromatography (silica; 80% $CH_2Cl_2$ in hexanes to 100% $CH_2Cl_2$ gradient) afforded pale yellow amorphous solid **12c**. Yield: 4.00 g, 8.86 mmol, 89%; $^1$H NMR ($CDCl_3$) δ 2.44 (s, 3H, S-$CH_3$), 5.51 (s, 1H, *meso* CH), 5.98 (s, 1H, pyrrole 3-H), 6.10 (t, J = 3.2 Hz, 1H, pyrrole(subst) 3-H), 6.15 (q, J = 2.8 Hz, 1H, pyrrole 4-H), 6.68 (dd, J = 2.4 Hz, 1.2 Hz, 1H, pyrrole 5-H), 6.78 (dd, 3.7 Hz, 2.5 Hz, 1H, pyrrole(subst) 4-H), 7.08 (d, J = 8.4 Hz, 2H, $CH_3$-S-Ar 2,6-H), 7.14 (d, J = 8.4 Hz, 2H, $CH_3$-S-Ar 3,5-H), 7.59 (d, J = 8.8 Hz, 2H, Br-Ar 3,5-H), 7.66 (d, J = 8.8 Hz, 2H, Br-Ar 2,6-H), 8.27 (bs, 1H, pyrrole NH), 9.99 (bs, 1H, pyrrole(subst) NH).

### 3.4.15 5,15-Di-p-tolyl-10,20-di-p-nitrophenylporphyrin (13a)

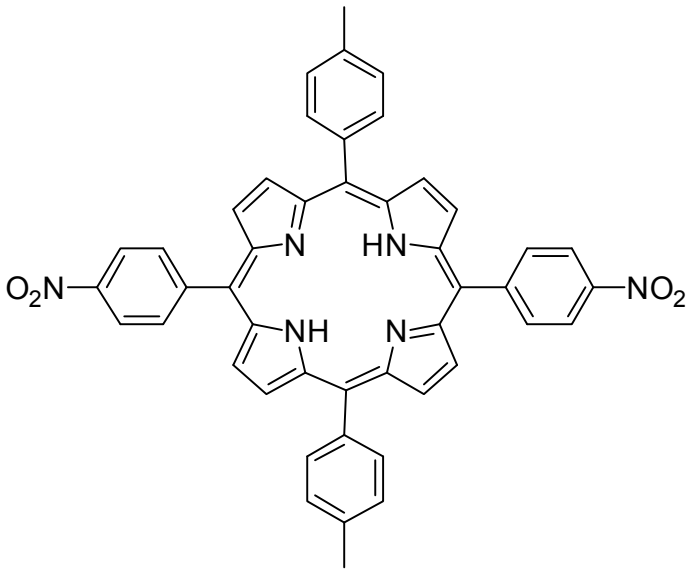


Following a published procedure[27] (scheme 4), $NaBH_4$ (600 mg, 16.0 mmol, 30 molar equiv.) was carefully and slowly added in small portions to a stirred solution of 1-(4-nitrobenzoyl)-5-toluoyldipyrromethane **12a** (200 mg, 0.52 mmol) in THF/methanol (3:1, 15 mL) at room temperature. The progress of the reduction was followed by TLC (silica, hexanes/ethyl acetate (9:1)). The reaction was complete after 20-30 min., the reaction mixture was then quenched with water (30 mL) and then poured into $CH_2Cl_2$ (30 mL). The organic phase was isolated, washed with water (2 x 30 mL), and then dried ($K_2CO_3$), filtered and solvent removed to afford the carbinol **12a'** as an orange/brown oil. The carbinol **12a'** (~0.52 mmol) was immediately dissolved in 200 mL of acetonitrile, and TFA (0.22 mL, 3.00 mmol) was added. The solution instantly darkened. After 3-5 min DDQ (230 mg, 1.00 mmol) was added and the mixture stirred at room temperature for 1 h. Then triethylamine (0.42 mL, 3.00 mmol) was added, and the entire reaction mixture was then filtered through a pad of alumina (eluted with $CH_2Cl_2$) until the eluent was no longer dark. Removal of the solvent gave a dark solid that was fully redissolved in $CH_2Cl_2$ (~20 mL) and filtered through a pad of silica (eluted with $CH_2Cl_2$) to afford **13a** as a purple solid (45.0 mg, 0.06 mmol, 24% starting from **12a)**; $^1$H NMR ($CDCl_3$) δ -2.79 (s, 2H, pyrrole NH), 2.72 (s, 6H, Ar-$CH_3$), 7.58 (d, J = 8.0 Hz, 4H, 5,15-Ar 3,5-H), 8.09 (d, J = 8.0 Hz, 4H, 5,15-Ar 2,6-H), 8.40 (d, J = 8.8 Hz, 4H, 10,20-Ar 2,6-H), 8.65 (d, J = 8.8 Hz, 4H, 10,20-Ar 3,5-H), 8.74 (d, J = 4.8 Hz, 4H, β-pyrrole), 8.93 (d, J = 4.8 Hz, 4H, β-pyrrole); MS (ESI$^+$) m/z $\{M+H\}^+$ calcd for $C_{46}H_{33}N_6O_4$ 733.3, obsd 733.2; FT-IR (powder, $cm^{-1}$) ν 1514 (NO stretch), 1345 (NO stretch). $\lambda_{max}$ ($CH_2Cl_2$)/nm (log ε) 421 (5.40), 517 (4.23), 554 (4.04), 591 (3.78), 648 (3.69).

### 3.4.16 5,15-Di-p-tolyl-10,20-di-m-nitrophenylporphyrin (13b)

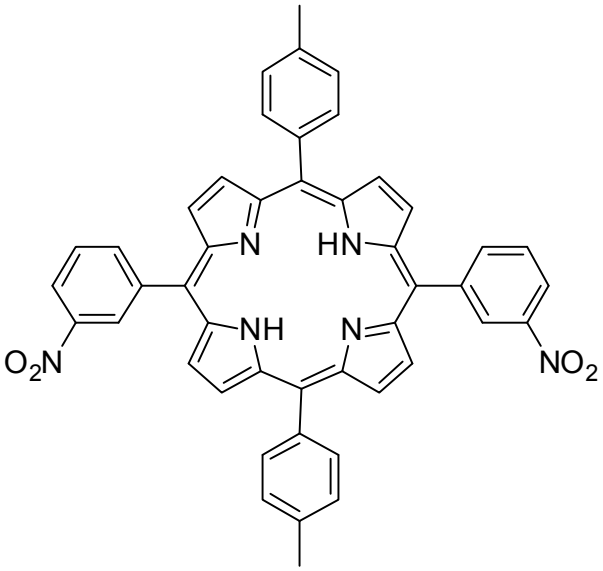


$NaBH_4$ (1.42 g, 37.5 mmol, 30.0 molar equiv.) was carefully and slowly added in small portions to a stirred solution of 1-(4-nitrobenzoyl)-5-toluoyldipyrromethane **12b** (480 mg, 1.25 mmol) in THF/methanol (3:1, 15 mL) at room temperature. The progress of the reduction was followed by TLC (silica, hexanes/ethyl acetate (9:1)). The reaction was complete after 20-30 min., so the reaction mixture was quenched with water (30 mL) and then poured into $CH_2Cl_2$ (30 mL). The organic phase was isolated, washed with water (2 x 30 mL), and then dried ($K_2CO_3$) and the solvent removed to afford the carbinol **12b'** as a brown oil. The carbinol **12b'** (~1.25 mmol) was immediately dissolved in 250 mL of acetonitrile, and TFA (0.60 mL, 8.00 mmol) was added. The solution instantly darkened. After 3-5 min DDQ (0.57 g, 2.50 mmol) was added and the mixture stirred at room temperature for 1 h. Then triethylamine (1.10 mL, 8.00 mmol) was added, and the entire reaction mixture was then filtered through a pad of alumina (eluted with $CH_2Cl_2$) until the eluent was no longer dark. Removal of the solvent gave a dark solid that was fully redissolved in $CH_2Cl_2$ (~20 mL) and filtered through a pad of silica (eluted with $CH_2Cl_2$) to afford **13b** as a purple solid (120 mg, 0.16 mmol, 26% starting from **12b**); $^1$H NMR ($CDCl_3$) δ -2.78 (s, 2H, pyrrole NH), 2.72 (s, 6H, Ar-$CH_3$), 7.58 (d, J = 7.6 Hz, 4H, 5,15-Ar 3,5-H), 7.96 (t, J = 7.6 Hz, 2H, 10,20-Ar 5-H), 8.10 (d, J = 7.6 Hz, 4H, 5,15-Ar 2,6-H), 8.55 (d, J = 7.2 Hz, 2H, 10,20-Ar 6-H), 8.69 (d, J = 8.0 Hz, 2H, 10,20-Ar 4-H), 8.73 (d, J= 4.0 Hz, 4H, β-pyrrole), 8.94 (d, J = 4.0 Hz, 4H, β-pyrrole), 9.1 (s, 2H, 10,20-Ar 2-H); MS (ESI$^+$) m/z $\{M+H\}^+$ calcd for $C_{46}H_{33}N_6O_4$ 733.3, obsd 733.2; FT-IR (powder, $cm^{-1}$) ν 1528 (NO stretch), 1344 ( NO stretch). $\lambda_{max}$ ($CH_2Cl_2$)/nm (log ε) 421 (5.61), 516 (4.37), 552 (4.07), 589 (3.92), 647 (3.68).

### 3.4.17 5,15-Di-p-tolyl-10,20-di-p-aminophenylporphyrin (14a)

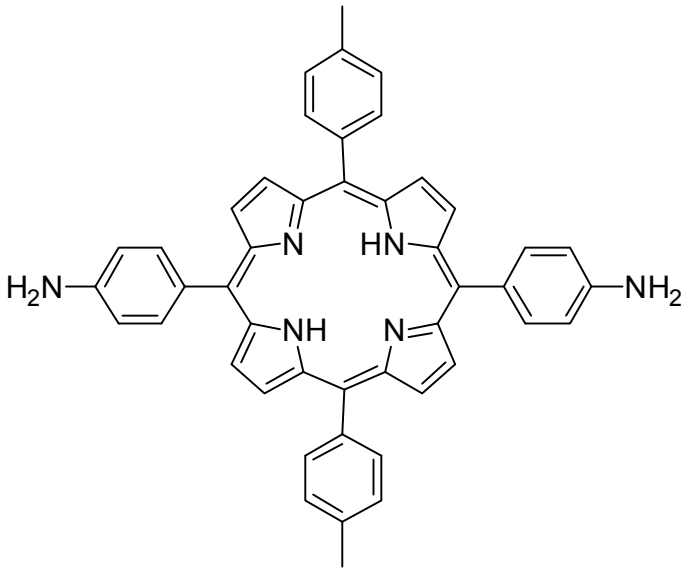


Following a literature procedure[32] (scheme 5), product **13a** (30.0 mg, 0.04 mmol) was dissolved in concentrated hydrochloric acid (30%, 10 mL) at 70 °C, to which was added $SnCl_2 \cdot 2H_2O$ (226 mg, 1.00 mmol). The resulting mixture was continued stirring at 70 °C for 30 min and then cooled to 0 °C. After neutralization with aqueous $NH_3$, the resulting product was extracted with dichloromethane, solvemt was evaporated and dried under vacuum, yielding **14a** as purple crystals (27.0 mg, 0.04 mmol, quant.). $^1$H NMR (DMSO-$d_6$): δ -2.82 (s, 2H, pyrrole NH), 2.67 (s, 6H, Ar-$CH_3$), 5.58 (s, 4H, Ar-$NH_2$), 7.0 (d, J = 7.2 Hz, 4H, 10,20-Ar 3,5-H), 7.62 (d, J = 7.2 Hz, 4H, 5,15-Ar 3,5-H), 7.85 (d, J = 7.2 Hz, 4H, 10,20-Ar 2,6-H), 8.09 (d, J = 7.2 Hz, 4H, 5,15-Ar 2,6-H), 8.80 (d, J = 4.0 Hz, 4H, β-pyrrole), 8.93 (d, J = 4.0 Hz, 4H, β-pyrrole); MS (ESI$^+$) m/z $\{M+H\}^+$ calcd for $C_{46}H_{37}N_6$ 673.3, obsd 673.2; FT-IR (powder, $cm^{-1}$) ν 3345 (NH stretch), 2917 (NH stretch), 1612 (NH bend). $\lambda_{max}$ ($CH_2Cl_2$)/nm (log ε) 424 (5.48), 520 (4.22), 559 (4.16), 593 (3.87), 653 (3.86).

### 3.4.18 5,15-Di-p-tolyl-10,20-di-m-aminophenylporphyrin (14b)

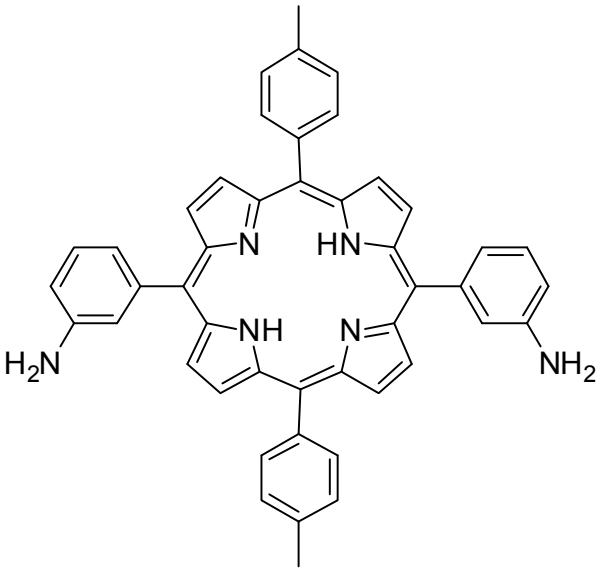


**13b** (60 mg, 0.08 mmol) was dissolved in concentrated hydrochloric acid (30%, 10 mL) at 70 °C, to which was added $SnCl_2 \cdot 2H_2O$ (1.13 g, 5.00 mmol). The resulting mixture was stirred at 70 °C and was monitored by TLC. After 30 minutes, the reaction mixture was cooled to 0 $^oC$. After neutralization with aqueous $NH_3$, the resulting product was extracted with dichloromethane, solvent was evaporated and dried under vacuum, yielding **14b** as purple crystals (55.0 mg, 0.08 mmol, quant.). $^1H$ NMR (DMSO-$d_6$): δ -2.77 (s, 2H, pyrrole NH), 2.70 (s, 6H, Ar-$CH_3$), 3.86 (bs, 4H, Ar-$NH_2$), 7.06 (d, J = 7.2 Hz, 2H, 10,20-Ar-H), 7.47-7.56 (m, 8H, 10,20-Ar-H, 5,15-Ar 3,5-H), 7.63 (d, J = 7.2 Hz, 2H, 10,20-Ar-H), 8.11 (d, J = 7.6 Hz, 4H, 5,15-Ar 2,6-H), 8.87 (d, J = 4.4 Hz, 4H, β-pyrrole), 8.94 (d, J = 4.4 Hz, 4H, β-pyrrole); MS ($ESI^+$) m/z $\{M+H\}^+$ calcd for $C_{46}H_{37}N_6$ 673.3, obsd 673.4; FT-IR (powder, $cm^{-1}$) ν 3342 (NH stretch), 2920 (NH stretch), 1598 (NH bend). $\lambda_{max}$ ($CH_2Cl_2$)/nm (log ε) 421 (5.43), 516 (4.18), 552 (3.94), 589 (3.79), 647 (3.61).

### 3.4.19 5,15-Di-p-tolyl-10,20-di-p-thiolphenylporphyrin (4')

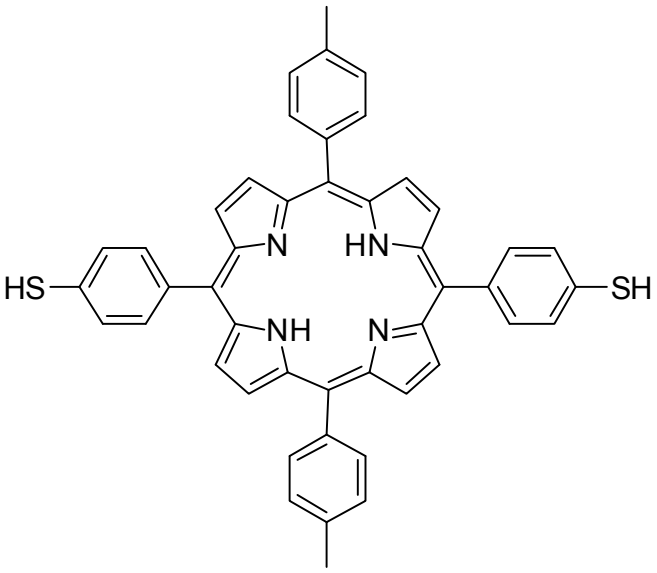


A Leuckart thiophenol reaction[34] (scheme 6) was performed to obtain pure *trans* dithiol porphyrin **4'**. 27.0 mg (0.04 mmol) of 5,15-di-p-tolyl-10,20-di-p-aminophenylporphyrin **14a** was dissolved in 10 mL of concentrated hydrochloric acid and heated until the slurry was transformed to a solution. The solution was cooled to 0-5 °C with continued

stirring. A 1 mL solution of sodium nitrite (0.05 M solution; 1.25 equiv.) was added and the mixture was stirred for an hour at 0-5 °C. Next, a 1 mL aqueous solution of potassium ethyl xanthate (0.10 M solution, 2.50 equiv.) was added and the reaction mixture was heated to 40-45 °C and stirred for another hour. A 1 M KOH solution was added until the pH was basic (pH = 12-13) and the solution was refluxed overnight. The pH was lowered to 6 using dilute hydrochloric acid and then the solution was extracted with 30 mL dichloromethane. The organic phase was washed with water (2 x 20 mL), dried with sodium sulfate, filtered and evaporated, yielding **4'** as purple crystals (20.0 mg, 0.03 mmol, 71%). $^1$H NMR ($CDCl_3$): δ -2.81 (s, 2H, pyrrole NH), 2.71 (s, 6H, Ar-$CH_3$), 7.57 (d, J = 8.0 Hz, 4H, 5,15-Ar 3,5-H), 7.74 (d, J = 8.4 Hz, 4H, 10,20-Ar 3,5-H), 8.09 (d, J = 8.0 Hz, 4H, 5,15-Ar 2,6-H), 8.14 (d, J = 8.4 Hz, 4H, 10,20-Ar 2,6-H), 8.81 (d, J = 4.8 Hz, 4H, β-pyrrole), 8.89 (d, J = 4.8 Hz, 4H, β-pyrrole); MS (ESI$^-$) m/z $\{M-H+Cl+H_2O\}^{2-}$ calcd for $C_{46}H_{35}ON_4S_2Cl$ 379.1, obsd 379.1. $\lambda_{max}$ ($CH_2Cl_2$)/nm (log ε) 419 (5.93), 515 (4.68), 551 (4.51), 588 (4.37), 646 (4.18).

## 3.4.20 5,10,15,20-tetrakis(4-aminophenyl) porphyrin (15)

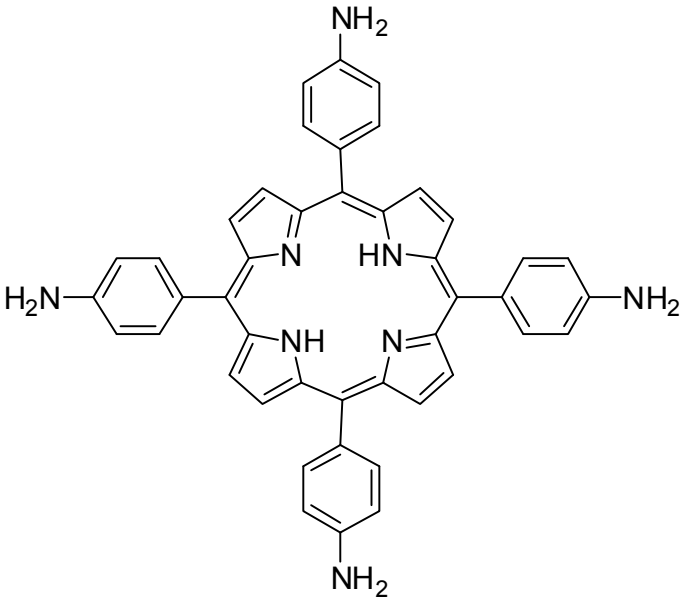


A literature procedure [32] was used to synthesize **15**. 4-nitrobenzaldehyde (5.5 g, 36.4 mmol) and acetic anhydride (6 mL, 63.6 mmol) were dissolved in propionic acid (150 mL). The solution was refluxed, to which pyrrole (2.5 mL, 36.0 mmol) was slowly added. After refluxing for 30 minutes, the resulting mixture was flitered to get black solid which was washed with water and methanol, and dried under vacuum. The dried powder was dissolved in pyridine (40 mL) which was refluxed for 1 hour. After cooling, the precipitate was collected by filtration and washed with acetone to give 5,10,15,20-tetrakis(4-nitrophenyl) porphyrin as purple crystals (1.0 g, 1.26 mmol, 14% yield). The product was dissolved in hot HCl (500 mL) at 70 $^o$C, to

which added $SnCl_2 \cdot 2H_2O$ in large excess (~ 25 equivalents). The resulting mixture was stirred at 70°C for 2 hours and reaction was monitored by TLC. After neutralization with aqueous $NH_3$, the resulting greyish product was collected by filtration and gradient flash chromatography ($CH_2Cl_2$/acetone) was perfomed to get the pure product **15** (770 mg, 1.14 mmol, 90 %). $^1$H NMR was similar to the reported values.[32]: $^1$H NMR ($CDCl_3$): δ -2.71 (s, 2H, pyrrole NH), 4.03 (bs, 8H, Ar-$NH_2$), 7.07 (d, J = 7.2 Hz, 8H, 5,10,15,20-Ar 3,5-H), 7.99 (d, J = 7.2 Hz, 8H, 5,10,15,20-Ar 2,6-H), 8.90 (s,8H, β-pyrrole).

## 3.4.21 5,10,15,20-tetrakis(4-bromophenyl) porphyrin (16)

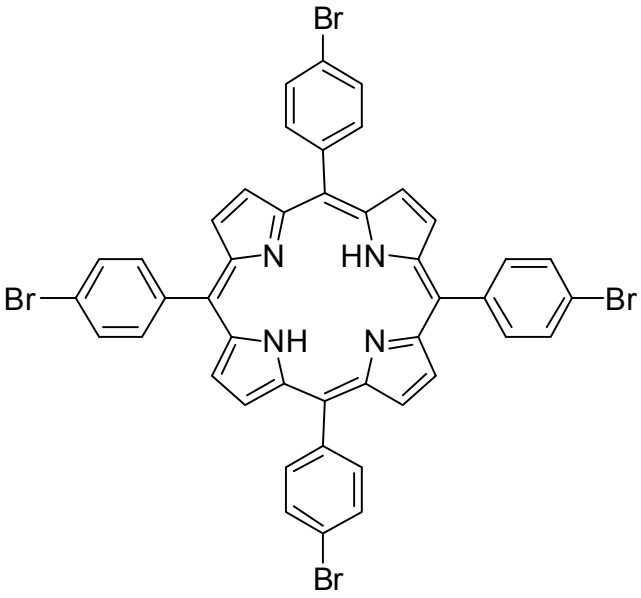


Classical Adler and Longo method [11] was used to synthesize 5,10,15,20-tetrabromophenyl porphyrin. Freshly distilled pyrrole (6.94 mL, 0.1 mole) and reagent grade 4-bromobenzaldehyde (18.5 g, 0.1 mol) were added to 400 mL of refluxing reagent grade propionic acid. After 30 minutes, the solution is cooled down to room temperature and filtered. The filter cake was washed thoroughly with methanol and with hot water. The resulting purple crystals were dried in vacuum oven yielding **16** as tetrabromophenyl porphyrin (13.95 g, 15 mmol, 15 %). $^1$H NMR was similar to the reported values.[42]: $^1$H NMR ($CDCl_3$): δ -2.86 (s, 2H, pyrrole NH), 7.91 (d, J = 8Hz, 8H, 5,10,15,20-Ar 3,5-H), 8.07 (d, J = 8 Hz, 8H, 5,10,15,20-Ar 2,6-H), 8.84 (s,8H, β-pyrrole).

## 3.4.22 5,10,15,20-tetrakis(*p*-thiomethoxyp*henyl*) porphyrin (17)

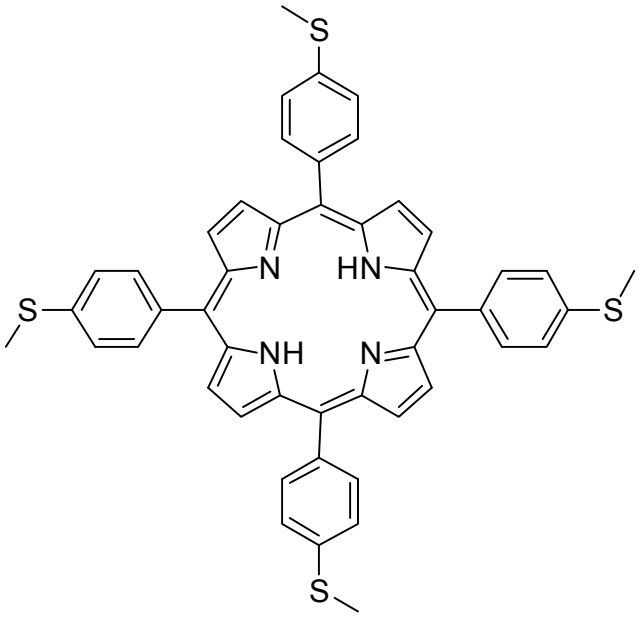


A similar method as described above was used for the synthesis of **17**.[43] Pyrolle (0.69 mL, 0.01 mole) and reagent grade 4-methylthio benzaldehyde (1.33 mL, 0.01 mol) were added to 50 mL of refluxing reagent grade propionic acid. After 30 minutes, the solution was cooled down to room temperature and filtered. The filter was washed thoroughly with methanol. The resulting purple crystals were dried in vacuum oven yielding **17** of tetra(thiomethoxy)phenyl porphyrin (0.8 g, 1 mmol, 10 %). $^1$H NMR was similar to the reported values.[43]: $^1$H NMR ($CDCl_3$): δ -2.81 (s, 2H, pyrrole NH), 2.78 (s, 12H, ArS-$CH_3$), 7.61 (d, J = 8 Hz, 8H, 5,10,15,20-Ar 2,6-H), 8.11 (d, J = 8 Hz, 8H, 5,10,15,20-Ar 3,5-H), 8.85 (s,8H, β-pyrrole).

## 3.4.23 {5,15-Di-p-tolyl-10,20-di-p-thiolphenylporphyrinato}zinc (18)

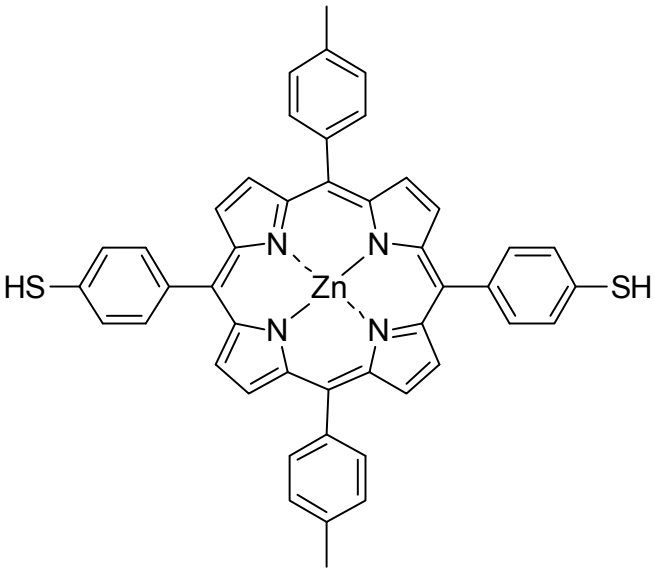


A similar method as described in [31] was used to prepare Zn derivative of **4'**. A solution of $Zn(OAc)_2 \cdot 2H_2O$ (10 mg, 45.5 μmol) in MeOH (2.5 mL) was added to a solution of **4'** (5 mg, 7.0 μmol) in THF (7.5 mL). The mixture was stirred at room temperature for 2 hours. The reaction was monitored by TLC, which shows the completion of the reaction. Solvent was evaporated and product was dissolved in

dichloromethane and excess Zinc acetate was removed by washing twice with water. Removal of the solvent yielded pure product **18** (5.4 mg, 7.0 μmol, quantitative yield). We were not able to get a proper $^{1}$H-NMR, but the spectra shows clear disappearance of pyrrolic-NH protons. MS (ESI$^{-}$) m/z $\{M-H+CF_3COO+2DMSO+CH_3CN\}^{2-}$ calcd for $C_{54}H_{48}F_3N_5O_4S_4Zn$ 538.6, obsd 538.7.

## 3.4.24 {5,10,15,20-tetrakis(4-aminophenyl)porphyrinato}zinc(II) (19)

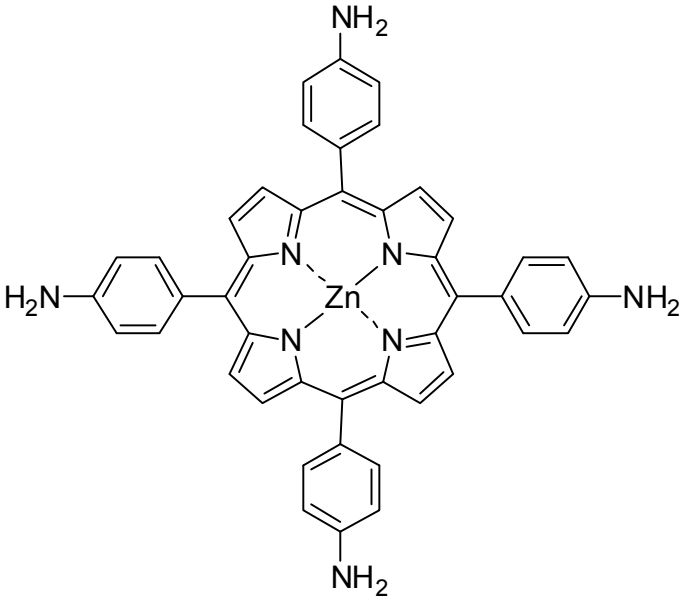


Zinc metal insertion in tetraaminophenyl porphyrin 15 above was performed by the method desribed in the literature [31]. A solution of $Zn(OAc)_2 \cdot 2H_2O$ (0.2 g, 0.91 mmol) in MeOH (5 mL) was added to a solution of xx (0.1 g, 0.15 mmol) in THF (15 mL). The mixture was stirred at room temperature for 2-3 hours. The reaction was monitored by TLC, which shows the completion of the reaction. Solvent was evaporated and product was dissolved in dichloromethane and excess Zinc acetate was removed by washing twice with water. Removal of the solvent yielded pure product (0.11 g, 0.15 mmol, quantitative yield). $^{1}$H-NMR clearly shows the disappearance of pyrrolic-NH protons. $^{1}$H NMR (DMSO): δ 5.45 (s, 8H, Ar-$NH_2$), 6.97 (d, J = 8.0 Hz, 8H, 5,10,15,20-Ar 3,5-H), 7.81 (d, J = 8.0 Hz, 8H, 5,10,15,20-Ar 2,6-H), 8.84 (s,8H, β-pyrrole).

## 3.5 References


1. Anderson, H.L., *Building molecular wires from the colours of life: conjugated porphyrin oligomers.* Chemical Communications, 1999(23): p. 2323-2330.
2. Grill, L., et al., *Nano-architectures by covalent assembly of molecular building blocks.* Nature Nanotechnology, 2007. **2**: p. 687-691.
3. Sedghi, G., et al., *Single molecule conductance of porphyrin wires with ultralow attenuation.* Journal of the American Chemical Society, 2008. **130**(27): p. 8582-+.
4. Winters, M.U., et al., *Probing the efficiency of electron transfer through porphyrin-based molecular wires.* Journal of the American Chemical Society, 2007. **129**(14): p. 4291-4297.
5. Kang, B.K., et al. *Electrical transport properties and their reproducibility for linear porphyrin arrays*. in *Meeting of the European-Materials-Research-Society*. 2005. Strasbourg, FRANCE.
6. Kanehara, M., H. Takahashi, and T. Teranishi, *Gold(0) porphyrins on gold nanoparticles.* Angewandte Chemie-International Edition, 2008. **47**(2): p. 307-310.
7. Sivanesan, A. and S.A. John, *Amino group position dependent orientation of self-assembled monomolecular films of tetraaminophthalocyanatocobalt(II) on Au surfaces.* Langmuir, 2008. **24**(5): p. 2186-2190.
8. Satake, A., et al., *Single supramolecular porphyrin wires bridging gold nanoparticles.* Chemical Communications, 2009(10): p. 1231-1233.
9. Gryko, D.T., C. Clausen, and J.S. Lindsey, *Thiol-derivatized porphyrins for attachment to electroactive surfaces.* Journal of Organic Chemistry, 1999. **64**(23): p. 8635-8647.
10. Jagessar, R.C. and J.M. Tour, *Synthesis of porphyrins bearing trans-thiols.* Organic Letters, 2000. **2**(2): p. 111-113.
11. Adler, A.D., et al., *A Simplified Synthesis for Meso-Tetraphenylporphin.* Journal of Organic Chemistry, 1967. **32**(2): p. 476-&.
12. Meng, G.G., et al., *Porphyrin Chemistry Pertaining to the Design of Anticancer Drugs .2. the Synthesis and in-Vitro Tests of Water-Soluble Porphyrins Containing, in the Meso Positions, the Functional-Groups - 4-Methylpyridinium, or 4-Sulfonatophenyl, in Combination with Phenyl, 4-Pyridyl, 4-Nitrophenyl, or 4-Aminophenyl.* Canadian Journal of Chemistry-Revue Canadienne De Chimie, 1994. **72**(12): p. 2447-2457.
13. Lee, C.H. and J.S. Lindsey, *One-Flask Synthesis of Mesosubstituted Dipyrromethanes and Their Application in the Synthesis of Trans-Substituted Porphyrin Building-Blocks.* Tetrahedron, 1994. **50**(39): p. 11427-11440.
14. Littler, B.J., Y. Ciringh, and J.S. Lindsey, *Investigation of conditions giving minimal scrambling in the synthesis of trans-porphyrins from dipyrromethanes and aldehydes.* Journal of Organic Chemistry, 1999. **64**(8): p. 2864-2872.
15. Geier Iii, G.R., B.J. Littler, and J.S. Lindsey, *Investigation of porphyrin-forming reactions. Part 3.1 The origin of scrambling in dipyrromethane[space]+[space]aldehyde condensations yielding trans-A2B2-tetraarylporphyrins.* Journal of the Chemical Society, Perkin Transactions 2, 2001(5): p. 701-711.
16. Lindsey, J.S., *Synthetic Routes to meso-Patterned Porphyrins.* Accounts of Chemical Research, 2009. **43**(2): p. 300-311.

17. Kruper, W.J., T.A. Chamberlin, and M. Kochanny, *Regiospecific Aryl Nitration of Meso-Substituted Tetraarylporphyrins - a Simple Route to Bifunctional Porphyrins.* Journal of Organic Chemistry, 1989. **54**(11): p. 2753-2756.
18. Zhang, H.L., W.M. Shi, and J. Wu, *Regiospecific aryl nitration of meso-tetraarylporphyrins: The directive effect of para-substituent.* Heterocycles, 2005. **65**(12): p. 3001-3006.
19. Ostrowski, S. and A.M. Raczko, *Selective double functionalization of meso-tetraphenylporphyrin complexes on the same pyrrole unit by tandem electrophilic/nucleophilic aromatic substitution.* Helvetica Chimica Acta, 2005. **88**(5): p. 974-978.
20. Ostrowski, S. and B. Lopuszynska, *Preparation of meso-tetraarylporphyrins nitrated in two neighboring aromatic rings.* Synthetic Communications, 2003. **33**(23): p. 4101-4110.
21. Pollard, M.M. and J.C. Vederas, *A convenient preparation of thioether functionalized porphyrins.* Tetrahedron, 2006. **62**(51): p. 11908-11915.
22. Gryko, D.T. and M. Tasior, *Simple route to meso-substituted trans-A(2)B(2)-porphyrins bearing pyridyl units.* Tetrahedron Letters, 2003. **44**(16): p. 3317-3321.
23. Gill, H.S., et al., *Facile oxidative rearrangement of dispiro-porphodimethenes to nonplanar and sheetlike porphyrins with intense absorptions in the near-IR region.* Angewandte Chemie-International Edition, 2004. **43**(4): p. 485-490.
24. Dogutan, D.K., M. Ptaszek, and J.S. Lindsey, *Rational or statistical routes from 1-acyldipyrromethanes to meso-substituted porphyrins. Distinct patterns, multiple pyridyl substituents, and amphipathic architectures.* Journal of Organic Chemistry, 2008. **73**(16): p. 6187-6201.
25. Ravikanth, M., et al., *Trans-substituted porphyrin building blocks bearing iodo and ethynyl groups for applications in bioorganic and materials chemistry.* Tetrahedron, 1998. **54**(27): p. 7721-7734.
26. Imaoka, T., R. Tanaka, and K. Yamamoto, *Investigation of a molecular morphology effect on polyphenylazomethine dendrimers; Physical properties and metal-assembling processes.* Chemistry-a European Journal, 2006. **12**(28): p. 7328-7336.
27. Rao, P.D., et al., *Efficient synthesis of monoacyl dipyrromethanes and their use in the preparation of sterically unhindered trans-porphyrins.* Journal of Organic Chemistry, 2000. **65**(4): p. 1084-1092.
28. Littler, B.J., et al., *Refined synthesis of 5-substituted dipyrromethanes.* Journal of Organic Chemistry, 1999. **64**(4): p. 1391-1396.
29. Abdelrazzaq, F.B., R.C. Kwong, and M.E. Thompson, *Photocurrent generation in multilayer organic-inorganic thin films with cascade energy architectures.* Journal of the American Chemical Society, 2002. **124**(17): p. 4796-4803.
30. Naik, R., et al., *Facile synthesis of meso-substituted dipyrromethanes and porphyrins using cation exchange resins.* Tetrahedron, 2003. **59**(13): p. 2207-2213.
31. Grozema, F.C., et al., *Supramolecular control of charge transport in molecular wires.* Journal of the American Chemical Society, 2007. **129**: p. 13370-+.
32. Yuasa, M., et al., *Micellar cobaltporphyrin nanorods in alcohols.* Journal of the American Chemical Society, 2004. **126**(36): p. 11128-11129.
33. Michael B. Smith, J.M., ed. *March's Advanced Organic Chemistry: Reactions, Mechanisms, and structure, 6th Edition*. 6th ed. 2007, John Wiley & Sons, Inc. 2384.
34. Tarbell, D.S. and M.A. McCall, *The Basic Isomerization of Allyl Aryl Sulfides to Propenyl Aryl Sulfides.* Journal of the American Chemical Society, 1952. **74**(1): p. 48-56.

35. Rillema, D.P., et al., *Redox Properties of Metalloporphyrin Excited-States, Lifetimes, and Related Properties of a Series of Para-Substituted Tetraphenylporphine Carbonyl-Complexes of Ruthenium(Ii)*. Journal of the American Chemical Society, 1981. **103**(1): p. 56-62.
36. Rao, P.D., et al., *Rational syntheses of porphyrins bearing up to four different meso substituents.* Journal of Organic Chemistry, 2000. **65**(22): p. 7323-7344.
37. Pinchart, A., et al., *Efficient formation of aromatic thiols from thiomethylated precursors.* Tetrahedron Letters, 1999. **40**(30): p. 5479-5482.
38. Falvo, R.E., L.M. Mink, and D.F. Marsh, *Microscale synthesis and H-1 NMR analysis of tetraphenylporphyrins.* Journal of Chemical Education, 1999. **76**(2): p. 237-239.
39. Clausen, C., et al., *Investigation of tightly coupled porphyrin arrays comprised of identical monomers for multibit information storage.* Journal of Organic Chemistry, 2000. **65**(22): p. 7371-7378.
40. Geier, G.R., et al., *A survey of acid catalysts in dipyrromethanecarbinol condensations leading to meso-substituted porphyrins.* Journal of Porphyrins and Phthalocyanines, 2001. **5**(12): p. 810-823.
41. Zaidi, S.H.H., et al., *9-Acylation of 1-acyldipyrromethanes containing a dialkylboron mask for the alpha-acylpyrrole motif.* Journal of Organic Chemistry, 2004. **69**(24): p. 8356-8365.
42. Nielsen, C.B. and F.C. Krebs, *Aspects of investigating scrambling in the synthesis of porphyrins: different analytical methods.* Tetrahedron Letters, 2005. **46**(35): p. 5935-5939.
43. Dattagupta, N., et al., *Synthesis and Properties of 3 Sulfur-Containing Porphyrins, One Water-Soluble.* Bulletin of the Chemical Society of Japan, 1988. **61**(6): p. 2274-2276.

# CHAPTER 4

## Au Nanorods as Bottom-up Nanoelectrodes

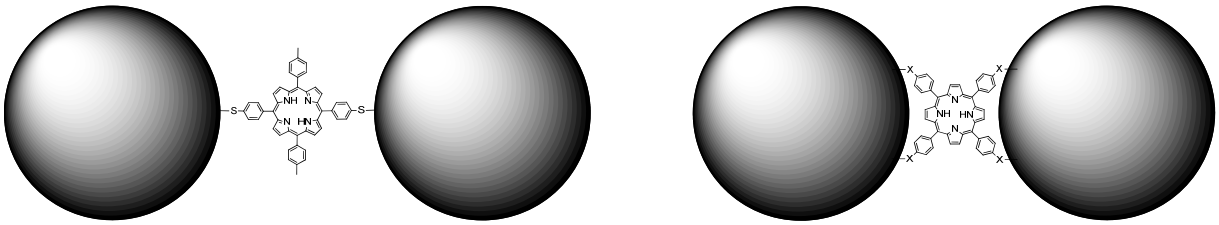

Porphyrin molecules interacting with gold nanoparticles in different orientations based on number of linker groups present on the porphyrins.

With the aim to investigate the potential of Au nanorods as bottom-up nanoelectrodes for contacting single molecules, the interaction of porphyrin molecules with gold nanoparticles and gold nanorods was studied to get insight into their binding affinity and electronic properties of the Au-nanoparticle – porphyrin assemblies. Porphyrins were chosen for such studies because of their interesting spectroscopic and electronic properties and possibility to tune electronic and magnetic properties via the central metal atom. The results show that these molecules indeed interact with gold nanoparticles and nanorods, but binding is dependent on the number of linker moieties present on the porphyrin molecules and on the morphology of the nanoparticles. Tetraaminophenyl porphyrin causes unspecific binding of nanoparticles, resulting in agglomeration of nanoparticles, whereas controlled binding of nanoparticles was achieved using trans-dithiolphenyl porphyrins, where 2-3 nanoparticles were specifically connected to each other. Individual Au nanorods were successfully contacted with micro electrodes and were also aligned by end-to-end linkage using cysteine, however attempts to contact aligned Au nanorods with microelectrodes were unsuccessful because of their movement on the silicon wafer upon micro fabrication.

## 4.1 Introduction

In molecular electronic studies, the reliable fabrication of nanoelectrodes with a single molecule contact is of significant importance, but has so far relied on stochastic approaches with associated low yields and high uncertainty. A promising approach towards such contacts is the use of metallic nanoparticles spaced by bridging molecules. In this context Au nanorods are of special interest because elongated shape allows use of such rods as bottom-up nano electrodes, which can be easily contacted further to complete the electronic arrangement. Recent work has shown that such nanorods can be selectively functionalized at their ends,[1] because molecules are more easily exchanged, presumably due to higher curvature and larger defect density.

Au nanorods have been known to align with each other and make end-to-end contact e.g. formation of Au-nanorod dimers via aromatic and aliphatic dithiols[2, 3]. Long chain formation of aligned gold nanorods has been achieved via covalent connection or small molecule supramolecular interactions,[4-8] protein-substrate recognition[9-12] oligonucleotide hybridization[13], and amphiphilic triblock copolymers[14]. The growth of nanoparticles, functionalized with dithiol-polyethylene glycol, to aligned nanorods is an alternative strategy to prepare such nanoelectrodes.[15] Other strategies to link molecules between nanoelectrodes include the in situ stepwise synthesis of functional multi-junction molecular wires on gold electrodes and gold nanoparticles[16], controlled assembly of gold nanoparticles in one dimensional array between electrodes using an electrophoresis process[17], and the fabrication of two-dimensional nanoparticle arrays using DNA motifs.[18]

These and other nanoparticle-molecule assemblies have frequently been used to study electronic interactions and charge and energy transport between inorganic nanoparticles and organic molecules. For instance, conducting probe atomic force microscopy with gold nanoparticles to study the conductance of single dithiolated molecules, as well as conductance of conjugated oligomers with thiol end-groups inserted between two dimensional gold nanoparticle arrays was measured.[19, 20] The photoconductance properties of oligo(phenylene vinylene) molecules in metal-molecule-metal junctions were investigated recently. These molecules were electrically contacted in a two-dimensional array of gold

nanoparticles, where nanoparticles were separated by few nanometers.[21] The charge transport properties of gold nanoparticle networks linked by terthiophene molecules have been observed and such systems have potential to be used in nano-scale electronics.[22] Additionally, molecular electronic measurements on a single gold nanoparticle for the assessment of a nanoparticle bridge platform have been achieved.[23] Gold nanoparticles have been used in nonvolatile memory electronic devices using bifunctional π-conjugated molecules as linkers between nanoparticles and reduced graphene oxide sheets.[24]

Despite these successes, so far there are only few reports on the use of molecular spaced gold nanorod assemblies as nanoelectrodes [15, 25, 26]. The aim of this work is to investigate the potential of Au nanorods as bottom-up nanoelectrodes for contacting single molecules. For the molecules, the focus of this study was on porphyrin molecules because of their conjugated structure, interesting spectroscopic and electronic properties;[27, 28] and possibility to tune electronic and magnetic properties via the central metal atom.[29, 30] There are few examples in literature, where porphyrins have been shown to interact with gold nanoparticles,[31, 32] however these examples lack any details on the electronic properties of these hybrid materials.

To get further insights for porphyrin–nanorod interaction, an interesting aspect for such studies was to use model systems such as interaction of gold nanoparticles and gold nanorods with porphyrins in solution, which may afford valuable information about molecule-nanoparticle interactions, and will guide further single molecule studies on porphyrin junctions.

In this work the potential of gold nanorods as bottom-up nanoelectrodes for contacting single molecules is investigated. Spherical and rod-shaped gold nanoparticles have been synthesized following literature protocols, and their interactions with various porphyrin molecules have been studied (figure 1). These porphyrins differ in the nature and number of gold-binding groups located at their periphery. Their synthesis has been described in chapter 3.

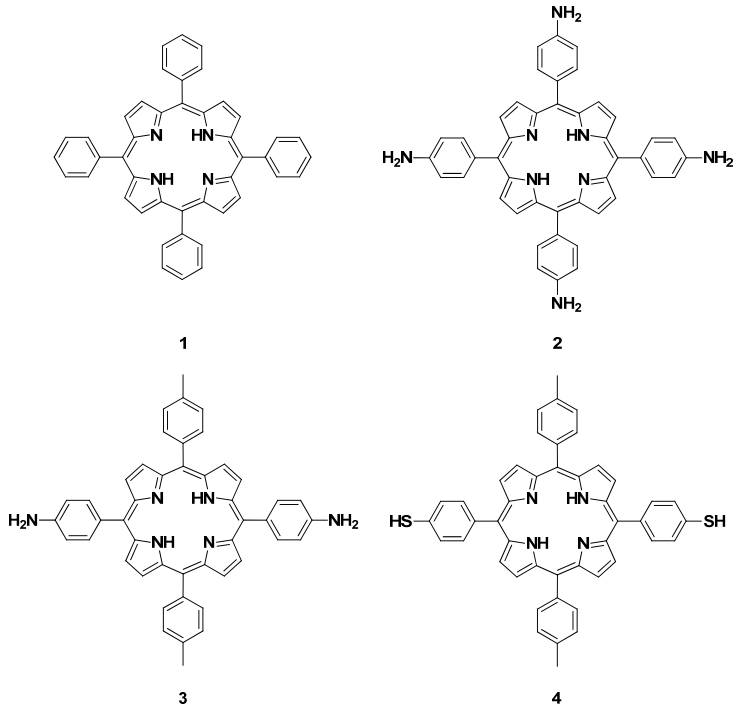


Fig. 1: Porphyrins used to study their binding with Au-NPs.

UV-Vis spectroscopy, fluorescence spectroscopy, gel permeation chromatography (GPC), dynamic light scattering (DLS) and scanning electron microscopy (SEM) were used to investigate interaction of porphyrins with gold nanoparticles and gold nanorods in our studies. Finally, attempts to contact such rods as nanoelectrodes are described.

## 4.2 Results and discussions

### 4.2.1 Synthesis of gold nanoparticles

#### 4.2.1.1 Spherical nanoparticles

Gold nanoparticles (Au-NPs) were synthesized in organic phase and aqueous phase according to the literature procedures.[33, 34]. For aqueous phase Au-NPs, $HAuCl_4$ salt solution was reduced by sodium borohydride in presence of sodium citrate. The solution immediately turned orange-red, indicating the formation of gold nanoparticles, which were further grown by aqueous solution of $HAuCl_4$, CTAB and ascorbic acid. For organic phase Au-NPs, dodecylamine was initially dissolved in cyclohexane, and then aqueous formaldehyde was added. After vigorously stirring at room temperature, the cyclohexane phase was separated

out. Aqueous $HAuCl_4$ solution was added into the separated cyclohexane. The color turned to deep ruby red indicating the formation of gold nanoparticles. For organic phase gold nanoparticles, the UV-Vis absorption spectrum showed a strong band at 515 nm characteristic for a gold plasmon band, indicating that gold nanoparticles with a diameter of 6-9 nm were formed.[35] This was confirmed by DLS, which revealed that nanoparticles with a diameter of 7.6 ± 0.8 nm were formed.

The formation of gold nanoparticles in aqueous phase was confirmed by UV-Vis absorption spectroscopy, which shows a strong band at 525 nm, characteristic for a gold plasmon band, indicating that gold nanoparticles with a diameter of 18-20 nm were formed. Scanning electron microscopy (figure 2), showed that the average size of these aqueous phase Au nanoparticles corresponded to 22 ± 3 nm. Size distribution was determined by counting size of ~50 individual nanoparticles under SEM microscope.

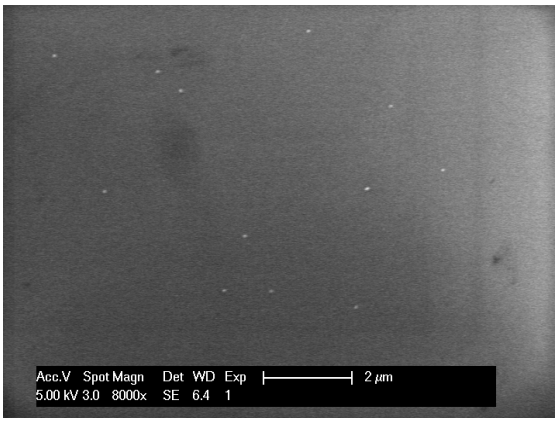


Fig. 2: SEM image of spherical Au-NPs prepared in aqueous phase.

#### 4.2.1.2 Concentration of gold nanoparticles

In order to find out the binding affinity of porphyrins to a nanoparticle and quantify porphyrin molecules bound to a single gold nanoparticle, we needed to know the concentration of nanoparticles. The extinction coefficient of nanoparticles solution can also calculated, once the concentration is known. However, determining the concentration of nanoparticles is difficult because the precursor salt is reduced to nanoparticles solution, where each nanoparticle constitute number of gold atoms. If the size of nanoparticles is determined, then by using a standard formula, number of gold atoms in each particle can be calculated, which leads us to the concentration of gold nanoparticles.

The concentration of gold nanoparticles in solution (organic phase) was determined by the method described by Huo et al [36] and Guo et al [37], using the average Au-NP size. Repeated DLS measurements showed that the average particle consisting of an Au core and a surfactant shell had a hydrodynamic diameter of 7.6 ± 0.8 nm. Assuming a length of 1.6 nm for an extended dodecylamine surfactant molecule, the particles contain an Au core of approximately of 4.4 ± 0.8 nm. This corresponds to 2650 ± ~1450 atoms for each nanoparticle, if it is assumed that all the particles are spherical in shape. Face-centered cubic gold density parameters were used to calculate the number of Au atoms per nanoparticle. [36, 38].

On dividing the concentration of total Au atoms with the number of Au atoms present in each nanoparticle, the concentration of Au-NPs can be estimated, assuming that all the precursor gold salt has been transformed into nanoparticles. Starting from 5 mM solutions of $AuCl_3.3H_2O.HCl$, the concentration of gold nanoparticles in the organic phase is estimated as $1.9 \times 10^{-6}$ M in THF. All fluorescence and UV experiments were carried out with same nanoparticle solution for accuracy purposes. However for GPC experiments, a new batch was synthesized, where DLS showed slightly larger nanoparticles.

#### 4.2.1.3 Rod-shaped nanoparticles

Gold nanorods (Au-NRs) of aspect ratio ~ 25 were synthesized in aqueous phase according to the literature procedure.[39, 40] Gold-seeds were initially produced by reducing $HAuCl_4$ salt with sodium borohydride in presence of sodium citrate. The colour of gold nanoparticles seed solution was orange. These seeds were grown to gold nanorods by introducing them to three different growth solutions containing cetyltrimethylammonium bromide, $HAuCl_4$, ascorbic acid and NaOH. A small quantity of seed solution was introduced to first growth solution, from which a small fraction was taken and introduced to second growth solution. Similarly a small part from second growth solution was taken and added to third growth solution. The resulting solutions had a reddish brown color, indicating the formation of gold nanorods. The UV-Vis absorption indeed showed two absorption maxima confirming the formation of Au nanorods. The strong band at 525 nm was assigned to the transverse plasmon band, and the relatively weak band at roughly 660 nm to the longitudinal plasmon band of the Au nanorods. These rods were separated from spherical side products by centrifuging them at 1500 rpm for 20 minutes and the supernatant fluid was discarded. Addition of water redispersed nanorods

in the solution. Scanning electron microscopy (SEM) confirmed the formation of gold nanorods with diameters of 20 ± 4 nm, and lengths of 500 ± 100 nm (figure 3). The statisitical distribution was measured for 50 individual rods from the SEM image.

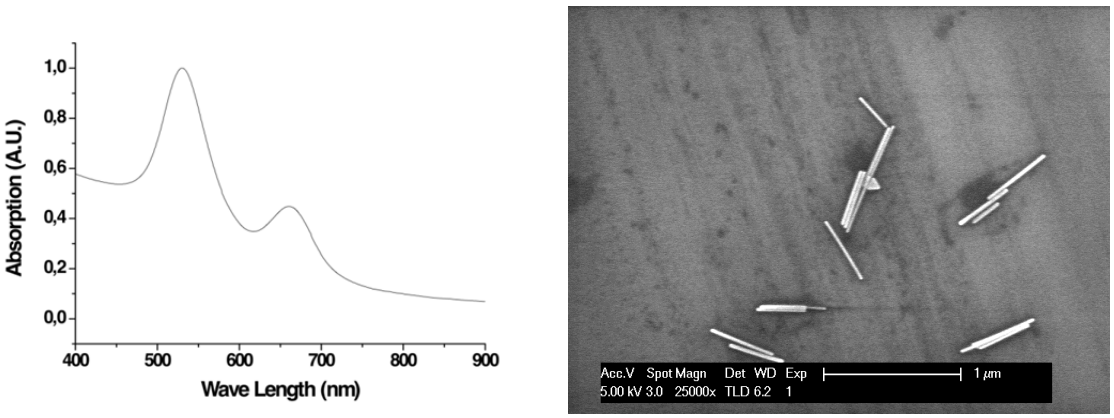


Fig. 3: Surface plasmon resonance of non-spherical gold nanorods having both transverse and longitudinal absorption peaks and SEM picture of gold nanorods with average 500 nm length.

### 4.2.2 Binding of porphyrins to spherical gold nanoparticles

In this section, we studied binding of porphyrins to Au-NPs as a model surface for molecular electronic studies. UV-Vis and fluorescence spectroscopy techniques were used because changes in electronic spectra were expected upon addition of gold nanoparticles because of the electronic interactions between porphyrins and gold nanoparticles. UV-Vis spectroscopy can be used to observe any change in size of particles or the agglomeration of particles by monitoring change in the absorption peak of nanoparticles. It was also used to determine the number of porphyrins attached to each nanoparticle (see paragraph 4.2.5).

In a first series of experiments, UV-Vis spectrophotometric titrations of porphyrins **1**, **2**, **3**, and **4** by Au-NPs were performed. Figure 4 shows a series of UV-Vis spectra obtained upon adding increasing amounts of Au-NP solution to a solution of porphyrin **4**.

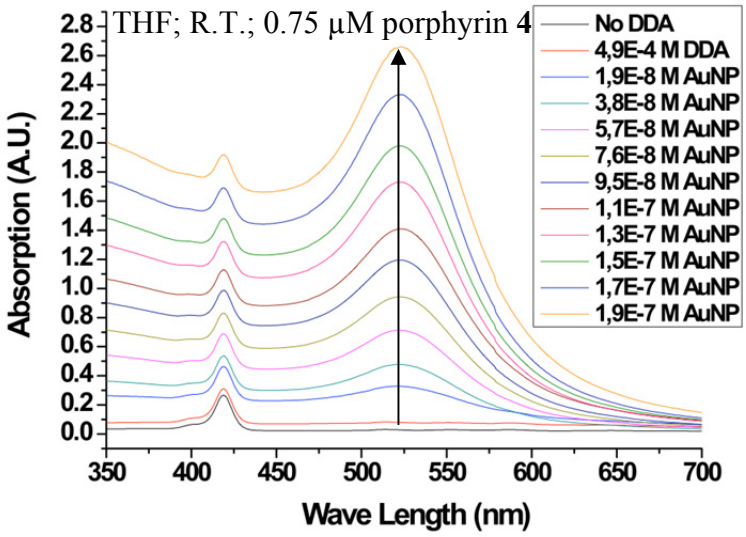


Fig. 4: UV-Vis absorption spectra of porphyrin **4**, which shows that increase in absorption is due to increase in absorption of Au-NPs. The intensity of the porphyrin peak around 420 nm remains same for all titration measurements, obvious from height of the peak from the base line for each peak.

Analysis revealed that the change of the spectra shown in figure 4 with each aliquot of nanoparticles was due to absorption of gold nanoparticles only. The absorption spectrum of porphyrins was not changed by the addition of Au nanoparticles. Similar results were obtained for porphyrins **1**, **2**, and **3**. The absence of changes in the porphyrin indicates that either the porphyrins did not bind to the Au-NPs, or that there is only a (very) weak electronic interaction between the porphyrins and the Au-NPs.

Fluorescence spectroscopy was used to investigate binding of porphyrins to gold nanoparticles, because fluorescence quenching is usually more sensitive to electronic interactions. The steady state fluorescence was expected to decrease with each and every addition of Au-NPs, as the porphyrins linked to nanoparticles were expected to transfer their excitation energy to nanoparticles. The steady state fluorescence studies were complemented by lifetime fluorescence measurements, to reveal whether fluorescence quenching is static or dynamic in nature.

Steady state and life time fluorescence spectroscopy techniques were used to study the interaction of gold nanoparticles with various porphyrin molecules. Titrations were carried out with Au-NPs of average size 4.4 nm in THF. The porphyrins were excited at their Soret

band (around 420 nm), where the extinction coefficient is very high. The Au-NPs have their surface plasmon resonance at around 515 nm. Stern-Volmer plot was calculated as $F_o/F$ versus Au-NP concentration. $F_o$ and F represents the fluorescence intensity of porphyrins before addition of quencher and after the addition of quencher, respectively, and [Q] represents concentration of quencher, in this case the Au-NPs.

First, as a control the effect of Au-NPs on the fluorescence of tetraphenyl porphyrin (TPP) **1** was studied. Since TPP **1** does not have any groups capable of binding to Au-NPs, strong quenching of the fluorescence was not expected.

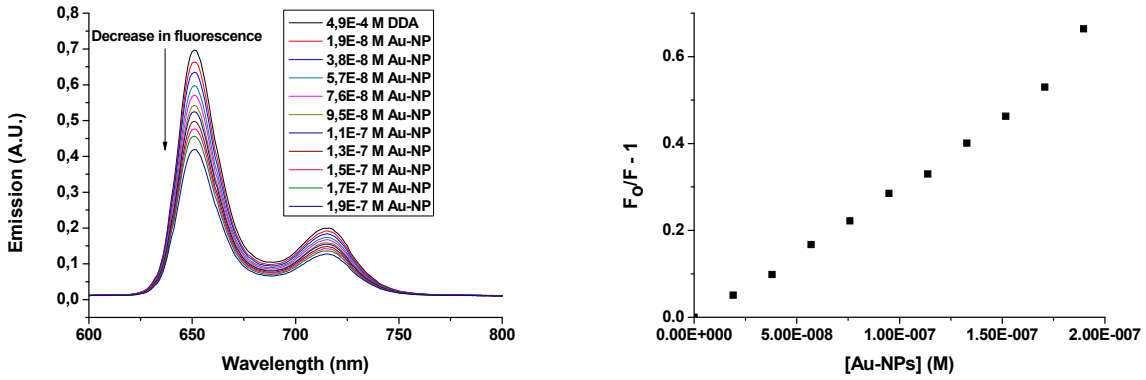


a b

Fig. 5: (a) Fluorescence quenching of TPP (1) by addition of Au-NPs. Excitation at 417 nm, emission maxima at 651 nm and 716 nm and (b) Stern-Volmer Plot for TPP (**1**) quenching with Au-NPs.

Remarkably, the addition of Au-NPs to solution of **1** resulted in a significant decrease of the porphyrin fluorescence (figure 5a). The Stern-Volmer plot generally represents quenching constant, which in case of static binding, represents binding constant. The Stern-Volmer plot for TPP (figure 5b) gives a value of $3 \times 10^6$ $M^{-1}$ as quenching constant. This measurement can be considered as the standard interaction of porphyrins with gold nanoparticles without any functional group present. Most likely, the observed decrease in fluorescence intensity of partly attributed to inner filter effects of Au-NPs because of their high absorption at around 420 nm, and partly due to unspecific binding of TPP to the Au-NP by interaction with the aliphatic monolayer covering the Au-NPs. We were able to calculate the contribution of inner filter effects (vide infra), and we attribute the remaining quenching effect to unspecific binding. Consequently, any additional quenching effects present in other porphyrins in a first

approximation may be regarded as resulting from of specific binding of the porphyrin by their functional groups to the Au-NPs.

Figure 6 shows the effect of nanoparticles on the fluorescence of porphyrin **2**, which has four additional amino groups compared to TPP.

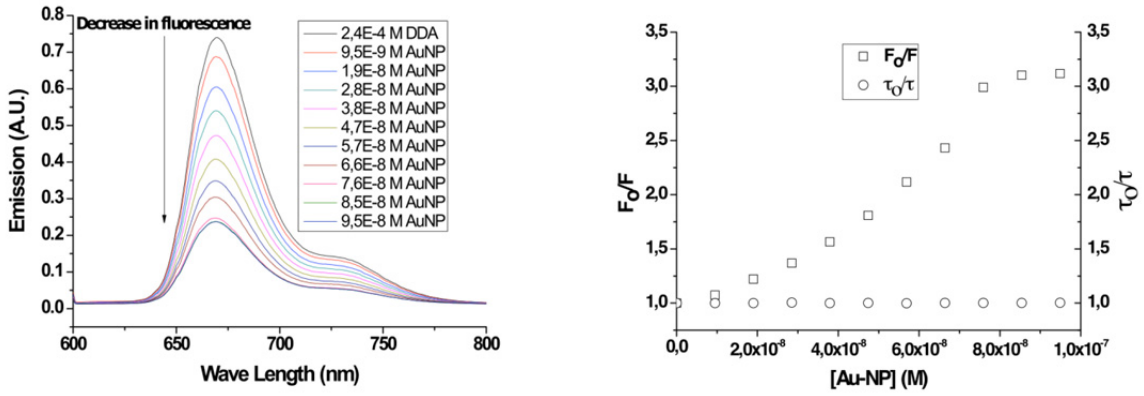


a b

Fig. 6: (a) Fluorescence quenching of porphyrin **2** when Au-NPs are added and (b) quenching constant and binding constant of Au-NPs with porphyrin **2** is 3 x $10^7$ $M^{-1}$, calculated from the Stern-Volmer plot. Life time fluorescence measurement of porphyrin **2** when mixed with Au-NPs.

The addition of Au-NPs to solutions of porphyrin **2** also resulted in quenching of its fluorescence, although much stronger than for porphyrin **1**. The quenching can be described by the Stern Volmer equation, and the Stern Volmer constant of porphyrin **2** with Au-NPs amounted to 3 x $10^7$ (figure 6b). This value is significantly higher than was found for porphyrin **1**, indicating a stronger interaction between **2** and Au-NPs. Time resolved fluorescence measurements revealed that the fluorescence lifetime was not affected by the addition of Au-NPs, indicating that quenching of the fluorescence of **2** by Au-NPs is a static process, where gold nanoparticles inhibit the excited state formation by forming a non-fluorescent complex. Inner filter effects were kept to a minimum during these measurements by using fluorescence cuvette of 3mm path length, but cannot be excluded completely. As a result, the Stern Volmer quenching constant is only an approximation of the binding constants of the porphyrin to the Au-NPs. Nevertheless, these measurements reveal that porphyrins with four amino groups have high binding affinity with Au-NPs compared to porphyrin **1** with no amino groups.

Because these results clearly indicate that porphyrin **2** with four amino groups binds strongly to Au-NPs, the interaction of porphyrin **3** having two amino groups at *trans* positions with Au-NPs was also investigated. Also for this porphyrin the addition of Au-NPs led to quenching of the porphyrin fluorescence, however, the Stern Volmer quenching constant amounted to only 4 x $10^6$ (figure 7b), indicating that binding of porphyrin **3** with only 2 amino groups at trans positions, is not as strong as for porphyrin **2** with four amino groups.

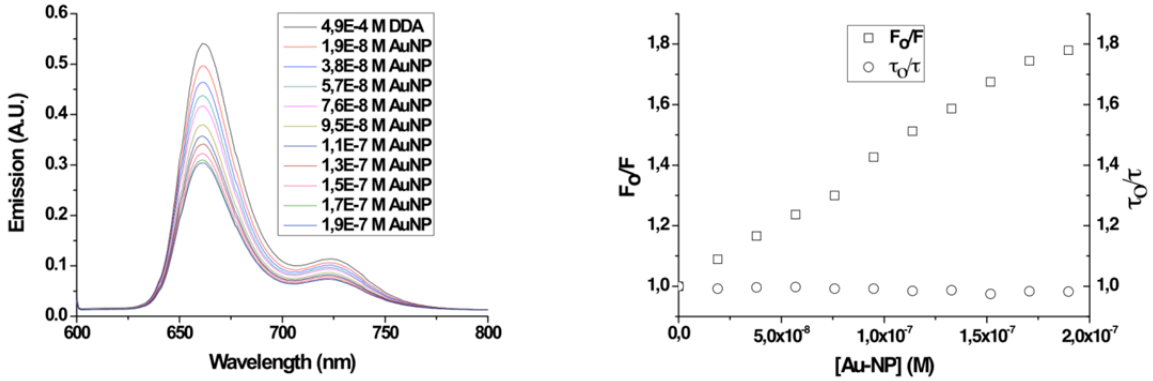


a b

Fig. 7: (a) Fluorescence quenching spectra of porphyrin **3** and (b) Stern Volmer plot for quenching constant. Life-time fluorescence measurements show it is static quenching, confirming that quenching constant is binding constant.

The life time fluorescence measurement (figure 7b) also shows that it is static quenching rather than dynamic quenching, which confirms that quenching constant is binding constant. It is clear that porphyrin **3** has affinity for Au-NPs, but interaction is nearly same as TPP **1**.

Studies with four amino versus two amino groups present in porphyrins reveal that there was much stronger binding for the tetra-amino functionalized porphyrin **2** as compared to the bis-amino functionalized porphyrin **3**. Since thiol functional groups have a higher binding affinity to gold surface as compared to amino groups,[41] it was interesting to study the interaction of thiol-functionalized porphyrins with Au-NPs. The fluorescence quenching of porphyrin **4** results is shown in figure 8a.

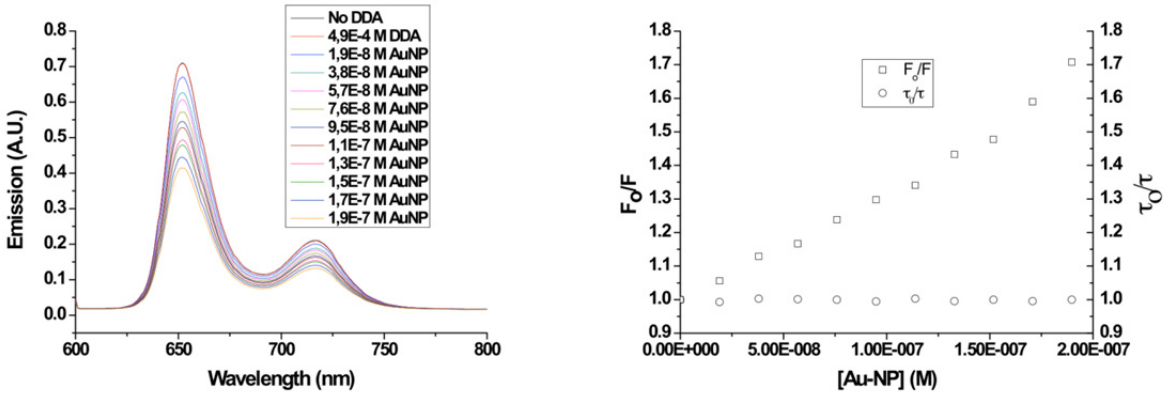


a b

Fig. 8: (a) Fluorescence quenching spectra of porphyrin **4** and (b) Stern Volmer plot for quenching constant. Life-time fluorescence measurements show that it is static quenching, which confirms that the quenching constant is the same as the binding constant.

The Stern-Volmer plot for porphyrin **4** (figure 8b) did not show significant difference in the quenching constant compared to porphyrin **3**, that is 3 x $10^6$. It was slightly lower than porphyrin **3** and similar to TPP (porphyrin **1**), indicating that the presence of two thiol groups at *trans* positions did not lead to significantly stronger interactions with Au-NPs.

Summarizing, porphyrin **2** has binding constant around one order of magnitude higher as compared to porphyrins **1**, **3** and **4**. Porphyrin **3** with two amino groups have marginally higher binding constant as compared to porphyrin **1** without any functional group and porphyrin **4** with two thiol groups present. Porphyrins **1** and **4** show almost similar behavior, which suggests that quenching is due to non-specific binding and/or inner filter effects, and not related to presence or absence of binding groups.

### 4.2.3 Binding of porphyrins to Au-NPs and inner filter effects

Unspecific binding and inner filer effects have been studied in more detail to discriminate between their contributions and gain insight into the nature of the interactions between porphyrins and surfactant-protected Au-NPs. Inner filter effects arise from strong absorption which overlap with the excitation and emission spectrum of interest, leading to partial absorption of the excitation beam as well as emitted light, which in turn results to a decrease of the observed fluorescence intensity. In the situation of porphyrins with Au-NPs, the inner filter effects are due to the strong absorption of the Au-NPs and increase with each addition in

a titration experiment. Inner filter effects can in part be reduced by using a cuvette with short path-length to avoid excessive absorption of the light, but cannot be completely eliminated because of the high extinction coefficient of Au-NPs. These inner filter effects can cause large errors in the evaluation of quenching efficiencies.

It was clear from UV-Vis and fluorescence measurements that there were considerable inner filter effects, during these fluorescence measurements. Inner filter effects were minimized by using cuvette of 3mm path length in all of our measurements. We needed to know the extent of inner filter effects of these nanoparticles on fluorescence measurements, because they heavily influence the calculation of binding constants.

It should be noted that the systems described so far also contain surfactant molecules as stabilizer for the Au-NPs, which have to be replaced in part upon binding of the porphyrin. It is known that dye molecules attached to gold nanoparticles can be replaced by addition of surfactant molecules, resulting in increase of fluorescence, as more dye molecules are liberated from the nanoparticles.[42] It appeared to us that this feature can be exploited to discriminate between fluorescence intensity decrease due to inner filter effects and due to binding, by performing a competitive displacement experiment with an electronically non-absorbing surfactant while keeping the porphyrin and Au-NPs concentrations responsible for the strong absorption and eventual inner filter effects constant. Hence, we carried out such a surfactant displacement experiment with porphyrin **2**, which has the highest binding of the four porphyrins used in our studies, in combination with the gold nanoparticles observed via fluorescence quenching studies. These studies were performed in dichloromethane as solvent. With the fluorescence quenching studies of porphyrin **2** (figure 6), it is clear that at a certain concentration of porphyrins and gold nanoparticles, there is no further fluorescence quenching observed any more. Further addition of gold nanoparticles only result in further inner filter effects and no binding.

Since these concentrations were known already, the simple strategy we used was to treat the porphyrins ($7{,}5 \times 10^{-7}$ M) with gold nanoparticles with the highest concentration ($9{,}5 \times 10^{-8}$ M), obtained from fluorescence quenching studies (figure 9, curve A). Although dodecylamine does not fluoresce, neither it is responsible for inner filter effects, it was realized that dodecylamine by itself could act as a fluorescence quencher. Addition of dodecyl amine to a solution of **2** resulted, however, in only a minor (5%) increase of the fluorescence

of **2** (figure 9, curve B), probably due to deprotonation of any residual protonated amines in **2**. For other porphyrins (e.g. TPP), addition of dodecylamine did not led to an increase or decrease of the fluorescence levels. Because the effect is only minor and specific for **2**, we did not further investigate the cause of increase of fluorescence of porphyrin **2** on addition of dodecyl amine.

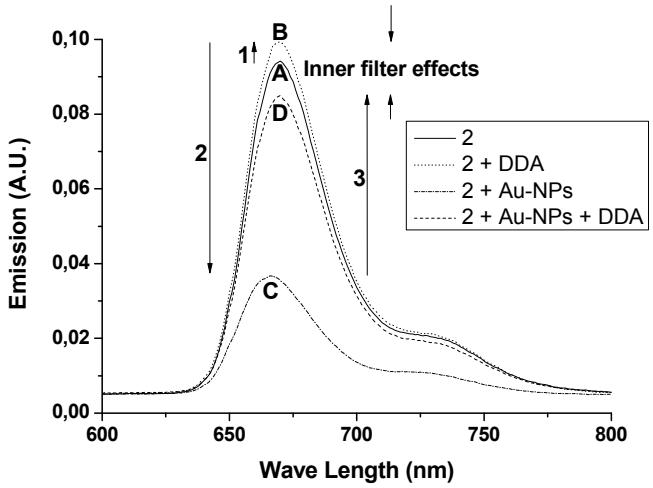


Fig. 9: Effect of DDA, Au-NPs, and inner filter effects on the fluorescence of porphyrin **2**.

Addition of gold nanoparticles (9,5 x $10^{-8}$ M) to a 7,5 x $10^{-7}$ M solution of porphyrin **2** resulted in an immediate quenching of the porphyrin fluorescence (figure 9, curve C). However, addition of DDA liberates porphyrins from the Au-NPs leading to a (partial) restoration of the fluorescence (figure 9, curve D). At this stage there is no interaction of porphyrins with gold nanoparticles and only inner filter effects are visible. The contribution of inner filter effects can now be determined from the difference in fluorescence intensity between curve B compared to the total maximal quenching (curve C). From the intensities in figure 9 it was deduced that the total inner filter effects contribute up to 23 % of total quenching, whereas 77% of the fluorescence decrease of **2** upon addition of Au-NPs is due to binding of porphyrin molecules to gold nanoparticles. These values will be influenced by the amount of gold nanoparticles added, because of change in inner filter effects. Because the binding of porphyrins **1**, **3** and **4** is relatively weak compared to binding of **2,** the possible contribution of inner filter effects to the total quenching was not further investigated.

### 4.2.4 DLS and GPC as complimentary techniques to study porphyrins – gold nanoparticles binding

The fluorescence quenching studies strongly suggest that porphyrin **2** binds to Au-NPs. Further evidence for binding of porphyrin **2** to Au-NPs, was obtained by separation of porphyrins bound to Au-NPs from unbound porphyrin molecules in solution by means of gel permeation chromatography. To this extend, a relatively concentrated 15 mL (~300 μM) solution of porphyrin **2** in THF was added to 1 mL (1 μM) of Au-NPs in THF, and the fraction of porphyrins bound to the gold nanoparticles was determined by gel permeation chromatography (GPC) and UV-Vis spectroscopy.

The Au-NPs used in these experiments had a hydrodynamic diameter of 8.9 nm as measured by DLS, before passing them over the GPC column. When a solution of such 8.9 nm Au-NPs was treated with porphyrin **2** as explained above, and then passed through GPC column to remove the excess porphyrins, a significant increase of the hydrodynamic diameter of the particles was observed by DLS. The agglomerated size of particles was bigger than 1 μm, as is clear from the particle size distribution shown in figure 10a. As a control experiment also Au-NPs without added porphyrin were passed over a GPC column, which unfortunately, also already caused agglomerated of Au-NPs to clusters with a size of ~100 nm. Most likely, the access of surfactant present in the Au-NPs solution was removed through this process resulting in some agglomeration of the Au-NPs.

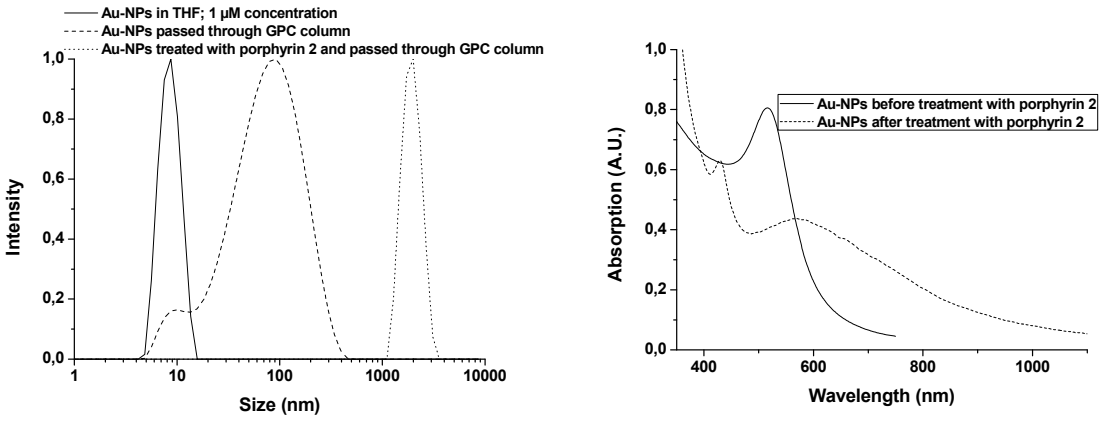


a b

Fig. 10: (a) Normalized intensity distribution curves from DLS measurements for Au-NPs (i) in THF at 1 μM concentration (ii) passed through GPC column (iii) treated with porphyrin **2** and passed through GPC column. (b) UV-Vis absorption spectrum of Au-NPs before and after treatment with porphyrin **2**. Free porphyrins were separated by GPC.

Despite this undesired destabilization of Au-NPs, GPC still could be used to separate porphyrins bound to Au-NPs from the free porphyrins in solution. Figure 10b shows the UV-Vis absorption spectra of the Au-NPs fractions collected from the GPC column in the absence and presence of porphyrin **2.** The spectrum of the Au-NPs treated with porphyrin **2** shows a clear absorption band with a maximum around 420 nm, characteristic for the Soret band of the porphyrin. This clearly indicates that porphyrin **2** is attached to gold nanoparticles. The peak for the Au-NPs has moved from 525 nm to 570 nm, which is a sign that the size of Au-NPs has increased because of huge aggregation. This enhanced aggregation is due to use concentrated solutions of porphyrins and Au-NPs, and removal of surfactants by GPC, resulting in larger overall plasmon resonance leading to red shift in the absorption spectrum.

### 4.2.5 Estimation of number of porphyrins attached to single Au-NP

Estimation of number of porphyrins attached to each Au-NP was next logical step to get further knowledge of the porphyrin – Au-NPs binding. The extinction coefficient of porphyrins and gold nanoparticles in dichloromethane have been determined to be 2,484 x $10^5$ L $mol^{-1}$ $cm^{-1}$ (at 428nm) and 9 x $10^6$ L $mol^{-1}$ $cm^{-1}$ (at 515nm), respectively. Nanoparticles and porphyrins were mixed as described in the previous section, and Au-NP - porphyrin complexes were separated from unbound porphyrin by GPC.

The UV-Vis absorption spectra of the Au-NPs linked with porphyrins are shown in figure 11a.

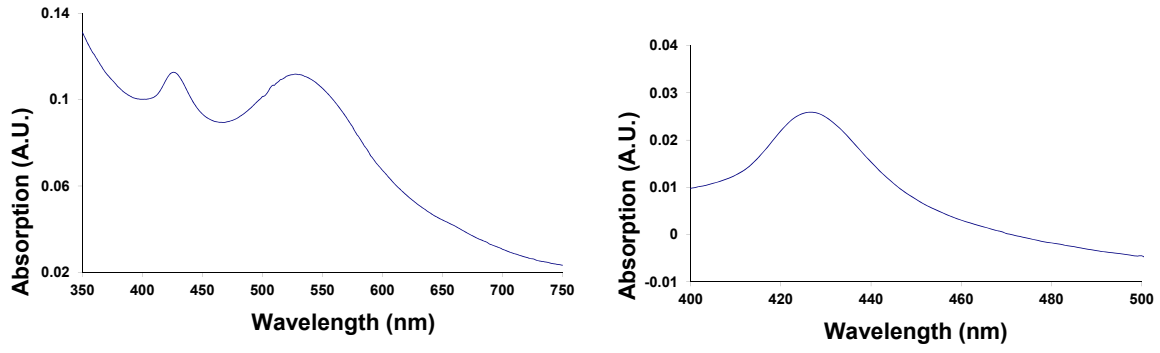


a b

Fig. 11: (a) UV-Vis absorption spectrum for Au-NPs treated with porphyrin **2** and passed through an analytical GPC column. (b) Background corrected for porphyrins.

It was observed that the absorbance maximum associated with the Au-NPs had shifted from 515 nm to 528 nm, which also points to agglomeration of particles due to interaction with porphyrins **2**. The contribution of porphyrin absorption to the total absorption was obtained by subtracting the nanoparticles absorption. From the absorption of the resulting peak at 427 nm (figure 11b) it was calculated that the concentration of porphyrins amounts to ~100 nM, whereas the concentration of Au-NPs is 12-13 nM, which corresponds to roughly 7-9 porphyrins for each Au-NP. It should be noted that these results should be interpreted with care, because distortion of the Au-NPs spectra due to agglomeration prohibited a reliable deconvolution of the spectra.

As an alternate strategy to calculate number of porphyrins attached to each nanoparticle, we measured UV-Vis spectra of porphyrin **2** ($8.25 \times 10^{-7}$ M) and Au-NPs ($8.77 \times 10^{-8}$ M) independently. With various attempts, we were able to regenerate the spectrum in figure 11a of porphyrin coupled to Au-NPs (figure 12), by varying weight (a) and weight (b) according to the following scheme.

Weight (a) x porphyrin spectrum + weight (b) x Au-NPs spectrum = spectrum (figure 11a)

The weight (a) appeared to be 1/16.525 and weight (b) appeared to be 1/7.225. The concentrations of porphyrin and Au-NPs were calculated according to the following formula.

Concentration of porphyrins in figure 11a = weight (a) x concentration of porphyrins only
Concentration of Au-NPs in figure 11a = weight (b) x concentration of nanoparticles only

The concentration of porphyrin appeared to be $5 \times 10^{-8}$ and concentration of Au-NPs appeared to be $1.214 \times 10^{-8}$, which gives a ratio of ~4 porphyrin molecules per nanoparticle.

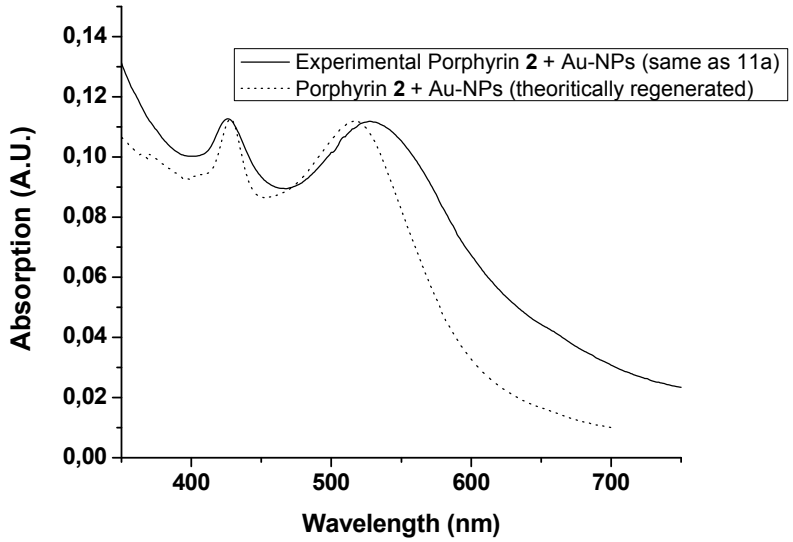


Fig. 12: Regeneration of spectra in figure 11a by adding individual spectra of porphyrins and gold nanoparticles of known concentrations.

### 4.2.6 Coupling of gold nanoparticles in water

The studies described above were performed with spherical Au-NPs in organic phase because of the limited solubility of the porphyrins in water. However, the rod-shaped Au-NPs have been synthesized in aqueous solutions. A suitable common solvent system for both porphyrins and Au-NPs prepared in aqueous solutions appeared to be DMSO in water. Interestingly, the addition of dilute DMSO solution of dithiol porphyrin **4** (0.5 mmolar, 0.4 mL) to 1 μM nanoparticles aqueous solution (1.6 mL) with excess CTAB, resulted in the selective attachment of two or three Au nanoparticles, as observed from the following SEM pictures (figure 13).

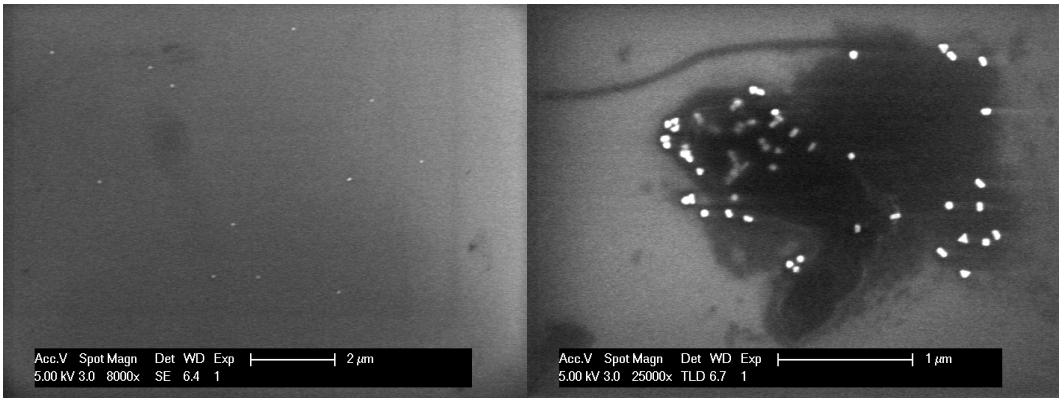


a b

Fig. 13: Selective connection of Au-NPs while using porphyrin 4 in mixture of water and DMSO (20%). (a) Au-NPs appear as isolated particles before treatment with porphyrins, whereas (b) after treatment with porphyrin 4; the Au-NPs appear as small clusters of two to three particles.

UV-Vis absorption spectra of Au-NPs were also measured before and after treatment with porphyrins. After the treatment, the solution (a mixture of DMSO and water) with porphyrins and Au-NPs was extracted with dichloromethane until all the free porphyrins were extracted into the organic layer. The UV-Vis absorption spectrum of aqueous solution was taken, which shows the Soret band of porphyrins in addition to a new shoulder peak for the Au-NPs (figure 14). This shoulder corresponds to the shift of surface plasmon, when two or three particles are joined together as seen from the SEM pictures above.

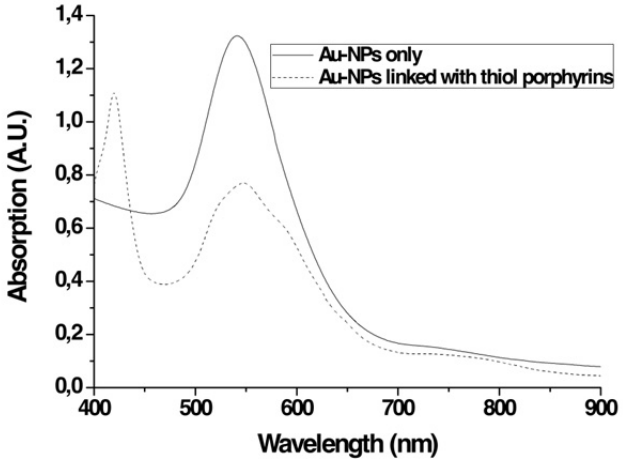


Fig. 14: UV-absorption spectrum of gold nanoparticles with and without thiol porphyrin molecules attached.

### 4.2.7 Binding of porphyrins to gold nanorods

With the successful selective binding of gold nanoparticles in aqueous phase using dithiol porphyrins, we approached to the final step, where linking of two or more gold nanorods as bottom-up nanoelectrodes using porphyrin molecules was considered (figure 15).

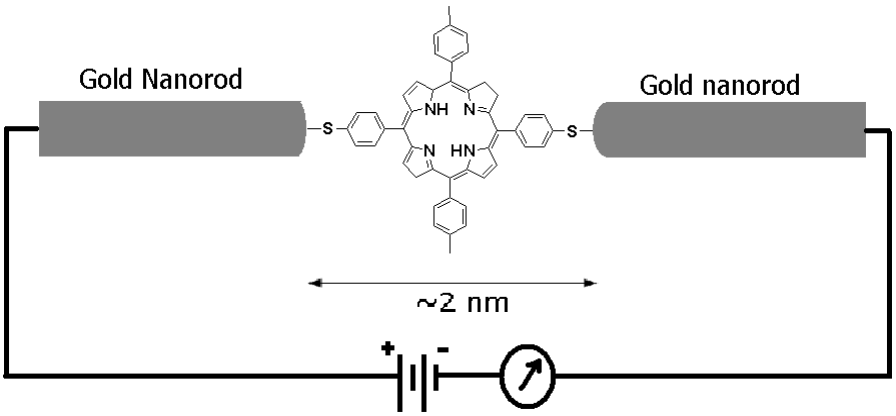


Fig. 15: Cartoon diagram showing a single porphyrin molecule present in between two gold nanorods, which are further connected to electronic circuitry. The relative size of molecule and rods is not according to scale.

In the diagram above, a single porphyrin molecule is placed between two nanorods with spacing of ~2 nm, which is roughly the size of one porphyrin molecule. The rods could be further connected to electronic circuitry using micro electrodes. Addition of a metal cation in the porphyrin core could possibly change the I-V characteristics of the molecule.

In order to achieve this goal, we used many combinations of solvents to solubilize gold nanorods (aqueous phase) and porphyrins (organic phase) in a single homogenized system to make rods linked to each other, as we did in our aqueous nanoparticle approach. Those combinations were not successful as gold nanorods either precipitated immediately or they did not show any linking observed under scanning electron microscopy. We did not consider synthesizing any water soluble porphyrins with polar functional groups, as we were focusing on amine and thiol functionalized porphyrins. Therefore we decided to use two other approaches to solve this problem.

1) Solubilize gold nanorods in an organic phase by the ligand exchange method, and try to link them via porphyrins.

2) The rods are first connected via end-to-end linkage by any water-soluble molecule (e.g. cysteine), put the structure on a silicon wafer, and then a porphyrin molecule is linked between the rods by exchange.

The first approach seemed feasible as described in literature,[43-46] where Au-NR ligands were exchanged with some thiol or amine functionalized surfactants via phase transfer mechanism in presence of ethanol or acetonitrile.[3, 47] This enables rods to become suspended in organic solvents.

It was tried to dissolve our gold nanorods in different organic solvents such as THF, toluene, ethanol, methanol, acetonitrile, acetone, and propanol in excess of dodecanethiol. Although the surfactant present on rods was exchanged successfully as observed from the immediate transfer of rods from aqueous to dodecanethiol phase in case of either acetone or acetonitrile, the rods were not dissolved in a stable manner and precipitated within 30 minutes. Other solvents e.g. THF, ethanol, methanol and propanol, gold nanorods precipitated immediately. The length of the rods was at least 10 times larger (~500 nm) than the size of the rods in literature (length ~50 nm), where they exchanged the surfactant successfully.[3]. Presumably, the reason for the low stability of our Au-NR solutions in acetone or acetonitrile was the large size of the rods, leading to very fast agglomeration.

Since it was not possible to obtain stable solutions of gold nanorods in any organic phase, and making of smaller rods was not of interest for subsequent micro fabrication steps, the direct connection of Au-NRs by porphyrins by approach that was pointed out above was not further pursued.

### 4.2.8 Contacting of gold nanorods

It is known that thiol containing amino acid cysteine can induce end-to-end linkage in Au-nanorods.[5] Referring to method 2 in section 4.2.7, a dilute solution of cysteine was added to a solution of gold nanorods. Their end-to-end assembly was followed by observing change in the UV-Vis spectrum in time. The emergence of a long-wavelength band in UV-Vis over time was clearly observed (figure 16).

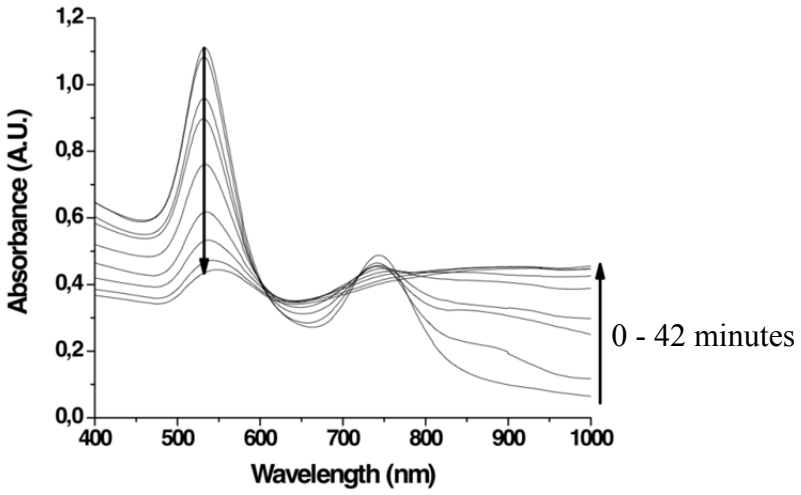


Fig. 16: UV-Vis spectrum for gold nanorods changes with respect to time after the addition of cysteine solution. Spectra were measured by a difference of 6 minutes each.

Scanning electron microscopy (SEM) confirmed that these rods were connected via end-to-end assembly (figure 17).

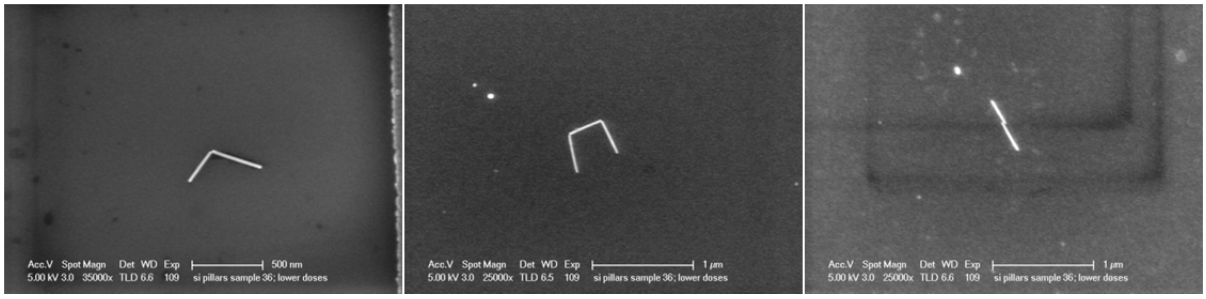

Fig. 17: Individual cases where two or three gold nanorods are linked via cysteine molecules.

After this successful connection of the rods via cysteine using literature protocols, it was important to know if microelectrodes can be fabricated along the rods. Using standard e-beam lithography techniques, it was possible to connect the rods with micro gold electrodes as shown in the following diagram (figure 18). This work was done by our collaborators at Kavli institute of nanosceince, Delft university of technology.[48]

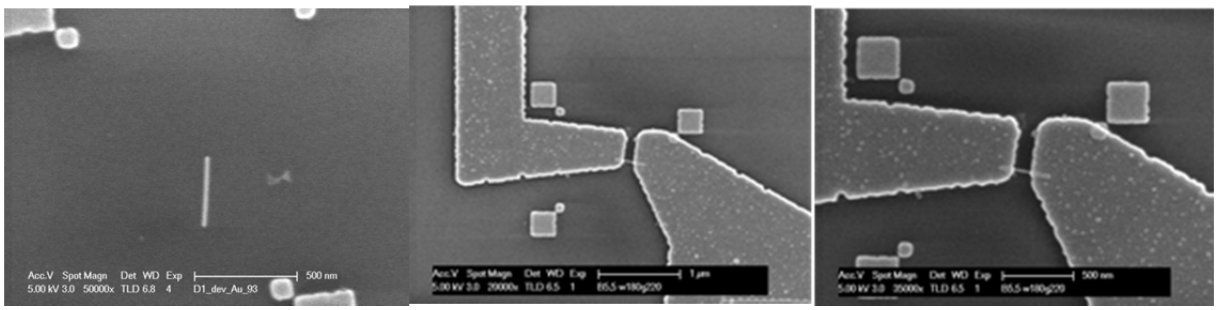

a b c

Fig. 18: SEM pictures (a) single gold nanorod, (b and c) single nanorod connected with microelectrodes.

These nanorods were conducting as single rod in contact with the microelectrodes, formed via standard e-beam lithography techniques. The contact was reliably low ohmic and the resistance was 180 Ω.[48] However, making the contacts was not straight forward and there was high probability for the microlectrodes to short. Additionally, the rods were not strongly attached to the silicon wafer surface. This resulted in movement of the rods on the surface of the silicon wafer, during the fabrication process. This harmed our intention to micro-fabricate the linked rods and we did not further pursue in this direction.

## 4.3 Conclusions

With our aim to investigate the potential of Au nanorods as bottom-up nanoelectrodes for contacting single molecules, binding interaction of porphyrin molecules with gold nanoparticles and gold nanorods was studied to get valuable insights, which is essential for understanding the behavior of single molecules contacted between nanoelectrodes.

UV-Vis titration experiments showed that addition of gold nanoparticles does not affect the absorption of porphyrins. Fluorescence studies revealed that porphyrins with four amino functionalities (porphyrin **2**) have highest binding interaction with gold nanoparticles as compared to other porphyrins, we used. Binding constant of porphyrin **2** was an order of magnitude higher than other porphyrins. The life time fluorescence measurement revealed that the binding is static rather than dynamic by showing similar decay constant for porphyrins before and after addition of nanoparticles.

The increase in Stern-Volmer plot for all porphyrins is partly due to the inner filter effects of gold nanoparticles, confirmed by UV-Vis absorption spectroscopy of the same solutions. A method to calculate the inner filter effects of gold nanoparticles by addition of dodecylamine, which replaces bound porphyrins was described. The highest fluorescence in presence and absence of gold nanoparticles keeping porphyrins free in solution allowed for an estimation of the inner filter effects of gold nanoparticles.

Porphyrins **2** induce non-selective and uncontrolled binding of gold nanoparticles as was observed by DLS. Nanoparticles agglomerated upon addition of porphyrin solution. The number of porphyrins attached to each gold nanoparticle was calculated using a combination of gel permeation chromatography and UV-Vis absorption spectroscopy. Selective and controlled binding of two or three particles by using porphyrin **4** was achieved by combining DMSO solubilized porphyrins and aqueous phase nanoparticles. As a result, porphyrins **2** and **4** were chosen for further studies. Binding is dependent on the number and type of linker moieties present on the porphyrin molecules and morphology of the nanoparticles.

Attempts to align gold nanorods using porphyrins were unsuccessful due to very large size of gold nanorods and their instability in organic solvents upon ligand exchange. Individual rods were successfully fabricated with micro electrodes; however contacting already aligned nanorods (by use of cysteine) with microelectrodes was not feasible due to the movement of rods on the silicon surface.

## 4.4 Experimental

### 4.4.1 Materials and methods

Porphyrins were synthesized and characterized as described in previous chapter. Extinction coefficient of porphyrin **2** was calculated to be 2,484 x $10^5$ L $mol^{-1}$ $cm^{-1}$ by measuring UV-Vis absorption at 428 nm of five different dilutions in dichloromethane. The life-time fluorescence decay for porphyrin **2** is 7.35 ns, 7.72 ns for porphyrin **3** and 7.24 ns for porphyrin **4**.

Cysteine and dodecanethiol, dodecaneamine and other organics / inorganics were available commercially and were used without further purification. All solvents used for reactions were

purified with the use of MBRAUN Solvent purification system MB SPS-800, MilliQ-water was used in case of measurements and preparation of aqueous phase gold nanoparticles and gold nanorods.

### 4.4.2 Synthesis of Au nanoparticles and nanorods

Gold nanoparticles (Au-NPs) were synthesized in organic phase and aqueous phase according to the literature procedures.[33, 34]

For aqueous phase Au-NPs, 20 mL aqueous solution containing 2.5 x $10^{-4}$ M $HAuCl_4$ and 2.5 x $10^{-4}$ M trisodium citrate was prepared. To this solution was added 0.6 mL of ice cold 0.1 M $NaBH_4$ with stirring. The solution immediately turned orange-red, indicating the formation of seed gold nanoparticles. A growth solution was prepared separately, where 100 mL aqueous solution of 2.5 x $10^{-4}$ M $HAuCl_4$ was taken in a conical flask. To this was added 3 g of solid CTAB (0.08 M final CTAB concentration), and the resulting solution was heated with stirring. The solution was cooled to room temperature and used as a stock solution. 1.0 mL of the seed solution was added with vigorous stirring to a mixture of 9 mL sample of the growth solution and 50 $\mu$L of 0.1 M ascorbic acid. Stirring was continued for 10 minutes. 1 mL from this solution was added to another 9 mL sample of the growth solution mixed with 50 $\mu$L of 0.1 M ascorbic acid solution. Vigorous stirring was continued for 10 minutes. The resulting purple-colored solution indicated formation of gold nanoparticles. The formation of gold nanoparticles in aqueous phase was confirmed by UV-Vis absorption spectroscopy. The mixture showed a strong band at 525 nm, characteristic for a gold plasmon band, from which we concluded that gold nanoparticles with a diameter of 18-20 nm were formed. Scanning electron microscopy showed that the average size of these aqueous phase Au nanoparticles was 22 ± 3 nm. Size distribution was determined by counting the size of ~50 individual nanoparticles under the SEM microscope.

Synthesis of gold nanoparticles in organic phase was carried out by dissolving 0.75 g dodecylamine in 25 mL cyclohexane, then 6 mL aqueous formaldehyde (37%) was added. After vigorously stirring for 10 min at room temperature, the cyclohexane phase was separated and washed twice with water. Next, 10 mL aqueous $HAuCl_4$ solution (1 g $HAuCl_4$ in 250 mL $H_2O$) was added into the cyclohexane solution under vigorous stirring. Stirring was continued at room temperature for 40 min, the color of the organic phase turned to deep ruby

red indicating the formation of gold nanoparticles. The aqueous phase was separated and organic solution of gold nanoparticles was obtained. The UV-Vis absorption spectrum showed a strong band at 515 nm. DLS confirmed that nanoparticles with a diameter of 7.6 ± 0.8 nm were formed. The extinction coefficient of Au-NPs was calculated to be 9 x $10^6$ L $mol^{-1}$ $cm^{-1}$ by measuring UV-Vis absorption at 515 nm of five different dilutions in dichloromethane.

Gold nanorods were prepared according the literature procedure.[39, 40] The preparation of gold nanorods was initiated with gold-seed production. 0.5 mL of 0.01 M $HAuCl_4$ trihydrate in water and 0.5 mL of 0.01 M sodium citrate in water were added to 18 mL of deionized water and stirred. Next, 0.5 mL of freshly-prepared 0.1 M $NaBH_4$ was added and the solution color changed from colorless to orange. Stirring was stopped and the solution was left undisturbed for 2 hours. For gold nanorod growth from the seeds, three flasks were labeled A, B, and C. Growth solutions A and B consisted of 9 mL of 0.1 M cetyltrimethylammonium bromide (CTAB) in water, 0.25 mL of 0.01 M $HAUCl_4$ trihydrate in water, 50 μL of 0.1 M ascorbic acid and 100 μL of 0.1 M NaOH. Growth solution C was prepared with 90 mL of 0.1 M CTAB, 2.5 mL of 0.01 M $HAuCl_4$, 0.5 mL of 0.1 M ascorbic acid and 0.5 mL of 0.1 M NaOH.

To grow the gold nanorods, 1.0 mL of the seed solution was added to growth solution A. Growth solution A was shaken for approximately 3-5 seconds and 1.0 mL of solution A was added into B. Solution B was shaken for ~3-5 seconds, then all of B was poured into growth solution C. The solution color of C changed from colorless to a reddish brown indicating the formation of gold nanorods. This solution was kept overnight. The UV-Vis absorption indeed showed two absorption maxima confirming the formation of Au nanorods with a strong band at 525 nm and relatively weak band at roughly 660 nm. To separate the gold Nanorods from spherical side products, four 10 mL portions of solution C were centrifuged at 1500 rpm for 20 minutes; the supernatant fluid was then poured off and 100 μL of water was added to the precipitate in each tube to redisperse it. 5 μL of this solution was evaporated on a silicon wafer and imaged under SEM microscope confirming gold nanorods (Au-NRs) with diameters of 20 ± 4 nm, and lengths of 500 ± 100 nm with aspect ratio ~ 25. The statistical distribution was measured for 50 individual rods from the SEM image.

### 4.4.3 UV-Vis and fluorescence measurements

UV-Vis measurements were performed in AnalytikJena Specord 250 spectrometer equipped with a deuterium-lamp and a halogen-lamp. Quartz cuvettes were used with path-lengths of 10mm. Fluorescence spectroscopy was performed on a Jasco J-815 CD-spectrometer. The cuvette was quartz with dimensions 3x3mm. For determination of luminescence lifetimes, a LifeSpecs-ps (Edinburgh instruments) was used with excitation pulses of 70 ps at 405 nm.

Samples were prepared by combining the correct amounts and appropriate ratios from stock solutions of gold nanoparticles and porphyrins in THF. For fluorescence and UV-Vis measurements, the concentration of porphyrins was kept constant at 0.75 μM. The addition of gold nanoparticles was from 0 - 100 μL (1 μM) with difference of 10 μL for each measurement. Final concentrations were calculated for a solution of 2 mL each sample. 70 μL from 2 mL of each prepared sample were used for fluorescence measurements and the rest was used for UV-measurements. Samples were not used twice. In general, the samples were mixed and kept overnight and next day measurements were recorded. For the measurements of inner filter effects, the concentration of porphyrins was kept constant at 0.75 μM. The concentration of DDA was approximately kept same as the concentration of DDA present in gold nanoparticles as the exact concentration of DDA in gold nanoparticles could not be estimated. The addition of gold nanoparticles was 100 μL (1 μM) and the final concentration was calculated for a solution of 2 mL.

### 4.4.4 Gel permeation chromatography

Gel permeation chromatography (purification and purity-trace) was performed on a Waters Gel Permeation chromatography machine, LC-8A pump with a Waters 2487 dual λ absorbance detector. The column used here was the reprogel PS-GPC 500, 5μm particle size dimensions 300x30mm for preparative with a 6 ml/min (THF) flow, for analytical measurements the same column with dimensions 30x8mm was used with a flow of 1 ml/min (THF). Porphyrin bound gold nanoparticles were separated from free porphyrins by these columns.

### 4.4.5 Dynamic light scattering

Dynamic light scattering (DLS) measurements were performed on the Zetasizer Nano ZS from Malvern Instruments Limited using the 173° angle non-invasive back-scatter mode and the M3-phase analysis light scattering mode, respectively. The instrument had a red 4.0 mW 633 nm He–Ne laser. The multiple peak high-resolution fitting procedure was used to obtain the particle size distribution from the auto-correlation function. DLS spectra were measured at room temperature in THF. Intensity distribution curves for Au-NPs were considered for particle size distribution. Measurements were performed with nanoparticles at 1 μM concentration, nanoparticles passed through GPC column and nanoparticles treated with porphyrin **2** and passed through GPC column.

### 4.4.6 Scanning electron microscopy

Inspection and pictures of gold nanoparticles and gold nanorods were realized with a Philips XL30SFEG scanning electron microscope (SEM) present in cleanroom nanofacility at Delft University of Technology.

For this purpose, silicon wafers were cut into 1 x 1 $cm^2$ pieces and cleaned with a mixture of sulfuric acid and hydrogen peroxide. These were further rinsed with deionized water and dried with flow of nitrogen gas. 5-10 μL solution of homogenized Au-NPs or Au-NRs were dropped on the cleaned silicon wafer and left for 3-5 minutes. The remaining solution was removed with a flow of nitrogen gas in order to avoid excess particle accumulation on silicon surface. These gold particle containing silicon wafer pieces were used for imaging under SEM microscope. Particle size distribution was determined by calculating size of ~50 particles under the microscope.

## 4.5 References


1. Jebb, M., et al., *Ruthenium(II) trisbipyridine functionalized gold nanorods. Morphological changes and excited-state interactions.* Journal of Physical Chemistry B, 2007. **111**(24): p. 6839-6844.
2. Joseph, S.T.S., et al., *Gold nanorods to nanochains: Mechanistic investigations on their longitudinal assembly using alpha,omega-alkanedithiols and interplasmon coupling.* Journal of Physical Chemistry B, 2006. **110**(1): p. 150-157.
3. Pramod, P. and K.G. Thomas, *Plasmon Coupling in Dimers of Au Nanorods.* Advanced Materials, 2008. **20**(22): p. 4300-4305.
4. Joshi, H., et al., *Isothermal titration calorimetry studies on the binding of amino acids to gold nanoparticles.* Journal of Physical Chemistry B, 2004. **108**(31): p. 11535-11540.
5. Hu, X.G., et al., *Well-ordered end-to-end linkage of gold nanorods.* Nanotechnology, 2005. **16**(10): p. 2164-2169.
6. Varghese, N., et al., *A calorimetric investigation of the assembly of gold nanorods to form necklaces.* Chemical Physics Letters, 2008. **450**(4-6): p. 340-344.
7. Kawamura, G., Y. Yang, and M. Nogami, *End-to-end assembly of CTAB-stabilized gold nanorods by citrate anions.* Journal of Physical Chemistry C, 2008. **112**(29): p. 10632-10636.
8. Sudeep, P.K., S.T.S. Joseph, and K.G. Thomas, *Selective detection of cysteine and glutathione using gold nanorods.* Journal of the American Chemical Society, 2005. **127**(18): p. 6516-6517.
9. Caswell, K.K., et al., *Preferential end-to-end assembly of gold nanorods by biotin-streptavidin connectors.* Journal of the American Chemical Society, 2003. **125**(46): p. 13914-13915.
10. Gole, A. and C.J. Murphy, *Biotin-streptavidin-induced aggregation of gold nanorods: Tuning rod-rod orientation.* Langmuir, 2005. **21**(23): p. 10756-10762.
11. Zareie, M.H., X.D. Xu, and M.B. Cortie, *In situ organization of gold nanorods on mixed self-assembled-monolayer substrates.* Small, 2007. **3**(1): p. 139-145.
12. Chang, J.Y., et al., *Oriented assembly of Au nanorods using biorecognition system.* Chemical Communications, 2005(8): p. 1092-1094.
13. Pan, B.F., et al., *End-to-end self-assembly and colorimetric characterization of gold nanorods and nanospheres via oligonucleotide hybridization.* Nanotechnology, 2005. **16**(9): p. 1776-1780.
14. Nie, Z.H., et al., *Self-assembly of metal-polymer analogues of amphiphilic triblock copolymers.* Nature Materials, 2007. **6**: p. 609-614.
15. Jain, T., et al., *Self-Assembled Nanogaps via Seed-Mediated Growth of End-to-End Linked Gold Nanorods.* Acs Nano, 2009. **3**(4): p. 828-834.
16. Ashwell, G.J., B. Urasinska-Wojcik, and L.J. Phillips, *In Situ Stepwise Synthesis of Functional Multijunction Molecular Wires on Gold Electrodes and Gold Nanoparticles.* Angewandte Chemie International Edition, 2010. **49**(20): p. 3508-3512.
17. Cheon, D., S. Kumar, and G.-H. Kim, *Assembly of gold nanoparticles of different diameters between nanogap electrodes.* Applied Physics Letters, 2010. **96**(1): p. 013101-3.
18. Zheng, J., et al., *Two-Dimensional Nanoparticle Arrays Show the Organizational Power of Robust DNA Motifs.* Nano Letters, 2006. **6**(7): p. 1502-1504.
19. Morita, T. and S. Lindsay, *Determination of Single Molecule Conductances of Alkanedithiols by Conducting-Atomic Force Microscopy with Large Gold Nanoparticles.* Journal of the American Chemical Society, 2007. **129**(23): p. 7262-7263.

20. Jianhui, L., et al., *Interlinking Au nanoparticles in 2D arrays via conjugated dithiolated molecules.* New Journal of Physics, 2008. **10**(6): p. 065019.
21. Mangold, M.A., et al., *Resonant Photoconductance of Molecular Junctions Formed in Gold Nanoparticle Arrays.* Journal of the American Chemical Society, 2011. **133**(31): p. 12185-12191.
22. Noguchi, Y., et al., *Charge transport in various dimensions of small networks composed of gold nanoparticles and terthiophene wire-molecules.* Applied Physics Letters, 2011. **98**(26): p. 263114-3.
23. Jafri, S.H.M., et al., *Assessment of a nanoparticle bridge platform for molecular electronics measurements.* Nanotechnology, 2010. **21**(43): p. 435204.
24. Cui, P., et al., *Nonvolatile Memory Device Using Gold Nanoparticles Covalently Bound to Reduced Graphene Oxide.* Acs Nano, 2011. **5**(9): p. 6826-6833.
25. Tang, Q., et al., *Self-assembled nanogaps for molecular electronics.* Nanotechnology, 2009. **20**(24): p. 245205.
26. Ni, W., et al., *Evidence for Hydrogen-Bonding-Directed Assembly of Gold Nanorods in Aqueous Solution.* The Journal of Physical Chemistry Letters, 2010. **1**(8): p. 1181-1185.
27. Lee, J.-E., J. Yang, and D. Kim, *Single-molecule fluorescence dynamics of a butadiyne-linked porphyrin dimer: the effect of conformational flexibility in host polymers.* Faraday Discussions, 2012. **155**(0): p. 277-288.
28. Wang, K.-R., et al., *Excitonic coupling interactions in the self-assembly of perylene-bridged bis([small beta]-cyclodextrin)s and porphyrin.* Chemical Communications, 2012. **48**(30): p. 3644-3646.
29. Calvete, M., G.Y. Yang, and M. Hanack, *Porphyrins and phthalocyanines as materials for optical limiting.* Synthetic Metals, 2004. **141**(3): p. 231-243.
30. Liao, M.-S. and S. Scheiner, *Electronic structure and bonding in metal porphyrins, metal=Fe, Co, Ni, Cu, Zn.* The Journal of Chemical Physics, 2002. **117**(1): p. 205-219.
31. Cormode, D.P., J.J. Davis, and P.D. Beer, *Anion sensing porphyrin functionalized nanoparticles.* Journal of Inorganic and Organometallic Polymers and Materials, 2008. **18**(1): p. 32-40.
32. Kanehara, M., H. Takahashi, and T. Teranishi, *Gold(0) porphyrins on gold nanoparticles.* Angewandte Chemie-International Edition, 2008. **47**(2): p. 307-310.
33. Gole, A. and C.J. Murphy, *Seed-mediated synthesis of gold nanorods: Role of the size and nature of the seed.* Chemistry of Materials, 2004. **16**(19): p. 3633-3640.
34. Chen, Y.Y. and X.K. Wang, *Novel phase-transfer preparation of monodisperse silver and gold nanoparticles at room temperature.* Materials Letters, 2008. **62**(16): p. 2215-2218.
35. Yang, Y., et al., *Precise size control of hydrophobic gold nanoparticles using cooperative effect of refluxing ripening and seeding growth.* Nanotechnology, 2008. **19**(17): p. 175603.
36. Liu, X.O., et al., *Extinction coefficient of gold nanoparticles with different sizes and different capping ligands.* Colloids and Surfaces B-Biointerfaces, 2007. **58**(1): p. 3-7.
37. Ding, Y.H., et al., *Comparative studies on adsorption behavior of thionine on gold nanoparticles with different sizes.* Journal of Colloid and Interface Science, 2008. **327**(1): p. 243-250.
38. Mucic, R.C., et al., *DNA-Directed Synthesis of Binary Nanoparticle Network Materials.* Journal of the American Chemical Society, 1998. **120**(48): p. 12674-12675.
39. Busbee, B.D., S.O. Obare, and C.J. Murphy, *An Improved Synthesis of High-Aspect-Ratio Gold Nanorods.* Advanced Materials, 2003. **15**(5): p. 414-416.
40. Park, W.M., Y.S. Huh, and W.H. Hong, *Aspect-ratio-controlled synthesis of high-aspect-ratio gold nanorods in high-yield.* Current Applied Physics, 2009. **9**(2): p. E140-E143.

41. Nath, S., et al., *Ligand-stabilized metal nanoparticles in organic solvent.* Journal of Colloid and Interface Science, 2010. **341**(2): p. 333-352.
42. Nerambourg, N., et al., *Quenching of molecular fluorescence on the surface of monolayer-protected gold nanoparticles investigated using place exchange equilibria.* Langmuir, 2007. **23**(10): p. 5563-5570.
43. Feng, X.L., et al., *Aqueous-organic phase-transfer of highly stable gold, silver, and platinum nanoparticles and new route for fabrication of gold nanofilms at the oil/water interface and on solid supports.* Journal of Physical Chemistry B, 2006. **110**(25): p. 12311-12317.
44. Misra, T.K., T.-S. Chen, and C.-Y. Liu, *Phase transfer of gold nanoparticles from aqueous to organic solution containing resorcinarene.* Journal of Colloid and Interface Science, 2006. **297**(2): p. 584-588.
45. Wijaya, A. and K. Hamad-Schifferli, *Ligand customization and DNA functionalization of gold nanorods via round-trip phase transfer ligand exchange.* Langmuir, 2008. **24**(18): p. 9966-9969.
46. Wijaya, A., et al., *Selective Release of Multiple DNA Oligonucleotides from Gold Nanorods.* Acs Nano, 2009. **3**(1): p. 80-86.
47. Nandanan, E., N.R. Jana, and J.Y. Ying, *Functionalization of Gold Nanospheres and Nanorods by Chitosan Oligosaccharide Derivatives.* Advanced Materials, 2008. **20**(11): p. 2068-2073.
48. Oliveros, E.A.O., *Quantum transport through single molecules*. 2009, Delft University of Technology: Delft.

# CHAPTER 5

## Porphyrins and semiconductor quantum dots:

## Binding and charge / energy transfer studies

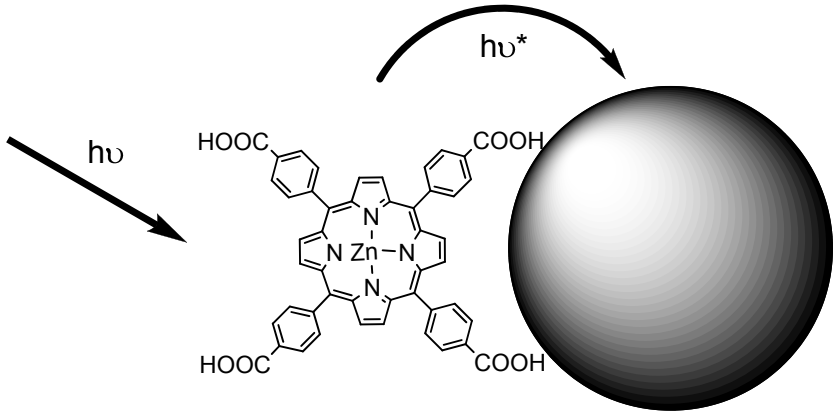


Energy transfer from a porphyrin molecule to a quantum dot

Previous studies revealed binding of functionalized porphyrins to metallic nanoparticles. In this chapter, binding interaction of functionalized porphyrins with semiconductor quantum dots and charge / energy transfer studies between porphyrins and quantum dots is described. These studies are part of our goal in molecular electronics to have a better understanding of charge or energy transfer in such organic-inorganic hybrid systems. We observed binding of porphyrins with specific functional groups and uni-directional charge transfer from porphyrins to quantum dots. These studies show that porphyrins have potential for charge transfer in single molecule electronic studies.

## 5.1 Introduction

In this chapter, we will make porphyrins-quantum dot hybrids by the selective binding of porphyrin molecules to quantum dots. The idea of making these hybrids is to study binding interaction of porphyrins with semiconductor quantum dots and once they bind, to determine if charge or energy transfer happens between porphyrins and quantum dots or not. Because the main goal of this thesis is to exploit porphyrins for single molecule electronics, these studies may add to our understanding of charge or energy transfer through porphyrin molecules.

Research on semiconductor nanoparticles or quantum dots is often focused towards charge and / or energy transfer studies to obtain a better understanding of behavior of molecules in molecular electronic devices. For example, mixing of semiconductor nanocrystalline quantum dots and Ru-polypyridine complexes resulted in the formation of electronically coupled assemblies. Photoexcitation of such assemblies resulted in oxidation of the adsorbed complex via efficient hole transfer (charge transfer) from the nanocrystalline quantum dot.[1] Electrochemiluminescence and energy transfer of quantum dots can also be used for the detection of organic molecules.[2]

The hybridization and binding of organic ligands and specifically porphyrins with semiconductor quantum dots is known in literature. Such studies reveal the mechanism of binding, energy or charge transfer processes and applications and uses of such hybrids in various biological, medical, photovoltaic and other specific fields. For example, assemblies of QDs with photosensitizing dyes provided a novel approach to photo-dynamic therapy (PDT). In PDT, these hybrid materials can selectively destroy malignant tissues, such as cancer cells.[3] Other possibilities include biosensor applications,[4] significant improvement in the functionality of biological systems,[5] and applications in solar cells and light emitting diodes.[6, 7]

The electron transfer properties of a typical semiconductor and semiconductor nanocrystal are of particular importance.[8] Nanoassemblies of CdSe/ZnS quantum dots and tetra pyridyl-substituted free-base porphyrin molecules have shown QD photoluminescence quenching and spectral changes of porphyrins. In some cases FRET occurs from QDs to porphyrins, which is a qualitative tool to identify well defined formation of QD-porphyrin complexes, where photo

induced charge transfer takes place in the matrix in time scales of up to seconds.[9] These nanoassemblies are metastable and interfacial rearrangement occurs, leading to a more effective photoluminescence quenching.[10] Computational studies suggest that such hybrid systems can transfer excitation from QD to oxygen through porphyrin, generating singlet oxygen for medical applications. Electron transfer from the QD to the dye is one of the main competing mechanisms, because the porphyrins tend to be better electron-acceptors than hole-acceptors, however longer distances between QD and porphyrin molecules disfavors electron transfer.[11]

Energy transfer from water soluble quantum dots to porphyrins, specifically meso-tetra(4-sulfonatophenyl)porphine dihydrochloride (TSPP), is observed by steady-state and time-resolved spectroscopy. In this case, the Dexter type electron exchange mechanism is the dominant transfer mechanism in addition to the Forster type nonradiative energy transfer.[12] Other studies show direct sensing of metal ions by CdSe quantum dots functionalized with tetrapyridyl-substituted porphyrin, which is a cation selective carrier. Porphyrins coordinate to Cd atoms of the CdSe quantum dots through the Lewis basic pyridyl groups. When nitrogen atoms of the pyridyl moieties of pyridyl-substituted porphyrins are coordinated with zinc cations, increase in the fluorescence efficiency of CdSe through activating binding interaction with the quantum dots surface is observed. It is due to surface passivation by the inorganic shell, attributed to charge carrier confinement in the nanoparticle core.[13]

Since we are working towards porphyrin dye – QD energy transfer studies, our aim is to study energy or charge transfer processes occurring from porphyrins to quantum dots and vice versa. In order to better understand these underlying processes between porphyrins and quantum dots, we consider our porphyrins as good candidates to analyze our aims. These studies are important in our understanding for our goal to obtain a better understanding of single molecule electronics.

## 5.2 Results and discussions

In this study we explored the interaction of various functionalized porphyrins with PbSe quantum dots. The PbSe QDs were synthesized following the method of Maksym V. Kovalenko.[14] The resulting PbSe QDs are stabilized by a surface layer of oleyl amine, and have a mean diameter of ~2.8 nm excluding the interfacial layer, determined by a curve fit

[15] from absorbance measurements. The QDs are well soluble in iso-propanol, and have absorption and emission maxima at 1088 nm and 1166 nm, respectively. Because PbSe QDs are not stable in air, all experiments have been carried out in a nitrogen atmosphere.

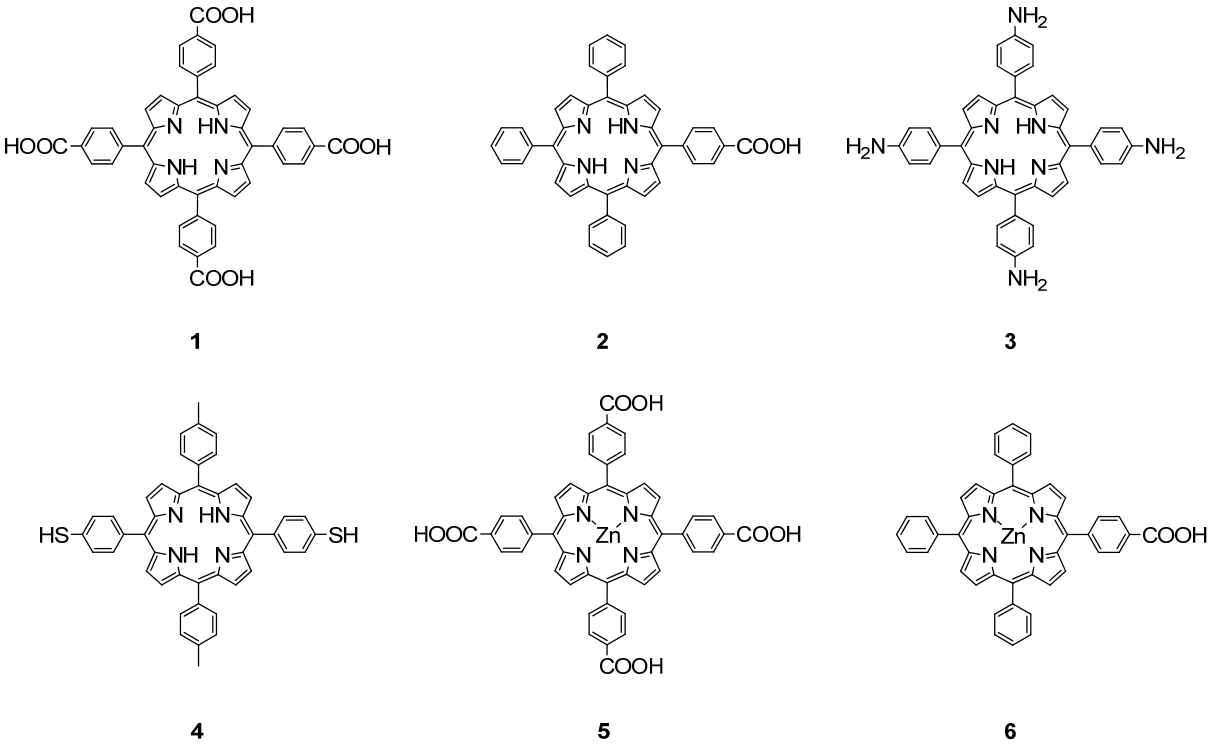


Fig. 1: Porphyrin molecules with four carboxylic acid functional groups **1**, mono carboxylic functional group **2**, four amino groups **3**, *trans* dithiol functionality **4**, four carboxylic functional groups with zinc atom in the inner core **5** and mono carboxylic acid functional group with zinc atom in the inner core **6**.

In literature, we find that PbSe quantum dots can be synthesized with capping agents containing carboxylic acid groups,[16-19] amines[20] and thiols,[20, 21] indicating that these functional groups can bind to PbSe QDs. Therefore we explored the binding of porphyrins bearing one or more of such functional groups with PbSe QDS. The porphyrins used in this study are listed in figure 1, synthesis of porphyrin **3** and **4** has been described in chapter 3 of this thesis. Porphyrins **1**, **2**, **5**, and **6** were obtained commercially.

### 5.2.1 Porphyrin-quantum dot binding studies using UV-Vis and fluorescence spectroscopy

The interaction of porphyrins **1** - **4** with PbSe QDs was first explored by absorption and fluorescence spectroscopy, because it was expected that binding of porphyrin to PbSe QDs

would be accompanied by a change of the porphyrin fluorescence due to electronic interactions with the QDs.

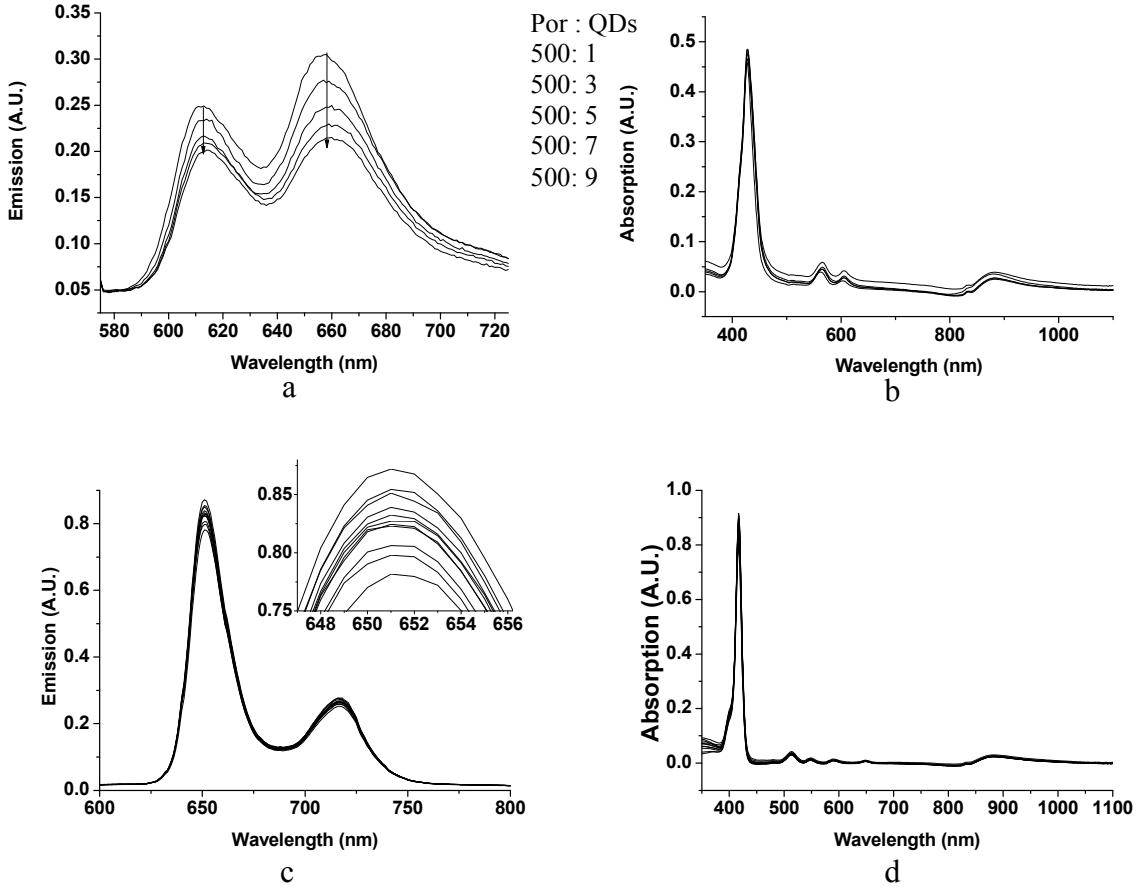


Fig. 2: (a) Fluorescence and (b) absorption spectra of a 2.5 μM solution of porphyrin **1** in THF, in the presence of increasing concentrations of PbSe quantum dots ($\lambda_{exc}$=428 nm) (c) Fluorescence and (d) absorption spectra of 2.5 μM solution of porphyrin **2** in THF treated with PbSe QDs to a final concentration of 0.05 μM ($\lambda_{exc}$=416 nm). The inset in (c) shows close up view of fluorescence peak at ~ 650 nm.

Fluorescence spectrophotometric titrations of porphyrins **1** - **4** dissolved in THF with PbSe-QDs were performed to observe changes in the emission spectra of the porphyrins after titrating porphyrins with QDs. In figure 2a above, porphyrin **1** fluorescence decreases with addition of quantum dots, while absorption spectra remain constant (figure 2b). The change in baseline of one of the samples in UV is possibly due to handling error. The decrease of the emission intensity is a clear indication that porphyrin **1** binds to the PbSe QDs, although the absence of changes in the absorption spectra indicate that this interaction does not lead to notable exciton coupling between the porphyrin and the QDs.

When porphyrin **2** with a single carboxylic acid functional group (2.5 μM) was treated with PbSe QDs up to 0.05 μM concentration, we found that there was no quenching effect as seen from the fluorescence spectra (figure 2c). Similarly, the absorption spectra were similar for all the samples (figure 2d). These studies show that porphyrin **2** with a single carboxylic acid functional group does not bind to quantum dots. Similar titration experiments of porphyrins **3** and **4** with amine and thiol functional groups, respectively, did not lead to any significant changes in the absorption and fluorescence spectra, indicating that PbSe QDs do not interact with these porphyrins.

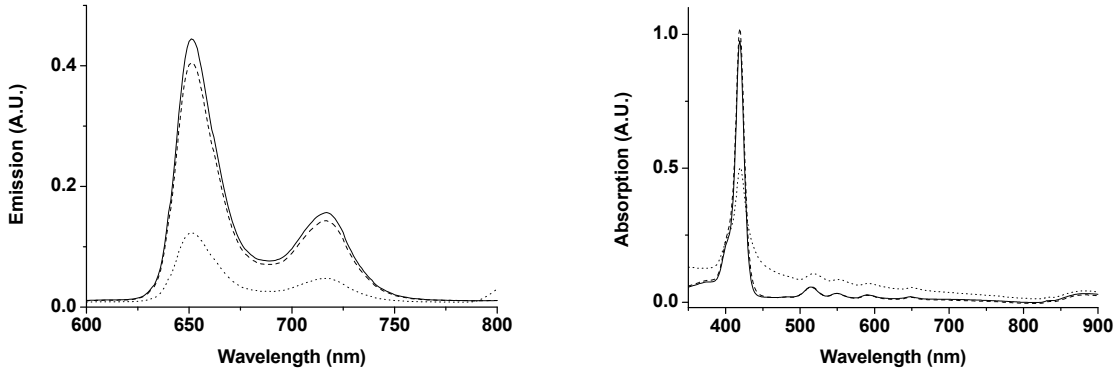


a b

Fig. 3: Fluorescence (left) and absorption spectra (right) of a 30 μM tetracarboxylic acid porphyrin **1** in THF (____), in the presence of 30 μM oleylamine (----), and in the presence of 1 μM PbSe QDs (.....).($\lambda_{exc}$=428 nm).

Previous results show that tetra carboxylic acid porphyrin **1** is bound to the PbSe QDs. However, the PbSe QD preparations still contain excess of oleylamine, which was added as a capping agent to stabilize the QD preparations. Such aliphatic amines are also know to act as fluorescent quenching agent themselves,[22] and therefore we verified whether the observed porphyrin fluorescence quenching is not caused by the added oleyl amine rather than the QDs. Upon addition of 30 μM oleylamine(figure 3a), we observed a slight quenching of fluorescence of porphyrin **1**, whereas addition of QDs resulted in a more pronounced quenching of fluorescence (figure 3a), clearly indicating that quenching is indeed caused by interaction of porphyrins with the QDs. Interestingly, we observed a significant decrease and broadening of the porphyrin B-band at 428 nm upon addition of the QDs (figure 3b). It should be noted that in these experiments, the porphyrin concentration was 30 μM, giving a porphyrin to QD ratio of 30:1. This large excess of porphyrin with respect to the QDs mostly likely results in binding of multiple porphyrin molecules on a single QD and likely, the

enhanced quenching of the porphyrin fluorescence and changes of the absorbance spectra are caused by interactions between porphyrin molecules bound to the same QD.

Further analysis of quenching of the porphyrin **1** fluorescence by the QDs revealed that the quenching can be described by Stern-Volmer equation with quenching constant of $8 \pm 2 \times 10^6$. Fluorescence lifetime measurements revealed that the lifetime decreases upon addition of the QDs. For example, porphyrin **1** lifetime was measured (figure 4a) at two different wavelengths i.e. 654 nm and 720 nm.

We have repeated the fluorescence life time measurements with zinc-porphyrin **5** instead of free-base porphyrin **1**, and found that also with **5** the addition of PbSe QDs led to quenching of the fluorescence together with a decrease of the fluorescence life time (figure 4b). The decrease of the fluorescence lifetimes upon binding of porphyrins (**1** and **5**) with four carboxylic groups to PbSe QDs, indicates that the binding is a dynamic rather than a static process on fluorescence timescale, in contrast to the porphyrins - gold nanoparticles binding described in the previous chapter. As our main focus was to study energy / charge transfer from porphyrins to quantum dots and vice versa, we did not further pursue the lifetime measurements.

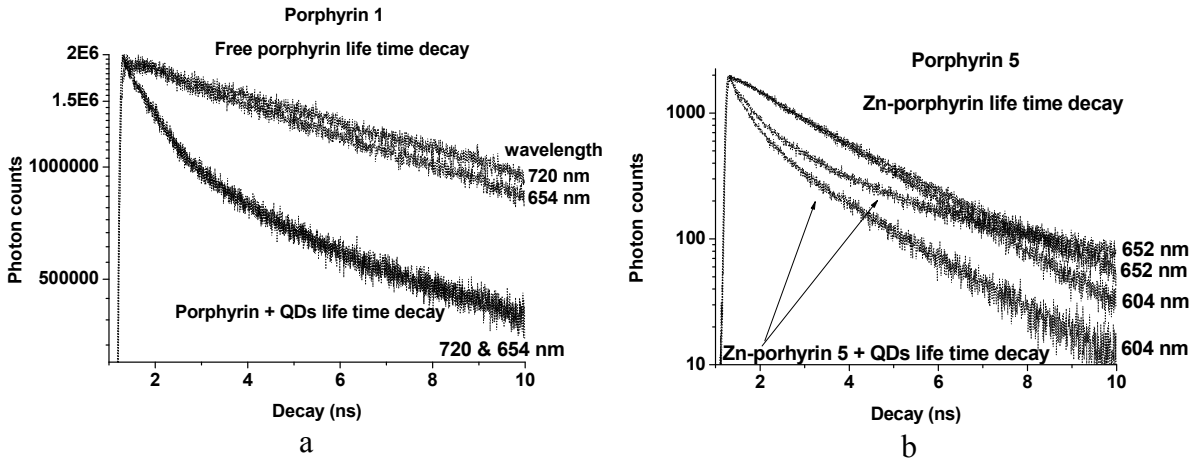


Fig. 4: Fluorescence life time decay measurements of porphyrins in THF (2.5 μM) in presence and absence of PbSe QDs (0.05 μM) (a) Porphyrin **1** ($\lambda_{exc}$=654 nm and 720 nm). (b) Porphyrin **5** ($\lambda_{exc}$=604 nm and 652 nm). The wavelength selection was based on fluorescence peaks of the porphyrins.

## 5.2.2 Quantum dots absorption and fluorescence upon binding to porphyrins

Previously, we were focused on absorption and fluorescence spectra of porphyrins, which remained generally the same over all the experiments with exception of porphyrin **1** and **5**. Quantum dots in general do not have any effect on the absorption spectrum of porphyrins. The absorption wavelength remains same in remaining all cases. We studied the change in absorption spectra of quantum dots before and after they were treated with porphyrins. In this case, a possible red shift of the absorption wavelength of quantum dots may indicate an increase of the QD size, e.g. by particle agglomeration, whereas a blue shift may point to size reduction, e.g. due to dissolution / de-aggregation.

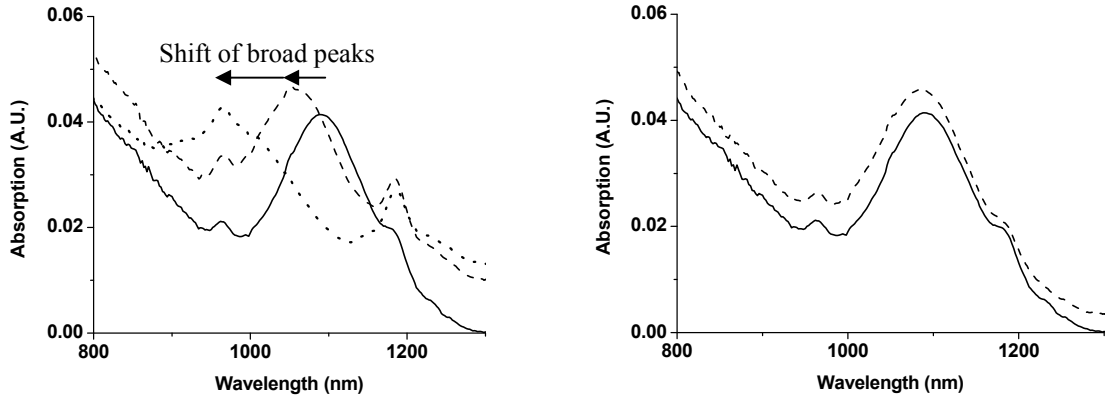


Fig. 5: (a) Change in absorption spectra of a 1 μM solution of PbSe quantum dots in isopropanol (____), and upon addition of a solution of porphyrin **2** in iso-propanol ($[\mathbf{2}]_{final}$ = 10 μM), recorded after 40 h (------) and 70h (…...). (b) Absorption spectrum of a 1 μM solution of PbSe quantum dots in iso-propanol, recorded after 40 h (____) and 70h (------). The sharp peaks around 970 nm and 1200 nm arise from water absorption, present as impurity in iso-propanol. All measurements were performed at room temperature.

In these measurements, iso-propanol was used as solvent with a ratio of 10:1 for porphyrin : QDs. In the graph above (figure 5a), three absorption peaks are visible. The broad absorption around 1100 nm originates from the PbSe quantum dots, and the sharp peaks around 970 nm and 1200 nm appear due to absorption of minute water impurity present in iso-propanol.[23] When we treat the quantum dots with porphyrin **2**, i.e. mono carboxylic acid porphyrin, the peak for the quantum dots shifts to the blue with a maximum absorption at ~1050 nm. This absorption spectrum was taken 40 hours after addition of porphyrins to quantum dots. The

third absorption spectrum was taken after 70 hours of interaction of porphyrins with quantum dots, and revealed an even larger blue shift of the absorption to a maximum around 950 nm. This progressive blue shift with time points to an increase of the band gap of the PbSe quantum dots, which suggests that the quantum dots size gradually decreases with time. However separate measurements of the absorption spectra of the QDs in iso-propanol as solvent without added porphyrin **2** did not result in any shift (figure 5b) shows that QDs remain stable in absence of porphyrins. Similar blue shifts of the absorption peak of quantum dots, observed upon binding with porphyrin **2** (figure 5a) was observed for the other carboxylic acid functionalized porphyrins, i.e. porphyrins **1**, **5** and **6**. Altogether, these results clearly indicate that the presence of porphyrins results in a decrease in size of the quantum dots, presumably due to dissolution of the QDs caused by the acidic carboxylic function of the porphyrins.

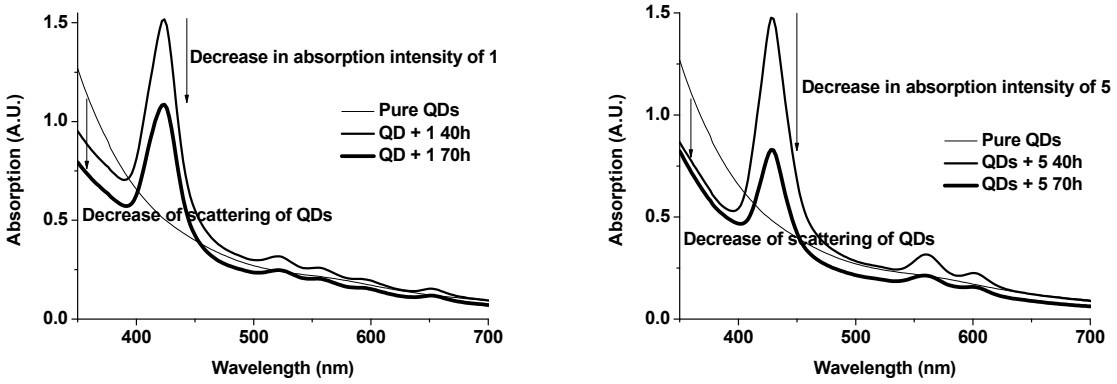


a b

Fig. 6: Porphyrins **1** and **5** does not change in shift of peak. However we see decrease in absorption of peaks over time for both porphyrins. The scattering of QDs also decreases upto 600 nm regime.

The scattering of quantum dots lies up to ~600 nm in UV-Vis spectra, which changes with particle size and goes $1/\lambda^4$ with wavelength, and has no special feature in the spectrum. We observe decrease of scattering of QDs when they are treated with tetra functionalized porphyrins **1** (figure 6a) and **5** (figure 6b) and we also see a decrease of the porphyrin (**1** and **5**) absorption over time (figure 6a and 6b). Both of these observations indicate that porphyrin – QD hybrids precipitates in time as well. From these experiments, we can conclude that carboxylic acid porphyrins are stable molecules themselves, but presence of carboxylic groups lead to slow dissolution of the quantum dots and porphyrin – QD hybrids precipitate over time as well.

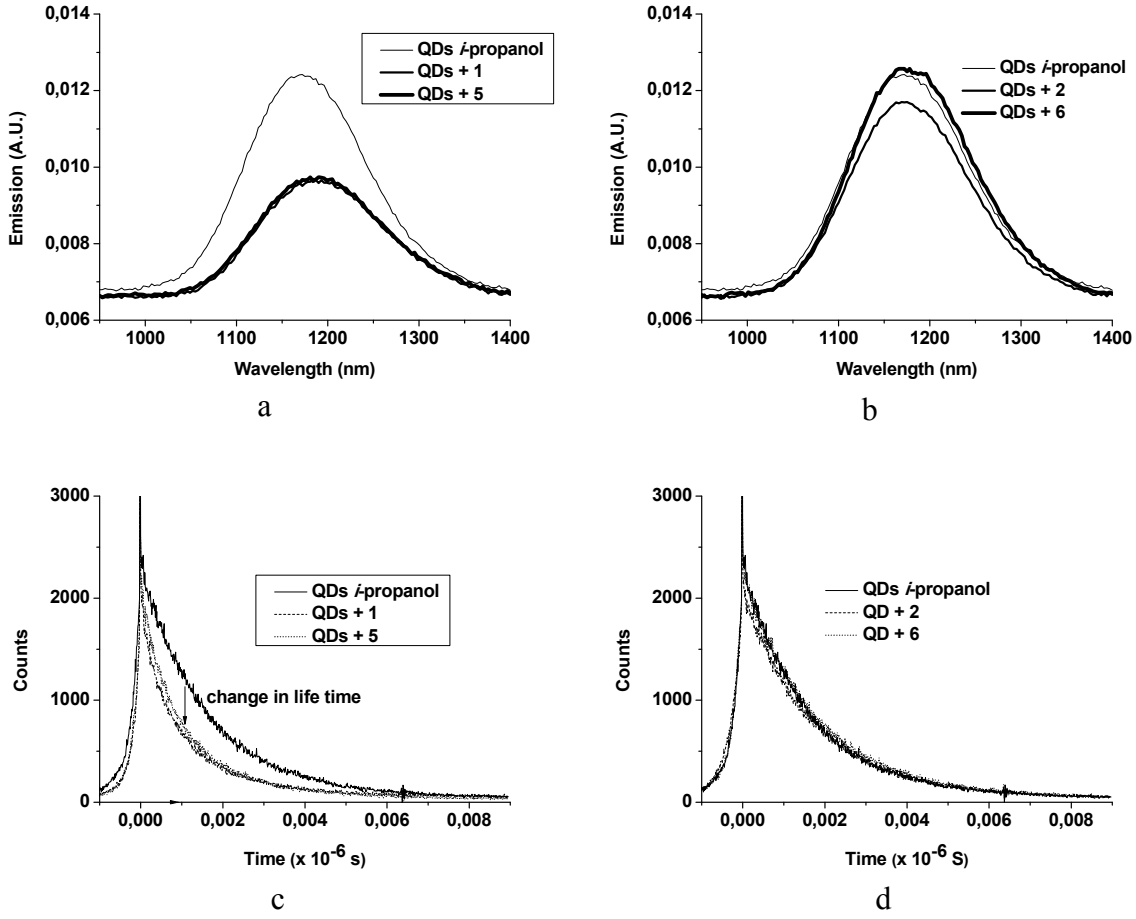


Fig. 7: Luminescence spectra of PbSe QDs ($\lambda_{exc}$=650 nm) (a) effect of tetra carboxylate porphyrins **1** and **5** (10μM each) (b) effect of mono carboxylate porphyrins **2** and **6** (10μM each). Fluorescence life time decay of QDs (c) effect of porphyrin **1** and **5** and (d) effect of porphyrins **2** and **6**.

Until now, we have shown the effect of QDs on the absorption and fluorescence of porphyrins as well as the effect of porphyrins on the absorption of QDs. We also investigated possible photo-induced electron or energy transfer from porphyrins to quantum dots, by studying the effect of porphyrins on the fluorescence of QDs. In these explorative experiments, the samples were excited at the porphyrin Q-band at 650 nm and the B-band at 435 nm respectively, and emission of the PbSe QDs was measured at between 950-1400 nm. Time-resolved fluorescence measurements were also measured at the same wavelengths. This strong absorption by the porphyrin might interfere with the measurements due to inner filter effects, but nevertheless we can differentiate between mono and tetra carboxylic acid functionalized porphyrins as well as effect of Zn cation present in the core of porphyrin. Luminescence spectra of QDs treated with porphyrins **1**, **2**, **5** and **6** are shown in figure 7a and 7b. The spectra in figure 7a clearly show that the luminescence of PbSe QDs is quenched

upon mixing with the tetracarboxylate porphyrins **1** and **5**. In contrast, treatment of the PbSe QDs with mono-carboxylate porphyrins **2** and **6** does not lead to significant changes in the luminescence of QDs (figure 7b). Time resolved fluorescence measurements revealed a decrease of the fluorescence lifetime of the PbSe quantum dots upon addition of porphyrin **1** and **5** (figure 7c), while addition of mono-carboxylate porphyrins **2** and **6** does not significantly affect the fluorescence lifetimes (figure 7d). Very similar results were obtained for excitation at 435 nm instead of 650 nm. Separate control experiments revealed that addition of isopropanol alone causes only a minor (<10%) decrease of the PbSe quantum dot luminescence, while the fluorescence lifetime remains the same. These results are in excellent agreement with the fluorescence quenching experiments described above, and confirm that binding of tetracarboxylate porphyrins **1** and **5** to the PbSe QDs is a dynamic process on the fluorescence lifetime timescale. In contrast, under the conditions of these experiments there is no significant interaction between the monocarboxylate porphyrins and PbSe quantum dots. Interestingly, the luminescence quenching and decrease of luminescence lifetime are also indicative of an electronic interaction between porphyrins **1** and **5** and the PbSe quantum dots during the contact time. We speculate from these measurements that photo-induced resonance energy transfer is not possible between porphyrins and QDs because there is no spectral overlap between porphyrin emission and PbSe QDs absorption. Moreover we would expect increase of QDs emission upon energy transfer from porphyrin to QD, which is not the case. However electron exchange quenching by Dexter interaction or photo-induced electron transfer by exciplex (excited complex) formation is quite possible, since this would be expected to lead to decrease of both porphyrins and QDs emission and relaxation of the charge transfer complex to the ground state without emission of a photon. More detailed investigations are required to reveal the exact mechanism of charge transfer.

### 5.2.3 Charge transfer studies by transient absorption spectroscopy

We also carried out preliminary transient absorption spectroscopy experiments as a final tool to study charge transfer from porphyrins to quantum dots or vice versa. For these experiments, we chose porphyrin **5** as our model porphyrin. Iso-propanol was used as the solvent of choice. To investigate the higher order charge recombination on a sub-nanosecond time scale, we applied femtosecond time-resolved transient optical absorption spectroscopy (TA).

The first part was to study charge transfer from quantum dots to porphyrins. For this purpose, we excited first quantum dots only and then a mixture of quantum dots and porphyrins at 800 nm (porphyrins cannot be excited at this wavelength).

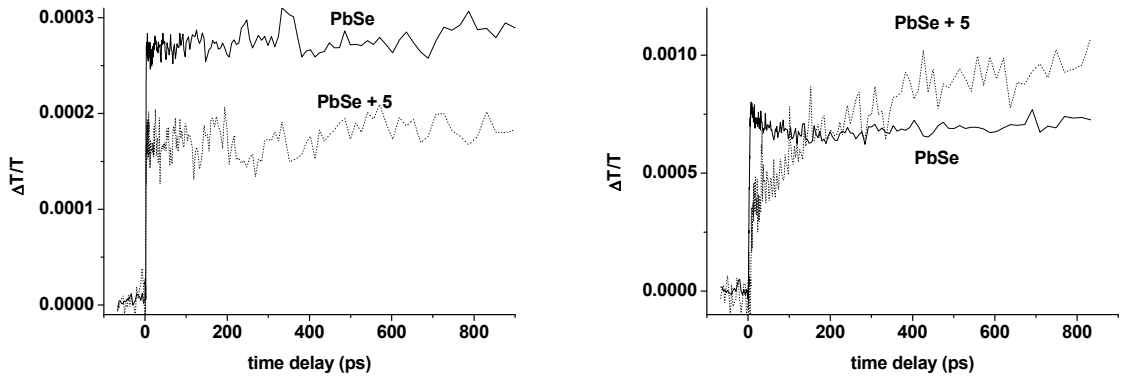


Fig. 8: Transient absorption (TA) spectroscopy of quantum dots and quantum dots mixed with porphyrin **5**. Solid line represents PbSe quantum dots and dotted line represents QDs + **5** (a) excited at 800 nm and probed at 1044 nm, (b) excited at 400 nm and probed at 1000 nm.

The transient absorption traces at 1044 nm of both solutions shown in figure 8a, remain constant in time and we do not see a decrease in absorption (or increase in transmission), when quantum dots are mixed with porphyrins. This indicates that there is no charge transfer from quantum dots to porphyrins. It was according to our expectations as porphyrins are excited at higher energy than quantum dots, so energy transfer is not probable in this case.

However, we did expect that charge transfer from porphyrins to quantum dots will occur. For this purpose, we excited the quantum dots alone or in the presence of porphyrins, at 400 nm, and probed the system at 1000 nm (figure 8b). The transient absorption traces shown in figure 8b) reveals a relatively moderate increased transmission (decreased absorption) when quantum dots are treated with porphyrins. This strongly suggests that excitation of the porphyrin indeed leads to photo-induced charge transfer to the PbSe quantum dots.

## 5.3 Conclusions

We performed experiments to study binding interaction of porphyrins with quantum dots and observed charge transfer from porphyrins to quantum dots. We did not observe charge transfer from quantum dots to porphyrins, based on our observations in transient absorption

spectroscopy experiments. As mentioned earlier, these studies were part of our goal in molecular electronics (next chapter) to have more understanding of charge / energy transfer in hybrid systems. Because charge transfer occurs from porphyrins to quantum dots, therefore these molecules can further be used for charge transfer through nanoelectrodes and are good candidates for single molecule electronic studies.

Besides the general conclusions, several observations were made. Porphyrin – QD hybrid materials should be handled in air free atmosphere, and porphyrins containing amino groups or thiol groups do not bind to QDs, however only tetra carboxylic acid functionalized porphyrins does bind with quantum dots. In general, there is no pronounced effect in energy / charge transfer, whether Zn ion is present in the core of porphyrin or not. Mono-carboxylic acid functional group containing porphyrins do not bind with QDs. These binding interactions were unveiled using fluorescence quenching, UV-Vis-IR absorption, and life time decay change.

Transient absorption spectroscopy confirmed that there is energy transfer from porphyrins to quantum dots. There was no energy / charge transfer from quantum dots to porphyrins used in this study. Quantum dots appear to change size or may precipitate slowly in time, when they are exposed for longer times to any porphyrin containing carboxylic acid functional group, as was observed from a blue shift in the absorption of quantum dots and the decrease of scattering at short wavelengths.

## 5.4 Experimental

### 5.4.1 Materials and methods

All solvents used for reactions and measurements were purified with the use of MBRAUN Solvent purification system MB SPS-800

### 5.4.2 PbSe quantum dots

Oleylamine capped PbSe QDs were synthesized with standard air and moisture free techniques i.e. using schlenk line and nitrogen glove box, following the method of Maksym V. Kovalenko.[14] 14.0 mL of oleylamine and 0.38 g $PbCl_2$ were degassed under vacuum at 100 $^oC$ for half hour, and then heated to 140 $^oC$ under nitrogen. Then two solutions of 260 μL

$Sn(N(SiMe_3)_2)_2$ dissolved in 2 mL trioctylphosphine (TOP) and 6 mL of 1M Se-trioctylphosphine were prepared in different vials in a glove box. The two solutions were mixed in a syringe and immediately injected into the $PbCl_2$/oleylamine solution. The reaction mixture was kept at 112 $^oC$ for 2 minutes, and then cooled using a water bath. These QDs were precipitated by adding butanol, centrifuged and redissolved in hexane. We estimated the average size of the nanoparticles using the relationship between the bandgap $E_0$ and the size of the nanoparticles. From the curve fit using the published data and method [15], we calculate a value of ~ 2.8 nm.

### 5.4.3 Porphyrins

Porphyrins **1**, **2**, **5** and **6** were obtained from commercial sources, whereas porphyrin **3** was synthesized according to the method described in literature.[24] Porphyrin **4** was synthesized as described in third chapter of this thesis.

### 5.4.4 UV-Vis and fluorescence spectroscopy

UV-Vis measurements were performed in AnalytikJena Specord 250 spectrometer or a Perkin-Elmer Lambda 900 spectrometer, equipped with a deuterium-lamp and a halogen-lamp. Quartz cuvettes were used with path-lengths of 10mm. Fluorescence spectroscopy was performed on a Jasco J-815 CD-spectrometer. The cuvette used here was quartz with dimensions 3x3mm. For determination of luminescence lifetimes, a LifeSpecs-ps (Edinburgh instruments) was used with excitation pulses of 70 ps at 405 nm.

In the fluorescence experiments, the concentration of porphyrins was kept constant at 2.5 μM, unless otherwise specified. The concentration of PbSe QDs (added) was constant at 1 μM. QDs were generally added to the solution of porphyrins with amounts ranging from 10 – 1000 μL (0.005 μM – 0.5 μM). The mixtures were stabilized for few hours before the measurements were taken. The excitation wavelength was initially taken at the Soret band of the specific porphyrin. In the last few measurements, the excitation wavelength was fixed at 404 nm and mentioned in the results & discussion part of this chapter. The solvent used in these experiments was THF, TCE or *iso*-propanol.

### 5.4.5 Transient absorption spectroscopy

The samples were excited and monitored by pump and probe pulses from a chirped-pulse amplified laser system (Mira-Legend USP, Coherent Inc.), running at 1 kHz and delivering pulses of 60 fs, 2.2 mJ and at a wavelength of 795 nm. Tunable infrared and visible pulses (<100 fs) were generated by optical parametric amplification (Topas-800-fs and Opera, Coherent Inc.). Pump and probe beams were imaged onto InGaAs pin photodiodes (Hamamatsu G5853-23, G8605-23). The two beams were spatially separated downstream of the sample. Orthogonal polarization of the beams allowed further separation by means of a polarizer.

## 5.5 References


1. Sykora, M., et al., *Photoinduced Charge Transfer between CdSe Nanocrystal Quantum Dots and Ru−Polypyridine Complexes.* Journal of the American Chemical Society, 2006. **128**(31): p. 9984-9985.
2. Liu, X., et al., *Anodic Electrochemiluminescence of CdTe Quantum Dots and Its Energy Transfer for Detection of Catechol Derivatives.* Analytical Chemistry, 2007. **79**(21): p. 8055-8060.
3. Samia, A.C.S., X.B. Chen, and C. Burda, *Semiconductor quantum dots for photodynamic therapy.* Journal of the American Chemical Society, 2003. **125**(51): p. 15736-15737.
4. Chen, M., et al., *Functionalized Self-Assembled InAs/GaAs Quantum-Dot Structures Hybridized with Organic Molecules.* Advanced Functional Materials, 2010. **20**(3): p. 469-475.
5. Rakovich, A., et al., *Resonance Energy Transfer Improves the Biological Function of Bacteriorhodopsin within a Hybrid Material Built from Purple Membranes and Semiconductor Quantum Dots.* Nano Letters, 2010. **10**(7): p. 2640-2648.
6. Huang, J., et al., *Photoinduced Ultrafast Electron Transfer from CdSe Quantum Dots to Re-bipyridyl Complexes.* Journal of the American Chemical Society, 2008. **130**(17): p. 5632-5633.
7. Issac, A., S. Jin, and T. Lian, *Intermittent Electron Transfer Activity From Single CdSe/ZnS Quantum Dots.* Journal of the American Chemical Society, 2008. **130**(34): p. 11280-11281.
8. Tisdale, W.A., et al., *Hot-Electron Transfer from Semiconductor Nanocrystals.* Science, 2010. **328**(5985): p. 1543-1547.
9. Zenkevich, E., et al., *Nanoassemblies designed from semiconductor quantum dots and molecular arrays.* Journal of Physical Chemistry B, 2005. **109**(18): p. 8679-8692.
10. Zenkevich, E.I., et al., *Identification and assignment of porphyrin-CdSe hetero-nanoassemblies.* Journal of Luminescence, 2007. **122**: p. 784-788.
11. Kilin, D.S., et al., *Ab initio study of exciton transfer dynamics from a core-shell semiconductor quantum dot to a porphyrin-sensitizer.* Journal of Photochemistry and Photobiology a-Chemistry, 2007. **190**(2-3): p. 342-351.
12. Wen, Y.N., et al., *Activation of porphyrin photosensitizers by semiconductor quantum dots via two-photon excitation.* Applied Physics Letters, 2009. **95**(14).
13. Frasco, M.F., V. Vamvakaki, and N. Chaniotakis, *Porphyrin decorated CdSe quantum dots for direct fluorescent sensing of metal ions.* Journal of Nanoparticle Research, 2010. **12**(4): p. 1449-1458.
14. Kovalenko, M.V., et al., *Quasi-Seeded Growth of Ligand-Tailored PbSe Nanocrystals through Cation-Exchange-Mediated Nucleation.* Angewandte Chemie International Edition, 2008. **47**(16): p. 3029-3033.
15. Moreels, I., et al., *Composition and size-dependent extinction coefficient of colloidal PbSe quantum dots.* Chemistry of Materials, 2007. **19**(25): p. 6101-6106.
16. Moreels, I., et al., *Surface Chemistry of Colloidal PbSe Nanocrystals.* Journal of the American Chemical Society, 2008. **130**(45): p. 15081-15086.
17. Gautam, U.K. and R. Seshadri, *Preparation of PbS and PbSe nanocrystals by a new solvothermal route.* Materials Research Bulletin, 2004. **39**(4-5): p. 669-676.
18. Sun, Y.Y., et al., *Preparation and characterization of nanocrystalline PbSe in poly(acrylic acid-co-styrene).* Journal of Materials Research, 2001. **16**(10): p. 2922-2927.

19. Gao, S.Y., et al., *Synthesis of Se nanospheres and PbSe nanoshells in solution under refluxing and stirring.* Smart Materials & Structures, 2007. **16**(6): p. 2350-2353.
20. Gao, Y., et al., *Photoconductivity of PbSe Quantum-Dot Solids: Dependence on Ligand Anchor Group and Length.* Acs Nano, 2012. **6**(11): p. 9606-9614.
21. Etgar, L., E. Lifshitz, and R. Tannenbaum, *Synthesis of water-soluble PbSe quantum dots.* Journal of Materials Research, 2008. **23**(04): p. 899-903.
22. Goodpaster, J.V. and V.L. McGuffin, *Selective Fluorescence Quenching of Polycyclic Aromatic Hydrocarbons by Aliphatic Amines.* Analytical Chemistry, 2000. **72**(5): p. 1072-1077.
23. Clevers, J.G.P.W., L. Kooistra, and M.E. Schaepman, *Using spectral information from the NIR water absorption features for the retrieval of canopy water content.* International Journal of Applied Earth Observation and Geoinformation, 2008. **10**(3): p. 388-397.
24. Yuasa, M., et al., *Micellar Cobaltporphyrin Nanorods in Alcohols.* Journal of the American Chemical Society, 2004. **126**(36): p. 11128-11129.

# CHAPTER 6

## Single Molecule Conductance of Porphyrin Derivatives

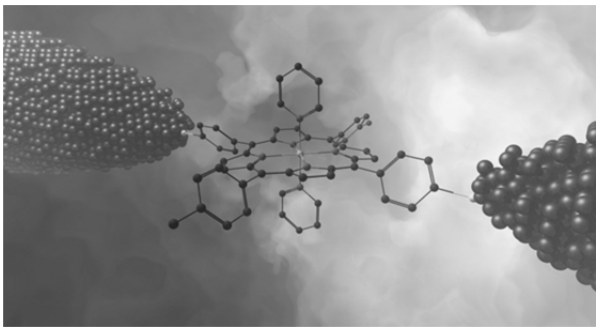

Artistic impression of a single porphyrin molecule bridging between source and drain electrodes.

In this chapter, the electronic conductance characteristics of porphyrins using single molecule devices are described. The formation of single-molecule devices based on nanometer-spaced platinum electrodes using a self-breaking electromigration method yielded nanogaps with long-term stability at room temperature. A detailed comparison of the device electrical properties before and after deposition of the molecules was studied. Additionally, charge transport in thiol-functionalized porphyrin molecular junctions using the mechanically controllable break-junction (MCBJ) technique at room temperature and cryogenic temperature (6K) show that molecules can take on different junction configurations, having an observable effect on the trace histograms and the current–voltage ($I(V)$) measurements. Our MCBJ studies also suggests that porphyrin molecules with added thiol end groups and pyridine axial groups form more stable single molecule junctions with an increased spread in low-bias conductance with different bridging geometries. In contrast, rod-like molecules show one preferential binding geometry.

The work described in this chapter was published:

1. Perrin, M. L.; Prins, F.; Martin, C. A.; **Shaikh, A. J.**; Eelkema, R.; van Esch, J. H.; Briza, T.; Kaplanek, R.; Kral, V.; van Ruitenbeek, J. M.; van der Zant, H. S. J.; Dulić, D., Influence of the Chemical Structure on the Stability and Conductance of Porphyrin Single-Molecule Junctions. *Angewandte Chemie International Edition* **2011,** *50* (47), 11223-11226.

2. Perrin, M. L.; Martin, C. A.; Prins, F.; **Shaikh, A. J.**; Eelkema, R.; van Esch, J. H.; van Ruitenbeek, J. M.; van der Zant, H. S. J.; Dulić, D., Charge transport in a zinc–porphyrin single-molecule junction. *Beilstein Journal of Nanotechnology* **2011,** *2*, 714-719.

3. Prins, F.; **Shaikh, A. J.**; van Esch, J. H.; Eelkema, R.; van der Zant, H. S. J., Platinum-nanogaps for single-molecule electronics: room-temperature stability. *Physical Chemistry Chemical Physics* **2011**, 14297–14301.

## 6.1 Introduction

Metal-bound porphyrins could find use as conductive platforms in single molecule electronic devices, such as transistors and sensors. Trans-functionalized porphyrins such as the ones described in Chapter 3 possess a conjugated pathway spanning from one terminus to the other, while having a central cavity capable of binding a metal cation. The cation can be used to bind analytes, introduce an unpaired electron in the system, or change the frontier orbital energies of the porphyrin to influence the conductance characteristics of the overall device. In general, for incorporation in single molecule devices, the porphyrin should be contacted to nano-scale metal electrodes reliably and reproducibly. It is the purpose of this chapter to evaluate the stability and conductance behavior of *trans*-functionalized porphyrins in nano-scale electronic devices.

### 6.1.1 Transport through junctions

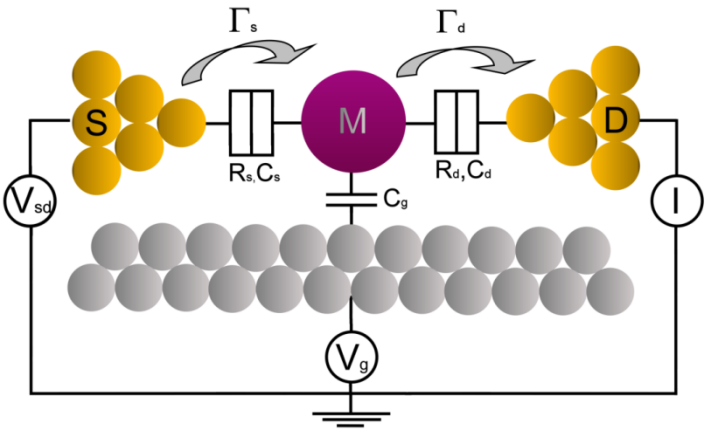


Fig. 1: Schematic representation of a single molecule electronic device. The electronic coupling between the source (S), the molecule (M) and the drain (D) determines the transport $\Gamma_s$ (S - M) and $\Gamma_d$ (M - D) via tunnel barriers, allowing charge carriers to tunnel to and from the molecule with resistance (R) and conductivity (C). $V_{sd}$ and $V_g$ represents bias and gate voltage respectively.[1]

Nanoscale single molecule electronic devices are typically made up of nanoscale source and drain electrodes, and a molecule bridging between these two electrodes. In more sophisticated devices, a third gate electrode is introduced, allowing manipulation of the frontier orbital energy levels of the bridging molecule by applying a potential difference. Conductance in

single molecule electrical devices generally depends both on the conductivity of the molecule itself, as well as the coupling to the source and drain electrodes (figure 1).

Further details on the conduction of electrons through single molecule, transport mechanisms, coulomb blockade effect, Fermi levels of electrodes, and HOMO-LUMO levels of molecules, various techniques to measure single molecule conductance, and relevant previous research achievements are described in chapter 2 of this thesis.

## 6.1.2 Device fabrication and characteristics

The behavior of specific porphyrins was tested in two types of nanoscale electronic devices: electromigrated platinum nanogaps, and mechanically controlled break junctions with gold electrodes. The basic principles and some fabrication procedures of both types will be discussed below.

### 6.1.2.1 Platinum nanogaps made by electromigration

A common technique to fabricate three-terminal single molecule devices (e.g. transistors) is through electromigration of thin metal wires on top of $Al/Al_2O_3$ gate structures.[2-7] In the process of electromigration atoms in a metal migrate at high current-density, due to momentum transfer to the metal ions from the current-carrying electrons. Resistive heating assists this process and in this way small wires can be thinned and eventually broken to form nanoscale electrodes separated by a nanometer wide gap. It is unfortunately not possible to control the gap size with atomic precision, and electromigration will therefore always result in a distribution of gap sizes. Until recently, three-terminal measurements on single molecules were performed at low temperatures due to the instability of the commonly used gold electrodes. In nanoscale electronics, gold is a preferred electrode material because of its superior noble character. However, at room temperature the atomic mobility is so high that in electromigrated devices the electrodes tend to retract and the separation between them becomes too large for a molecule to bridge. To obtain a device capable of functioning at room temperature, the Molecular Electronics and Devices group at TU Delft has made platinum-based nanogaps by electromigration.[8] The room-temperature stability of these gaps is a result of the larger cohesive energy of the Pt–Pt bond (5.8 eV) as compared to the Au–Au bond (3.4 eV). The advantages of the stable Pt-electrodes are that they can be plasma-cleaned,

re-used, and repeatedly cycled to low temperature without significant changes in the gap-resistance.

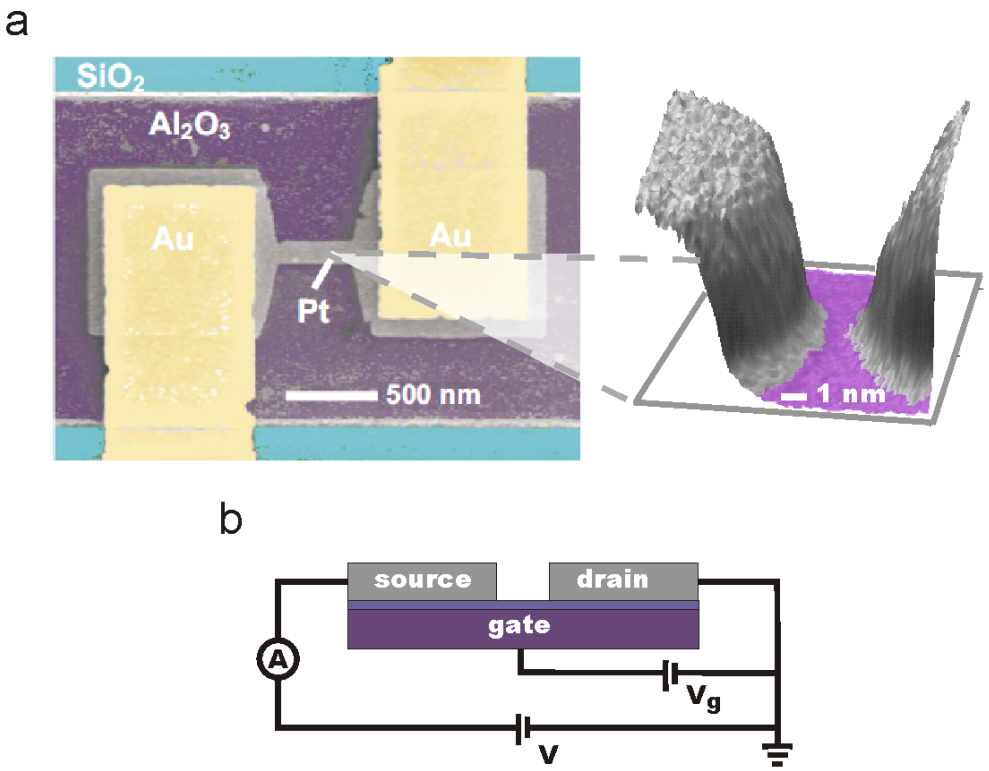


Fig. 2: a) Colorized scanning electron microscopy image of the device structure. The Pt nanowire (grey) is positioned on top of a $Al/Al_2O_3$ gate electrode (purple) which in turn lies on the $SiO_2$ surface (blue). Contact to the Pt nanowire is made through thick Au pads (yellow). Inset: 3D-model of an electromigrated Pt nanogap, constructed from a transmission electron microscopy image (from our collaborators) b) Schematic representation of the measurement setup.

The inherent stability of a platinum device makes it possible to perform electrical characterizations of the gap prior to molecule deposition. In this way, changes in the current–voltage characteristics after molecule deposition can be unambiguously attributed to the molecule. Molecules can be deposited from solution and their transport behavior can be studied under ambient conditions, in a three terminal device.

With an electromigrated break junction, it is typically possible to measure current-voltage (I-V) characteristics of bound molecules. When a gate is included in the design, the dependence of I-V measurements on the gate voltage can be measured, often depicted as so called “stability diagrams”. A stability diagram is a 3-dimensional plot of dI/dV versus the bias voltage and the gate voltage.

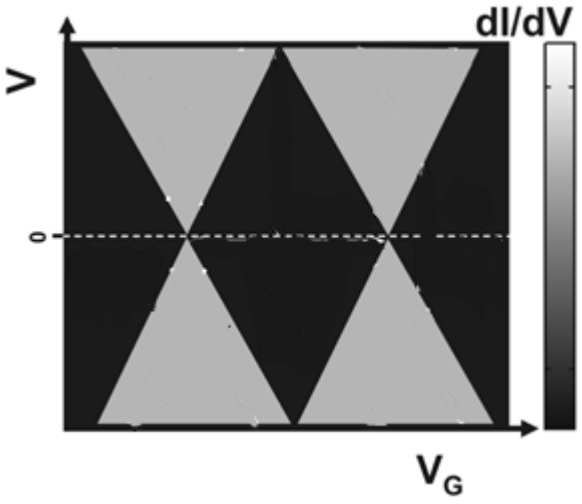


Fig. 3: Conductance map of the differential conductance, d*I*/ d*V*, versus $V$ and $V_G$ (stability diagram). The edges of the diamond-shaped regions (black) correspond to the onset of current (gray).

When the transport Γ is very small compared to the coulombic interactions, the system is in the weak coupling limit. In the weak coupling, Coulomb blockade regime, a low current is observed over a wide voltage range. Figure 3 illustrates the result of a typical transport measurement in the form of a stability diagram. Slanted lines separate regions of high conductance (single-electron tunneling (SET) regime, grey regions) from enclosed diamond-shaped regions (Coulomb diamonds) with almost zero conductance (black regions). Inside the black diamond-shaped regions the number of electrons on the molecule is fixed to an integer value. Between consecutive black regions (charge states) the charge on the molecule increases (or decreases) by one unit as we go to more positive (or negative) gate voltages. It should be noted that it is difficult to assign a particular charge state of the free molecule to these states. For instance, the charge state measured at zero bias and zero-gate voltage may not be the neutral charge state of the molecule. At zero bias, partial charging of the molecule can take place in order to equilibrate the chemical potentials across the junction. Background charges from electron-traps in the vicinity of the device may also introduce an offset in the level positions of the molecular quantum dot.

#### 6.1.2.2 Mechanically controllable break junctions

A high precision technique for electrical characterization of single molecules is the mechanically controllable break junction (MCBJ). In this device, a gold wire is attached to a substrate. Through lithographic techniques, a thinned, freestanding bridge of gold is created

on the substrate (figure 4). Bending of the substrate leads to additional thinning and eventually breaking of the gold bridge. Subsequently, the electrode displacement can be controlled with sub-Å precision via the deflection of the substrate center (the pushing rod). In principle, the bending can be considered elastic, resulting in a gap size between the two electrodes (Δd) that is proportional to the lateral displacement (Δz) (figure 5). The ratio Δd/Δz is called the reduction factor "r" and "1/r" is the attenuation factor. The high attenuation factor in MCBJ results in picometer control of electrode spacing. The junctions have high stability at cryogenic temperatures and high vacuum (~$10^{-7}$ mbar).

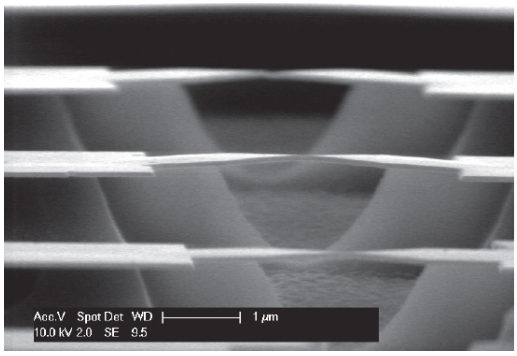


Fig. 4: SEM picture of typical MCBJ sample. Adopted from reference[9]

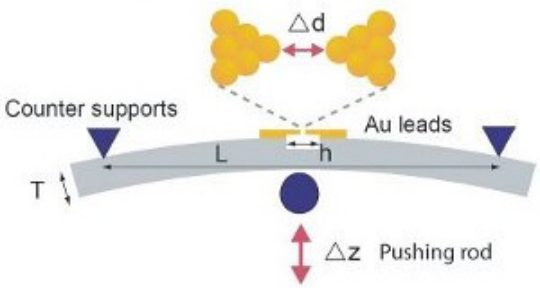


Fig. 5: Mechanism of a mechanically controllable break junction. A Push rod bends the flexible substrate, resulting in atomic sized gaps (contacts) by breakage of the metallic constriction on top.

In an MCBJ, molecules are typically assembled from solution, on an unbroken gold wire. After removal of excess solvent, a monolayer of molecules is assumed on the gold surface of the device. Upon subsequent mechanical breaking of the wire, one or a few molecules will bridge the gap between the nanoscale gold electrodes. Whether a single molecule is present between the electrodes can generally be assessed from the subsequent conductance characteristics of the device, when the electrodes are separated further (figure 6). The intrinsic softness of the gold wire results in the formation of a single atom gold wire at the breaking

point, just before breaking. The single atom gold wire has a single quantum conductance $2e^2/h$ that is clearly visible as a plateau in the conductance *vs* displacement traces that are typically recorded for these devices. In most measurements, device and molecular conductance in the MCBJ are listed in relation to this fundamental conductance, known as $G_0$.

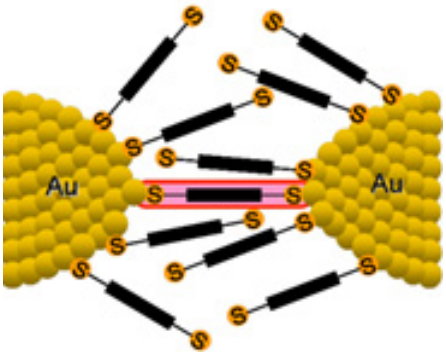


Fig. 6: Two gold nanoelectrodes near to each other at molecular distances. Molecules containing two thiol groups are stuck on both the sides of the electrodes.

The atomic-level geometry of the electrode-molecule contact has an effect on the molecular conductance and can vary from one experiment to the other. Because the mechanical behavior of an MCBJ is reversible, numerous breaking and making experiments can be performed on a single device, with or without molecules present. In this way, statistical information on the conductance behavior of the device can be obtained, often displayed in so-called 'trace histograms'. These histograms show the conductance (log(G)) versus the electrode displacement (d), and map the breaking dynamics of the junctions beyond the point of rupture ($G_0$, defined as d=0). Areas of high counts represent the most typical breaking behavior of the molecular junction.

Overall, the major advantage of the MCBJ is that it allows precise and dynamic control over electrode spacing. As different spacing will likely lead to changes in molecular conformation in the gap, and thereby conductance, the MCBJ makes it possible to mechanically control single molecule conductance.

## 6.2 Results and discussion

The main goal of the experiments on conductance of porphyrins in nanoscale electronic devices was two-fold: first, the porphyrins were used to test the device characteristics and stability of both electromigrated and mechanically controlled break junctions. Second, when successful, the transport characteristics of the various porphyrins could be investigated, to obtain a relationship between conductance behavior and molecular structure in said nanoscale devices. Overall, this study gives insights into the use of both these device architectures and molecular design in nanoscale electronics.

### 6.2.1 Porphyrins

The single molecule conductance behavior of a range of porphyrins was studied using electromigrated platinum nanogaps and gold mechanically controlled break juntions. As different metals are used in these two device setups, porphyrins with anchoring groups known to display a high affinity for either platinum (amines) or gold (thiols) were used. The synthesis is described in Chapter 3. For various control experiments, porphyrins without anchoring groups were either synthesized (**2**, Chapter 3) or obtained commercially (**3**). The influence on conductance behavior of steric bulk on the π-surface of the porphyrin was studied using porphyrins containing a central metal ion, capable of binding a pyridine ligand (**5** and **6**). The synthesis of Zn-porphyrin **5** is described in Chapter 3, Ru-porphyrin **6** was obtained from Prof. V. Kral, University of Prague.

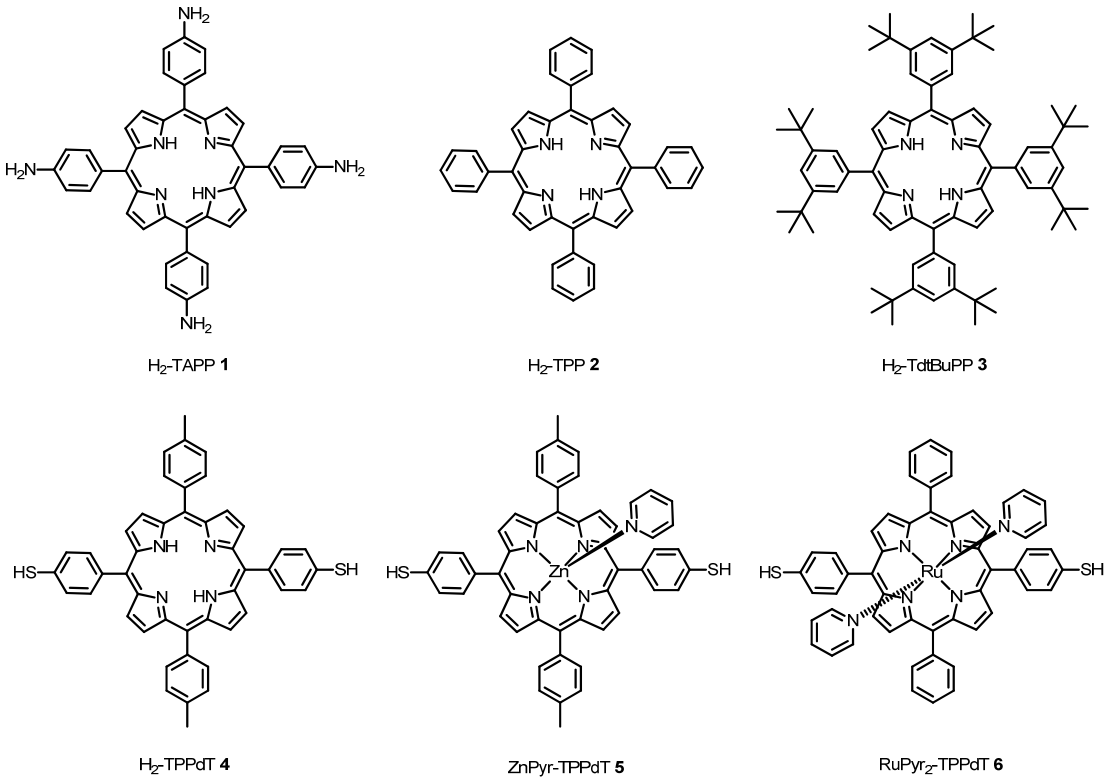


Fig. 7: Various porphyrin molecules used for single molecule studies.

### 6.2.2 Electromigrated break junctions (platinum nanogaps)

For this part of our research, platinum nanogaps obtained by electromigration were used to observe current-voltage characteristics of single porphyrins. The molecule that was applied here was tetra-aminophenyl porphyrin **1** as the amino group is known to have a greater affinity for platinum surfaces.[10]

These single-molecule devices are fabricated by using a self-breaking electromigration method which yields nanogaps with long-term stability at room temperature[8]. This stability allows detailed comparison of the device electrical properties before and after deposition of the molecules. In this way, conductance as a result of direct tunneling between the electrodes can be distinguished from conductance through the molecule. After molecule deposition, some devices display transport in the strong coupling regime while others are in the weak-coupling Coulomb blockade regime. Gated transport is observed in the latter case.

#### 6.2.2.1 Measurements

Nanogaps were prepared by feedback controlled electromigration followed by self-breaking according to the process described in ref [8]. To make optimal use of the stability of the nanogaps, the empty gaps were characterized electrically at room temperature and at low temperature (10 K). In this way, changes that occur after molecule deposition can be distinguished from the background conductance due to direct tunneling between the electrodes.

After the detailed empty-device characterization, molecules are introduced into the gap from solution. The electrodes are immersed in a 0.1 mM solution of $H_2$–TAPP **1** in acetone for 5 minutes after which they are rinsed with pure acetone, blow-dried, and placed back in the probe station vacuum chamber. After deposition, 8 out of 29 devices show a clear change in the current–voltage characteristics which is an indication that molecules have been trapped in the nanogap; we will refer to these devices as molecular junctions. It should be noted that control experiments (15 devices) with only solvent did not show any significant changes in the current–voltage characteristics.

#### 6.2.2.2 Results

Figure 8 displays four characteristic current–voltage characteristics before and after deposition. The conductance before deposition (black lines in figure 8) is a result of direct tunneling between source and drain and can be seen as an intrinsic background signal of the device. After deposition two types of current increase are observed (red lines in figure 8). The first, and predominant type (6 devices, see figure 8a and b for example), displays an increase in conductance across the entire voltage range. The conductance increases in the low-bias conductance range from two-fold up to ten-fold. The second type, which was observed in two molecular devices (see figure 8c and d), shows increased conductance only at higher bias values whereas the low-bias region superimposes with the background conductance of the device before deposition. This suggests that at low bias only direct tunneling contributes to the conductance while the conductance via the molecular levels is only possible at higher bias.

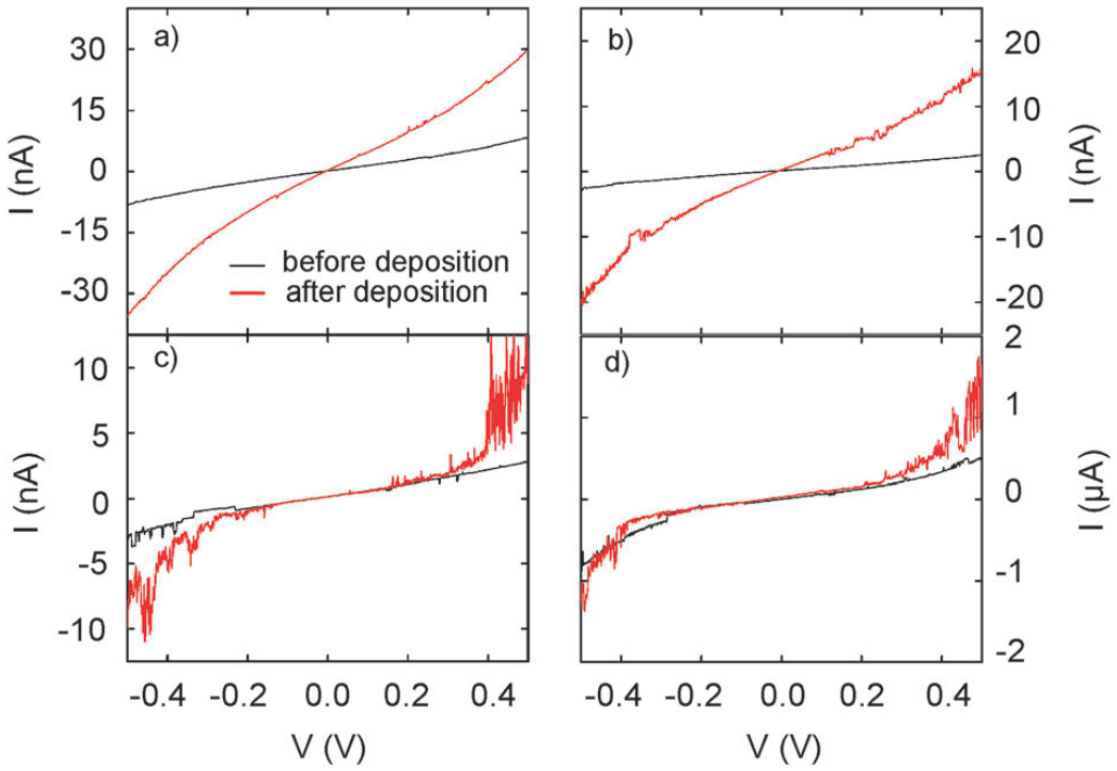


Fig. 8: Room-temperature current–voltage characteristics of four devices, before (black curves) and after (red curves) deposition of $H_2$–TAPP **1**. The increases in conductance after deposition show that transport is through one or more molecules. Two types of conductance increase are observed. The first type (a and b) shows increased conductance across the entire voltage range. The second type (c and d) shows increased conductance only at higher bias values whereas the low-bias region superimposes with the background conductance of the device before deposition. It is interesting to note that the current– voltage characteristics of this type show increased fluctuations at high bias, possibly due to small reconfigurations of the molecule in the junction.

Cooling the devices down to low temperature shows that some of the molecular devices display features in the current–voltage characteristics. Broad resonances are observed in the devices that showed increased conductance across the entire voltage range (see figure 9a for an example, same device as figure 8a). In the other device category, we see that also at low temperature the low-bias conductances before and after molecule deposition are the same (see figure 9b for an example, same device as figure 8c). Only at high bias clear differences are seen; in figure 9b only at negative bias voltage, as the red curve shows. At low temperature the increase in conductance is more abrupt, as can be expected since the thermal broadening is decreased.

Besides the two-terminal current–voltage characteristics we have also performed three-terminal characterization on 7 out of 8 molecular junctions using the $Al/Al_2O_3$ gate electrode

(in the device of figure 8d the gate electrode was not functioning properly due to higher than normal gate-drain currents). Most of the molecular junctions do not show gate-dependent transport. For example, the current–voltage characteristic of figure 9a does not change when the gate voltage ($V_g$) is varied between ±2.5 V (the maximum range in our devices). In one sample however, a clear gate-dependent onset in conductance is observed (see figure 9b, green and blue dashed lines).

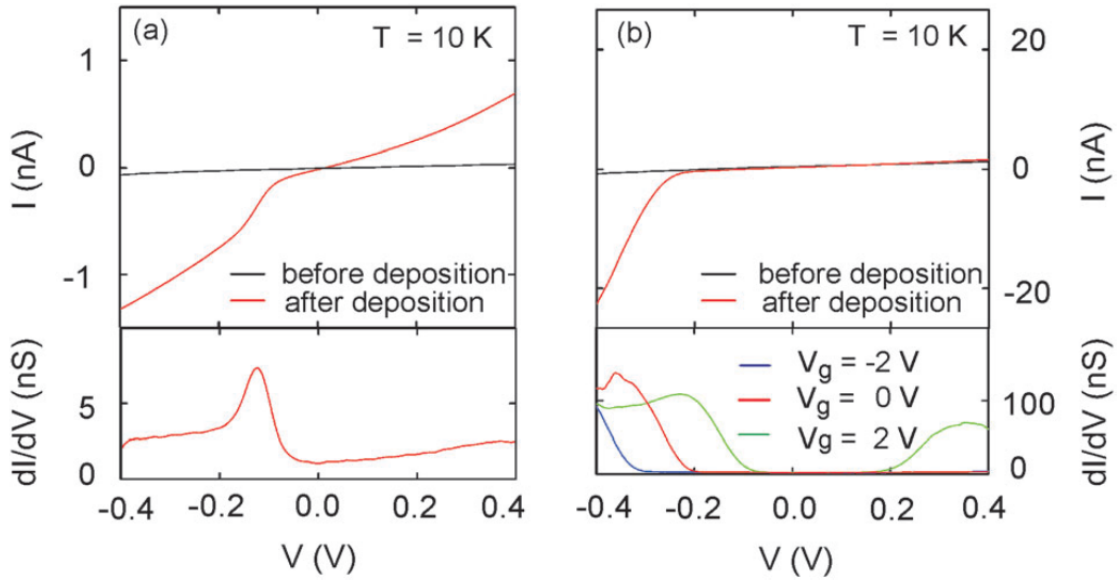


Fig. 9: (a) Current–voltage characteristic of a molecular device (the one from figure 8a) at low temperature (10 K) before (black line) and after (red line) deposition of H2–TAPP. The bottom panel shows the first derivative of the current, dI/dV after deposition. (b) Same for a second molecular device (the one from figure 8c). In the bottom panel dI/dV curves at different gate-voltages are displayed illustrating the gate dependent nature of the transport in this device.

To characterize the gate-dependent transport of the device in figure 9b in more detail, we constructed a conductance map (see figure 10). Before and after molecule deposition current–voltage characteristics are taken at low temperatures at different gate voltages, with the bias voltage ranging from −0.5 to 0.5 V and the gate voltage ranging from −2 to 2 V before deposition and −2.5 to 2.5 V after deposition. On the left panel a color-scale plot of the differential conductance (dI/dV) of the device as a function of bias voltage and gate voltage before deposition is displayed ($V_g$ = ±2 V). The current–voltage characteristics are smooth and therefore the corresponding dI/dV curves do not show any features (figure 10, left panel). Furthermore, no gate dependence is observed. After deposition, part of what is known as a Coulomb diamond becomes visible.[11] As figure 10 (right panel) indicates, in the dark blue

region transport through the molecule is blocked due to Coulomb repulsion, while in the red regions a molecular charge state has entered the bias window and transport occurs via single electron tunneling through a double barrier potential. The presence of only one (partial) Coulomb diamond indicates that transport occurs through a single molecule.

Although the Coulomb diamond is incomplete, we can deduce some important parameters. First, from the slope of the diamond edge we deduce that the crossing point of the diamond lies at positive gate voltage, estimated around $V_g = 3.5$ V. At positive gate voltages, molecular levels are shifted downwards in energy with respect to the Fermi level, which means that transport in the red regions occurs through the lowest unoccupied molecular orbital (LUMO) of the porphyrin molecule.

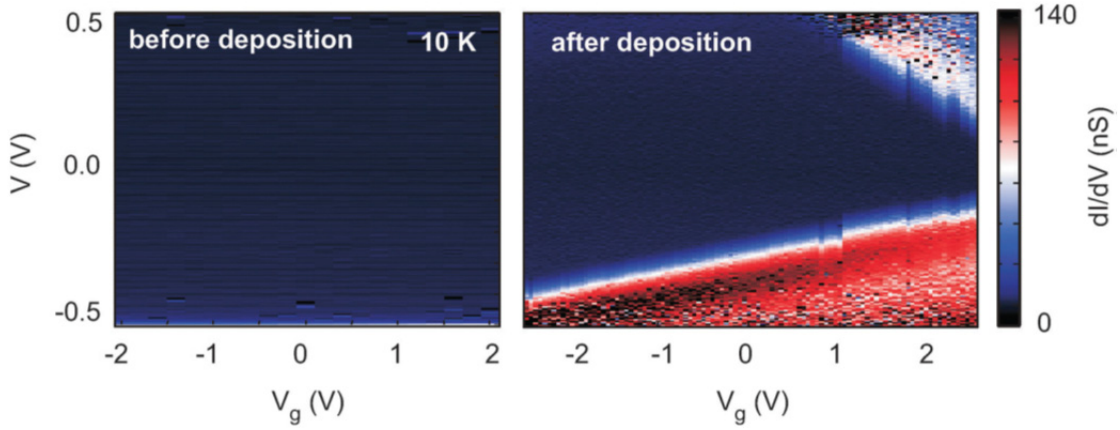


Fig. 10: Color-scale plots of the first derivative of the current (dI/dV) vs. bias (V) and gate voltage (Vg) before (left panel) and after (right panel) molecule deposition, at 10 K (same sample as displayed in Fig. 8c and 9b). Before deposition the conductance map is featureless whereas after deposition clear gate-dependent onsets of conductance are visible.

#### 6.2.2.3 Discussion

When the conductance only increases at higher bias, while at low bias the current is Coulomb-blockaded, transport occurs through a double-barrier potential and sequential tunneling is the main transport mechanism (figure 8c, d). A likely configuration that may establish such a double barrier is a porphyrin molecule bridging the source and drain electrodes through the amino-groups (see figure 11, right hand side). In contrast, an overall change of the current–voltage characteristic (Fig. 8a and b) indicates a (partial) lowering of a single tunnel barrier. This can be understood as follows: in the absence of a molecule bridging the gap, the

transport mechanism is direct tunneling through the vacuum barrier. In the presence of a molecule, a molecular level with an energy lower than the vacuum level results in a lower effective barrier. Off-resonant transport (i.e. superexchange) is then the main transport mechanism; the current at any non-zero voltage will be larger than in the absence of molecular levels. At higher bias resonances may be present if a molecular level is included in the bias window (resonant transport).

A single barrier configuration can be obtained if the molecule is very strongly coupled (and hybridized) to one electrode only (for example if it lies flat on one of the electrodes). This situation is then very similar to an STM-like configuration where the molecule interacts with the conducting substrate. The strong coupling to one of the electrodes would also explain the absence of gate-dependence in these devices where hybridization pins the molecular level to the Fermi-level of the metallic electrode. In this respect, it is interesting to compare the current–voltage characteristics of the gate-independent molecular junctions in our setup with previous STM experiments on porphyrin derivatives.

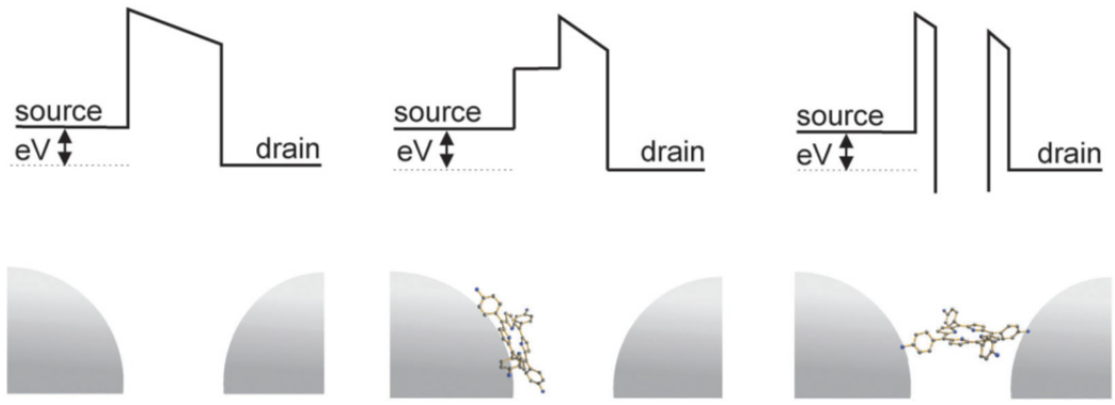


Fig. 11: Top: barrier landscapes of the observed transport mechanisms; direct tunneling (left), off-resonant tunneling (middle) and single electron tunneling (right). Bottom: sketch of the empty gap and two possible configurations of the porphyrin molecule between electrodes, which can lead to the corresponding barrier landscapes.

Finally, in view of room-temperature operation it is interesting to compare the low-temperature and the room-temperature current–voltage characteristics of the gate-dependent device. For both temperatures we find that the low-bias conductance is equal to the one before molecule deposition, while an onset in conductance is observed at higher bias. This suggests that even at room temperature Coulomb blockade is maintained in this device. Although this

is a promising aspect when looking for room temperature single-molecule transistors, the preferred strong coupling of the body of $H_2$–TAPP **1** to the electrodes suggests that this system is not the ideal candidate for this purpose. Modifications to the molecular system that would decouple the π-conjugated ring structure from the surface could help to improve the yield of weakly coupled molecules.

#### 6.2.2.4 Conclusions for the electromigrated breakjunctions

In conclusion, we have presented a method to contact single molecules in a three-terminal geometry. The stability of Pt enables operation at room temperature for which initial experiments have been performed with porphyrin molecules. A comparison between the current–voltage characteristics before and after deposition allows us to distinguish molecular transport from background-tunneling conductances. This information is important in the understanding of transport through single molecules. We have found that the $H_2$–TAPP **1** porphyrin derivative prefers to be situated flat on one of the electrodes, very similar to the situation studied in a scanning tunneling microscopy setup; gate-dependent transport is absent in this case. In some cases the molecule couples weakly to the electrodes and gate-dependent measurements shows Coulomb-blockaded transport. Further studies will be directed towards new molecular systems with less electrode–molecule interaction, promoting a single-molecule to bridge source and drain electrodes. The goal is a single-molecule, single-electron transistor at room temperature.

### 6.2.3 Mechanically controlled break junctions

In this section, we study the interaction of π-conjugated porphyrin molecules with nanoscale electrodes by means of time and stretching-dependent conductance measurements on mechanically controlled molecular break junctions. Strategies to reduce interactions of the molecular π-electrons with the metal electrodes by modifying the chemical structure of the porphyrin molecules are included.

#### 6.2.3.1 Measurements

To achieve a selective and strong affinity for the gold surface of the MCBJ electrode surface, we used the thiol-derived porphyrins **4** and **6** (figure 7) in the study of the influence of the

molecular structure on the formation of porphyrin single-molecule junctions. Since the thiol group is most commonly used to contact rod-like molecules to form straight molecular bridges[12], we first compared $H_2$-TPP **2**, without thiol termination (figure 7) to a nearly identical molecule with two thiol groups on opposite sides of the molecule ($H_2$-TPPdT **4**). To investigate the influence of the molecular backbone geometry on the junction formation we further studied a thiol terminated porphyrin molecule with two bulky pyridine axial groups attached via an octahedral $Ru^{II}$-ion ($RuPyr_2$-TPPdT **6**). Due to steric hindrance these groups can be expected to reduce the direct interaction of the metal electrodes with the π-face of the porphyrin [13].

Prior to electrical characterization, the molecules of interest were deposited using self-assembly from solution. To study the conductance of these molecules we used lithographic mechanically controllable break junctions (MCBJ) in vacuum at room temperature. The lay-out and characteristics of a MCBJ device in a three-point bending mechanism are described in Section 6.1.2.2. As the device is bent, the suspended electrodes on the substrate surface are stretched and broken at their thinnest point. Subsequently, the electrode displacement can be controlled with sub-angstrom precision via the deflection of the substrate center. During repeated breaking and fusing of the electrodes, the current was measured at a fixed bias voltage and the junction conductance was determined as a function of electrode stretching. To obtain the conductance value of the most probable contact geometry we repeatedly break and fuse the electrodes[14-16] between conductances of $1 \cdot 10^{-5}$ $G_0$ and 10 $G_0$, while measuring the current at a fixed bias voltage (100 mV). Sets of 1000 consecutive breaking traces from individual junctions were then analyzed numerically to construct 'trace histograms' of the conductance (log(G) versus the electrode displacement d)[17, 18]. This statistical method maps the breaking dynamics of the junctions beyond the point of rupture of the last monatomic gold contact (defined as d=0), which has a conductance of one quantum unit $G_0=2e^2/h$. Areas of high counts represent the most typical breaking behavior of the molecular junctions. Figure 12 presents 'trace histograms' as well as examples of individual breaking traces for an acetone reference sample (a) and junctions exposed to $H_2$-TPP **2** (b), $H_2$-TPPdT **4** (c) and $RuPyr_2$-TPPdT **6** (d). For all three porphyrin molecules as well as for the reference sample which was exposed to pure acetone several junctions have been measured. Here, we only show a typical set of measurements.

In the junction which was exposed to the pure solvent without porphyrin molecules (figure 12a), the Au-bridge initially gets stretched until a plateau around the conductance quantum (G ~ $G_0$) is observed (only visible in the individual traces shown in black), which corresponds to a monatomic contact [17]. Upon further stretching, the last gold-gold contact is broken and the conductance decreases sharply and abruptly to ~$10^{-3}$ $G_0$. Beyond this point, electron tunneling between the electrodes leads to a fast conductance decay with stretching (visible as the orange tail), as expected for tunneling across a vacuum barrier.

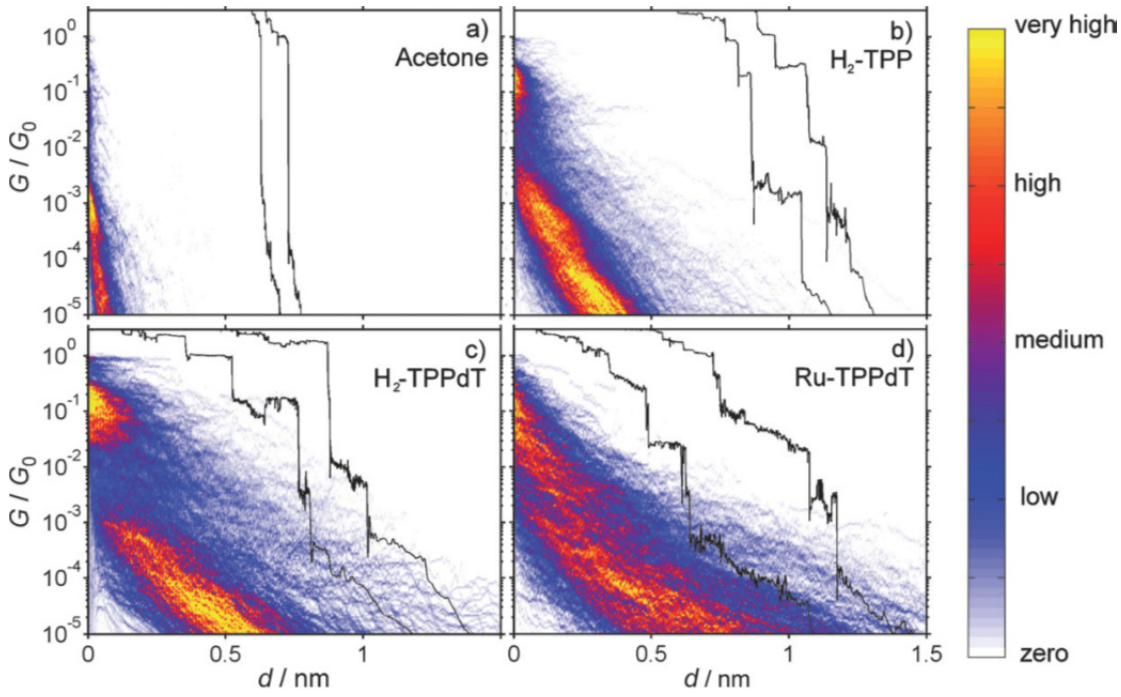


Fig. 12: Trace histograms constructed from 1000 breaking traces for junctions exposed to pure acetone, $H_2$-TPP, $H_2$-TPPdT, and Ru-TPPdT. The black curves are examples of individual breaking traces (offset for clarity). For the construction of the histograms, d=0 for each curve was set to the point where the conductance drops sharply below 1 $G_0$. All histograms were taken at a bending speed of 30 $mms^{-1}$ (on the scale of the electrodes, this bending is translated into a stretching on the order of 1.8 $nms^{-1}$) and a bias voltage of 150 mV. No data selection schemes were utilized. For additional trace histograms see the Supporting Information. For (a) we found a decay constant of 2 $Å^{-1}$.

### 6.2.3.2 Results

Introducing the porphyrins **2**, **3**, **4** or **6** by self-assembly on the junctions leads to pronounced plateaus at different conductance values in the sub-$G_0$ regime. These plateaus can be flat or sloped.[19, 20] The representative breaking traces that are included in Fig. 12b-d display a set

of such plateaus. Averaging over 1000 traces does not lead to a narrow region of high counts in the histograms, in contrast to measurements on rod-like molecules [16-18, 20]. In the trace histograms of porphyrins **2** and **3**, (figure 13a and b), however, there are two distinct regions with high counts; a high-conductance region (HCR) around $10^{-1}$ $G_0$, and a sloped low-conductance region (LCR) below $10^{-3}$ $G_0$. For $H_2$-TPPdT **4** (figure 12c) both the HCR and LCR are longer than for **2** and **3**; thus, adding the thiol end groups to $H_2$-TPP increases the plateau length. Adding the thiol to $H_2$-TPP **2** also reduces the slope of the LCR. In $RuPyr_2$-TPPdT **6** (figure 12d) the HCR and LCR can hardly be distinguished anymore: a single long region with a slight dip in the middle, sloping from $10^{-1}$ $G_0$ to $10^{-5}$ $G_0$ is present, which has a shallower slope compared to $H_2$-TPP **2** and $H_2$-TPPdT **4**, and an increased length.

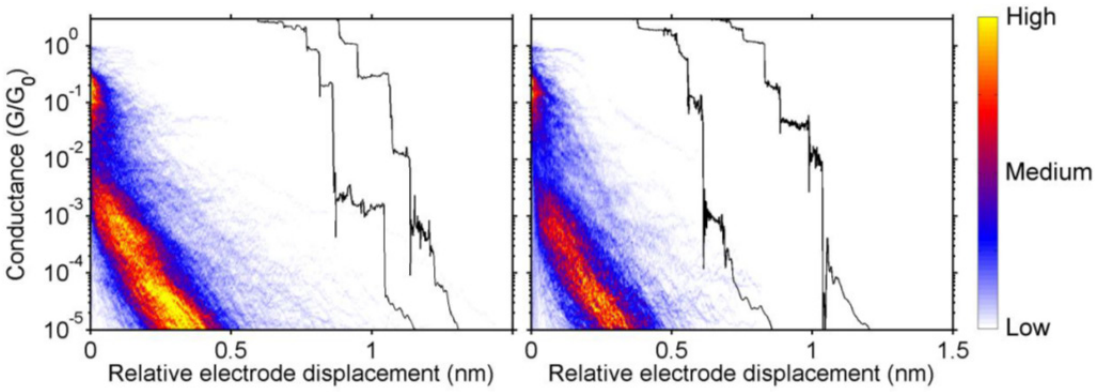


Fig. 13: Trace histogram obtained from a junction exposed to TPP **2** (left) and tetra butyl TPP **3** (right). Due to steric hindrance, tetra butyl TPP cannot form a molecular junction via π-stacking. Qualitatively, the plots exhibit similar transport features.

From the trace measurements we come to the following conclusions. First, a stable molecular junction can be formed even when no chemically distinct anchoring groups are present. Second, there is no qualitative difference between the trace histograms of **2, 3** and **4**. There is only an increased length of the area of high counts, which can be interpreted as an increase in junction stability versus stretching. Third, by adding two pyridine axial groups to the molecules (that is, for $RuPyr_2$-TPPdT **6**), the region of high counts in the trace histogram becomes even longer, and the variability in conductance increases.

Additional information about molecular junction configurations can be gained by measuring the evolution of the junction conductance over large time intervals at fixed electrode distances.[21] To obtain such 'time traces', we opened the junction in small steps using a

servo motor at 77K. This low temperature enhances their stability due to a reduced surface diffusion without causing extensive changes in molecular conductance.[9] We then measured the conductance in the range from 1 $G_0$ to $10^{-4}$ $G_0$ at various fixed electrode spacings and for time periods exceeding several hours. Due to the exceptional control over the electrode separation in the MCBJ,[9, 22] conductance jumps in these measurements can be attributed to reconfigurations of the molecule in the junction rather than mechanical interference of the setup.

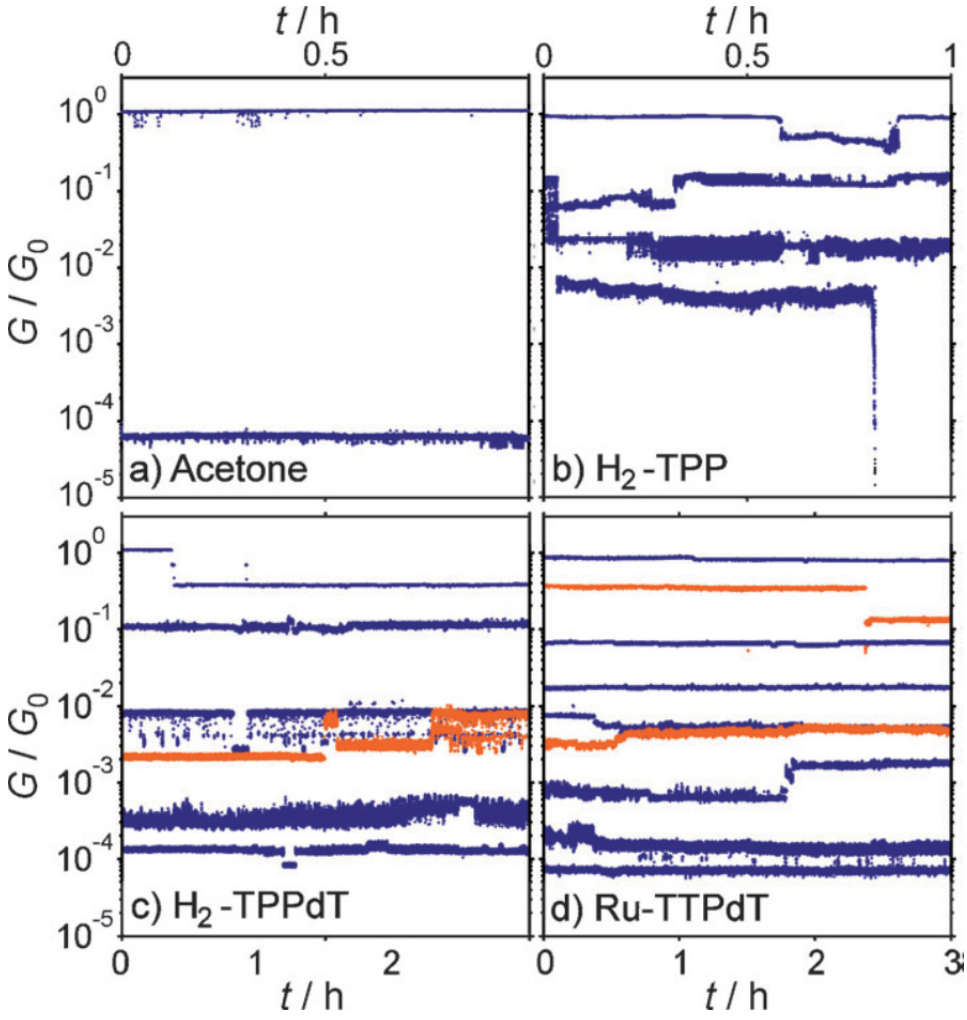


Fig. 14: Conductance-versus-time plots for acetone, H2-TPP, H2-TPPdT, and Ru-TPPdT taken at a bias voltage of 150 mV. The traces originate from the same opening event and are taken at intervals of 50 pm. Several lines are displayed in orange for clarity.

Typical time traces of junctions exposed to pure acetone, $H_2$-TPP **2** , $H_2$-TPPdT **4** and $RuPyr_2$-TPPdT **6** are presented in figure 14 a-d. As can be seen in figure 14a, a stable contact is formed at 1 $G_0$ in the clean junction. A slight increase in the electrode spacing leads to abrupt

breaking of the contact to a conductance value around $10^{-4}$ $G_0$. In contrast to this sharp drop, the presence of porphyrin molecules leads to the formation of junctions with conductances in the region between 1 $G_0$ and $10^{-3}$ $G_0$ ($H_2$-TPP **2** figure 14b, $H_2$-TPPdT **4** figure 14c and $RuPyr_2$-TPPdT **6** figure 14d). Below $10^{-3}$ $G_0$, the $H_2$-TPP molecule (figure 14b) exhibits a sudden conductance drop to below $10^{-5}$ $G_0$. In contrast, thiol terminated $H_2$-TPPdT **4** and Ru-TPPdT **6** (figure 14 c-d) form molecular junctions over the whole range between 1 $G_0$ and $10^{-4}$ $G_0$. The observations support the conclusions drawn from the trace histograms: adding thiol and pyridine groups increases the junction stability and leads to a variety of molecular geometries with different conductance values. To examine the contribution of π-stacking of multiple molecules to those configurations, we measured trace histograms on junctions exposed to the bulkier $H_2$-TdtBuPP **3**. Due to steric hindrance of the butyl groups, the possibility of π-stacking between two molecules is reduced. Resulting trace histograms are shown in figure 13. There is no qualitative difference between the trace histogram of **3** and **2** molecules, which demonstrates insignificant influence of π-stacking on the formation of different configurations.

A closer inspection of the time traces reveals interesting information on the behavior of the molecule in the junction. Since the electronic noise of the junction is much smaller than the width of the observed bands of the measured conductance values, we conclude that what appears to be noise in the time traces is in fact a sign of small variations in the molecular configuration[22]. Large jumps in the conductance (figure 14c-d) indicate that a molecular junction can spontaneously change configuration. In figure 14c random telegraph noise between two conductance values is observed indicating the possibility of forming several meta-stable configurations. Furthermore, figure 14d shows that a particular junction conductance can be reached from different starting values (blue and orange traces in the middle of the figure).

The presence of such a large range of molecular adsorption geometries contrasts with most studies on long rod-like molecules, which typically assume a straight bridging configuration of the molecule with both thiol groups connected to the electrodes (see figure 15a). For $H_2$-TPPdT **4**, such a configuration could be expected. However, the high affinity of the porphyrin π-cloud for metal surfaces likely stabilizes other configurations, such as sketched in figure 15b and 15c (the configuration shown in figure 15b is likely destabilized by adding the

pyridine axial groups, as the one shown is figure 15c may be stabilized, as displayed in figure 15d). Although a stable junction configuration can be formed without thiol groups,[23] recent break junction experiments have indeed demonstrated that benzene moieties can bind directly to gold electrodes [24]. Furthermore, it has been reported that the lateral coupling of π orbitals to the electrodes can influence the single-molecule conductance of rod-like molecular wires [25, 26]. Such coupling can only become more likely when laterally extended molecules are probed. In addition these molecules have internal degrees of freedom, which can influence the charge transport on a single molecule level [27]. STM studies have indicated that tetraphenyl porphyrins can bind to Au(111) through an interaction with their phenyl side groups [28]. On gold surfaces their conformation can change through rotations of side groups and buckling of the center [29]. Such variations in the adsorption geometry, which can be expected to lead to different conductances, are likely the origin of the variety of junction configurations that we observe.

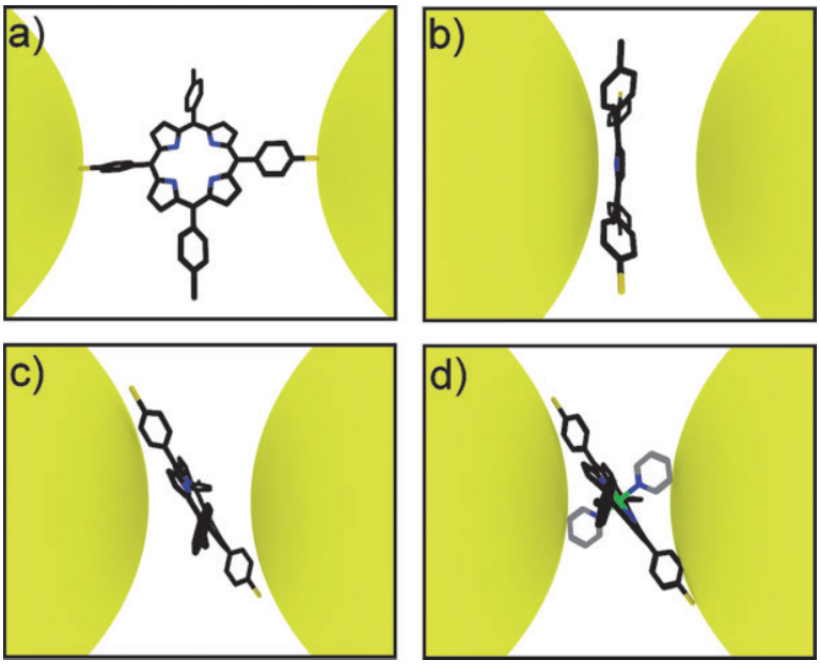


Fig. 15: Illustration of four possible configurations of a porphyrin molecule in the junction. a) Bridging configuration, b) STM-like configuration, and c) intermediate configuration of $H_2$-TPPdT; d) intermediate configuration of Ru-TPPdT (pyridine groups shown in gray).

#### 6.2.3.3 Current voltage characteristics

To get a better insight into the current voltage characteristics of porphyrins in a mechanically controlled break junction setup, in this section, we investigate both the low-bias and the high-bias regime charge transport through zinc porphyrin **5** with an axial pyridine ligand. Porphyrins are ideal for this purpose as they are complex, non-rod-like molecules, which can form various stable configurations [28, 30], especially in the presence of the axial pyridine group [31]. Using the mechanically controllable break junction technique (MCBJ), we here study the low-bias conductance as a function of electrode displacement. In addition, we use current-voltage measurements for different electrode spacings to gain spectroscopic information in the high-bias regime.

##### 6.2.3.3.1 Measurement setup

All experiments are performed in high vacuum ($<10^{-6}$ mbar). Prior to the experiments, ZnPyr-TPPdT **5** is dissolved in dichloromethane (DCM) and deposited on the unbroken electrodes using self-assembly from solution. After deposition, the junctions are broken in vacuum at room temperature. The aforementioned stability of the electrodes allows us to characterize charge transport through ZnPyr-TPPdT **5** by performing two types of experiments. First, we measure at room temperature the low-bias conductance of the molecule as a function of electrodes stretching. Second, we perform spectroscopy of the molecular levels by measuring current-voltage characteristics, *I-Vs,* at fixed electrode spacings, both at room temperature and cryogenic temperature (6K).

##### 6.2.3.3.2 Results

In figure 16 we show trace histograms as well as examples of individual breaking traces for a junction exposed to (a) the solvent DCM and (b) ZnPyr-TPPdT **5**. All measured curves are included, i.e., no data selection has been employed. We measured several samples with ZnPyr-TPPdT **5** molecules as well as DCM references. The features shown in figure 16a and 16b are representative for all these measurements.

In the junction that was exposed to the pure solvent without porphyrin molecules (figure 16a), the Au-bridge is stretched until a single-atom contact is formed, visible (only in the individual traces in the inset) as a plateau around the conductance quantum ($G \sim G_0$). Upon further

stretching, the monatomic contact is broken and the conductance decreases sharply and abruptly to ~$10^{-3}$ $G_0$ due to relaxation of the electrode tips. Beyond this point, electron tunneling between the electrodes leads to a fast conductance decay with stretching (visible as the orange tail), as expected for tunneling through a single barrier.

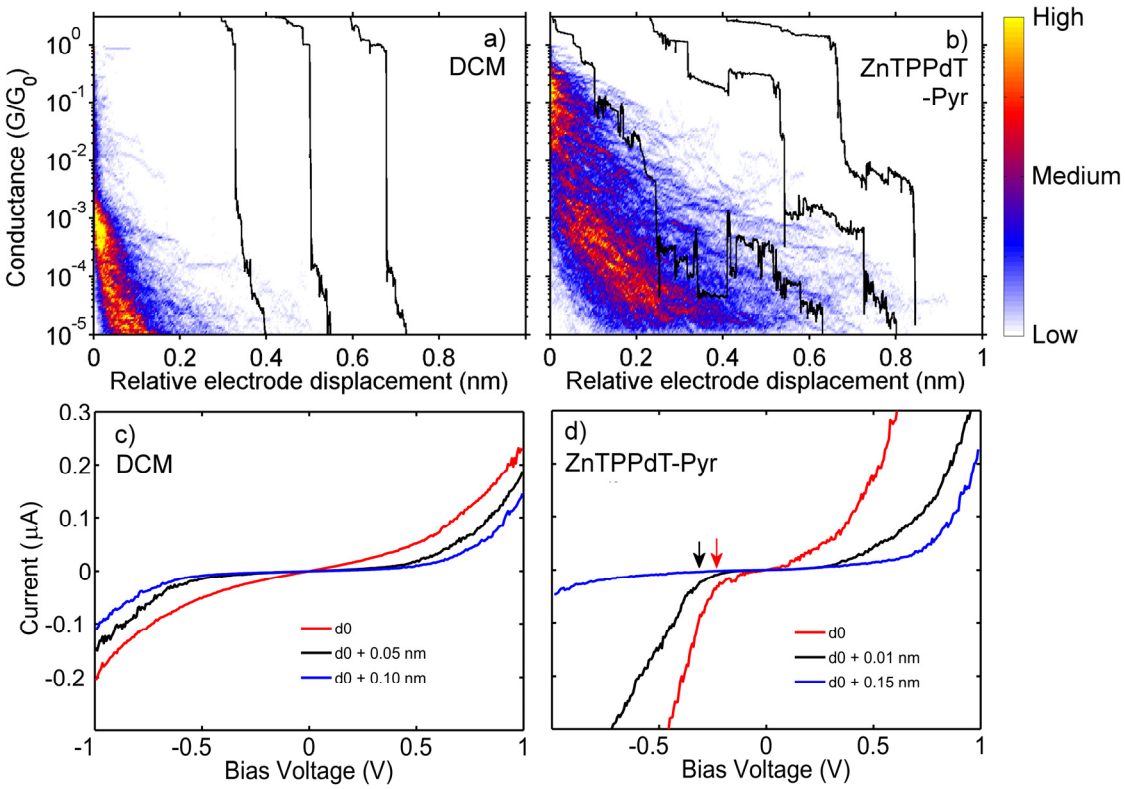


Fig. 16: Trace histograms constructed from 500 consecutive breaking traces taken at room temperature and 100mV bias for junctions exposed to (a) the solvent DCM only, (b) ZnTPPdT-Pyr. Regions of high counts represent the most probable breaking behavior of the contact. The black curves are examples of individual breaking traces (offset along the horizontal axis, d, for clarity). For the construction of the trace histograms the zero of the relative electrode displacement for each curve was set to the point where the conductance drops sharply below 1 $G_0$. (c) Current-voltage characteristics taken at room temperature for various electrode spacings starting from the initial value $d_0$ of junctions exposed to the solvent DCM, and (d) ZnTPPdT-Pyr.

In contrast to this fast tunneling decay, introducing the porphyrin molecules by self-assembly on the junction leads to pronounced plateaus at different conductance values in the sub-$G_0$ regime. The observation of such plateaus in the breaking traces is commonly taken as a signature of the formation of a molecular junction.[14-16]. Figure 16b shows that the plateaus can be horizontal or sloped. Some traces consist of a few plateaus at different conductance values. The representative breaking traces that are included in figure 16b display a set of such

plateaus. Some traces also show an abrupt increase in conductance for increasing electrode spacing. In strong contrast to measurements on rod-like molecules, averaging over 500 traces does not lead to a narrow region of high counts in the trace histograms. Instead, two distinct regions with high counts are visible; a high-conductance region around $10^{-1}$ $G_0$, and a sloped low-conductance region ranging from $10^{-3}$ $G_0$ to $10^{-5}$ $G_0$. Although clear plateaus are observed in the single breaking traces, averaging over hundreds of traces washes out the molecular signature. Hence, a complementary method is required to study charge transport in more detail.

We have therefore measured current-voltage (*I-V*) characteristics at fixed electrode spacing, in the $10^{-2}$ - $10^{-5}$ $G_0$ conductance region. In between the *I-V*s, the inter-electrode distance was gradually increased or decreased in steps of about 10 pm, without fusing the electrodes to form a metallic contact. In this way, changes in molecular junction configurations occurring as a function of electrode spacing can be accurately probed. *I-V*s taken at room temperature for a few settings of the electrodes spacing of junctions exposed to DCM and ZnPyr-TPPdT **5** are presented in figure 16c and figure 16d, respectively. For each series, all presented *I-V*s are taken from the same breaking sequence.

*I-V*s of a junction exposed to DCM (figure 16c) exhibit the characteristic single-barrier tunneling shape and show the expected current decrease upon increasing the electrode spacing. In contrast, *I-V* characteristics on the porphyrin junction show a sharper current onset, marked by arrows in figure 16d. This observation may be viewed as a molecular fingerprint as they correspond to the onset of resonant transport through an energy level of the molecule (either vibrational or electronic). Interestingly, the current onset strongly depends on the inter-electrode distance. At $d_0$ it is located around -250 mV. After a step of about 10 pm in the electrode distance, the onset shifted to around -350mV. Increasing the inter-electrode distance with an additional 140 pm, shifts the onset at negative bias to a location outside the bias window. Note furthermore the asymmetry in the curves in figure 16d, which increases as they electrode moves further apart (e.g. the blue curve in this figure). For the three *I-V*s we have also determined the conductance at the same bias voltage as used to construct the trace histograms, i.e., at 100mV. For the red, black and blue *I-V* curve we obtain conductance values of $2.0 \cdot 10^{-3}$, $1.6 \cdot 10^{-4}$ and $1.6 \cdot 10^{-4}$ $G_0$ respectively. Interestingly, small changes in electrode distance (~10 pm) can induce big changes in the shape of the *I-V* characteristics and

the low-bias conductance (compare e.g. the red and black curves). Opening the junction further (black and blue curves) results in an equal conductance value at 100 mV, but different *I-V* shapes.

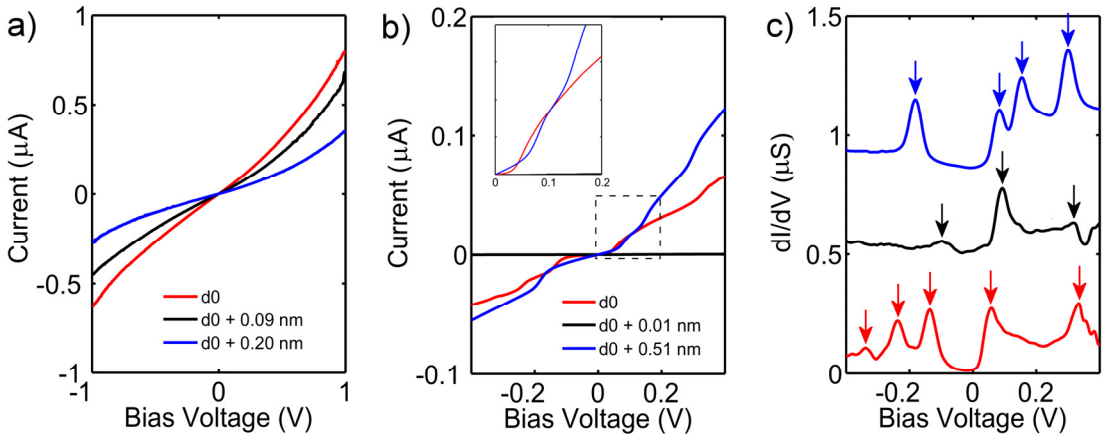


Fig. 17: Low-temperature *I-V* characteristics of junctions exposed to (a) DCM and (b) ZnTPPdT–Pyr. The DCM sample clearly shows vacuum- tunneling behavior. The porphyrin sample exhibits Coulomb blockade and steps. (c) dI/dV of a junction exposed to a ZnTPPdT–Pyr solution; curves are offset vertically for clarity. Resonances correspond to electronic or vibrational energy levels of the molecular junction. Note, for the black line the dI/dV has been scaled by a factor of 100.

Spectroscopic features become more pronounced at low temperature as the junction stability increases, and both the thermal noise and thermal broadening decrease. We therefore cooled down the junctions to cryogenic temperature (6 K) while keeping the zero-bias conductance at a fixed value (around $1 \cdot 10^{-4}$ $G_0$) with a feedback loop. In figure 17 a and b, we present low temperature *I-V* characteristics of junctions exposed to (a) DCM and (b) ZnPyr-TPPdT **5** solution, for different electrode spacings. *I-V*s of the junction exposed to DCM show the characteristic tunneling shape, without any molecular signature, as was also found at room temperature. A notable difference, however, is the significant reduction of the noise.

The *I-V*s of the ZnPyr-TPPdT **5** containing junction now show sharp step-like features, which are more pronounced than that in figure 16d. We numerically determined the differential conductance (dI/dV) as displayed in figure 17c. In the dI/dVs, the step-like features are visible as resonances, which have been marked in the figure with arrows of the corresponding color. For clarity, the dI/dVs have been offset vertically, and the dI/dV representated by the black curve magnified 100 times. The origin of those resonances can be electronic or vibrational

[32-34]. Independently on their origin, their position reveals the alignment of the corresponding energy level with respect to the Fermi energy of the electrodes.[11] For a distance of $d_0$ (red curve), five pronounced resonances are present, located at -339mV, -283mV, -153mV, 58mV and 334mV. For the conductance at 100mV we obtain a value of $2.1 \cdot 10^{-3}$ $G_0$. Increasing the distance by 10pm (black curve) drastically changes the molecular energy spectrum, with one distinct resonance at 94mV, and two fainter peaks around -99mV and 319 mV. Here, the conductance at 100 mV is $1.2 \cdot 10^{-5}$ $G_0$. Increasing the distance with an additional 500pm (blue curve) again leads to changes in the molecular energy spectrum; four pronounced resonances are now located at -238mV, -136mV, 58mV and 334mV. For the conductance we again obtain a value of $2.1 \cdot 10^{-3}$ $G_0$.

Comparing first the red and black curve in figure 17c, we see that within an electrode displacement of 10 pm, the number of energy levels involved in the electronic transport as well as their energy has drastically changed. A jump of more than two orders of magnitude in the low-bias conductance is observed as well. This suggests an abrupt change in the molecule-electrode interaction, presumably caused by a change in molecular configuration. A similar change in molecular configuration was also observed in the room temperature *I-V*s for the red and black curve; the onset for current shifted by -100mV and the conductance dropped one order of magnitude within 10 pm. These observations support the conclusion drawn from the trace histogram measurements: The molecule can adopt different stable configurations, leading to plateaus at different conductance values in the breaking traces. Comparing the red and blue curve in figure 17c, which are taken are at a separation of 0.51 nm, we see that their molecular energy spectrum strongly differ, but that their low-bias conductance is similar (figure 17b, inset). Similar behavior is also observed at room temperature (figure 16d). This suggests that different stable junction configurations with very different spectroscopic signatures can exhibit the same low-bias conductance. Looking at the conductance evolution of the three *I-V*s as a function of electrode spacing, we first see a sharp drop of more than two orders of magnitude within 10 pm. Although at 0.51nm the initial conductance is recovered, from the molecular energy spectrum we see the molecular junction has now adopted a different configuration. Such sharp decrease and increase in conductance are also observed in the room temperature histogram measurements (see first black trace in figure 16b). However, in such measurements, no distinction can be made between two different configurations with similar conductance values.

For most of the low-bias break junction measurements on rod-like molecules it is assumed that repetitive fusing and breaking of the molecular junction provides the most probable conductance value.[14-16] Multiple conductance peaks are often attributed to the formation of multiple molecular bridges connected in parallel.[14, 35] The strength of the metal-molecule chemical bond is considered to play a central role in determining the single molecule conductance values. Our results on the Zn porphyrin molecule with a pyridine axial group show that different conductance values can also result from stretching or fusing a molecular junction. As considerable changes in the conductance values and spectra already occur for a displacement as small as 10 pm, we conclude that neither the chemical molecule-electrode bond nor the electrode configuration itself can be held responsible. More likely, varying the electrode distance changes the molecular configuration, which in turn leads to abrupt changes in the molecule-electrode interaction. Our findings also show that *I-V* characteristics taken at different electrode spacings can exhibit very distinct spectroscopic features but a similar low bias conductance. This indicates that different junction geometries can lead to similar conductance values in the trace histograms. Therefore, as changes in the molecular junction conformation are not always reflected in the low-bias trace histograms, supporting high bias *I-V*-characteristics are essential for the interpretation of such histograms.

#### 6.2.3.4 Conclusions MCBJ

In summary, we have electrically probed different junction configurations of porphyrin molecules. We have demonstrated that porphyrin molecules can form stable bridging molecular junctions even without thiol anchoring groups. Adding the thiol end groups and pyridine axial groups to the porphyrin backbone, respectively increases the stability of the junctions and leads to an increased spread in conductance. This is a result of the formation of different junction configurations. To enable the reliable formation of stable porphyrin junctions, molecules with well-defined adsorption geometries will be required. Quantum chemistry calculations could yield more insight into their design as well as the configurations and the conductance of porphyrin single-molecule junctions. Finally, we expect that multiple junction configurations with considerable variation in the measured conductance values can also be observed for other non-rod-like molecules.

Additionally, we investigated charge transport in ZnPyr-TPPdT **5** molecular junctions using the lithographic MCBJ technique. We combined low-bias statistical measurements with

spectroscopy measurements of the molecular levels using *I-V* characteristics. This unique combination allows us to probe different junction configurations and monitor changes in the molecular level alignment upon fusing or breaking of a molecular junction. Both methods show that multiple stable single–molecule junction configurations can be obtained by stretching or fusing the junction. In addition we demonstrate that different ZnPyr-TPPdT **5** junction configurations can lead to different spectroscopic features for similar low-bias conductance values. Thus, *I-V* spectroscopy measurements provide valuable complimentary information about charge transport through a single molecule.

## 6.3 Conclusions

Overall, single molecule electrical measurements on functionalized porphyrins in nanoscale electronic devices show that it is possible to use this type of molecules for the formation of stable single molecule junctions. However, detailed analysis of such measurements reveals that the porphyrins can exist in several differently conducting configurations in these nanogaps, depending both on the device and on the molecular structure of the porphyrin. Moreover, the configuration can change rapidly and repeatedly over time. It is not unlikely that this behavior is not limited to porphyrins, and future design of single molecule electronic junctions should take this behavior into account.

## 6.4 Experimental

### 6.4.1 Electromigrated breakjunctions

In short, using standard electron-beam lithography and evaporation a thin Pt-wire (10 - 100 nm cross-section, 300 nm long) is defined on top of an $Al/Al_2O_3$ electrode (see figure 2a). Feedback controlled electromigration is performed at 420 K until a few-atom contact with a resistance of about 3 kΩ is created. The strain in the wire then causes the contact to break and a nanometer-sized separation between the two metal contacts is formed. Cooling down to room temperature suffices to stabilize the nanogap. On two different chips, out of a total of 56 devices, 29 (52%) underwent self-breaking to form nanometer-separated electrodes. The resistance of the other devices remained in the kΩ range. A device yield of 50%–70% is typical for this scheme of nanogap formation.[8] After gap-formation the devices are

UV/ozone cleaned for 10 minutes at room temperature and placed in a vacuum probe station ($10^{-4}$ mbar). To make optimal use of the stability of the nanogaps, the empty gaps were characterized electrically at room temperature and at low temperature (10 K). In this way, changes that occur after molecule deposition can be distinguished from the background conductance due to direct tunneling between the electrodes.

After the detailed empty-device characterization, molecules are introduced into the gap from solution. The electrodes are immersed in a 0.1 mM solution of $H_2$–TAPP in acetone for 5 minutes after which they are rinsed with pure acetone, blow-dried, and placed back in the probe station vacuum chamber. After deposition, 8 out of 29 devices show a clear change in the current–voltage characteristic which is an indication that molecules have been trapped in the nanogap; we will refer to these devices as molecular junctions. It should be noted that control experiments (15 devices) with the solvent only did not show any significant changes in the current–voltage characteristics.

### 6.4.2 Mechanically controlled break junctions

Sample fabrication is same as published in a previous paper from our collaborators.[9]

Porphyrins **2**, **3**, or **4** were dissolved in acetone to give solutions of concentrations of 0.1 mM. $RuPyr_2$-TPPdT **6** was dissolved in dimethylformamide (DMF) at concentrations of 0.1 mM. Devices were submerged in the molecular solution for 1 hour. After self-assembly, the devices were rinsed in pure solvent.

### 6.4.3 Experimental procedures and data processing

A home-made LabVIEW program was used to control the device bending, the measurement electronics and the data acquisition. Before each measurement, the setup was pumped to a pressure below $10^{-6}$ mbar. Conductance traces were acquired at a DC bias of 150 mV. All electrical measurements were carried out with home-built battery-operated equipment. We measured the junction currents using a DC voltage source with a logarithmic temperature-drift compensated current monitor, covering a range from less than 50 pA to more than 1 mA. Point wise calibration with standard resistors ranging from 100 Ω to 1 GΩ ensured the accuracy of this conversion. The junction conductance was calculated from the measured

current and the applied bias voltage. All current and voltage data were read into the PC using an Adwin-Gold data acquisition module (Jaeger).

During the histogram measurements the flexible MCBJ substrates were bent using a PC-controlled piezo actuator. The applied voltage ramp of 100V/s results in a substrate bending speed of 30 μm/s. On the scale of the electrodes, this bending is translated to a stretching on the order of 1.8 nm/s (for the calibration of the attenuation factor, see section 6.4.4). In order to acquire thousands of breaking curves the junctions were cycled repeatedly between the fused (10 $G_0$) and the open state (1 $\cdot 10^{-5}$ $G_0$). Complete opening of the contacts was guaranteed by an additional bending of 5 μm after the conductance had crossed the lower boundary of the studied conductance interval. Fusing to 10 $G_0$ ensured the atomic reconfiguration of the contact after each cycle.

We collected all conductance traces consecutively on individual junctions. Raw data were evaluated statistically without any data selection to obtain the trace histograms. The trace histograms were created using the procedure described.[36] On the y-axis we used logarithmic binning at 30 bins per decade of conductance. On the x-axis, we used 5 bins per V applied on the piezo actuator. In order to compare different measurements, the counts in the histograms were divided by the number of traces, the data acquisition rate (in Hz) and the 1/(bending speed) (in s/V). The resulting trace histograms were plotted using a color scale with a minimum of 0 and a maximum of $4 \cdot 10^{-3}$ counts. Data analysis and plotting of the histograms was carried out using the MATLAB package (The MathWorks™).

### 6.4.4 Calibration of the displacement ratio

In the metallic regime, the signature of atomic chains can be used to calibrate the displacement ratio of the MCBJ. Similar to a single- atom contact, chains of gold atoms exhibit a conductance of nearly 1 $G_0$.[37] The corresponding conductance plateaus in breaking traces show statistically preferred lengths, which can be related to an integer number of atoms in the chains.[36] We have carried out an analysis of the plateau lengths in the interval from 0.5 to 1.2 $G_0$ for a typical MCBJ device. Figure 18 presents a histogram of the conductance plateau length in micrometers of bending. The two peaks just above 4 and 8 μm indicate the formation of chains of gold atoms and can be used to calibrate the displacement ratio. Earlier experiments have established that the inter-atomic distance in these chains is 2.5 Å.[36] This allows us to estimate the displacement ratio, which is defined as $\Delta d/\Delta w$, where $d$ is the electrode displacement, and $w$ the change in motor position. This yields a displacement ratio of $6 \cdot 10^{-5}$. A similar value is obtained by analyzing the exponential decrease of the tunneling conductance with increasing substrate deflection.[38]

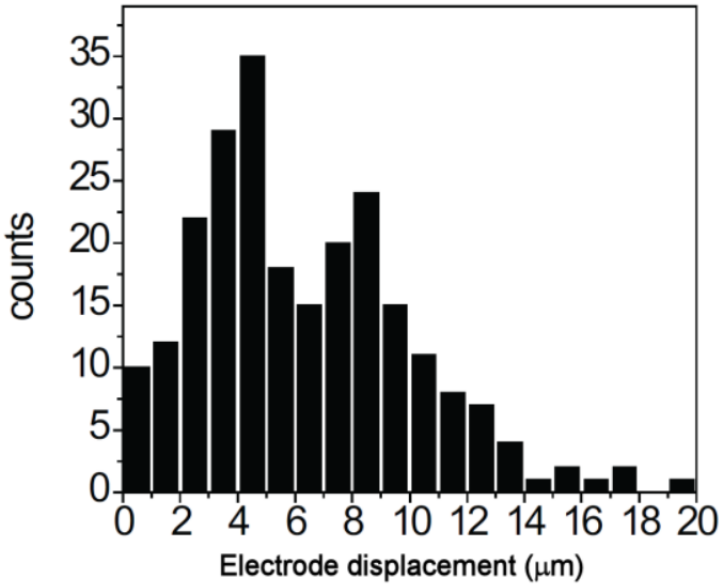


Fig. 18: Histogram of the motor displacement in the conductance interval between 0.5-1.2 $G_0$ used for the calibration of the displacement ratio of a clean gold MCBJ at 11 K. The data were obtained during 240 individual breaking and fusing cycles at a bias of 50 mV. The double peak structure indicates the formation of monatomic chains.

### 6.4.5 Experiments on other devices

To investigate the reproducibility of the features described in the main text, extensive measurements were performed on different MCBJ devices, for different bending speeds and bias voltages. At least three junctions for each porphyrin derivative and corresponding solvent were measured, showing similar features as described earlier.

Figure 19 presents trace histograms constructed from traces taken using the same settings as in the main text, but on different MCBJ devices. Figure 19 b-d display junctions that have been exposed to solutions of the different porphyrin derivatives. Since Ru-TPPdT was dissolved in DMF, figure 19a presents a typical trace histogram of a device exposed to DMF. Similar to the MCBJ devices submerged in acetone, the conductance sharply decreases from around $1G_0$ to $\sim 10^{-3}$ $G_0$ beyond which electron tunneling between the electrodes is observed. This is the characteristic of a clean junction.

To ensure that the formation of the molecular junction does not depend on the speed at which the histograms were taken, we also performed the experiments at a lower speed (0.18 nm/s). The corresponding trace histogram for a junction containing **2** is presented in figure 20b, which should be compared to the histogram of the main text which was taken at 1.8 nm/s (reproduced as figure 20a; the two histograms show the same features.

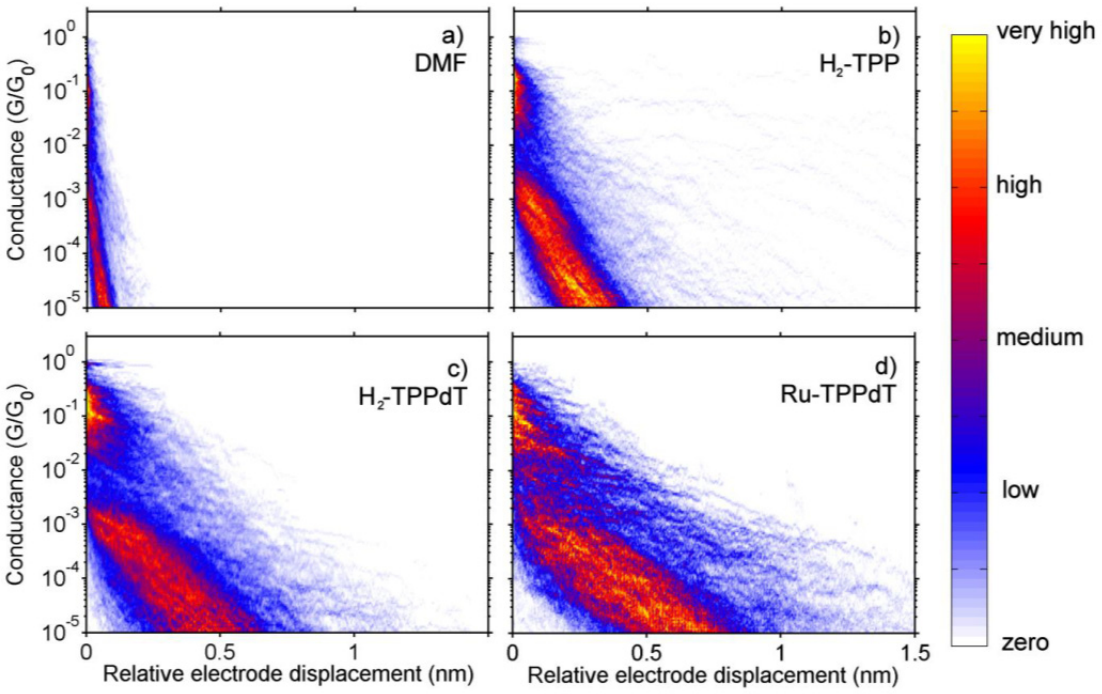


Fig. 19: Additional trace histograms constructed from 1000 breaking traces that were exposed to solutions of (a) DMF (b) H2-TPP (c) H2- TPPdT and (d) Ru-TPPdT. All histograms were taken at a bending speed of 1.8 nm/s, a bias voltage of 150 mV and from different samples from the ones shown in the main text. No data selection schemes have been utilized.

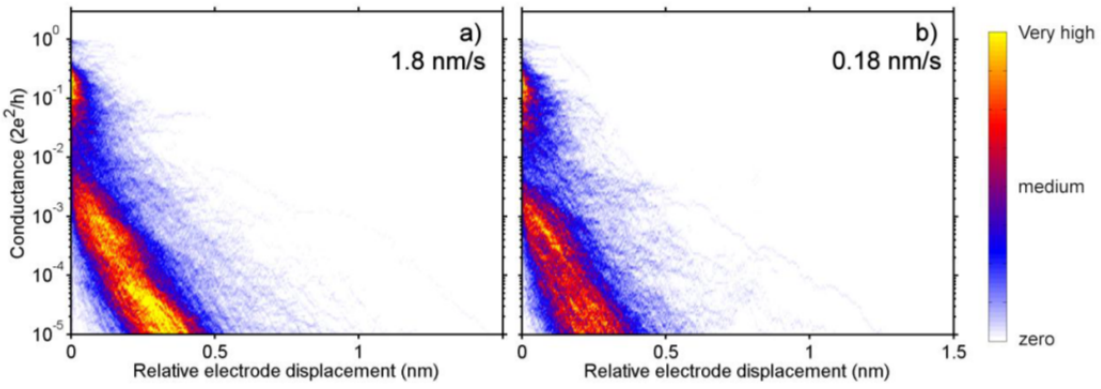


Fig. 20: Breaking speed dependence: Additional trace histograms of a junction that was exposed to a solution of $H_2$-TPP and taken at a bending speed of (a) 1.8 nm/s and (b) 0.18 nm/s. The bias voltage was set to 150 mV.

### 6.4.6 Conductance versus time traces at room temperature

Additional information about the molecular junction configurations can be obtained by measuring the evolution of the junction conductance over large time intervals. Such 'conductance traces' are obtained in the following way. Starting at a conductance of 1 $G_0$, the junction is opened in steps of 50 pm using a servo motor. After each step the inter-electrode distance is fixed and the conductance monitored for several hours. Figure 21 presents such an opening sequence at room temperature. From the figure it is clear that several molecular junction configurations can be formed below 1 $G_0$. We found that not all possible configurations can be achieved within the same opening sequence; consequently, the observed conductance values may differ from cycle to cycle. In addition, the allowed configurations are expected to be strongly depending on the exact shape of the electrodes, which are restructured in each fusing and breaking cycle. Furthermore, comparing figure 21 to figure 14 of the main text, in figure 21 the width of the observed bands of the measured conductance values are much broader, which is a direct consequence of the increased conformational flexibility of the molecule in the junction at this temperature.

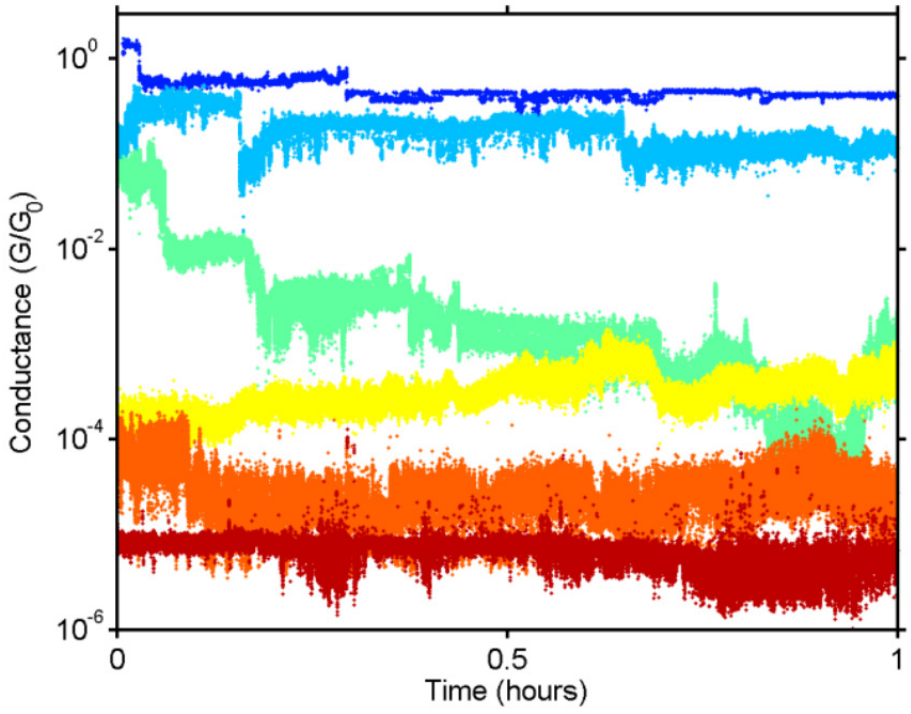


Fig. 21: Typical conductance versus time traces of RuTPPdT at room temperature originating from one opening sequence. Every step has been plotted in a different color for clarity.

### 6.4.7 Conductances versus time traces at 77K

Figure 22a reproduced figure 14c from the main text in which time traces of $H_2$-TPPdT at 77K are shown. Of those traces a histogram is shown in figure 22b. In some traces, notably the green one, several peaks are visible. This suggests that the molecule is switching between several configurations.

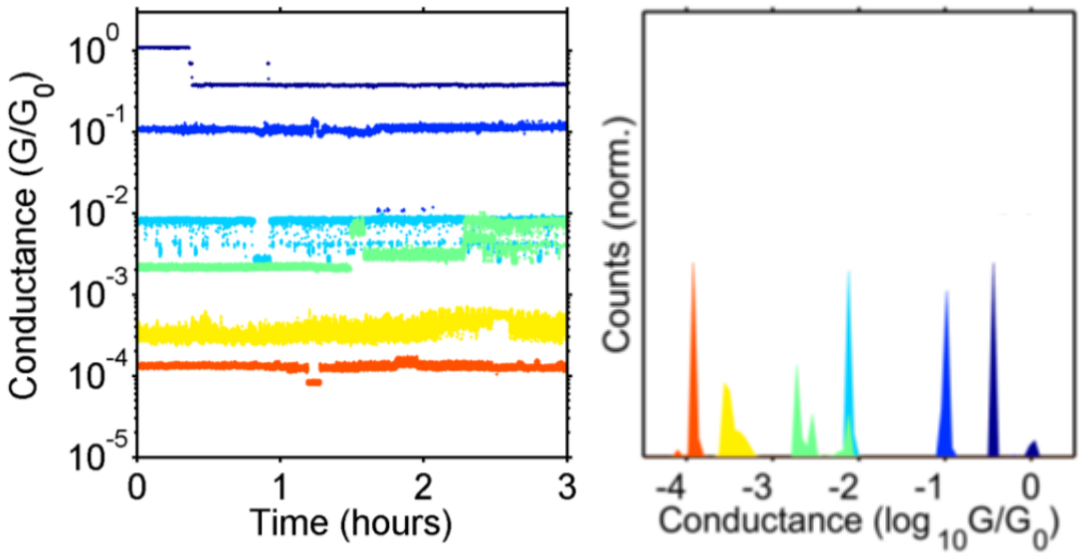


a b

Fig. 22: a) Typical conductance versus time traces of $H_2$-TPPdT at 77K originating from one opening sequence. Every step has been plotted in a different color for clarity. b) Histogram of the time traces shown in (a).

## 6.5 References


1. Osorio, E.A., *Quantum transport through single molecules*. 2009, Delft University of Technology: Delft. p. 126.
2. Park, H., et al., *Fabrication of metallic electrodes with nanometer separation by electromigration.* Applied Physics Letters, 1999. **75**(2): p. 301-303.
3. Park, J., et al., *Coulomb blockade and the Kondo effect in single-atom transistors.* Nature, 2002. **417**(6890): p. 722-725.
4. Yu, L.H. and D. Natelson, *The Kondo Effect in C60 Single-Molecule Transistors.* Nano Letters, 2003. **4**(1): p. 79-83.
5. Osorio, E.A., et al., *Single-molecule transport in three-terminal devices.* Journal of Physics-Condensed Matter, 2008. **20**(37): p. 374121.
6. Moth-Poulsen, K. and T. Bjørnholm, *Molecular electronics with single molecules in solid-state devices.* Nature Nanotechnology, 2009. **4**: p. 551-556.
7. Song, H., M.A. Reed, and T. Lee, *Single Molecule Electronic Devices.* Advanced Materials, 2011. **23**(14): p. 1583-1608.
8. Prins, F., et al., *Room-temperature stability of Pt nanogaps formed by self-breaking.* Applied Physics Letters, 2009. **94**(12): p. 123108.
9. Martin, C.A., et al., *Lithographic mechanical break junctions for single-molecule measurements in vacuum: possibilities and limitations.* New Journal of Physics, 2008. **10**: p. 065008.
10. Kim, K., H.B. Lee, and K.S. Shin, *Surface-enhanced Raman scattering characteristics of nanogaps formed by a flat Ag substrate and spherical Pt nanoparticles.* Spectrochimica Acta Part A: Molecular and Biomolecular Spectroscopy, (0).
11. Thijssen, J.M. and H.S.J. Van der Zant, *Charge transport and single-electron effects in nanoscale systems.* physica status solidi (b), 2008. **245**(8): p. 1455-1470.
12. Tao, N.J., *Electron transport in molecular junctions.* Nat Nano, 2006. **1**(3): p. 173-181.
13. Sedghi, G., et al., *Single molecule conductance of porphyrin wires with ultralow attenuation.* Journal of the American Chemical Society, 2008. **130**(27): p. 8582-+.
14. Xu, B. and N.J. Tao, *Measurement of Single-Molecule Resistance by Repeated Formation of Molecular Junctions.* Science, 2003. **301**(5637): p. 1221-1223.
15. Venkataraman, L., et al., *Single-molecule circuits with well-defined molecular conductance.* Nano Letters, 2006. **6**(3): p. 458-462.
16. González, M.T., et al., *Electrical Conductance of Molecular Junctions by a Robust Statistical Analysis.* Nano Letters, 2006. **6**(10): p. 2238-2242.
17. Martin, C.A., et al., *Fullerene-based anchoring groups for molecular electronics.* Journal of the American Chemical Society, 2008. **130**(40): p. 13198-13199.
18. Kamenetska, M., et al., *Formation and Evolution of Single-Molecule Junctions.* Physical Review Letters, 2009. **102**(12): p. 126803.
19. Quek, S.Y., et al., *Mechanically controlled binary conductance switching of a single-molecule junction.* Nat Nano, 2009. **4**(4): p. 230-234.
20. Mishchenko, A., et al., *Influence of Conformation on Conductance of Biphenyl-Dithiol Single-Molecule Contacts.* Nano Letters, 2009. **10**(1): p. 156-163.
21. Dulić, D., et al., *Controlled Stability of Molecular Junctions.* Angewandte Chemie International Edition, 2009. **48**(44): p. 8273-8276.
22. Dulic, D., et al., *Controlled Stability of Molecular Junctions.* Angewandte Chemie-International Edition, 2009. **48**(44): p. 8273-8276.

23. Osorio, E.A., et al., *Conductance Switching and Vibrational Fine Structure of a [2 × 2] CoII4 Gridlike Single Molecule Measured in a Three-Terminal Device.* Small, 2010. **6**(2): p. 174-178.
24. Schneebeli, S.T., et al., *Single-Molecule Conductance through Multiple π−π-Stacked Benzene Rings Determined with Direct Electrode-to-Benzene Ring Connections.* Journal of the American Chemical Society, 2011. **133**(7): p. 2136-2139.
25. Diez-Perez, I., et al., *Controlling single-molecule conductance through lateral coupling of [pi] orbitals.* Nat Nano, 2011. **6**(4): p. 226-231.
26. Haiss, W., et al., *Precision control of single-molecule electrical junctions.* Nat Mater, 2006. **5**(12): p. 995-1002.
27. Ruben, M., et al., *Charge Transport Through a Cardan-Joint Molecule.* Small, 2008. **4**(12): p. 2229-2235.
28. Qiu, X.H., G.V. Nazin, and W. Ho, *Mechanisms of Reversible Conformational Transitions in a Single Molecule.* Physical Review Letters, 2004. **93**(19): p. 196806.
29. Nazin, G.V., X.H. Qiu, and W. Ho, *Visualization and spectroscopy of a metal-molecule-metal bridge.* Science, 2003. **302**(5642): p. 77-81.
30. Brede, J. and et al., *Dynamics of molecular self-ordering in tetraphenyl porphyrin monolayers on metallic substrates.* Nanotechnology, 2009. **20**(27): p. 275602.
31. Perrin, M.L., et al., *Influence of the Chemical Structure on the Stability and Conductance of Porphyrin Single-Molecule Junctions.* Angewandte Chemie International Edition, 2011. **50**(47): p. 11223-11226.
32. Osorio, E.A., et al., *Addition Energies and Vibrational Fine Structure Measured in Electromigrated Single-Molecule Junctions Based on an Oligophenylenevinylene Derivative.* Advanced Materials, 2007. **19**(2): p. 281-285.
33. Reichert, J., et al., *Driving Current through Single Organic Molecules.* Physical Review Letters, 2002. **88**(17): p. 176804.
34. Kubatkin, S., et al., *Single-electron transistor of a single organic molecule with access to several redox states.* Nature, 2003. **425**(6959): p. 698-701.
35. González, M.T., et al., *Conductance values of alkanedithiol molecular junctions.* New Journal of Physics, 2008. **10**(6): p. 065018.
36. Untiedt, C., et al., *Calibration of the length of a chain of single gold atoms.* Physical Review B, 2002. **66**(8): p. 085418.
37. Yanson, A.I., et al., *Formation and manipulation of a metallic wire of single gold atoms.* Nature, 1998. **395**(6704): p. 783-785.
38. Martin, C.A., *Charge transport through single molecules in two- and three- terminal mechanical break junctions*. 2010, Delft University of Technology: Delft, The Netherlands.

# SUMMARY

**Single molecule electronics: a systematic approach to study the properties of single porphyrin molecules**

Porphyrins are an important class of molecules as they play a central role in many biological processes, such as photosynthesis, fixation and transport of oxygen in the respiratory system. These are highly-conjugated systems with delocalized π-electrons. Their great architectural flexibility, however, combined with their rich optical properties makes them interesting building blocks for prototypical molecular devices. In single molecule devices, although various (in)organic molecules have been studied with many different techniques, porphyrins were chosen for our studies. We were interested to know the behaviour of porphyrin molecules at the molecular level, and especially their conductance as single molecule junctions.

Organic synthesis of porphyrin molecules was the first important step for these studies. We devised an efficient route to synthesize exclusively trans-amine and thiol functionalized porphyrins, avoiding isomerization and scrambling of the functionalities. Trans-nitro porphyrin, obtained using the mono-carbinol strategy, was converted by reduction to the trans-amino porphyrin, which is a highly versatile intermediate for the synthesis of a wide variety of other functionalized porphyrins. This allowed for the production of trans-thiol functionalized porphyrins by Leuckart thiophenol synthesis in high yields, and less purification steps. These porphyrin molecules have the required conjugated structure and linkers at proper positions to be used in single molecule studies.

With the ultimate aim of studying these molecules in gold or platinum nanojunctions, we first investigated the potential of Au nanorods as bottom-up nanoelectrodes for contacting single molecules. The binding of porphyrin molecules with gold nanoparticles and gold nanorods in solution was studied to get valuable insights into their interaction strength and dynamics, which is essential for understanding the behavior of single molecules contacted between nanoelectrodes. Here, the gold nanoparticles were used as a model surface for gold nano-

electrodes. Fluorescence spectroscopy (steady state and life time measurements), UV-Vis absorption spectroscopy, gel permeation chromatography, dynamic light scattering, scanning electron microscopy, and mass spectrometry techniques were used to study their interaction and exchange of ligands on gold nanoparticles. UV-Vis spectroscopy showed that binding of the porphyrins to gold nanoparticles does not affect the absorption spectra, indicating that there is no or little electronic interaction between them. Fluorescence quenching studies revealed that porphyrins with four amino functionalities shows highest binding interaction i.e., an order of magnitude higher as compared to other porphyrins, we used. Difference in functional groups did not made any significant changes in the binding interaction studies, e.g. diamino porphyrins and dithiol porphyrins show similar binding constants. The life time fluorescence measurement revealed that the binding is static rather than dynamic.

DLS studies show that porphyrins with four amino groups induce non-selective association of gold nanoparticles to larger undefined particle clusters. However, the addition of trans-dithiol porphyrins to gold nanoparticles led to the selective formation of particle dimers or trimers. Gold nanorods could not be selectively aligned to each other while using porphyrins due to very large size of gold nanorods and their instability in organic solvents upon ligand exchange. Individual rods were successfully fabricated with microelectrodes; however contacting already aligned nanorods (by use of cysteine) with microelectrodes was not feasible due to the movement of gold nanorods on the silicon surface.

The most interesting porphyrins during the interaction studies of porphyrins with gold nanoparticles were tetraamino porphyrin and dithiol porphyrin. Therefore these were used later for single molecule studies. Tetraamino porphyrin shows highest interaction with gold nanoparticles and dithiol porphyrin selectively binds two or three gold nanoparticles under specific conditions.

We also investigated the binding interaction of porphyrins with PbSe quantum dots in order to study charge and energy transfer properties. These studies were also essential to gain more understanding of charge and energy transfer in hybrid systems. It was found that porphyrins containing a single carboxylic acid functional group or even multiple amine or thiol groups did not bind to QDs, however tetracarboxylic acid functionalized porphyrins do bind with quantum dots. This interaction appeared to be dynamic on fluorescence time scale. In general, there is no pronounced effect on binding, whether Zn is present in the core of porphyrin or

not. Transient absorption spectroscopy confirmed that there is photo-induced charge transfer from porphyrins to quantum dots, indicating that these porphyrins are good candidates for single molecule electronic studies. Unfortunately, the quantum dots appear to change size or precipitate slowly in time, when they are exposed for longer times to any porphyrin containing carboxylic acid functional group, as was observed from a blue shift in the absorption of quantum dots and the decrease of scattering at short wavelengths. These results increase our interest to study porphyrins in single molecule setup as these molecules can be used for charge transfer through nanoelectrodes.

Final part of this thesis was focused on single molecule electronic behavior of porphyrins, which have significant potential for both bulk and single molecule electronics. Porphyrins were studied as single molecules using platinum electromigration and mechanically controllable break junction techniques. The stability of Pt enables operation at room temperature for which experiments have been performed with porphyrin molecules. A comparison between the current-voltage characteristics before and after deposition allows us to distinguish molecular transport from background-tunneling conductances. This information is important in the understanding of transport through single molecules. In most experiments, gate-dependent transport was absent which we attribute to adsorption of the tetraaminophenyl porphyrin on one of the electrodes with the porphyrin plane parallel to the electrode surface. In some cases the molecule couples weakly to the electrodes and gate-dependent measurements shows Coulomb-blockaded transport. From these measurements, it is clear that the porphyrin molecules containing 4 amino functional groups are conductive and that single porphyrin molecules can be studied using nanogaps produced by platinum electromigration techniques. Also from the conductance maps, we are sure about the presence of single molecule as observed from clear single diamond edge structures.

Further studies with MCBJ were directed towards new molecular systems with less electrode-molecule interaction, promoting a single-molecule to bridge source and drain electrodes. Porphyrins were bound to the gold electrodes using thiol (-SH) anchoring groups. Conductance was either measured as a function of electrode stretching or measurement of I-V characteristics for fixed electrode spacing. When conductance was measured as function of electrode stretching, 1D histograms revealed a change in conductance when porphyrin molecules (with or without Zn) were present by observing higher conductance plateaus. It was

not possible to differentiate between two different porphyrin molecules in the 1D histograms because of the absence of clear molecular signatures. 2D histograms reveal differences between free base porphyrins and Zn-porphyrins as Zn-porphyrin contains side arm on one side, which reduces π-orbital interaction of porphyrin with nanoelectrodes, showing increase in conductance at longer electrode spacing indicating bridged conformations. Porphyrins show both i.e. planar (bridged, connected via thiol moieties) and also perpendicularly probed (lying flat on one of the electrode) configurations. Relative comparison of free porphyrin vs Zn-modified porphyrin, which has an extra pyridine arm, reduces the possibility of perpendicularly probed porphyrin.

Further studies towards understanding the influence of molecular geometry by using MCBJ technique revealed that porphyrin molecules can form stable bridging molecular junctions even without the thiol terminations. Adding the thiol groups and pyridine axial groups (using Ruthenium ion with octahedral geometry; two pyridine arms), respectively, leads to an increased spread in low-bias conductance, which is a result of the formation of different stable junction configurations. It furthermore increases the stability of the molecular junction. Moreover, the configuration can change rapidly and repeatedly over time. It is not unlikely that this behavior is not limited to porphyrins, and future design of single molecule electronic junctions should take this behavior into account.

As a result, these studies increase our understanding on the influence of metal – molecule interactions and electron transport in a single molecule, which is crucial for further development in nanoscale electronics. Porphyrins are perhaps one of the most interesting and important complex organic molecules used in molecular electronic devices. These molecules, although conductive, might not be the best candidates for molecular electronics, but certainly these studies improve our understanding of the behavior of molecular interaction and molecular electronics. The understanding from these systematic studies can be applied to other classes of organic molecules as well, in order to broaden the scope of molecular electronic studies and to be helpful in the quest for other interesting and useful classes of molecules.

Ahson Jabbar Shaikh

Abbottabad, Pakistan

March 2013

# SAMENVATTING

**Single molecule electronics: een systematische aanpak om de eigenschappen van enkele porfyrine moleculen te bestuderen**

Porfyrines zijn een belangrijke klasse van moleculen omdat ze een centrale rol spelen in vele biologische processen, zoals fotosynthese, en het vastleggen en transport van zuurstof in de luchtwegen. Deze moleculen zijn zeer geconjugeerde systemen met gedelokaliseerde π-elektronen. Hun grote structurele veelzijdigheid in combinatie met hun rijke optische eigenschappen maakt ze interessante bouwstenen voor prototypische moleculaire apparaten. Hoewel in single molecule onderzoek met verschillende technieken verschillende (an)organische moleculen onderzocht zijn, hebben wij porfyrines gekozen voor onze studies. We waren benieuwd naar het gedrag van porfyrinemoleculen op moleculair niveau, en vooral hun electronische geleiding in single molecule opstellingen.

Organische synthese van porfyrinemoleculen was de eerste belangrijke stap voor deze studies. We bedachten een efficiënte route om uitsluitend trans-amine en thiol gefunctionaliseerde porfyrinen te synthetiseren, terwijl isomerisatie en het vermengnen van de functionaliteiten vermeden moesten worden. Trans-nitro porfyrine, verkregen met de mono-carbinol strategie, werd omgezet naar het trans-amino porfyrine, een zeer veelzijdig tussenproduct voor de synthese van uiteenlopende andere gefunctionaliseerde porfyrinen. Dit maakte de productie mogelijk van trans-thiol gefunctionaliseerde porfyrinen door Leuckart thiofenol synthese in hoge opbrengsten en met maar weinig zuiveringsstappen. Deze porfyrinemoleculen bezitten de vereiste geconjugeerde structuur en verbindingsgroepen op de juiste posities voor gebruik in single molecule studies.

Met het uiteindelijke doel van het bestuderen van deze moleculen in goud of platina nanoschakelingen, moesten we eerst onderzoek gedaan naar de mogelijkheden van Au nanostaafjes als nanoelectrodes voor het contacteren van enkele moleculen. De binding van

porfyrinemoleculen met gouden nanodeeltjes en goud nanostaafjes werd in oplossing onderzocht om waardevolle inzichten krijgen in hun interactie sterkte en dynamiek, die essentieel is voor het begrijpen van het gedrag van enkele moleculen tussen nanoelectrodes. Hier werden de gouden nanodeeltjes als modeloppervlak voor goud nano-elektroden gebruikt. Fluorescentiespectroscopie (steady state en levensduur metingen), UV-Vis absorptiespectroscopie, gelpermeatiechromatografie, dynamische lichtverstrooiing, scanning elektronenmicroscopie en massaspectrometrische technieken werden gebruikt om de interactie en uitwisseling van liganden op goud nanodeeltjes bestuderen. UV-Vis-spectroscopie toonde aan dat binding van de porfyrinen aan goud nanodeeltjes niet de absorptiespectra beïnvloedt, wat aangeeft dat er geen of weinig elektronische interactie tussen hen is. Fluorescentiedoving studies toonden aan dat porfyrinen met vier amino funcionele groepen de hoogste bindingsinteractie met goud nanodeeltjes hadden, dwz een orde van grootte hoger in vergelijking met andere gebruikte porfyrinen. Verandering van bindingsgroepen heeft geen significante invloed op de bindingsinteractie studies, bijv. diaminoporfyrinen en dithiolporfyrinen vertonen vergelijkbare bindingsconstanten. De levensduur fluorescentiemetingen toonden dat de binding eerder statisch is dan dynamisch.

DLS studies tonen aan dat porfyrinen met vier aminogroepen niet-selectieve aggregatie van goud nanodeeltjes teweegbrachten, wat leidde tot grote, ongedefinieerde clusters van nanodeeltjes. De toevoeging van trans-dithiolporfyrinen aan goud nanodeeltjes leidde tot de selectieve vorming van dimeren of trimeren van nanodeeltjes. Het lukte niet om goud nanostaafjes selectief met elkaar te verbinden met behulp van porfyrinen, als gevolg van de zeer grote omvang van goud nanostaafjes en hun instabiliteit in organische oplosmiddelen bij ligand uitwisseling. Individuele staafjes werden succesvol verbonden aan micro-elektroden, maar contact van reeds uitgelijnde nanostaafjes (door middel van cysteïne) met micro-elektroden bleek niet haalbaar vanwege de beweging van goud nanostaafjes op het siliciumoppervlak.

De meest interessante porfyrinen tijdens de interactie studies met gouden nanodeeltjes bleken de tetraaminoporfyrine en dithiolporfyrine, die vervolgens werden gebruikt voor single molecule studies. Tetraaminoporfyrine toont de sterkste interactie met gouden nanodeeltjes en dithiol porfyrine bindt selectief twee of drie gouden nanodeeltjes in specifieke omstandigheden.

We hebben ook de bindingsinteractie van porfyrinen met PbSe quantum nanokristallen onderzocht om ladings- en energie-overdracht eigenschappen te bestuderen. Deze studies waren essentieel om meer inzicht te krijgen in de ladings- en energie-overdracht in hybride systemen. Het bleek dat porfyrinen met een carbonzuurgroep of meerdere amine- of thiolgroepen niet binden aan quantum nanokristallen. Alleen tetracarbonzuur gefunctionaliseerde porfyrinen binden aan dergelijke quantum nanokristallen. Deze interactie bleek dynamisch op fluorescentie tijdschaal. In het algemeen is er geen uitgesproken effect op de binding, als een Zn metaalion aanwezig in de centrale holte van de porfyrine. Tijdsafhankelijke absorptie spectroscopie toonde dat er fotogeïnduceerde ladingsoverdracht was van porfyrinen naar quantum nanokristallen, wat aangeeft dat deze porfyrinen goede kandidaten zijn voor single molecule elektronische studies. Helaas lijken de quantum nanokristallen van vorm of samenstelling veranderen wanneer ze voor langere tijd worden blootgesteld aan een porfyrine die carboxylzuurfunctionele groepen bevat, zoals waargenomen uit een blauwverschuiving in de absorptie van quantum nanokristallen. In het algemeen verhogen deze resultaten onze interesse om porfyrines te bestuderen in een single molecule opstelling, aangezien deze moleculen kunnen worden gebruikt voor ladingsoverdracht van en naar nanoelectrodes.

Het laatste deel van dit proefschrift was gericht op het single molecule elektronische gedrag van porfyrinen, die een significant potentieel hebben voor zowel bulk- als single molecule elektronica. Porfyrinen werden bestudeerd als single molecules met platina elektromigratie en mechanisch regelbare breekjunctie (MCBJ) technieken. De stabiliteit van Pt maakt het mogelijk experimenten uit te voeren met porfyrinemoleculen bij kamertemperatuur. Uit een vergelijking tussen de stroom-spanningskarakteristieken voor en na depositie kunnen we moleculair transport onderscheiden van achtergrond-tunneling geleidingen. Deze informatie is belangrijk voor het begrijpen van het transport door enkele moleculen. In de meeste experimenten was gate-afhankelijk transport afwezig, wat wij aan adsorptie van de tetraaminophenyl porfyrine op een van de elektroden met de porfyrine vlak evenwijdig aan het elektrodeoppervlak wijten. In sommige gevallen koppelt het molecuul zwak met de elektroden en tonen gate-afhankelijke metingen Coulomb-blokkade transport. Uit deze metingen blijkt dat de porfyrinemoleculen die vier amino functionele groepen stroom kunnen geleiden en dat die enkele porfyrines kunnen worden bestudeerd met nanoschakelingen verkregen door platina elektromigratietechnieken. Ook

kunnen we uit de duidelijke enkele diamant rand structuren in de geleidingskaarten zeker zijn over de aanwezigheid van enkele moleculen.

Verder onderzoek met de MCBJ was gericht op het bestuderen van deze nieuwe moleculaire systemen en hun interacties met de nano-electrodes. In deze techniek zijn de moleculen gebonden aan de gouden elektroden met thiol (-SH) bindingsgroepen. Geleiding werd gemeten als functie van elektrode uitrekking of de IV kenmerken werden gemeten bij een vaste elektrode-afstand. Als geleiding werd gemeten als functie van de elektrode afstand, bleek uit 1D histogrammen een verandering in geleiding wanneer porfyrine moleculen (met of zonder Zn-metaal) aanwezig waren, wat werd gemeten als een plateau van hogere geleiding. Het was niet mogelijk om tussen twee porfyrine moleculen onderscheiden in de 1D histogrammen wegens het ontbreken van duidelijke moleculaire signaturen. 2D histogrammen toonden verschillen tussen vrije base porfyrinen en Zn-porfyrinen, wanneer het Zn-porfyrine een zijwaarts gericht ligand gebonden had dat de π-orbitaal interactie van porfyrine met de nanoelectrodes verminderde. In de MCBJ opstelling tonen porfyrinen zowel vlakke (gebrugde, verbonden via thiol groepen) als loodrecht (plat liggend op een van de elektrodes) configuraties, opgemaakt uit de grote verschillen in geleidingsgedrag. Introductie van een zijwaarts georienteerd ligand aan een Zn gemodificeerd porfyrine, vermindert de mogelijkheid van het voorkomen van loodrecht porfyrine.

Bij verdere studies naar de invloed van de moleculaire geometrie met behulp van MCBJ techniek, werd gezien dat porfyrine moleculen zelfs stabiele overbruggingen van moleculaire schakelingen kunnen vormen zonder de thiol bindingsgroepen. Het toevoegen van de thiol groepen en pyridine axiale groepen (met een ruthenium ion met octaedrische geometrie en dus twee armen pyridine) leidt tot een verhoogde spreiding in de geleiding, die een gevolg is van de vorming van verschillende stabiele verbinding configuraties. Het verhoogt tevens de stabiliteit van de moleculaire verbinding. Bovendien kan de configuratie snel en herhaaldelijk veranderen. Het is niet onwaarschijnlijk dat dit gedrag zich niet beperkt tot porfyrinen, en bij toekomstige vormgeving van single molecule elektronische knooppunten moet met dit gedrag rekening gehouden worden.

Als gevolg van de bovenstaande studies hebben we een beter begrip van de invloed van metaal - molecuul interacties en elektrontransport in een enkel molecuul, wat cruciaal is voor de verdere ontwikkeling van nanoschaal elektronica. Porfyrinen zijn misschien wel een van de meest interessante en belangrijke complexe organische moleculen gebruikt in moleculaire elektronische opstellingen. Deze moleculen, hoewel geleidend, zijn misschien niet de beste kandidaten voor moleculaire elektronica, maar deze studies hebben zeker ons begrip van het gedrag van deze moleculen en de interactie met hun omgeving verbeterd. De kennis, opgedaan met deze systematische studies, kan worden toegepast op andere klassen van organische moleculen en om de reikwijdte van moleculaire elektronische studies en de zoektocht naar andere interessante en nuttige moleculen te verbreden.

Ahson Jabbar Shaikh

Abbottabad, Pakistan

Mars 2013.

# ACKNOWLEDGEMENTS

My time spent at University of Groningen and Delft University of Technology was like most other PhD students with a relatively relaxing first year (at Groningen), and then slowly intensifying research load (later years in Delft). This time which is almost coming to an end was filled with lot of challenges. The work contained in this dissertation is a result of great effort, however many people have contributed for the completion of this thesis.

First of all, I want to thank my promoter Jan for giving me an opportunity in Groningen to start my PhD under his supervision. I always admired and was inspired by your research ideas, as you are genius scientist and researcher for me. I have learnt a lot from you during this time spent in your lab. You have taught me, both consciously and un-consciously, how a good chemist tends to be. I appreciate all your contributions of time, research ideas, funding, moral support and everything you have done for me to make my Ph.D. experience productive and stimulating.

I am also thankful to my promoter from Groningen, Prof. J.C. Hummelen, accepting to be my promoter and giving important suggestions and corrections for thesis improvement.

Rienk, you have given me support on daily basis, where ever I was stuck, you were there to help me out. I am really grateful for your support, whether for bench work or suggesting corrections for the improvement of the thesis and manuscripts.

My special thanks to Prof. Herre van der Zant, Prof. Laurens Siebbeles, and Dr. Arjan Houtepen for giving me an opportunity to collaborate. I have always appreciated the collaboration with Yunan (for QDs), Edgar (for NPs and SEM), Ferry (platinum electromigration), and Diana (MCBJ), you guys were vital for my research projects and cannot forget help I have got from you. Thank you. Ruben, I am also thankful to you for teaching me how to use life time measurements instrument and discussing with me about various other social issues.

I would also like to thank my reading committee members for this dissertation, Prof. Stephen Picken, Prof. Gerard Roelfes and Prof. Alan Rowan for their time and interest to read my thesis.

I also thank Ger, Wolter, Louis, and Prof. Ernst Sudholter for giving me the opportunity to discuss experimental issues and research ideas at various occasions which directly or indirectly helped me in different research projects.

I have had the pleasure to work with the members of the Jan's group and many other short time research students who have come through the lab, and contributed immensely to my personal and professional time at Groningen and Delft. The group has been a source of friendships as well as good advice and collaboration. I have enjoyed discussions and company of all my colleagues during this time. Joost, Jochem, Aurelie, Patrick, Cristian, Job, Christophe, Danius, Iwona, Krishna and Mohan. I thank you all for the enjoyable time I had during my stay in the Netherlands.

Mieke, Louw and Lars, you guys are just great. You have provided all the support I needed either for paper work or for lab, whenever I needed you; you were always there to help me. Thank you.

Astrid, Marian, and Mieke (BOC group); though I had little contact with you during my stay, but I am thankful to you for the managerial support you have provided, whenever needed.

Daniela (BOC), Daniel (BOC), Judith (NOC), Venkatesh (NOC) and Ewold (Groningen), I really appreciate good talk time with you. Thank you for being good friends. Also a general thanks to the NOC (Nano-Organic Chemistry, now, Organic Materials & interfaces) group at ChemE and BOC (Biocatalysis & Organic Chemistry) group at Department of Biotechnology, who were immediate neighbors and good friends to Self-Assembling Systems (SAS) group [now Advanced Soft Matter (ASM) group].

I am also thankful to the Stratingh Institute for Chemistry and Zernike Institute for Advanced Materials for providing me funding, Department of Chemical Engineering, Delft University of Technology for providing lab space, and nanofacility at TUDelft for SEM facilities. I am also

thankful to two ladies, first is Asun (ChemE, for providing information about non-aqueous nanoparticles in the beginning and Hozanna Miro for providing me training for SEM instrument.

I am grateful for time spent with Mansoor & family, Khalid & family, Sajad, Waseem, Umar, and Ikram for not only being good Pakistani friends, but also made my time enjoyable in Groningen and Delft. Certainly these were not the only friends; therefore I am also thankful to all other Pakistani and Indian friends who made my time enjoyable while staying in the Netherlands.

I would also like to thank my family for all their love and encouragement. For my parents who raised me with a love of science and supported me in all my pursuits. I am also thankful to my brothers, sisters and other relatives, whom I remained in contact during this time and their good wishes for me also contributed to the completion of this thesis and my stay enjoyable in the Netherlands.

My lovely daughter Vanya, I love you deep from my heart. You are the main source of happiness for me since you are born. You are still young to read it, but when you will be grown up, and you read these words, I would like to let you know that Papa will always love you, as I love you now, even more.

Last but not the least, I acknowledge my wife Shazia with deep thanks, who was with me during all ups and downs in my life during PhD time and after wards. Her support, love and patience was of significant importance for the completion of this thesis. She has helped me morally and practically, as well as motivated me, where ever she could. I thank you deeply from my heart.

I have tried to recall and mentioned all those who have contributed, but if I have forgotten someone by chance, my sincere apologies and thank you to everyone who have helped me directly or indirectly for the completion of this thesis work, or have made my time enjoyable in the Netherlands.

Ahson Jabbar Shaikh

June 2013

# PUBLICATIONS


1. Perrin, M. L.; Verzijl, C. J. O.; Martin, C. A.; **Shaikh, A. J.**; Eelkema, R.; van EschJan, H.; van Ruitenbeek, J. M.; Thijssen, J. M.; van der Zant, H. S. J.; Dulic, D., Large tunable image-charge effects in single-molecule junctions. *Nat Nano* **2013,** *8* (4), 282-287.

2. Prins, F.; **Shaikh, A. J.**; van Esch, J. H.; Eelkema, R.; van der Zant, H. S. J., Platinum-nanogaps for single-molecule electronics: room-temperature stability. *Physical Chemistry Chemical Physics* **2011**, 14297–14301.

3. Perrin, M. L.; Prins, F.; Martin, C. A.; **Shaikh, A. J.**; Eelkema, R.; van Esch, J. H.; Briza, T.; Kaplanek, R.; Kral, V.; van Ruitenbeek, J. M.; van der Zant, H. S. J.; Dulić, D., Influence of the Chemical Structure on the Stability and Conductance of Porphyrin Single-Molecule Junctions. *Angewandte Chemie International Edition* **2011,** *50* (47), 11223-11226.

4. Perrin, M. L.; Martin, C. A.; Prins, F.; **Shaikh, A. J.**; Eelkema, R.; van Esch, J. H.; van Ruitenbeek, J. M.; van der Zant, H. S. J.; Dulić, D., Charge transport in a zinc–porphyrin single-molecule junction. *Beilstein Journal of Nanotechnology* **2011,** *2*, 714-719.

5. Wakchaure, V. N.; Mohanty, R. R.; **Shaikh, A. J.**; Nugent, T. C., A One-Pot Asymmetric Sequential Amination-Alkylation of Aldehydes: Expedient Synthesis of Aliphatic Chiral Amines. *European Journal of Organic Chemistry* **2007,** *2007* (6), 959-964.

6. Khan, K. M.; Maharvi, G. M.; Khan, M. T. H.; **Shaikh, A. J.**; Perveen, S.; Begum, S.; Choudhary, M. I., Tetraketones: A new class of tyrosinase inhibitors. *Bioorganic & Medicinal Chemistry* **2006,** *14* (2), 344-351.

# ABOUT THE AUTHOR

Ahson was born on 17th January, 1979 in Karachi, Pakistan. All his basic education and graduate studies were completed in Karachi. After getting his Masters of Science in Chemistry title in 2002, at the University of Karachi, he started working at HEJ Research Institute of Chemistry as junior research fellow. In February 2004, he moved to Bremen, Germany for his Masters in Nanomolecular science program. Upon successful completion of his studies in Germany, he started his PhD in February 2006 in Groningen. March 2007 was the time to move along his group to Delft University of Technology. During his PhD, he published papers in top class journals including Nature Nanotechnology and Angewandte Chemie. After completion of his bench work in Delft, he moved to Stellenbosch, South Africa in August, 2010 to work in the field of Polymer Chemistry. Due to a personal situation, he came back to Pakistan in March, 2011 and currently working as a lecturer in Chemistry at COMSATS Institute of Information technology, Abbottabad, Pakistan.